OCT 8 1957

ЖУРНАЛ
ЭКСПЕРИМЕНТАЛЬНОЙ И ТЕОРЕТИЧЕСКОЙ
ФИЗИКИ
АКАДЕМИЯ НАУК СССР

UNIVERSITY OF ILLINOIS
LIBRARY
APR 12 1960
CHICAGO

SOVIET PHYSICS

JETP

VOLUME 5 **NUMBER 2**

A Translation
of the
Journal of Experimental and Theoretical Physics
of the
Academy of Sciences of the USSR

Volume 32

SEPTEMBER, 1957

Published by the
AMERICAN INSTITUTE OF PHYSICS
INCORPORATED

DUPONT
EXPERIMENTAL STATION

SOVIET PHYSICS
JETP

A translation of the Journal of Experimental and Theoretical Physics of the USSR.

A publication of the

AMERICAN INSTITUTE OF PHYSICS

Governing Board

Frederick Seitz, *Chairman*
Allen V. Astin
Walter S. Baird
Jesse W. Beams
Hans A. Bethe
Raymond T. Birge
Richard H. Bolt
Franklin D. Dexter
Irvine C. Gardner
Samuel A. Goudsmit
Charles Kittel
Hugh S. Knowles
Winston E. Kock
R. Bruce Lindsay
William F. Meggers
Walter C. Michels
R. Ronald Palmer
Robert F. Paton
Joseph B. Platt
Ralph A. Sawyer
Henry D. Smyth
Mark W. Zemansky

Administrative Staff

Elmer Hutchisson
Director
Henry A. Barton
Associate Director
Mark W. Zemansky
Treasurer
Wallace Waterfall
Executive Secretary
Theodore Vorburger
Advertising Manager
Ruth F. Bryans
Publication Manager
Alice Mastropietro
Circulation Manager
Kathryn Setze
Assistant Treasurer
Eugene H. Kone
Director of Public Relations

American Institute of Physics Advisory Board on Russian Translatio

Robert T. Beyer, *Chairman*
Dwight Gray, Morton Hamermesh, Vladimir Rojansky,
Victor Weisskopf

Editor of Soviet Physics
Robert T. Beyer, Department of Physics, Brown University,
Providence, R.I.

Soviet Physics is a monthly journal published by the American Institute of Physics for the purpose of making available in English reports of current Soviet research in physics as contained in the Journal of Experimental and Theoretical Physics of the Academy of Sciences of the USSR. The page size of Soviet Physics will be 7⅞" x 10½", the same as other Institute journals.

Transliteration of the names of Russian authors follows the system employed by the Library of Congress.

This translating and publishing project was undertaken by the Institute in the conviction that dissemination of the results of researches everywhere in the world is invaluable to the advancement of science. The National Science Foundation of the United States encouraged the project initially and is supporting it in large part by a grant.

The American Institute of Physics and its translators propose to translate faithfully all the material in the Journal of EXPERIMENTAL AND THEORETICAL PHYSICS OF THE USSR appearing after January 1, 1955. The views expressed in the translated material, therefore, are intended to be those expressed by the original authors, and not those of the translators nor of the American Institute of Physics.

Two volumes are published annually, each of six issues. Each volume contains the translation of one volume of the Journal of EXPERIMENTAL AND THEORETICAL PHYSICS OF THE USSR. New volumes begin in February and August.

Subscription Prices:

Per year (12 issues)	
United States and Canada	$60.00
Elsewhere	64.00
Back Numbers	
Single copies	$ 6.00

Subscriptions should be addressed to the American Institute of Physics, 335 East 45th Street, New York 17, New York.

Copyright by American Institute of Physics 1957

SOVIET PHYSICS

JETP

A translation of the Journal of Experimental and Theoretical Physics of the USSR.

SOVIET PHYSICS—JETP VOL. 5, NO. 2, PP 157-343 SEPTEMBER, 1957

Emission of Negative Ions from Metallic Surfaces Bombarded with Positive Hydrogen Ions

I. M. MITROPAN AND V. S. GUMENIUK
Physico-Technical Institute, Academy of Sciences, Ukrainian SSR

(Submitted to JETP editor July 23,1956)
J. Exptl. Theoret. Phys. (U.S.S.R.) 32, 214–222 (February, 1957)

Results are presented of an experimental study of secondary negative ion emission from aluminum, stainless steel and copper targets bombarded by 200–1000 kev hydrogen and deuterium ions.

INTRODUCTION

WHEN metallic surfaces were bombarded by positive ions secondary emission of negative ions was observed together with secondary emission of electrons.[1–4] The experiments of Sloane and Love[3] show that the negative ions are partially due to the primary positive ions being converted into negative ones at the surface of the target.

The ejection of negative ions whose nature is different from that of the primary ones was observed in the work of Arnot[5] and of Veksler and Shuppe.[2] Arnot explained the appearance of the true secondary ions as a result of the excitation by the incident ion of the atoms adsorbed on the target. These ions, in giving up their excitation energy to the metal, capture an electron. Veksler and Shuppe consider that decomposition of electronegative impurities takes place at the surface of the target cathode. However, it remains unclear as to which of these processes is the dominant one when the elements bombarded by ions are those whose atoms have an electron affinity.

The object of the present work was to determine the coefficient of emission of secondary negative ions as a function of the energy of the primary hydrogen ions from metals ordinarily used in laboratory practice for the construction of high-voltage accelerating tubes. In addition, a mass spectrometric analysis of the resulting negative ions was carried out, and the influences of outgassing the target on the value of the coefficient of ejection K^- was studied.

APPARATUS AND EXPERIMENTAL PROCEDURE

An electrostatic generator was used for the production of accelerated hydrogen ions, with a mass analyzer (magnetic prism deflecting the beam through 90°) placed at the exit. The beam of ions selected by the magnetic analyzer was collimated by means of a number of diaphragms situated between the valve and the experimental setup shown schematically in Fig. 1).

The diaphragm D_1 (Fig. 1) with an opening 3 mm in diameter had a lead which was connected to a microammeter and which served to record the current. The next two diaphragms with openings 2 mm in diameter defined a beam whose cross-section at the target amounted to 2.5–3 mm.[2] The diaphragm D_4 with an opening 4 mm in diameter was insulated from the body of the apparatus, and was placed at a potential of –90 V with respect to ground in order to suppress secondary electrons and ions scattered by the collimating diaphragms.

The pressure in the high vacuum part of the apparatus produced by oil diffusion pumps and liquid nitrogen traps was $\sim 10^{-6}$ mm of Hg. In this investigation, H_1^+, H_2^+, D_2^+ and D_1^+ ions were used.

At first measurements were carried out on H_1^+ and D_2^+ ions, which allowed us to eliminate impurities of D_1^+ and H_2^+ as a result of the contamination of the source by deuterium. The contamination of H_2^+ in the work with D_1^+ was small as could be indirectly inferred from the shape of the curve $K^- = f(E_{kin})$, and introduced an error into the measured value of the coefficient of emission which was within experimental error.

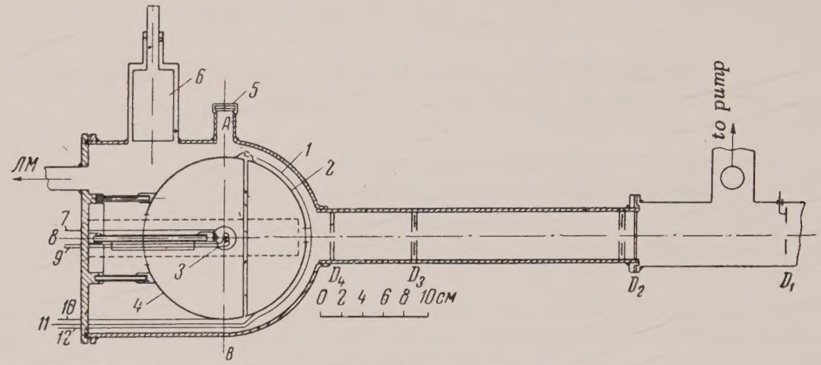

cross-section of the vacuum chamber along the line A-B

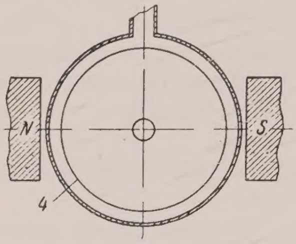

FIG. 1.

The main problem arising in the study of secondary negative ion emission is the separation of the electron and the ion components of secondary emission. This separation was achieved by subjecting the target-collector system, which was in the form of a spherical condenser, to a constant magnetic field. It may be shown that electrons originating on the surface of the inner sphere, with energies of several thousand ev and negative hydrogen ions of energies of a few ev may be separated in the magnetic field chosen for this work. Calculations show that the region in which the charged particles can move is bounded by a cylindrical surface whose axis coincides with the direction of the magnetic field. The radius of the cylindrical surface is given by

$$\rho = (v_\varphi / 2\omega) + \sqrt{(v_\varphi / 2\omega)^2 + 1}, \qquad (1)$$

where v_φ is the azimuthal component of the velocity, and $\omega = eH/mc$ (e and m are the charge and the mass of the particle, H is the intensity of the magnetic field, and c is the speed of light). For $H = 100$ oersted $\omega = 1.759 \times 10^9$ rad/sec for the electron and $\omega = 0.96 \times 10^6$ rad/sec for the negative hydrogen ion. If we assume that the electrons have a kinetic energy $E_{kin} \leq 3000$ ev, then the radius of the cylindrical surface which limits the region in which the electrons can move is $\rho_e \leq 1.7$ cm. For negative hydrogen ions of kinetic energy $E_{kin} \geq 10$ ev the radius of the cylindrical surface is given by $\rho \geq 5.75$ cm.

On the basis of the above calculations, we selected such parameters for our apparatus which allowed us definitely to separate secondary negative ions of energy $E \geq 10$ ev from secondary electrons of energy $E_{kin} < 3000$ ev. The spherical condenser used in our measurements consisted of an inner sphere *3* (Fig. 1) 20 mm in diameter, and an outer sphere *R* of diameter 160 mm. The inner sphere served as the target and was mounted on a porcelain insulator. A tungsten spiral was placed inside the inner sphere, was issulated from the target and was provided with insulated leads. By means of this spiral the target was heated to 1000° C during operation. The spherical segment *2* cut off by the plane passing perpendicular to the incident beam at a distance of 10 mm from the surface of the target served as the collector for the negative ions. The spherical segment was insulated from the remainder of the sphere. The target-collector system was situated inside a cylindrical copper chamber outside of which was placed an electromagnet with plane pole tips 100 mm in diameter The spherical segment was screened on the outside by a hemissphere of aluminum foil 1. The hydrogen ion beam, after passing through the collimator passed through an opening 10 mm in diameter in the screening hemisphere, and then through an opening 11 mm in diameter in the spherical segment, after which it reached the target.

Such a choice of the apparatus geometry allowed us to prevent the arrival at the collector of scattered particles and of particles ejected from the diaphragms, which was experimentally checked by placing the target inside a screening cylinder (shown by dotted lines in Fig. 1) with a 10 mm diameter opening in its end and situated coaxially with the direction of the beam. By sending the beam through the apparatus we established that no current is observed from the collector to ground.

The targets utilized in this work made of copper, aluminum and stainless steel of the EI–1 type were in the form of polished spherical surfaces. Before being placed in the apparatus, the target was washed with acetone and was then conditioned at a temperature of 900° C in a vacuum for 20–30 min with a subsequent cooling of the target for 1.5–2 hours before each measurement. The carbon target was obtained by depositing a thick layer of aquadag on a spherical copper base.

Because of fluctuations in intensity of the ion beam we used for the measurement both of the primary and the secondary ion current the method of accumulating charge on electrical capacitances during a time much smaller than the time constant for the discharge of these capacitances. The electrostatic field in the spherical condenser was set up by applying a potential to the target. The whole electrical supply system was insulated from ground. Both parts of the outer sphere were maintained at the same (zero) potential. Therefore the field of the spherical condenser was practically not distorted at all by the separation of the sphere into two parts insulated from each other.

The quantity of charge carried by the negative ions to the spherical segment (when the target was bombarded by primary ions) was measured by means of the electrometer *1*. The quantity of charge originating at the target and the quantity of charge carried by the secondary electrons to the capacitances part of the outer sphere were algebraically added by the circuit and were measured by means of the electrometer *2*.

The integrated coefficient of emission of negative ions was defined by the relation

$$K^{-} = q_1/(q_2 - q_1), \tag{2}$$

where q_1 and q_2 are the charges accumulated during the time of measurement in systems containing electrometers *1* and *2* respectively. The magnetic field set up by the electromagnet could be varied from 0 to 300 oersted and was practically homogeneous inside a cylinder 4 cm in diameter.

In order to determine the nature of the negative ions, a simplified mass-analyzer was used; it is schematically shown in Fig. 2. The plane surface of the target was placed at an angle of 45° to the direction of the beam and at an angle of 45° to the direction of the mass-analyzer axis. The target was cut out of copper foil of 0.1 mm thickness and was of oval shape. A tungsten spiral was mounted at the rear of the target in order to heat the target prior to measurement.

The ions emitted by the copper target bombarded by hydrogen ions were focussed by an electrostatic three-electrode lens. The focussing properties of the lens were checked by using electrons. The current focussed by the lens amounted to ~ 2% of the total emission current of a tungsten cathode used in place of the target. The magnetic field of the mass-analyzer was limited to a sector with 60° apex angle. The distance between the pole tips was 20 mm, and the radius of curvature of the ion trajectory was 100 mm.

A Faraday cup with an entrance opening 6 mm in diameter served as the collector of negative ions. The Faraday cup was screened on the outside by a cylinder with an opening 5mm in diameter insulated from the detecting cylinder. The ions originating at the target were accelerated by a potential difference of 650 V applied between the target and the grounded first electrode of the lens. A preliminary calibration of the mass analyzer was carried out using the positive ions Na^+, K^+, Li^+, which were emitted by heating a target covered by a layer consisting of a mixture of the aluminum silicates of Na, K, Li.

The scale of the mass-analyzer was calibrated by means of these ions. The investigation of the negative ion spectrum was carried out by smoothly varying the intensity of the magnetic field. The total ion current to the target was measured by a string electrometer which was connected to a 50 μF capacitance. A second string electrometer with a capacitance of 1000 pF in parallel was connected to to the Faraday cup. The measurements were made

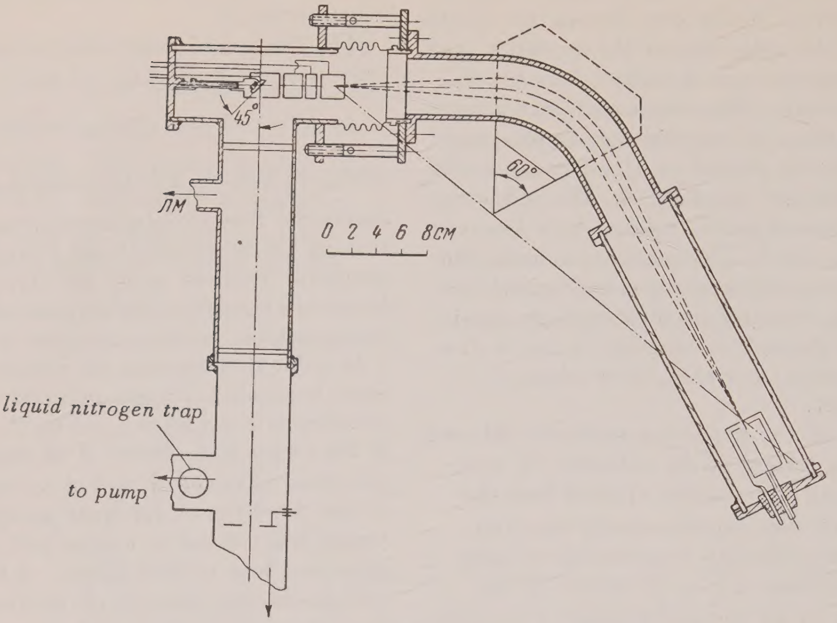

FIG. 2.

by the method described above. The coefficients for the emission of negative ions K^- were determined for potential differences of –100 and –400 V applied to the spherical condenser and with the intensity of the magnetic field varying from 100 to 300 oersted.

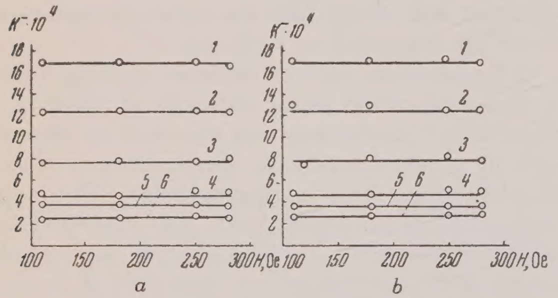

FIG. 3. Dependence of the coefficient of ejection of negative ions K^- on the intensity of the magnetic field frr various values of potential difference applied to the spherical condenser: *a*—200, *b*—400 V for the following energies of the H^+ ion: *1*—125, *2*—205, *3*—300, *4*—500, *5*—600, *6*—700 kev.

Figures 3*a* and *b* show the dependence of the coefficient K^- on the intensity of the magnetic field for a stainless steel target bombarded by protons of various energies. As may be seen from those Figures, the value of K^- for target potentials ranging from –200 to –400 V and for magnetic field intensity lying between 100 and 300 oersted, does not depend on the potential of the target and on the intensity of the magnetic field.

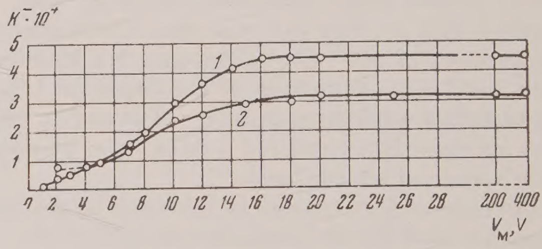

FIG. 4.

Measurements of secondary ion current were also carried out for lower values of target potential. Typical curves showing the results of such measurements for an aluminum target for a primary H_1^+ ion beam energy equal to 550 kev (curve *1*), 660 kev (curve *2*) and for a magnetic field intensity equal to 110 oersted are shown in Fig. 4.

The decrease in the coefficient K^- as the negative target potential is varied between 20 and 0V is explained by the presence of secondary positive ions of energy lying between 0 and 20 ev. By applying a positive potential to the target which retards the negative ions, we obtain the characteristic curves shown in Fig. 5. From these curves it may be seen that the energy of the negative ions does not exceed 10 ev. However, it is not possible to obtain from these curves the energy distribution of the ions at low energies since it may be seen from expression (1) that hydrogen ions of energies 2–3 ev may be partially held up by the magnetic field (H = 110 oersted). From the curves which show the manner in which the negative ions are retarded by the electric field (Fig. 5) we see that for the targets which we have investigated positive emission at energies higher than 150 kev is of the same order of magnitude as the emission of negative ions. The value of K^- which characterizes a given target for normal incidence of the beam at a given energy of bombarding ions was determined as the arithmetic mean of 8–10 measurements. The relative probable error amounts to ±3.7%.

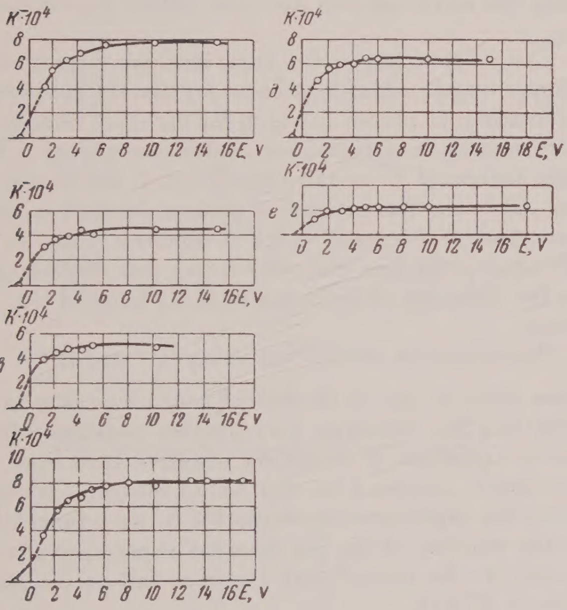

FIG. 5. Curves showing the retardation of negative ions for a magnetic field intensity of 110 oersted. a—aluminum target bombarded by H_1^+ ions of energy 175 kev; b—the same at an energy of 550 kev; c—the same at an energy of 660 kev; d—aluminum target bombarded by D^+ ions of energy 500 kev; e—stainless steel target bombarded by H^+ ions of energy 500 kev; f—carbon target bombarded by H^+ ions of energy 500 kev.

We have made a comparison of the coefficients for the ejection of negative ions by atomic and molecular ions of hydrogen and deuterium. We have compared the coefficients K^- obtained for molecular ions at energies of 1000 and 800 kev and for atomic H_1^+ and D_1^+ at energies of 500 and 400 kev respectively. The K^- measured for molecular ions of energy E_1 is twice as large as the K^- measured for atomic loss of energy $E_1/2$. From this we can conclude that the effectiveness of molecular hydrogen and deuterium ions from the point of view of secondary negative ion emission is equal to the effectiveness of two protons of the same speed. This enabled us to "join" the curves obtained for K^-, using atomic ions in the energy interval of 500 to 1000 kev, to curves obtained using molecular ions in the energy interval of ~ 150 to 500 kev and recalculated per atom.

The energy of the bombarding particles was determined by means of the magnetic analyzer. The radius of curvature of the trajectory in the magnetic field was 100 cm, the angle of deflection was 90°, as determined by the entrance and exit diaphragms with diameters of the openings given above. The magnetic poles were beveled at an angle of 45° at the points where the beam entered and left the magnetic field. The energy of the particles was measured with an accuracy of ±20 kev.

EXPERIMENTAL RESULTS AND DISCUSSION

Figure 6 shows curves obtained for the dependence of K^- on the kinetic energy of the bombarding hydrogen and deuterium ions using targets made of copper, stainless steel of type EIa–1, carbon and aluminum. Before the copper target was subjected to bombardment by primary ions it was conditioned over a long period of time in high vacuum at a temperature of 900° C and a pressure of ~ 10^{-6} mm of Hg in the absence of a beam during 1.5–2 hours. The measurements of the magnitude of K^- were made on a cold target free of oxides.

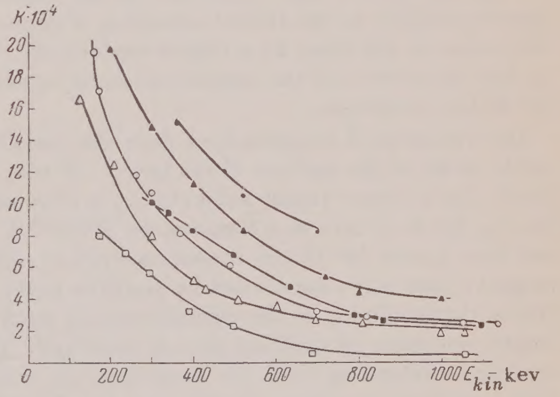

FIG. 6. Curves showing the dependence of the yield of negative ions on the kinetic energy of bombarding ions. Aluminum target: o—H_1^+, and o—D_1^+; carbon and stainless steel targets: Δ—H_1^+, ▲—D_1^+; copper target: □—H_1^+, ■—D_1^+.

As may be seen from the curves of Fig. 6, K^- decreases as the energy of the bombarding ions is increased. At the same energy of the primary ions K^- is larger when a given target is bombarded by D_1^+ ions than when it is bombarded by H_1^+ ions. Experiments carried out with stainless steel and carbon targets did not show any difference in the values of K^- and therefore the curves showing $K^- = f(E_{kin})$ obtained for a stainless steel target are also characteristic of a carbon target.

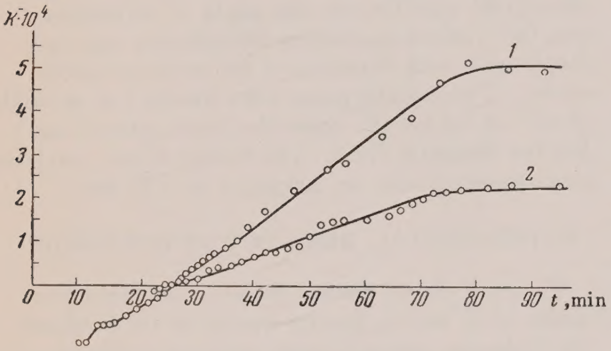

FIG. 7. Curve *1* refers to the bombardment by H_1^+ ions of kinetic energy 300 kev, curve *2* refers to thesame at an energy of 500 kev.

An aluminum target was also subjected to bombardment by the positive ions H_1^+ and D_1^+. As may be seen from Fig. 6, the shape of the curve $K^- = f(E_{kin})$ is the same as for the other targets. However, these experiments show that the value of K^- depends on the target material. Of the targets investigated by us the lowest emission of negative ions is exhibited by a copper surface which is free of oxides and the largest emission is exhibited by aluminum.

The emission of negative ions depends markedly on the state of the surface of the target. It was found that a copper target subjected to preliminary heating for 8–10 min at a temperature of 900° K and then cooled for 10 min shows no emission of negative ions when bombarded by positive ions. But at the beginning of the bombardment of such a target, emission of positive ions is observed. By applying a retarding field, we found that the positive ions have an energy greater than 400 ev and therefore we may suppose that these are primary ions scattered through large angles in the Coulomb field of the target nuclei.

The measurement of the current to the collector (from a cold target which had been previously heated) over a certain period of time shows that the positive current gradually decreases, passes through zero and a negative current begins to grow reaching a constant value after a time of the order of 70 min measured from the moment of stopping the heating of the target. Figure 7 shows the change with time of the emission of secondary ions from a copper target which was heated in a vacuum of 10^{-6} mm of Hg and which was subsequently allowed to cool in the absence of the ion beam for 8–10 min. A measurement of the coefficient of secondary electron emission γ for a copper target bombarded by hydrogen ions both before the target is heated in vacuum and after such heating does not exhibit at any time any difference in the value of γ. This experiment shows that the method used by us for outgassing the metal surface does not affect the value of γ.

The yield of secondary negative ions from a cold copper target, which had been previously subjected to heating, is shown in Fig. 8 for the case of bombardment by deuterium ions of 300 kev energy. The dependence of K^- on the time (Figs. 7 and 8) may be related to the formation of a surface layer of atoms adsorbed on the target which is apparently due to the adsorption from the surrounding gas medium and to the diffusion of hydrogen from the body of the metal.

Measurements carried out using H_1^+ and D_1^+ ions showed that in the energy range from 200 to 1000 kev the deuterium ions liberate considerably greater numbers of secondary negative ions from the target than do ions of atomic hydrogen. If one plots the experimental results for K^- as a function of the velocity of the ion then the experimental points for the ions of both isotopes fall on the same curves (Fig. 9).

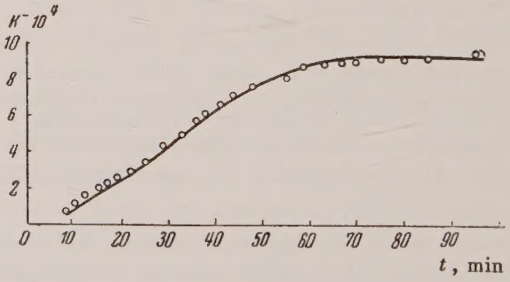

FIG. 8.

Concurrently with the study of the coefficient of emission of negative ions, we have also investigated their nature by analyzing their masses by means of the apparatus shown in Fig. 2. In the case of a copper target, we observed a large number of negative ions differing in their values of e/m

(Fig. 10). Under the same experimental conditions, the first peak has an intensity two orders of magnitude larger than the other groups, and is due to H^-_1 ions. The second group of peaks corresponds to masses 12, 16, 18. They correspond to C^{12-}, O^{16-}, and OH^- ions. The third group of negative ions apparently contained C_2^-, CH_2^-, $C_2H_2^-$ ions. When the target was heated by the method previously described, it was found that the hydrogen peak disappeared and was then reestablished during a time ~ 40 min.

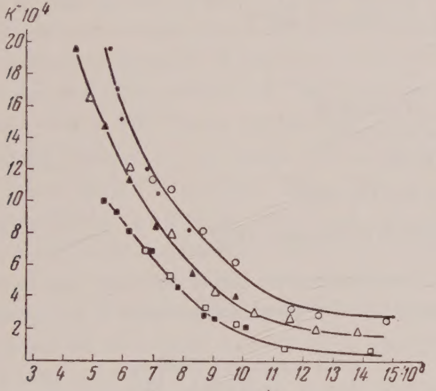

FIG. 9.

It would be of interest to investigate the dependence of K^- on the angle of incidence.

CONCLUSIONS

1. The coefficient of ejection of negative ions decreases monotonically as the energy of the primary hydrogen ions is increased. Within the investigated range of energies the maximum value of K^- at an energy near 200 kev is ~ 10^{-3} and falls to ~ 10^{-4} at an energy of 1000 kev.

2. The probability of forming negative ions by bombardment of metallic surfaces is determined by the speed of the primary ions and apparently does not depend on their mass.

3. The secondary emission of negative ions depends on the nature of the target. The value of the emission coefficient K^- progressively increases for the targets investigated in the following order: copper, stainless steel of type EIa–1, aluminum. No difference was observed in the values of K^- obtained for a stainless steel target add for a carbon target made by depositing a thick layer of aquadag on a copper support.

4. Outgassing the target decreases the value of K^- and the number of emitted negative ions may become less than the number of fast primary positive ions scattered by the Coulomb field. At the same time the coefficient γ remains constant.

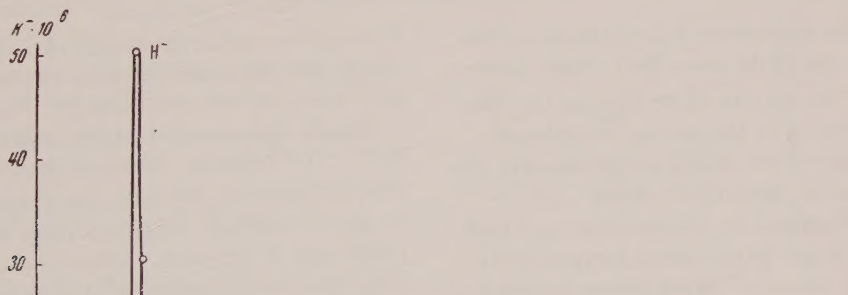

FIG. 10.

5. The coefficient of emission for negative

ions whose energy does not exceed 10 ev is of the same order as for slow positive ions.

The authors express their sincere gratitude to academician A. K. Val'ter and to Ia.M. Fogel' for valuable advice and for their continuing interest in this work.

---

[1] R. Arnal. Ann. de Phys. 10, 830 (1955).

[2] V.I. Veksler and G.N. Shuppe, J.Tech. Phys. (U.S.S.R.) 23, 1573 (1953).

[3] R.H. Sloane and H.M. Love. Nature 1599, 302 (1947).

[4] E. Ia. Zandberg, J.Tech. Phys. (U.S.S.R.) 25, 1386 (1955).

[5] F. L. Arnot and C. Beckett. Proc.Roy. Soc. (London) A168, 103 (1938).

Translated by G.M. Volkoff
51

SOVIET PHYSICS JETP VOLUME 5, NUMBER 2 SEPTEMBER, 1957

Some Cases of Very Small Life Times of Low Nuclear Levels

E. E. BERLOVICH AND G. V. DUBINKIN
Leningrad Physico-Technical Institute,
Academy of Sciecnes, USSR

(Submitted to JETP editor August 14,1956)
J. Exptl. Theoret. Phys. (U.S.S.R.) 32, 223-226 (February, 1957)

The life times of short-lived excited states of nuclei were studied by the delayed coincidence method. The life times of the lower levels of the Ti^{46} and Mo^{95} nuclei were found to be less than 10^{-10} sec.

The experimental half-life of the excited state of the Tl^{203} nucleus was found to be $(2.9 \pm 0.3) \cdot 10^{-10}$ sec., a result which does not agree with that of de-Waard. The method applied by de-Waard is discussed. The partial half-times for magnetic dipole and electric quadrupole transitions are compared with the values predicted by the formulas of the single-particle model.

BERLOVICH[1] has demonstrated the influence of the particle energy and of the pulse front shape associated with it on the results of measuring the lifetime of excited states by the method of delayed coicidences. This effect which is particularly important in the case of short-lived states (10^{-10} – 10^{-9} sec) was eliminated by introduction into both side channels of triple coincidence circuit amplitude analyzers by means of which it was possible to select the coincidences of only those pulses which lie in equivalent amplitude intervals.

In this article we present the results of investigating short-lived states of Ti^{46}, Mo^{95} and Tl^{203} nuclei. Before the measurements were made, the following control experiment was carried out: by means of investigating the curves of $\gamma\beta$–$\gamma\beta$–coincidences for the Co^{60} → Ni^{60} decay for which the limiting values of the energies of the β–spectrum and of the Compton distribution differ by a factor of more than 3½, we satisfied ourselves that when coincidences of pulses in energy–equivalent intervals were recorded no mutual displacement of the centers of gravity of the two curves occurred. This agrees with the results of Bay[2] according to which the life times for both excited states of the Ni^{60} nucleus are less than 10^{-11} sec.

Figure 1 shows the experimental results for the Sc^{46} → Ti^{46} decay. The maximum energy of the β-spectrum is 0.340 mev, the energies of the two γ-rays in cascade accompanying the β-decay are 0.880 and 1.120 mev. According to the data of Nag, Sen, and Chatterjee[3] the mean life of these levels is $\tau = 1.3 \times 10^{-5}$ sec. However, it follows from the measurements of Koicki, Ballini, and Chaminade[4] that this life-time must be less than 2×10^{-6} sec.

From the measurement of conversion coefficients,[5] and also from experiments on angular $\gamma\gamma$–correlation[6] and on angular correlation of the directions of polarization[7], it follows that both γ-transitions are of the E2 type. The life times of nuclear states for electric quadrupole transitions with energies of about one mev must (in accordance with the single particle formulas of Weisskopf[8] and of Moszkowsky[9] be smaller than the values given above by six or seven orders of magnitude.

It may be seen from Fig. 1 that the experimental curves for the $\beta\gamma$– and $\gamma\beta$–coincidences show no mutual displacment. When the experimental accuracy of our measurements is taken into account this means that for each of the two lowest excited states of the Ti^{46} nucleus $\tau < 10^{-10}$ sec.

Similar measurements for the $Nb^{95} \rightarrow Mo^{95}$ transition have shown that for the level of the Mo^{95} nucleus of 0.764 mev energy, which decays by a mixture of M1 and E2 transitions,[10] , the life time is also less than 10^{-10} sec.

Finally, Fig. 2 illustrates the experimental results on the lifetime of the level of the Tl^{203} nucleus of energy 0.279 mev. In an earlier paper,[11] we have obtained from the mutual displacement of the centers of gravity of the $\beta\gamma$– and $\gamma\beta$-coincidence curves (the method of "self–comparison") the value of 4×10^{-10} sec for the half life of this level which, however, we found useful to regard as the upper limit for the half life. The introduction of the amplitude analyzers, which for all practical purposes has eliminated the influence of the difference of the spectra of the two kinds of coincident particles (Compton electrons and β-particles), has enabled us to obtain a more definite result for the life time of the Ti^{203} level.

Curves similar to those shown in Fig. 2 were taken repeatedly with the amplitude intervals in the channels being varied and with both energy-equivalent and arbitrary intervals (within the limits of both spectra) being taken. In all cases, a displacement of the two curves ($\beta\gamma$– and $\gamma\beta$–coincidences) was observed in the same direction. The mean value for the half life obtained from measurements carried out with equivalent amplitude intervals turned out to be equal to

$$T = (2.9 \pm 0.3) \cdot 10^{-10} \text{ sec.}$$

In all the measurements, the possible coincidences of conversion electrons with x-rays were eliminated either by absorbing the latter by a lead filter or by choosing the amplitude intervals outside the region within which x-ray pulses could lie.

The value of 4×10^{-10} sec adopted in our earlier paper[11] for the upper limit on the half life turned out to be larger than in the present experiments apparently due to the difference in the upper limits of the β-spectrum ($E_{\beta\,max} = 0.215$ mev) and of the Compton distribution for γ-rays of energy 0.279 mev ($E_{Compt\ max} = 0.148$ mev) which should increase the mutual displacement of the $\beta\gamma$- and $\gamma\beta$-coincidence curves.

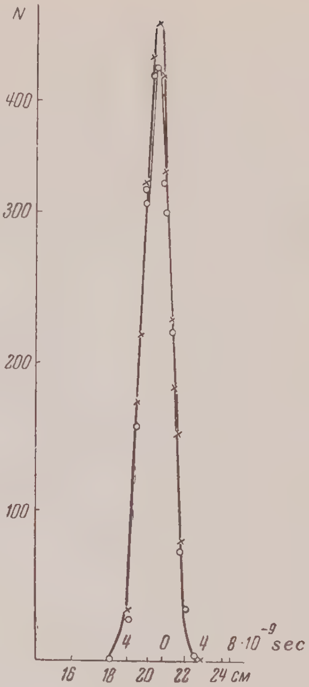

FIG. 1. Coincidence curves for the transition $Sc^{46} \rightarrow Ti^{46}$. O–$\beta\gamma$-coincidences, ×–$\gamma\beta$-coincidences. The number of coincidences is plotted along the vertical axis while the horizontal axis gives the readings of the variable delay line scale in units of time and in centimeters.

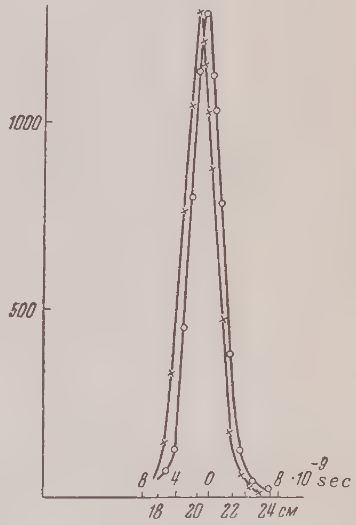

FIG. 2. Coincidence curves for the transition $Hg^{203} \rightarrow Tl^{203}$. O–$\beta\gamma$-coincidences, ×–$\gamma\beta$-coincidences. The number of coincidences is plotted along the vertical axis while the horizontal axis gives the readings of the variable delay line scale in units of time and in centimeters.

Recently, de-Waard[12] obtained (by the method of delayed coincidences) the value $T = (1.2 \pm 0.3) \times 10^{-10}$ sec for the level in question. The measurement was made by means of comparing the displacement of the curves for the $\beta\gamma$- and $\gamma\beta$-coincidences for the transition $Hg^{203} \rightarrow Ti^{203}$ with the displacement of similar curves for the transition ThB →ThC to the level with 0.238 mev excitation energy. In the second case the displacement could have been due only to instrumental effects since, according to the data of Graham and Bell,[13] the lifetime of the ThC level is less than 2×10^{-11} sec. The author assumes that the displacement due to instrumental causes is the same in both cases since the energies of the radiation are nearly the same (in thecase of Hg^{203} : $E_{\beta\max} = 0.215$ mev, $E_\gamma = 0.279$ mev; in the case of Thb: $E_{\beta\max} = 0.340$ mev, $E_\gamma = 0.238$ mev). The coincidences were registered only between β-particles and recoil electrons having an energy within the range from 75 to 150 kev.

It appears to us that the "instrumental" displacement of the $\beta\gamma$- and $\gamma\beta$-coincidence curves due to the influence of the difference in the pulse front shape must be larger in the case of ThB than in the case of Hg^{203} when measurements are made in the energy range 75–150 kev, since in the first case the average energy of the β-particles in this interval, which contains the neighborhood of the maximum of the β-spectrum (with the maximum value of 340 kev), is greater than in the second case of the softer β-spectrum (with a maximum energy of 215 kev) when the neighborhood of the maximum is strongly displaced and only the decreasing part of the spectrum falls within the working interval. Conversely, the average energy of the recoil electrons for the γ-rays of ThC ($E_\gamma = 0.239$ me v) whose maximum is near the limiting energy $E_{\text{Compt max}} = 0.115$ mev turns out to be lower over the working interval than in the case of the γ-rays from Tl^{203} ($E_\gamma = 0.279$ mev) for which the limit of the recoil electron distribution lies at $E_{\text{Compt max}} = 0.147$ mev. In the light of the detailed analysis of the effect of the steepness of the pulse fronts (which depends, in particular, on the energy of the particles) which was carried out in our earlier work,[1] it appears to us to be probable that the mutual displacements of the $\beta\gamma$- and $\gamma\beta$-coincidence curves brought about by instrumental causes must be different in the two cases under consideration and that the subtraction made by Zarubin[10] of the displacement of the curves for the ThB →ThC transition from the displacement of the curves for the $Hg^{203} \rightarrow Tl^{203}$ transition must lead to an underestimate of the lifetime of the Tl^{203} level. In order that the difference in the form of the spectra of β-particles and of recoil electrons should not lead to a displacement of the $\beta\gamma$- and $\gamma\beta$-coincidence curves, it is necessary to choose a considerably more narrow energy interval than was done in the work under consideration. This would have eliminated the necessity to subtract the displacements of the curves observed in the two transitions. Measurements made on a level with a negligibly small lifetime would then serve only to verify the absence of an "instrumental" displacement.

Using the value[14] $\alpha = 0.27$ for the total conversion coefficient, we obtain from the experimental value of the half-life the following value for the half life for radiative decay

$$T_\gamma = T\,(1 + \alpha) = (3.7 \pm 0.4) \cdot 10^{-10} \text{ sec.}$$

This value agrees well with the result of Barloutand, Grjebine and Rion,[15] who obtained $T_\gamma = (3.8 \pm 1.2) \times 10^{-10}$ sec from measurements of the cross section for Coulomb excitation.

The contradiction noted by de-Waard[12] with the result of Metzger's measurements[16] who obtained from experiments on the resonance scattering of γ-rays the value $T_\gamma = (6.9 \pm 2.8) \times 10^{-10}$ sec is considerably reduced since within experimental error this result almost overlaps with the two results given above. Nevertheless, taking into account the fact that Metzger's result has been obtained from three different ypes of experiment on the resonance scattering of γ-rays, one should suppose that the above difference is not accidental.

It is well established [14] that the transition in question is a mixture of 30% Ml and 70% E2 transitions. A calculation of the partial half lives for both types of transitions gives:

$$T_\gamma(M1) = 1.23 \cdot 10^{-9} \text{ sec.}$$

$$\text{and} \quad T_\gamma(E2) = 5.3 \cdot 10^{-10} \text{ sec.}$$

The second value is by a factor 9 less than the value calculated from Weisskopf's single particle formula (4.7×10^{-9} sec). This may be explained by the effect of the polarization of the nuclear core by the last odd proton. On the other hand a calculation using Weiskopf's formula for the Ml transition gives a value (1×10^{-12} sec) which is

1200 times less than the experimental value. Delayed magnetic dipole transitions have been studied by Graham and Bell,[13] who explained the reduction in the transition probability as being due to a forbidden change in orbital angular momentum: $\Delta l = 2$. The transition under consideration may be identified as the transition $d_{3/2} \rightarrow s_{1/2}$. A partial relaxation of the rule forbidding the transition in this case is apparently related to the meson exchange currents between nucleons.

Note added in proof. After the present article had been submitted for publication, the authors learned of the paper by Azuma[17] in which the estimate $\tau < 5 \times 10^{-11}$ sec is given for the upper limit on the lifetimes of both excited states of the Ti^{46} nucleus.

[1] E. E. Berlovich, Izv. Akad. Nauk SSSR, Fiz. Ser. 20, 1438 (1956).

[2] Bay, Henry and McLernon, Phys. Rev. 97, 561 (1955).

[3] Nag, Sen and Chatterjee, Nature, 164, 1001 (1949).

[4] Koicki, Ballini and Chaminade, Compt. rend. 236, 1155 (1955).

[5] Moon, Waggoner and Roberts, Phys. Rev. 79, 505 (1950).

[6] E. L. Brady and M. Deutsch, Phys. Rev. 78, 558 (1950).

[7] F. Metzger and M. Deutsch, Phys. Rev. 78, 551 (1950).

[8] J. Blatt and V. Weisskopf, *Theoretical Nuclear Physics.*

[9] S. Moszkowsky, Phys. Rev. 89, 1071 (1951).

[10] P. P. Zarubin, Bull. Acad. Sci. USSR Fiz. ser. 18, 563 (1954).

[11] E. E. Berlovich, Bull. Acad. Sci. USSR Fiz. Ser. 19, 343 (1955).

[12] H. de Waard, Phys. Rev. 99, 1045 (1955).

[13] R. L. Graham and R. E. Bell, Canad. J. Phys. 31, 377 (1953).

[14] N. Marty, Compt. rend. 240, 291 (1955).

[15] Barloutand, Grjebine and Rion, Compt. Rend. 240, 1207 (1955).

[16] F. R. Metzger, Proceedings of the 1954 Glasgow Conference on Nuclear and Meson Physics, Pergamon Press, London, 201 (1955); F. R. Metzger and W. B. Todd, Phys. Rev. 95, 627 (1954).

[17] R. E. Azuma, Phil. Mag, 46, 1031 (1955).

Translated by G. M. Volkoff
52

SOVIET PHYSICS JETP VOLUME 5, NUMBER 2 SEPTEMBER, 1957

Two Limiting Momenta in Scalar Electrodynamics

L. P. GOR'KOV
Institute for Physical Problems, Academy of Sciences, USSR

(Submitted to JETP editor December 15, 1955)
J. Exptl. Theoret. Phys. (U.S.S.R.) 32, 359-362 (February, 1957)

A study is made of the possibility of introducing two limiting momenta in scalar electrodynamics. It is shown that the difficulties connected with the vanishing of the renormalized charge in the limit of a point interaction appear also in the theory considered here.

KHALATNIKOV and the writer[1] have written integral equations for the Green's functions and vertex parts in the electrodynamics of charged mesons with spin zero [Eqs. (2), (4) and (7) in Ref. 1]. The last of these equations is valid only if in the photon function

$$D_{\mu\nu}(k) = \left(\delta_{\mu\nu} - \frac{k_\mu k_\nu}{k^2}\right)\frac{d_t(k^2)}{k^2} + \frac{k_\mu k_\nu}{k^2}\,\frac{d_l(k^2)}{k^2}$$

one chooses $d_l = d_t$, and was introduced in the approximation $e_1^2 \ll 1$. The solution of these equations was carried through in accordance with the general scheme of Landau, Abrikosov and Khalatnikov[2] for a smeared out interaction, in which the interaction factor β_σ is replaced by

$$\beta_\sigma \rightarrow \beta_\sigma \delta_{\Lambda_p}(p)\, \delta_{\Lambda_p}(p-l)\, \delta_{\Lambda_k}(l),$$

$$\delta_\Lambda(p) = \begin{cases} 1; & -p^2 \ll \Lambda^2 \\ 0; & -p^2 \gg \Lambda^2. \end{cases}$$

In Refs. 1 and 3, it was assumed that $\Lambda_p \sim \Lambda_k$; the changes appearing in the case in which there is a decided inequality between the two limiting values have been investigated by Abrikosov and Khalatnikov[4] in the ordinary electrodynamics and the pseudoscalar meson theory. In connection with a conclusion stated by Pomeranchuk[5] about the vanishing of the charge on the passage to a point interaction, the two-limit scheme takes on particular interest. We consider this question in the electrodynamics of particles with spin zero.

Two cases are possible:

I. $\Lambda_k \gg \Lambda_p$. The integration in Eq. (4) of Ref. 1 can be taken over two regions: a) $\Lambda_p \gg p \gg k$, and b) $\Lambda_k \gg p \gg \Lambda_p \gg k$. We turn our attention to the equation for the vertex part for $p \gg l$. The integration over k involves the region $\Lambda_p \gg k \gg p$. The vertex part is equal to zero for p or $l \gg \Lambda_p$ and is the same as the expression (6) of Ref. 3 for $\Lambda_p \gg p \gg l$. Therefore the region b) makes no contribution to the expression for the polarized tensor. If $l \gg p$, the vertex part contains in the right-hand member of Eq. 7 of Ref. 1 an integration only over the region $\Lambda_p \gg k \gg l$ (because of the factor $\delta_{\Lambda_p}(p-k)$ under the sign of integration), and is equal to zero for $l \gg \Lambda_p$. Thus for $\Lambda_k \gg \Lambda_p$, only the one limit Λ_p actually has any effect in the theory.

II. $\Lambda_p \gg \Lambda_k$. Let us consider the equation for the vertex part in this case. Let $p \gg l$. For the vertex part and $G(p)$, we try to find a solution in the form

$$G^{-1}(p) = [\hat{p} - m_1(p^2)] / \beta(p^2),$$

$$B_\sigma(p,\ p-l,\ l) = \beta_\sigma \alpha(p^2).$$

The region of integration is bounded by $\Lambda_k \gg k \gg p$. For $\Lambda_k \gg p \gg l$ we obtain the expression (6) of Ref. 3:

$$B_\sigma(p,\ p-l,\ l) = \beta_\sigma \alpha(p^2) \tag{1}$$

$$+ (\hat{l} l_\sigma - \beta_\sigma l^2)\, p^{-2} \alpha^2(p^2)\, d(p^2)\, S_0(p^2, l^2).$$

If $p \gg \Lambda_k \gg l$, then the integral does not make a logarithmic contribution, and

$$B_\sigma(p,\ p-l,\ l) \to \beta_\sigma. \tag{2}$$

We turn to the equation for the photon Green's function. If $k \gg \Lambda_k$, then $d_t(k^2) = 1$. Suppose $k \ll \Lambda_k$. Then, as before, in the integral for the polarization tensor there are two regions of integration

a) $\Lambda_p \gg \Lambda_k \gg p \gg k$, b) $\Lambda_p \gg p \gg \Lambda_k \gg k$.

In region a) one can use the expression (1) for $B_\sigma(p,\ p-l,\ l)$, and in region b) one can use Eq. (2). After some calculation we obtain:

$$d_t^{-1}(\eta) = 1 + 8\nu S(L_k, \eta) + (e_1^2/3\pi)\,\nu\,(L_p - L_k),$$

where we have at once introduced the effective number ν of different types of particles, and

$$\eta = \ln(-k^2/m^2), \qquad L_k = \ln(\Lambda_k^2/m^2).$$

For $S(\xi,\ \nu)$ we have

$$S(\xi, \eta) = (e_1^2/24\pi)(\xi - \eta)\,\beta(\xi).$$

But $\beta(\xi = L_k) = 1$. Therefore we get

$$d_t(k^2) = \begin{cases} [1 + (e_1^2/3\pi)\,\nu \ln(\Lambda_p^2/-k^2)]^{-1}; & \text{for } k \ll \Lambda_k, \\ 1; & \text{for } k \gg \Lambda_k. \end{cases} \tag{3}$$

Thus when two cut-off limits are introduced, the function $d_t(k^2)$ ceases to be continuous in the logarithmic scale, and takes a jump on passage through the value $-k^2 = \Lambda_k^2$. The formula for the charge will obviously be

$$e^2 = e_1^2 [1 + (e_1^2/3\pi)\,\nu \ln(\Lambda_p^2/m^2)]^{-1}.$$

The function $\alpha(\xi)$ is defined by the equation[3]

$$\alpha(\xi) = 1 - \frac{e_1^2}{8\pi} \int_{\xi}^{L_k} \alpha(z)\, d(z)\, dz.$$

Substituting the expression for $d(z) = d_t(z)$ into this equation and integrating, we obtain

$$\alpha(p^2) = \left[\frac{1 + (e_1^2/3\pi)\nu \ln(\Lambda_p^2/\Lambda_k^2)}{1 + (e_1^2/3\pi)\,\nu \ln(\Lambda_p^2/-p^2)} \right]^{3/8\nu} \tag{4}$$

for $-p^2 \ll \Lambda_k^2$,

$$\alpha(p^2) = 1 \qquad \text{for } -p^2 \gg \Lambda_k^2.$$

The expression for the function $\beta(p^2)$ can be obtained from an identity of Ward: $\alpha\beta = 1$; it will again be the renormalized value,

$$\beta(p^2) = [(e_1^2/e^2)\, d_t(\Lambda_k)]^{3/8\nu} [d_{tc}(-p^2)]^{-3/8\nu}. \tag{5}$$

The function $m_1(p^2)$ was defined in Ref. 1 as the renormalization ratio, which in the presence of two limits is written in the following way:

$$m_1(\Lambda_k, \Lambda_p, p^2, e_1^2)/m_1$$

$$= m(-p^2/m^2, e^2)/m(\Lambda_k^2/m^2, e^2),$$

$$\lim_{-p^2\to\Lambda_k} m_1(p^2) = m_1.$$

The correctness of such a normalization follows from the fact that in the equation for $G(p)$ the logarithmic contribution arises in the region $\Lambda_k \gg k \gg p$, and for $p \gg \Lambda_k$ the meson Green's function agrees with accuracy up to nonlogarithmic terms with its zeroth order value $(\hat{p} - m_1)^{-1}$. According to Ref. 1, we have

$$m(-p^2/m^2, e^2) = m[d_{tc}(p^2)]^{-9/8\nu},$$

from which we at once get

$$m_1(p^2) = m_1\left[\frac{1 + (e_1^2/3\pi)\nu\ln(\Lambda_p^2/-p^2)}{1 + (e_1^2/3\pi)\nu\ln(\Lambda_p^2/\Lambda_k^2)}\right]^{9/8\nu} \quad (6)$$

$$\text{for } -p^2 \ll \Lambda_k^2,$$

$$m_1(p^2) = m_1 \quad \text{for } -p^2 \gg \Lambda_k^2.$$

From Eq. (3) it can be seen that the vacuum polarization of particles with spin zero leads to a change of the photon Green's function in exactly the same way as in the case of the ordinary electrodynamics, studied in Ref. 4. Equations (4), (5) and (6) enable one to write out the expressions for the function $G(p)$ for $d_l = d_t$, according to Ref. 1. A gauge transformation to an arbitrary d_l can also be carried out.

It is now easy to convince oneself of the correctness of Pomeranchuk's result[5] for the scalar electrodynamics also. We consider the first of the diagrams for a vertex part which were not taken into account in Eq. (7) of Ref. 1 —a diagram with two intersecting virtual photon lines — and estimate the error incurred by neglecting this diagram $(d_l = d_t)$. For this purpose we put in place of $G(p)$, $B_\mu(p, p-k, k)$, and $D(k)$ the functions of the basic approximation, Eqs. (3)-(5), and assume that between the two limits there holds the inequality

$$\ln(\Lambda_p/\Lambda_k) \gg 1. \quad (7)$$

Ward's identity makes it possible to reduce all the functions β and α to only a single function α, which, as can be seen from Eq. (4), always satisfies $\alpha \lesssim 1$. On the other hand, since the integration over the photon quanta is taken up to the limiting momentum Λ_k, the two photon functions d_t will be smaller than

$$[1 + (e_1^2/3\pi)\nu\ln(\Lambda_p^2/\Lambda_k^2)]^{-1}.$$

The integral under consideration contains only one logarithmic integration, so that the relative size of the contribution from this diagram to the vacuum polarization will be less than

$$\sim e_1^4\ln(\Lambda_k^2/m^2)[1 + (e_1^2/3\pi)\nu\ln(\Lambda_p^2/\Lambda_k^2)]^{-2}.$$

For not too small $e_1{}^2$, this contribution does not depend on the priming charge and will be small, if instead of Eq. (7) we require

$$\ln(\Lambda_k^2/m^2)\ln^{-2}(\Lambda_p^2/\Lambda_k^2) \ll 1$$

(say $\Lambda_k = \sqrt{m\Lambda_p}$). It can easily be seen that all the remaining diagrams together give a power series

$$\sum_{n,m} C_{nm}\ln^n(\Lambda_k^2/m^2)\ln^{-m}(\Lambda_p^2/\Lambda_k^2), \text{where } m > n.$$

With a reservation regarding the asymptotic character of this series, there again follows from this basic conclusion of Pomeranchuk, that the charge goes to zero in the limit of a point interaction:

$$e^2 = [(\nu/3\pi)\ln(\Lambda_p^2/m^2)]^{-1} \to 0 \quad \text{for} \quad \Lambda_p \to \infty.$$

In conclusion I express my gratitude to I. M. Khalatnikov and A. A. Abrikosov for discussion of the work.

---

[1] P. L. Gor'kov and I. M. Khalatnikov, Dokl. Akad. Nauk SSSR **103**, 799 (1955).

[2] Landau, Abrikosov and Khalatnikov, Dokl. Akad. Nauk SSSR **95**, 497, 773, 1177 (1954).

[3] L. P. Gor'kov and I. M. Khalatnikov, Dokl. Akad. Nauk SSSR **104**, 197 (1955) .

[4] A. A. Abrikosov and I. M. Khalatnikov, Dokl. Akad. Nauk SSSR **103**, 993 (1955).

[5] I. Ia. Pomeranchuk, Dokl. Akad. Nauk SSSR **103**, 1005 (1955).

Translated by W. H. Furry
73

Measurement of the Relative Intensities of γ-lines by a Two-Meter Crystal Diffraction γ-Spectrometer

O. I. SUMBAEV
The National Scientific Research Institute of Metrology

(Submitted to JETP editor September 22,1956)
J. Exptl. Theoret. Phys. (U.S.S.R.) 32, 247–250 (February, 1957)

Results of measurements of the relative intensities of a number of lines in the γ-spectra of Ir^{192}, Ta^{182} and Ta^{183} are presented. In those cases when the relative intensities have been measured by different methods, the data for the Ir^{192} spectrum obtained by a crystal diffraction spectrometer agree satsifactorily with the results derived from photo-electron and recoil electron measurements.

THE relative intensities of the lines in the spectra of γ-radiation from Ir^{192}, Ta^{182} and Ta^{183} are measured on the two-meter crystal diffraction γ-spectrometer.[1] The high resolving power of the spectrometer (0.1 percent for γ-quanta with energies less than 1 mev, together with the exceptional simplicity of the spectra (each line is represented by a single peak in the spectrum on an almost constant background), permits the study of complicated spectra with closely spaced lines. In calculating the spectral sensitivity of the apparatus one must take into account self-absorption in the source, the reflection coefficient of the γ-radiation from the curved quartz crystal and the efficiency of the scintillation spectrometer, used as detector of the γ-radiation. The only specific dependence is the dependence of the reflection coefficient from the curved crystal (a quartz crystal with effective planes 3140 was used) on the wavelength. The investigations of DuMond and others[2] have shown that this relation is nearly quadratic. Detailed investigations carried out by us for energies of 191 (In^{114}), 279 (Hg^{203}), 412 (Au^{198}) and 1190 kev (the average energy of the group of hard lines in the spectrum of Ta^{182}) have confirmed DuMond's results and have led to the relation

$$\Gamma_i = k \cdot E^{-n},$$

where Γ_i is the reflection coefficient, E is the γ-ray energy and $n = 1.85 \pm 0.04$.

THE SPECTRUM OF Ir^{192}

A source of 1 curie activity, in the form of a foil of dimensions 30 × 5 × 0.2 mm, was used in investigating the spectrum of $Ir.^{192}$ The resolving power of the spectrometer

$$\delta = (1.5 \div 1.7) \cdot 10^{-3} E,$$

where δ is the relative line width at half maximum in percent and E is the γ-ray energy in kev.

Table I shows the relative intensities of the γ-lines in the spectrum of Ir^{192} from the results of Refs. 3–7.

TABLE I

Relative intensities of the lines in the spectrum of $Ir.^{192}$

E(kev)[5]	Intensities										
	our data		[3]		[4]		[5]		[6]	[7]	
205,75	0,30		0.27		0,25		0.23		—	4.35	
295.94	2,26	10.7	3.0	13,8	1,88	9.45	2,12	10,1	9.09	22.0	101.1
308.45	2.31		3.1		2,02		2,06			21.4	
316.46	6.10		7,7		5.55		5.90			57.5	
467,98	3.72		4.1		4,1		3.78		4.58	17.4	
484,75	0.34		—		0.37		0.23		—	0.64	
588,4	0.40	1.74	0.33	1,74	0,46	1.74	0.418	1.74	1.74	0.64	1.74
604.5	0.77		1.0		0.72		0.825			0.81	
612,9	0,56		0.41		0,55		0.495			0.29	

The results of Refs. 4 and 5, obtained from photo-electrons in magnetic spectrometers, and of Ref. 6, using recoil electrons in a magnetic spectrometer ("ritron"), in good accord with each other, are strongly in disagreement with the results obtained by DuMond on a crystal diffraction spectrometer.[7] As is apparent from the Table, our results, obtained with a crystal diffraction spectrometer of the DuMond type, agree with those of Refs. 3–6, carried out with magnetic spectrometers.

THE SPECTRA OF Ta^{182} AND Ta^{183}

The source used was in the form of a foil of dimensions 30 × 5 × 0.1 mm irradiated with neutrons. The overall activity of the source before the start of the measurements was 1.4 curies. The investigation has shown that besides the spectrum of Ta^{182}, the spectrum of Ta^{183}, obtained as the result of two consecutive neutron captures, Ta^{181} $(n\gamma)$ Ta^{182} $(n\gamma)$ Ta^{183}, is present.

Relative intensities for a number of lines, from the results of DuMond's group[7,8] and from our results, are shown in Table II. The ratio of the intensities of the soft and hard groups of lines from the results of Refs. 7 and 8 differ from each other markedly (approximately 3 times). Our results are closer to those of the earlier work.[7] In evaluating the reliability of the results, one should take into account the fact that our results were obtained using the same spectral sensitivity curve as was used in the investigation of the Ir^{192} spectrum (with the exception of a somewhat different value for the self-absorption) and also a much better ratio of signal to background for the group of hard lines than in the (previous) investigations[7,8] (Fig. 1).

TABLE II

Relative intensities of lines in the Spectrum of Ta^{182}

E (kev) [8]	Intensities		
	our data	[7]	[8]
152.41	13,9	12.5	35
156.37	5.85	3,98	11,5
179.36.	6.91	5,40	16
198,31	3.45	2,56	7,5
222.05	18.6	12,8	35
229.27	7.9	6.82	20
264.09	7.1	7,68	22
1122	100	100	100
1155	9.0	—	6.5
1189	59,5	44.6	45
1222 } 1231 }	136	95	145

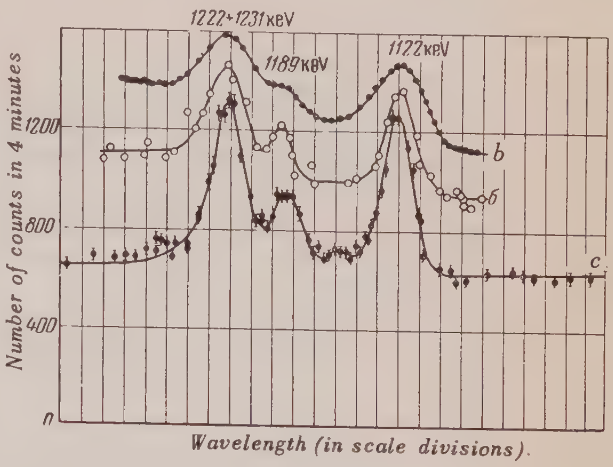

FIG. 1. Hard lines in the spectrum of Ta^{182} : *a*—from the results of the author; *b* and *c*—obtained on the DuMond spectrometer.[10]

TABLE III

Relative intensities of lines in the Spectrum of Ta^{183}

E (kev) [8]	Intensities	
	our data	[8]
144,12	10.7	8.5
160,53	11.9	10.5
161,36	33,6	31
162.33	16,5	16,5
208.81	1.8	2,6
209.87	16.0	16.5
244.26	29,7	34
246.05	100	100
291,71	14,8	20
313.03	24,8	30
354.04	39.1	40

Relative intensities of a number of lines in the spectrum of Ta^{183} from the results of Ref. 8 and from our results are displayed in Table III. Our results were obtained by using the same spectral sensitivity curves as in the cases of Ir^{192} and Ta^{182}. The resolving power of the spectrometer in the work of DuMond's group[8] was approximately twice as poor as in our work ($\delta = 3.10^{-3}\ E$). This last circumstance is important since groups of closely spaced lines appear in the spectrum (Fig. 2) and it would be necessary to use decomposition into components with a lower resolving power. The half

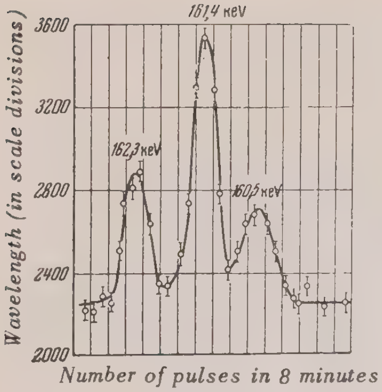

FIG. 2. Group of closely spaced lines in the spectrum of Ta^{183}

life of Ta^{183} was measured by us from the decrease in intensity of the most intense line in the spectrum with 246 -kev energy. The value of 5.0 ± 0.4 days found by us is in good agreement with earlier published results (5.2 days [8] and 5.3 days[9]).

---

[1] P. I. Lukirskii and O. I. Sumbaev, Izv. Akad. Nauk SSSR Ser. Fiz. 20, 903 (1956).

[2] Link, West and DuMond, Phys. Rev. 77, 475 (1950).

[3] Bashilov, Anton'eva and Dzhelepov, Izv. Akad. Nauk SSSR Ser. Fiz. 16, 264 (1952).

[4] M. W. Johns and S. V. Nablo, Phys. Rev. 96, 1599 (1954).

[5] Baggerly, Marmier, Boehm and DuMond, Phys. Rev. 100, 1364 (1955).

[6] Glazunov, Dzhelepov and Khol'nov, Iszv. Akad. Nauk SSSR Ser. Fiz. 19, 294 (1955).

[7] Muller, Hoyt, Klein and DuMond, Phys. Rev. 88, 775 (1952).

[8] Murray, Boehm, Marmier and DuMond, Phys. Rev. 97, 1007 (1955).

[9] E. der Mateosian, Phys. Rev. 97, 1023 (1955).

[10] J. W. M. DuMond, *Beta and Gamma-Ray Spectroscopy*. Edited by Kai Siegban (1955) (Intersoience Publishers Inc., New York; p. 126).

Translated by F. Ajzenberg-Selove
54

SOVIET PHYSICS JETP VOLUME 5, NUMBER 2 SEPTEMBER, 1957

Structure of the Periphery of Extensive Atmospheric Cosmic Ray Showers

IU. N. ANTONOV, IU. N. VAVILOV, G. T. ZATSEPIN,
A. A. KUTUZOV, IU. V. SKVORTSOV, G. B. KHRISTIANSEN
P. N. Lebedev Physical Institute, Academy of Sciences, USSR

(Submitted to JETP editor August 14, 1956)
J. Exptl. Theoret. Phys. (U.S.S.R.) 32, 227–240 (February, 1957)

An investigation of the lateral distribution of various components of extensive showers at their periphery (200–800 *m* from the axis) has been carried out. The data on the lateral distribution indicate that the contribution of the shower periphery to the total shower particle flux is significant.

The lateral distribution of the electron component at the periphery can be explained by means of the theory of multiple Coulomb scattering. Coulomb scattering also plays an important role in the divergence of the penetrating particles (μ-mesons); however the angles of emission in the elementary events of nuclear cascade processes of $\pi^{\pm}$-mesons which give rise to μ-mesons can apparently also lead to this type of divergence of μ-mesons.

An investigation of the intensity of the primary cosmic radiation at very high energies (10^{16} – 10^{17} ev) was also carried out.

A DETAILED investigation of the peripheral regions of extensive atmospheric showers is of considerable interest from the point of view of elucidating the qualitative characteristic features of the nuclear-cascade process which forms the foundation of the development of the shower. At the same time such an investigation also turns out to be necessary for the determination both of the total number of particles in the shower and of the ratios of the various components of the shower at any given depth of the atmosphere.

For the investigation of the periphery of showers, experimental arrangements are used involving counter systems situated at large distances D from each other which lead to a very large effective area of the recording system (of order D^2). This enables us to investigate the intensity of the primary cosmic radiation for ultra-high energies.

Up until now only a relatively small number of papers[1–5] has been published devoted to the study of the periphery of extensive atmospheric showers.

The majority of these papers (with the exception of that of Eidus et al.[5] describe work carried out by not very modern methods (the method of the correlation curve) which yield only qualitative results.[6]

In 1948 experiments were carried out in the Pamir[3] to determine the extent of the spatial distribution of the penetrating particles in extensive showers. Since these experiments were not published we shall describe them briefly.

Three groups of counters, each of 0.4 m^2 in area, were placed at a distance of approximately 2 m from each other and were separately screened be lead filters 22 cm thick. The number of coincidences between these three groups was determined.*

At the same time the number of coincidences was determined between this system of counter and either a group of counters shielded by lead or an uncovered counter of small area situated nearby.

We present below the experimental data:

	$C_3(\Sigma\Sigma\Sigma)$	$C_4(\Sigma\Sigma\Sigma\Sigma)$	$C_4(\Sigma\Sigma\Sigma, \sigma)$
Number of coincidences	119	32	20
Time of measurement (in hours)	18	8	10

$\Sigma = 0.4\ m^2$ $\sigma = 0.01\ m^2$

The counters of area Σ are screened by 22 cm of Pb. The counter of area σ is uncovered.

From these data the mean flux density penetrating particles reaching the screened counters was determined, and also the mean total flux density of charged particles over the uncovered counter. The ratio of these densities turned out to be equal to 0.06 for the central regions of the shower instead of the value 0.01 found in earlier investigations.[7,8]

This result was naturally interpreted as a slower rate of falling off from the core towards the periphery of the flux densities of penetrating particles as compared to the flux densities of electrons.

Further fluxes of penetrating particles were observed over distances up to 500 m from the shower core. We present below the data on the number of coincidences between groups of counters for various distances D between them both with screening (upper line) and without it:

	$D = 2\ m$	$D = 500\ m$
$C_4(0.4, \overline{08}; 0.4, \overline{08})$, hour^{-1}	(32.4 ± 2.2)	(0.52 ± 0.11)
$C_4(0.4, 08; 0.4, 08)$ hour^{-1}	(1892 ± 43)	$(3,64 \pm 0.54)$

These data showed that at the periphery of the shower, the flux density of penetrating particles falls off more slowly than the flux density of all charged particles.

In order to make a detailed quantitative study of the showers, a new method was used for the first time during the summer and fall of 1950 and 1951 by participants in the Pamir expedition of the Academy of Sciences, USSR at an altitude of 3860 m above sea level. By means of hodoscopic arrangements, the flux densities of all charged particles and of penetrating particles separately were simultaneously recorded at several stations in the observation plane (the method of correlated hodoscopes).

DESCRIPTION OF THE APPARATUS AND THE EXPERIMENTAL METHOD

The apparatus was in the form of a hodoscopic system consisting of several (from 3 to 5) hodoscopic stations operating in correlation when traversed by an extensive atmospheric shower. The system is shown in Fig. 1 where D = 1000 m and d = 600 m.

At hodoscopic station *3*, in addition to an indicator of flux densities, there was also placed a detector of penetrating particles which at the same time had sufficient sensitivity to detect particles from nuclear disintegrations. A cross-section of the detector is given* in Fig. 2. Such a hodoscopic system recorded showers which gave coincidences between 6 groups of counters each 0.8 m^2 in area, half of which (3 groups) was situated at station *1* while the other half was situated at station *3*.

---

*According to the data obtained in the present work, such coincidences are produced principally by showers whose cores lie at distances of the order of several hundred meters from the experimental setup.

The possibility of measuring the particle flux density at each of the stations over a wide range of densities was provided by using a set of hodoscopic counters of three different areas $\sigma = 330$, 100, 18 cm.[2] The use of 24 counters of a given area enables one to determine densities with an accuracy of the order of 30%.

In the Table below we present data on the number and the areas of the counters at the different stations.

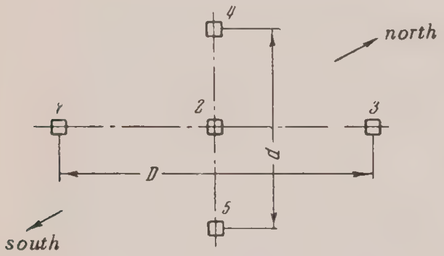

FIG. 1. Plan of the experimental arrangement. 1,2,3, 4,5, are the hodoscopic stations. The distances are $D = 1000$ m and $d = 600$ m.

At each hodoscopic station the hodoscopic counters were placed in a horizontal plane. The axes of all the counters in the whole hodoscopic system were oriented in the same direction parallel to the line 1–2–3.

The distance between the counters at any hodoscopic station was not less than half the diameter of these counters. As the analysis of the obtained data shows,[9] such a distance is quite sufficient to avoid distortions in the measurement of particle flux densities which are due to the presence at the periphery of the shower of a relatively large number of diffusely scattered particles.

Counter area, cm^2	Station number				
	1	*2*	*3*	*4*	*5*
330	72	48	$72+\overline{60}$	48	48
100	24	24	24	24	24
18		24			

The whole system was controlled in the following manner. At each of stations *1* and *3*, triple coincidence circuits were placed, into each channel of which were connected 24 counters of total area 0.8 m^2 (which were at the same time also connected to the hodoscope channels).

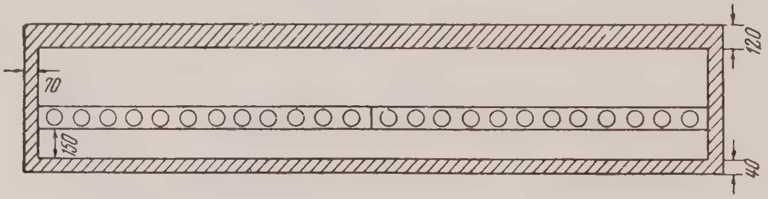

FIG. 2. Cross-section of the penetrating particle detector. The screening material is lead. The dimensions are given in mm. The screening of the counters at the ends is the same as at the sides.

Whenever a triple coincidence took place, each circuit produced a shaped pulse at its output. Such pulses from stations *1* and *3* were transmitted along a high frequency cable to station *2* where a two-channel coincidence circuit recorded sixfold coincidences. Whenever sixfold coincidences occurred, the two-channel circuit produced a shaped pulse which was sent out along several cables to all the hodoscopic stations including *1* and *3*. This pulse triggered the circuit controlling the hodoscope which emitted a controlling pulse to all the hodoscopic cells and which activated the photographic recording system.

---

*Next to the penetrating particle detector there was placed a group of 36 counters of dimensions $60 \times 550\,\text{mm}^2$ screened from above by 4 cm of Pb. On the basis of data on the flux densities of the particles in air, under 4 and under 12 cm of Pb (in the penetrating particle detector), the ratio of electron density under 4 cm of Pb to electron density in air was determined. This ratio turned out to be equal to 0.3 over the whole range of distances from the shower cores investigated by us. From this ratio we computed that the electron flux density under 12 cm of Pb must amount to 5×10^{-3} of their flux density in air. Since over the range of distances from the shower cores investigated by us the fraction of penetrating particles has a value of 0.1 or more (see the Section "Results" below) we may neglect the contribution due to electrons under 12 cm of Pb.

The resolving time for the triple coincidence circuits was chosen as 3 microseconds. This, in particular, made allowance for the possible retardation of some particles with respect to others at the periphery of the shower.

The two-channel coincidence circuit which recorded the coincidence of pulses arriving from stations *1* and *3* had a resolving time $\tau = 5 \times 10^{-6}$ sec which guaranteed a high efficiency of recording all showers, including oblique ones, which caused the firing of counters in each of the six controlling groups. It is obvious that in order to record oblique showers it is necessary that τ should be approximately given by $\sim D/c = 3.3 \times 10^{-6}$ sec, where c is the velocity of light. The number of sixfold coincidences was equal to 0.4 pulses per hour.

The additional hodoscopic stations 2,4,5 easily enabled us to differentiate the true sixfold coincidences produced by the passage of a single shower consisting of a large number of particles from accidental coincidences which are primarily due to the passage of two independent showers containing a small number of particles through stations *1* and *3*. With the circuit parameters chosen by us, the relative number of accidental sixfold coincidences* amounted to 20%.

The hodoscopes in the present experiment consisted of self-quenching counters of different dimensions (filled with a mixture of 70% argon and 30% ethylene at a pressure $p = 100$ mm of Hg) connected to hodoscopic cells of type GK–3.[10]

The inefficiency of the hodoscope as a whole was primarily determined by the inefficiency associated with the dead time of the counters connected to the hodoscope.

The resolving time of the hodoscopic cells had an average value of 30 microseconds with values for individual cells scattered between 10 and 40 microseconds. Such a resolving time guaranteed reliable operation of all the hodoscopic cells in spite of the appreciable (up to 5×10^{-6} sec) possible delays of the controlling pulse with respect to pulses from the counters (for example, at hodoscopic stations situated at a distance from the central station *2*). On the other hand, such a resolving time gives not more than one accidental firing of the hodoscopic cell for each 1000 controlling pulses, which is (by a large factor) less than the frequency of firing of the cells due to particle fluxes even in the least energetic extensive atmospheric showers which are still to a noticeable extent registered by the apparatus.**

The experimental setup described above enabled us to determine the spatial distribution of all the charged particles and separately of the penetrating particles. It is evident that a complete solution of this problem requires the knowledge of the individual characteristics of the shower, i.e., the position of the core of each shower and the number of particles in it. In the most highly developed variant of the method of correlated hodoscopes[11] where the number of stations containing indicators of density is large the problem of determining the individual characteristics is dealt with separately from the problem of finding the spatial distribution. For the experimental setup under discussion these two problems turn out to be inseparable.

Let us consider the specific solution of these two problems in two cases: *a*) the hodoscopic system consists of three stations containing density indicators; *b*) the hodoscopic system consists of five such stations.

a) We denote by N the total number of particles in the shower and by $\rho\ (r) = kNf\ (r)$ the function giving the spatial distribution of the shower particles.*** Let ρ_1, ρ_2, ρ_3 be the particle flux densities observed in a given shower at stations 1,2,3; and let r_1, r_2, r_3 be the distances from the shower core to stations 1,2,3.

Then on the basis of this notation and of Fig. 1, and also making use of the axial symmetry of the spatial distribution function of the shower particles, we can write the following system of equations relating the unknown quantities r_1, r_2, r_3, kN and the unknown function $f\ (r)$ to the quantities ρ_1, ρ_2, ρ_3 and the apparatus geometry

$$\rho_i = kNf\,(r_i)\ \ (i = 1,\ 2,\ 3); \tag{1}$$

$$D^2\quad 2 = r_1^2 + r_3^2 - 2r_2^2.$$

It is seen that this system of equations cannot be solved simultaneously with respect to r_1, r_2, r_3, kN and also with respect to $f(r)$. The function $f\ (r)$ must be found on the basis of additional data.

---

*The number of such coincidences increases as $\sigma^{2\varkappa}$, where $\varkappa = 1.5$, and for areas of the order of 1 m^2 attains values comparable with the number of true coincidences which increases as σ^{2-1}.

** In view of the large number of different elements in the experimental setup (600 counters were used in the investigation, of which 144 were used for the control circuit, and 600 hodoscopic cells GK–3 were also employed) particular attention was paid to monitoring the operation of the apparatus. All questions concerning the monitoring of the apparatus are dealt with in Khristiansen's thesis.[9]

***k is a constant factor (see below).

Such additional data may be obtained if we consider the characteristics not of an individual shower but of the totality of showers recorded by the apparatus. Such characteristics are for example the spectra of particle densities at stations 1,2,3.

The above integral characteristics are sensitive only to the general character of the behavior of the spatial distribution function, since they are obtained by integrating the function $f(r)$ within certain limits (see below). Taking into account the results of the analysis of the correlation curve carried out by Skobel'tsyn,[12] it is useful to represent the dependence on r in the form $f(r) = r^{-n}$, where n is the parameter to be determined.

The quantity most sensitive to the value of n turns out to be the spectrum of particle flux densities at station *2* (see Ref. 9). This spectrum can be calculated theoretically for a given value of n and for a given form of the shower spectrum with respect to the number of particles $F(>N) \sim N^{-\varkappa}$. If $\varkappa$ is determined in addition, then the theoretical characteristics obtained in this way may be compared with the corresponding experimental characteristics and from this one can determine the desired parameter n for the function $\rho(r) \sim 1/r^n$.

The solution of the problem of the individual shower characteristics for $\rho(r) = kN/r^n$ has the following form:

$$r_1 = (D/\sqrt{2})\,[1 + (\rho_1/\rho_3)^{2/n} - 2(\rho_1/\rho_2)^{2/n}]^{-1/2} \text{etc.}$$

$$kN = (D^n/2^{n/2})\,[(1/\rho_1)^{2/n} + (1/\rho_3)^{2/n} - 2(1/\rho_2)^{2/n}]^{-n/2}. \qquad (2)$$

b) Using the same notation, we can write the following equations which relate the individual shower characteristics and the spatial distribution function to the geometry of the apparatus and the particle flux densities produced over stations 1,2,3,4,5 (see Fig. 1)

$$\rho_i = kNf(r_i) \quad (i = 1 \ldots 5) \qquad (3)$$

$$D^2/2 = r_1^2 + r_3^2 - 2r_2^2,$$

$$d^2/2 = r_4^2 + r_5^2 - 2r_2^2.$$

We see that in this case one could formulate the problem of finding the spatial distribution function in a form which would depend on two parameters for each individual shower. In such a case, the above system of equations would enable us to obtain an analytic solution of the above problem.

However, such a solution of the problem for an individual shower in the case when the number of hodoscopic stations is small (as is the case in our arrangement) is not worth while for the following reasons. In each shower we obtain information on densities at several distances from the core. Thus the parameters of the desired distribution function will in each individual case be determined by the accidental combination of distances from the core selected in a given shower , and therefore will not give an overall picture of the spatial distribution function. This leads to the necessity of a statistical approach to the problem.*

The possibilities of applying the new method are due to our being able to identify each recorded shower in two independent ways, by utilizing data on observed flux densities of shower particles at all five stations.

We restrict ourselves to finding the spatial distribution function in the form $1/r^n$. Then for each recorded shower, Eq. (3) leads to two sets of values characterizing the number of particles and the position of the shower core

$$kN_{\rm I} = (D^n/2^{n/2})\,[(1/\rho_1)^{2/n} + (1/\rho_3)^{2/n} - 2(1/\rho_2)^{2/n}]^{-n/2}; \qquad (4)$$

$$kN_{\rm II} = (d^n/2^{n/2})\,[(1/\rho_4)^{2/n} + (1/\rho_5)^{2/n} - 2(1/\rho_2)^{2/n}]^{-n/2};$$

$$r_{2\rm I} = (D/\sqrt{2})\,[(\rho_2/\rho_1)^{2/n} + (\rho_2/\rho_3)^{2/n} - 2]^{-1/2};$$

$$r_{2\rm II} = (d/\sqrt{2})\,[(\rho_2/\rho_4)^{2/n} + (\rho_2/\rho_5)^{2/n} - 2]^{-1/2}.$$

On the basis of these formulas we can obtain the probability distributions for the numbers $N_{\rm I}$, $N_{\rm II}$ in each individual shower if we know the distributions of $\rho_1 \ldots \rho_5$. The index of the function n may evidently be found from the requirement of optimum overlapping of the distributions for $N_{\rm I}$ and $N_{\rm II}$, and of the simultaneous optimum overlapping of the regions I and II of the possible points struck by the core of the shower. As has been mentioned earlier, it is not worthwhile to solve this problem for an individual shower. Therefore one should examine analogous data simultaneously for a large number of showers selected according to some definite criterion (approximate number of particles in the shower or the selected range of distances to the apparatus). In this way we shall average the ratios ρ_i/ρ_k appearing in expressions (4) over the whole range of the practically continuously varying values of r. The index n may then evidently be found from the requirement of optimum overlapping of the sum of the distributions for N and also of the regions containing the points struck by the shower cores.

---

* We do not stress that the determination of the spatial distribution function for an individual shower is also impossible because of large errors in the determination of $\rho_1, \rho_2 \ldots \rho_5$.

It should be noted that an approximate identification of each recorded shower is possible on the basis of an approximate value of n (for example, from the method of integral characteristics). Therefore, by means of the method described above, it is possible to determine the spatial distribution function in the form $1/r^n$ for various ranges of N and r and in this way to obtain an idea of the dependence of n on the ranges of N and r under investigation. The method of integral characteristics does not allow one to do this.

We note in conclusion that the determination of the spatial distribution of the penetrating component from the readings of the penetrating particle detector presents no difficulties if we know the individual characteristics of each recorded shower.

RESULTS

During the entire time of the experiment (1200 hours), approximately 500 cases of sixfold coincidences were recorded from which 370 cases which were in each case due to the passing of a single extensive atmospheric shower * were selected by examining the hodoscopic photographs.

The following stations participated in the recording of these extensive atmospheric showers:

Number of showers	Stations taking part in recording
80	*1, 2, 3*
70	*1, 2, 3* and penetrating particle detector
120	*1, 2, 3, 4*
100	*1, 2, 3, 4, 5* and penetrating particle detector

On the basis of the data obtained it is possible to determine the absolute intensity of extensive atmospheric showers containing a number of particles N larger than some given number. Indeed the number of sixfold coincidences may be represented by the expression

$$C_6 \frac{}{hour} \tag{A}$$

$$= A\int_0^\infty N^{-(\varkappa+1)}\int_{s'}(1-e^{-kN/r_1^n})^3\,(1-e^{-kN/r_2^n})^3\,ds\,dN.$$

The quantity $\varkappa$ may be determined by the method of varying the areas of the counters.[13] Since the controlling counters were connected to the hodoscope at the same time, we obtained several practically independent series of measurements of the number of showers by counters of different areas, which gave the average value $\varkappa = 2.15 \pm 0.15$.

The constant A was then found by means of numerical integration over S and N. The expression for the absolute intensity of showers containing a number of particles greater than N obtained by the method described above has the form:

$$F(>N) = 1 \cdot 10^{11}\,\frac{1}{m^2 \cdot hour \cdot sterad}\,N^{-2.1}.$$

In order to investigate the structure of the periphery of the recorded showers we utilized the methods described earlier.

In order to determine the form of the spatial distribution of charged particles, we plotted the spectra of the particle flux densities for each of stations 1,2,3,4,5 on the basis of the experimental data. The transition from the direct hodoscopic data on the number of counters which had fired to the values of ρ was carried out in the usual way (see for example Ref. 5).

We compared the experimental spectra obtained by us with the spectra calculated by means of numerical integration on the basis of different assumptions with respect to n and $\varkappa$.[9] Figure 3 shows experimental spectra of the flux densities at stations 1,2,3,4,5 and the theoretically calculated spectra of the flux densities at the same stations based on different assumptions* with respect to n and $\varkappa$. As may be seen, there is good agreement between the experimental spectra of the flux densities at identical stations 1 and 3 and 4 and 5. The theoretically calculated spectra of the flux densities show a very strong dependence on n for station *2* and practically a complete lack of dependence on n for station *1* (or *3*). As may be seen from the diagram, the theoretically calculated spectra using the values $n = 3$ and $\varkappa = 2.1$ agree well with the experimental spectra both for station *2* and also for station *4* (or *5*).

Figure 4 shows the range of distances from the shower core over which the exact shape of the function is averaged in constructing the spectra of the flux densities at the various stations. Figure 5 shows a spectrum with respect to the number of particles in the shower as given by the apparatus.

---

* The remaining coincidences, with the exception of one special case, apparently represent accidental coincidences caused by the passage of two independent showers of relatively small energies.

*As calculations have shown, the assumptions made with respect to the form of ρ (r) at small distances from the shower core play no significant role.

In constructing these spectra, r and N were determined by the experimental values of ρ_i with the index having the value $n = 3$ in accordance with Eqs. (2). The constant k was found on the assumption that

$$\rho(r) = kN / r^n \qquad \text{for} \quad r > R(n-1),$$

$$\rho(r) = k_1 N e^{-r/R} r^{-1}$$

$$\text{for} \quad r < R(n-1), \; R=80 \text{ м}.$$

The curve $r^{-1} e^{-r/R}$ gives good agreement with the experimental curve of the spatial distribution of shower particles for $r < R\ (n-1)$ and goes over smoothly into the function r^{-n} *for* $r > R\,(n-1)$. From the conditions $kN/r^n = k_1\ Ne^{-r/R} r^{-1}$ for $r = R\,(n-1)$ and $N = \int_0^\infty \rho\ (r)\ 2\pi r dr$ for $n = 3$ we obtain $k = 3$.

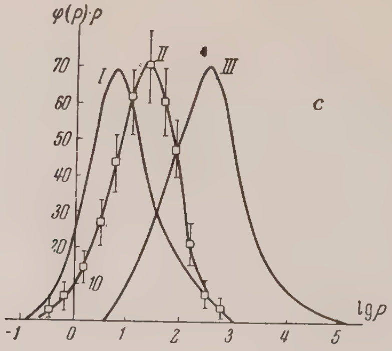

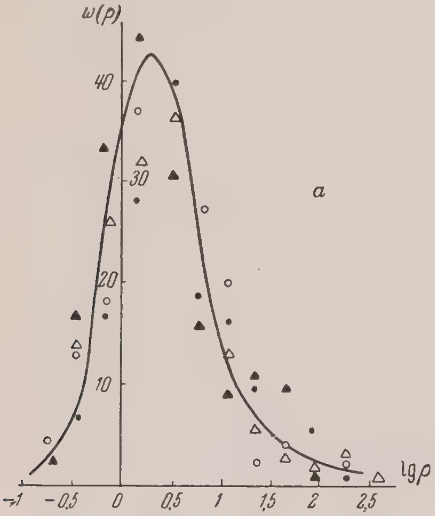

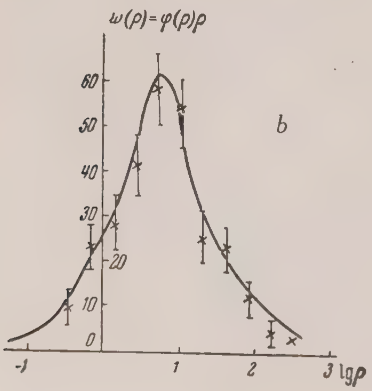

FIG. 3. Spectra of the densities of showers recorded at the different hodoscopic stations. lg ρ is plotted along the horizontal axis (ρ in units of $1/m^2$), the number of showers of density ρ in the interval ρ is plotted along the vertical axis- *a*— for stations 1,3; *b*—for stations 4,5; Δ and ▲ are the experimental points for 1950 and 1951 for station 1, O and ●—the same for station 3, ×—the same for stations 4 and 5. In Figs. 3*a* and 3*b* the solid curves are theortical curves for $n = 3$ and $\varkappa = 2.1$; in Fig. 3*c* for station 2 the curves *I, II, III* are theoretical curves for $n = 2.6$, $n = 3$ and for $\rho\ (r)$ given by the cascade theory[14] ; $\varkappa = 2.1$, are the experimental data.

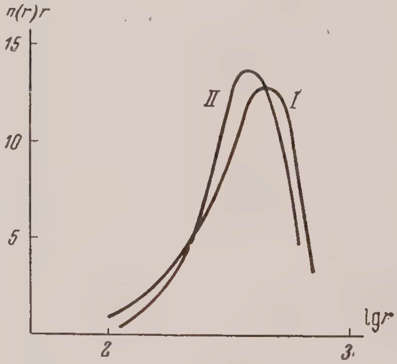

FIG. 4. Distances from the shower core to the hodoscopic stations. *I* is the distribution of distances to stations *1,2,3* ; *II*—the same for stations *1,3,4* (*5*).

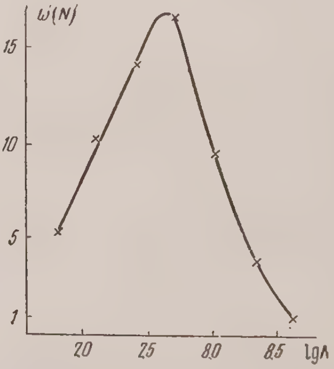

FIG. 5. The spectrum of recorded showers with respect to the number ofparticles.

In order to find the dependence of the index n on the number of particles in the shower N and on the distance r, we made use of the second method. In breaking up all the observed showers into groups belonging to different ranges of r and N preliminary values for the latter were obtained on the assumption $n = 3$. For showers belonging to each group we then determined the sums $\Sigma(N_I - N_{II})/\bar{N}$ for different values of the index n.* Here N_I is the number of particles in a shower determined on the basis of the values of ρ_1, ρ_2, ρ_3; N_{II} is the number of particles in a shower determined on the basis of ρ_4, ρ_5, ρ_2.

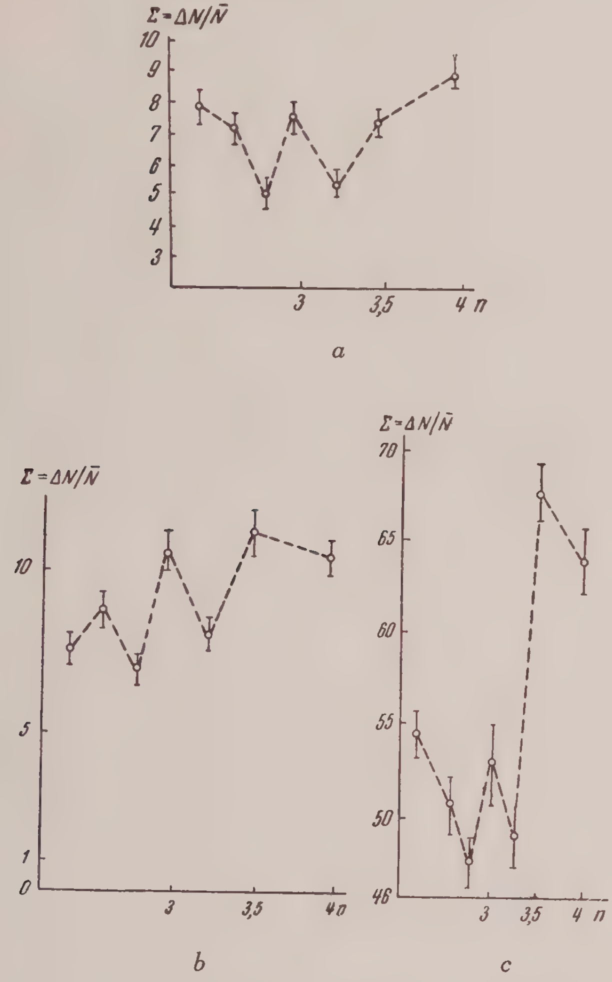

a

b

c

FIG. 6. The quantities $\Sigma(N_I - N_{II})/\bar{N}$ for showers with different ranges of r and N. a—200 $m < r <$ 600 m, $5 \times 10^6 < N < 5 \times 10^7$; b—400 $m < r <$ 800 m, $5 \times 10^6 < N < 5 \times 10^7$; c—for all the 100 showers each of which was simultaneously recorded at all five stations.

The quantity $\sum \frac{N_I - N_{II}}{\bar{N}}$, regarded as a function of n, must show the following behavior: near the value $n = n_0$ which best of all characterizes the average behavior of the function $\rho(r)$, it must have two minima, and at the value $n = n_0$ it must have a relative maximum.**

We carried out the calculation for several discrete values of n in the neighborhood of the expected value $n = 3$. Figure 6 shows some of the results of these calculations.

As may be seen from the graphs and from the results of calculations, the index n which best characterizes the average behavior of the functions is in each case close to 3, and thus (within $\Delta n = \pm 0.2$) does not depend on the ranges of r and N over which the function $\rho(r)$ is averaged.

On the basis of the individual characteristics obtained by us, we also found the spatial distribuion of the penetrating component. For the construction of this spatial distribution, the whole available range of distances was divided into a number of separate intervals, for each of which the average flux density of penetrating particles was found by using all the showers falling within this interval.

Since the distance between the shower core and the penetrating particle detector was determined with a fairly large error, we made allowance for the probability of those showers falling within the given interval which correspond to an average value $\bar{r}$ belonging to other intervals. Figure 7 shows the spatial distribution of penetrating particles in showers with an average number of particles given by $\bar{N} \approx 10^8$.

If the spatial distribution of penetrating particles is represented by means of a power law $\sim r^{-n}$ then the use of the method of least squares will yield for showers with $\bar{N} \sim 10^7$ $n = 1.6 \pm 0.3$ and for showers with $\bar{N} \sim 10^8$ $n = 2.0 \pm 0.4$.

It is also of interest to find the fraction of penetration particles at various distances from the

---

*Due to the lengthy calculations involved, we restricted ourselves to a comparison of two measurements of the number of particles, and did not compare measurements involving a change of axis.

**The existence of minima in the sum Σ near $n = n_0$ and not at $n = n_0$ is explained by the fact that the experimental values of ρ for each individual shower cannot exactly satisfy the distribution $\rho(r)$. They agree better with a distribution with an index n, which, although close to n_0, is nevertheless different from it.

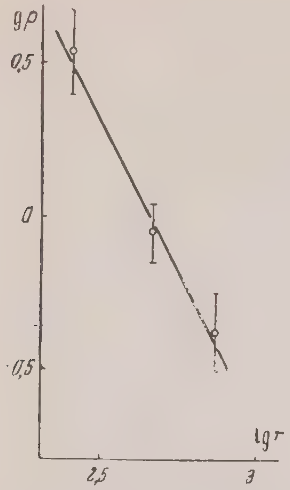

FIG. 7. The spatial distribution of penetrating particles (μ-mesons) for showers with the number of particles: $\bar{N} \approx 10.^{8}$

shower core. Since an indicator of the particle flux densities was situated at station *3*, the fraction of penetrating particles could be easily determined as the average value of the ratio of the flux density of penetrating particles to the flux density of all charged particles taken over all the showers under consideration. Figure 8 gives the fraction of penetrating particles as a function of the distance from the shower core. It may be seen that the fraction of penetrating particle increases continuously as the distance from the core increases and reaches a value $\delta = 0.4$ at distances of the order of 800 m. At the same time it should be noted that the observed value of the fraction of penetrating particles signifies that in addition to μ-mesons and electrons in equilibrium with them, a considerable contribution to the flux density of charged particles up to distances of the order of 800 m is made by electrons of origin different from those which are in equilibrium with the μ-mesons. Figure 8 also gives for comparison the data of Eidus et al.[5]

The analysis of hodoscopic photographs obtained for the penetrating-particle detector shows that group firings of neighboring counters situated under a lead screen are extremely rare. The frequency of firings of two neighboring counters is in good agreement with the theoretically expected effect due to δ-electrons. At the same time, we observed three cases (in the total number of 100 investigated showers) in which more than three neighboring counters fired simultaneously. However, all these cases corresponded in general to a large density of penetrating particles (showers with a large N and a relatively small r). Thus the group firings in these cases may be explained by the large density of penetrating particles and there is no need to suppose that they are caused by particles coming from nuclear disintegrations.

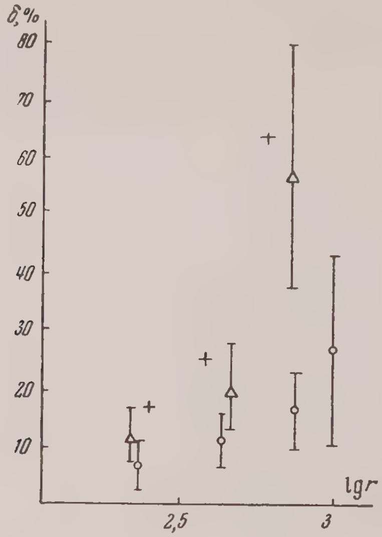

FIG. 8. The ratio of the number of penetrating particles (μ-mesons) to the number of all charged particles at different distances from the shower core. Δ—for showers with $N = 10^7$; O— for showers with $N = 10^8$; +— data for Ref. 5 for showers with $N \sim 10^7$ (at sea-level).

DISCUSSION OF RESULTS

The relatively slow falling off of the flux densities of all charged particles ($\sim 1/r^3$), and particularly of the penetrating particles ($\sim 1/r^2$) at the periphery of the shower, points to the important contribution of the periphery to the total number of shower particles and particularly to the number of penetrating particles in it.

Making use of the present data, and also of the data of Refs. 11 and 15, we can construct curves which characterize the contribution of the different parts of the shower situated at different distances from its core to the total number of shower particles. Such curves are given in Fig. 9. The fraction of penetrating particles in the hole shower (including its periphery) obtained from these curves is not less than 5%, which exceeds by severalfold the previous estimates[15] of this quantity for mountain altitudes.

At the same time the slow falling off of the flux densities of shower particles at the periphery shows that a study of the periphery is absolutely essential for the correct investigation of the problem of the spatial divergence of particles in a nuclear-cascade process. The spatial divergence

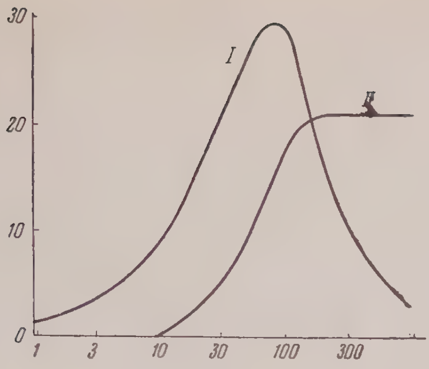

FIG. 9. Contribution of the different parts of the shower to the total number of shower particles of different kinds: *I*—for electrons, *II*—for μ-mesons. The density of shower particles multiplied by r^2 is plotted along the vertical axis, the distance r from the shower core in meters is plotted along the horizontal axis.

of charged particles in a shower may be due to the following causes: 1) the emission at relatively large angles in individual nuclear interaction events either of the directly recorded particles or of their predecessors ($\pi^{\pm}$-mesons if we are considering μ-mesons); 2) Coulomb scattering of particles by nuclei of atoms of air; 3) their deflection under the influence of the earth's magnetic field. These various causes play different roles in the divergence of shower particles of different kinds.

Let us first examine this question for that part of the electron component at the periphery of the shower which is not caused by the observed flux of μ-mesons, i.e., which is not of "equilibrium" nature. The spatial distribution of this "non-equilibrium" electron component can evidently be obtained from the distributions of all the charged particles and of the penetrating particles

$$\rho_{el}(r) \sim \frac{1}{r^3} - k\frac{1}{r^2},$$

where k is a coefficient which takes into account the flux density of μ-mesons and of electrons in equilibrium with them. Figure 10 shows the spatial distribution of the electrons. The coefficient k has been calculated for a μ-meson energy equal to 10^9 ev.*

These electrons are the cascade descendants of γ-quanta originating in the decay of π^0-mesons generated in nuclear collisions. In our further discussion of the spatial distribution of electrons, we shall have in mind only this fraction of the electrons. As is well known, electrons in electron-photon avalanches undergo considerable scattering by charged nuclei of atoms of air. Their spatial distribution at large distances from the core originating in this manner apparently has been calculated most accurately in recent papers by Nishimura and Kamata.[16]

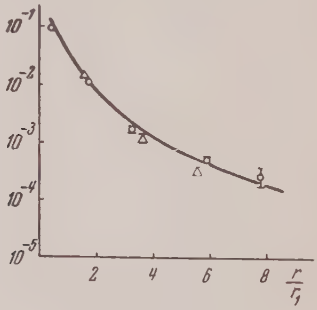

FIG. 10. The spatial distribution of the electron component which is not in equilibrium with the penetrating particles (μ-mesons) at the periphery of the shower—Δ—experimental points for $N = 10,^7$ O—for $N = 10.^8$ The solid curve is the theoretical spatial distribution of electrons in an electron-photon avalanche with $S = 1.0$ (Nishimura and Kamata). The distance from the shower core expressed in characteristic units of length r_1 (at the altitude of 3860 m $r_1 = 125$ m) is plotted along the horizontal axis. The density of non-equilibrium electrons multiplied by r/r_1 is plotted along the vertical axis.

According to these papers the spatial distribution of electrons at the periphery of the shower depends in an essential way on their energy spectrum in the avalanche, and may become quite flat for $S > 1$.

We shall compare the spatial distribution of electrons obtained by us with their distribution in an electron-photon avalanche as calculated by Nishimura and Kamata.[16] Figure 10 shows a theoretical curve[16] which corresponds to the cascade theory parameter $S = 1.0$. A good agreement is observed between the experimental and the theoretical curves over the whole range of distances investigated by us.* We note that the experimental data do not disagree with the theoretical curve for $S = 1.2$. One should thus conclude that Coulomb scattering of electrons is by itself sufficient to explain their considerable spatial divergence. The angular divergence of electron avalanches associated with the angles of emission of π°-mesons in the elementary events of the nuclear cascade process in this case plays a relatively insignificant role.* We shall now consider the spatial divergence of penetrating particles, (μ-mesons) brought about by Coulomb scattering. It depends markedly both on their energy spectrum and on the altitude of the point at which they are produced, An approximate estimate shows that as a result of multiple scattering μ-mesons may reach the periphery of the shower.

---

* The value of this coefficient depends very little on the μ-meson energy. We used the average energy of the μ-mesons in a shower as taken from Cocconi et al.[15]

*It should be noted that in accordance with Ref. 16, Fig. 10 shows the spatial distribution of electrons of total energy $E > m_e c,^2$ while in the experiment a dense substance (counter wall, roof of the building) amounting to 2 gm/cm^2 is situated above the sensitive volume of the counter, which corresponds to the absorption of electrons of energy < 7 mev. However, since the value of Z for the dense substance is close to that for air the production of electrons by photons compensates for their absorption.

Indeed, according to the theory of multiple scattering of charged particles the mean square divergence of particles of energy E which have traversed in the atmosphere a path from the altitude $h_0 + h$ to the altitude h_0 is given, without taking ionization losses into account, by:

$$\overline{r^2(E)} = \int_0^h h'^2 \left(\frac{E_s}{E}\right)^2 \frac{dh'}{L_0 e^{\alpha h'}}, \qquad \text{(B)}$$

where α is the coefficient in the barometric formula, $\alpha = 1/8000\ m^{-2}$, L_0 is the value of one radiation length in meters at the altitude h_0, $E_s = 21$ mev.

We substitute into the above formula the average μ-meson energy $E = 10^9$ ev according to Cocconi et al,[15] and their mean altitude of origin of 10,000 m above sea-level according to Bassi et al.[18] Then, for observations carried out at an altitude of 3860 m ($h = 60 \times 10^3$ m and $L_0 = 410$ m), we obtain $\sqrt{\overline{r^2}} = 200$ m. Concerning the third reason for the divergence of charged shower particles—the earth's magnetic field— it is found to give a deflection

$$r_M(E) = \int_0^H h \frac{dh}{\rho}, \text{ where } \rho = \frac{1.1 \cdot 10^{-2}}{\cos\lambda} E; \lambda = 30^\circ{}^{**}.$$

On substituting the above values we obtain $r_M = 150\ m$. We should thus conclude that the Coulomb scattering of μ-mesons and the earth's magnetic field have a pronounced effect on the spatial distribution of μ-mesons. At the same time, it can be easily seen that these causes evidently cannot completely explain the observed divergence of μ-mesons.

Indeed, on the basis of the experimental data obtained by us and of the data of Vavilov et al[11] we can evaluate:

$$\overline{r^2} = \int r^2 \rho_\mu(r)\, 2\pi r dr \Big/ \int \rho_\mu(r)\, 2\pi r\, dr.$$

Such an evaluation gives $\sqrt{\overline{r^2}} > 400\ m.$***

This forces us to conclude that the angular dedivergence of $\pi^\pm$-mesons born in elementary events of the nuclear-cascade process also plays a significant role in determining the spatial divergence of μ-mesons.

CONCLUSIONS

In the present work we have carried out a quantitative study of the different components of an extensive atmospheric shower at large distances from its core (200–800 m).

1. The part of the shower which we have studied consists of an electron-photon and a penetrating (apparently a μ-meson) component.

The relative role played by the penetrating component increases considerably as the distance from the shower core increases and at a distance of $r = 800$ m the flux densities of penetrating particles and of electrons become the same. According to Eidus et al,[5] a similar situation is also observed at sea-level.

2. The spatial distribution of the total flux of electrons and penetrating particles is given by $\rho(r) \sim 1/r,^n$ with $n = 3.0 \pm 0.2$.

The spatial distribution of the flux of penetrating particles is given by $\rho(r) \sim 1/r^n$ with $n \approx 2.0$.

3. The relatively slow falling off of the flux densities of shower particles leads to the shower periphery playing an important role in the overall balance of the flux of shower particles. For penetrating particles, this role even becomes the dominant one. Thus a quantitative investigation of the shower cannot be restricted to the study of its central regions as is usually done (see also Ref. 5).

4. The mechanism for the transfer to the periphery of the shower of electrons which are not in equilibrium with μ-mesons is accounted for by the Coulomb scattering of these electrons by nuclei of atoms of air.

5. The transfer to the periphery of the shower of μ-mesons occurs both by means of Coulomb scattering, and apparently also as a result of the large angles of emission in elementary events of the nuclear cascade process of $\pi^\pm$-mesons giving rise

---

* The divergence associated with the influence of the earth's magnetic field does not play any significant role for electrons in electron-photon avalanches as is shown by Cocconi.[17]

**The value of the geomagnetic latitude of the station at which our measurements were made.

***Since the shape of $\rho_\mu(r)$ is known experimentally only up to distances ~ 800 m it is clear that we can give only a minimum estimate.

to these μ-mesons.

In the present work we have also obtained data on the intensity of primary cosmic ray particles of ultra high energies of $10^{16}-10^{17}$ ev by observing extensive atmospheric showers of corresponding energies (with the numbers of particles given by $N = 10^7 - 10^8$): the absolute number of showers with the number of particles $> N$ is given by the expression $F\,(>N) = AN,^{-\varkappa}$ where $A = 1 \times 10^{11}$ ($1/m^2$ hour); the index $\varkappa$ of the integrated energy spectrum of primary particles in the energy range $10^{16}-10^{17}$ ev does not exceed 2.15.

In conclusion, the authors wish to express their deep gratitude to N. A. Dobrotin for his assistance in this work, and for valuable advice, and to S. B. Vernov for participating in the discussion of results, and also to D. Parfanovich, Iu. Anishchenko, M. Kazarinova, Iu. Prokhorov, M. Khachaturian, V. Sarantsev, M. Shafranov who all took part in this work in the course of carrying out the practical work for their diplomas, and to E. S. Levit.

---

[1] G. T. Zatsepin and V. V. Miller, J. Exptl. Theoret. Phys. (U.S.S.R.) 17, 939 (1947).

[2] D. M. Alekseev, Zatsepin and Morozov, Dokl. Akad. Nauk SSSR 63, 375 (1948).

[3] Zatsepin, Khristiansen, and Shuvaev, Report of the cosmic ray laboratory of the Physical Institute of the Academy of Sciences, USSR, 1948.

[4] Zatsepin, Rosental', Zakharova, Khrebet and Khristiansen, Dokl. Akad. Nauk SSSR 74, 29, 1950.

[5] L. Kh. Eidus et al., J. Exptl. Theoret. Phys. (U.S.S.R.) 22, 440, (1952).

[6] J. Blatt, Phys. Rev. 75, 1584, (1949).

[7] Zatsepin, Kuchai and Rosental', Dokl. Akad. Nauk SSSR 61, 47 (1948).

[8] Cocconi, Tongiorgi-Cocconi and Greisen, Phys. Rev. 75, 1063 (1949).

[9] G. B. Khristiansen, Thesis, Moscow, Physical Institute of the Academy of Sciences, USSR (1953).

[10] L. N. Korablev, Dokl. Akad. Nauk SSSR 69, 643(1949).

[11] Vavilov, Nikol'skii and Tukish, Dokl. Akad. Nauk SSSR 93, 233 (1953).

[12] D. V. Skobeltsyn, Dokl. Akad. Nauk SSSR 67, 45 (1949).

[13] G. T. Zatsepin, Thesis, Moscow, Physical Institute of the Academy of Sciences USSR (1950).

[14] I. Molliere. Die kosmiche Strahlung, Herausgegeben von W. Heisenberg, Berlin, Springer, (1953).

[15] Cocconi, Cocconi-Tongiorgi and Greisen, Phys. Rev. 76, 1020, (1946).

[16] L. Nishimura and K. Kamata. Progr. Theor. Phys. 262, 628 (1951). L. Nishimura and K. Kamata. Progr. of the Int. Conf. of Theor. Phys., Tokio, (1954).

[17] J. Cocconi, Phys. Rev. 93, 646; 95, 1705 (1954).

[18] Bassi, Klark and Rossi. Phys. Rev. 92, 441 (1953).

Translated by G. M. Volkoff
53

SOVIET PHYSICS JETP VOLUME 5, NUMBER 2 SEPTEMBER, 1957

Soft 15–800 kev Radiation Accompanying the Thermal Neutron Fission of Uranium

V. K. VOITOVETSKII, B. A. LEVIN, AND E. V. MARCHENKO
Institute of Atomic Energy, Academy of Sciences, USSR

(Submitted to JETP editor September 24, 1956)
J. Exptl. Theoret. Phys. (U.S.S.R.) 32, 263–268 (February, 1957)

A scintillation spectrometer investigation of the γ-rays coincident with fission has established the presence of a series of lines. It has been shown that γ-quanta having energies of 101, 119, 142, 207, 295, 360, 490, and 590 kev are emitted in fission. It is suggested that these γ-quanta are emitted by excited fragments following neutron emission. Intense radiation having a maximum at 27 kev apparently consists of the K x-rays of heavy fragments.

INTRODUCTION

THE γ-rays accompanying the thermal neutron fission of U^{235} have been the subject of a series of investigations[1–3] These studies have yielded a value for the total energy emitted in the form of γ-rays; the average number of γ-rays per fission has been determined and likewise the general character of the spectrum.

Kinsey, Hannah, and Van Patter[1] have shown that γ-rays are emitted within a time $T \leq 0.7$ microsecond following fission, and that the total γ-ray energy is 4.6 ± 1 mev. The method used in this work was not one that could give a correct result concerning the spectral distribution of the radiation and in fact contradicts later results.[2–3] The work of Rose and Wilson[2] concerned the angular distribution of the γ-rays. The experimental results suggest that at least some of the γ-quanta are emitted by the fragments. Analyzing the composition of the radiations, the authors concluded that, on the average, 6 quanta are emitted in fission with a wide energy distribution (up to 2.5 mev) and that the total energy is 5.2 ± 0.5 mev.

The data of Gambla and Francis[3] show that the radiation intensity falls exponentially with the energy. The average number per fission is less than 7.5, the total energy is less than 7.5 mev and the upper limit of the energy is approximately equal to 7 mev.

A study of the soft component (15–250 kev) of the γ-ray spectrum accompanying the thermal neutron fission of U^{235} established a presence of a series of lines.[4] The present work extends the energy region investigated up to 800 kev. It is shown that in the energy region 15–800 kev there are 8 monochromatic lines and an intense radiation having a maximum at 27 kev.

EXPERIMENTAL ARRANGEMENT

An ionization chamber with U^{235} registering fission fragments is placed in a beam of thermal neutrons (Fig. 1). The γ-rays emitted in fission are detected in a scintillation counter γ-spectrometer. A coincidence circuit and gate circuit (Fig. 2) select for amplitude analysis the pulses from the scintillation counter that are coincident with the fission fragment pulses.*

The beam of neutrons is collimated by a channel in the pile (Fig. 1). This figure also shows the distribution of the neutron flux over the chamber. The chamber is made out of thin walled aluminum. The five lower foils of the chamber carry films of uranium oxide (approximately 3 mg/cm^2). The chamber is filled with one atmosphere of argon; the working voltage is a thousand volts. The rise time of the amplified pulses from fission was $\leq 0.3\ \mu$ sec. After discrimination the shaped pulses were put into the coincidence circuit and simultaneously registered by a scalar (multiplication factor 10^4).

The spectrometer was made from a type C photo multiplier and a NaI–Tl crystal ($\phi = 29$ mm, $h = 12$ mm) with magnesium oxide reflectors. The scintillator was protected from the slow neutrons and γ-rays by a boron and lead shield. The amplified pulse from the photo multiplier was sent through the gate circuit into a 20 channel pulse height analyzer.[5] The same pulse after discrimination and shaping was sent into the coincidence circuit governing the gates. The analyzer was constructed on the principle of converting an amplitude into a delay and makes possible a pulse height analysis into 80 channels with subsequent use of 20 of them.

In order to get the characteristics and calibrate the spectrometer there were obtained pulse height analyses from γ-rays of several isotopes. The resolving power of the spectrometer for the Cs^{137}

---

*The resolving time of the coincident circuit was $2\tau = 0.4\ \mu$sec. Increasing this by a factor of 1.5 increased the number of coincidences only by 5–6%.

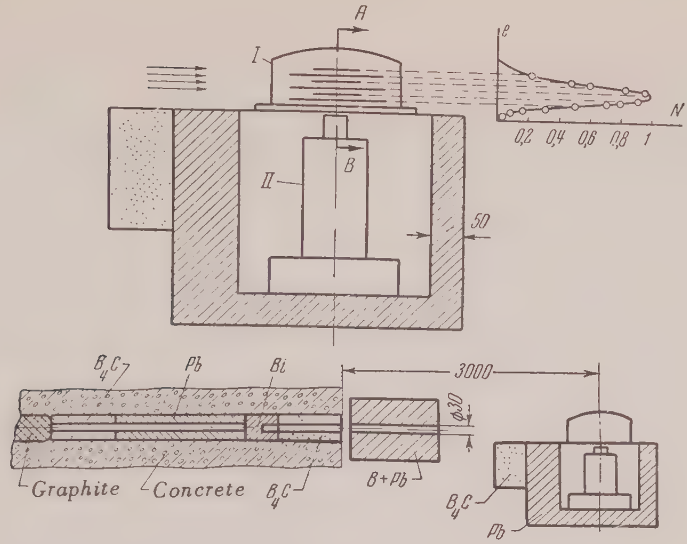

FIG. 1. *I* – Multifoil ionization chamber; *II* – Scintillation counter. Above on the right is given the distribution of neutron flux across the cut *AB*. The arrows on the left indicate the neutron direction of motion.

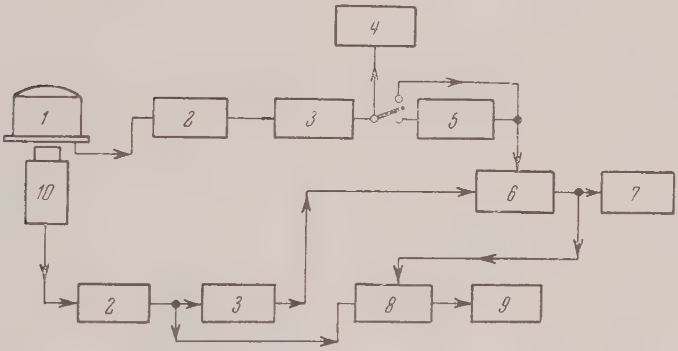

FIG. 2. Block Diagram of Electronics. *1*–Ionization chamber, *2*–Amplifier, *3*–Discriminator, *4*–Scalar (× 10^4), *5*–Delayline, *6*–Coincidence circuit, *7*–Scalar (× 64). *8*–Gate circuit, *9*–20 channel analyzer. *10*–Scintillation counter.

line (662 kev) was 8%; for the Ce^{141} line (145 kev) it was 16%. In this energy region the position of the photo-peaks is a linear function of the γ-ray energy. The stability of the spectrometer was controlled with known photo-peaks. The displacement of these photo-peaks during long measurements (8–12 hours) did not exceed 1%.

In order to check the operation of the spectrometer together with the gate circuits, the radiations coming from the uranium in the chamber were analyzed. The spectrum obtained with the chamber registering α-particles and the gate circuits governed by $\alpha-\gamma$ coincidences (Fig. 3) had the same appearance as a spectrum of γ-rays from uranium taken without coincidences.

RESULTS OF THE MEASUREMENTS

The measurements were carried out in the following fashion. Simultaneously with the amplitude analysis of the pulses from the γ-rays, the number of fissions and the number of coincidences were recorded; this allowed a normalization from one part of the work to another. The number of fissions registered per second was about 5×10^3; the number of coincidences was about 200. In order to

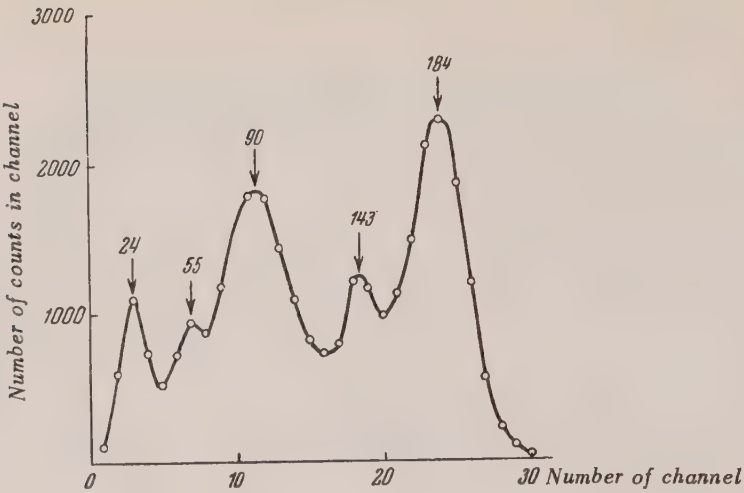

FIG. 3. The numbers on the peaks are given in kev.

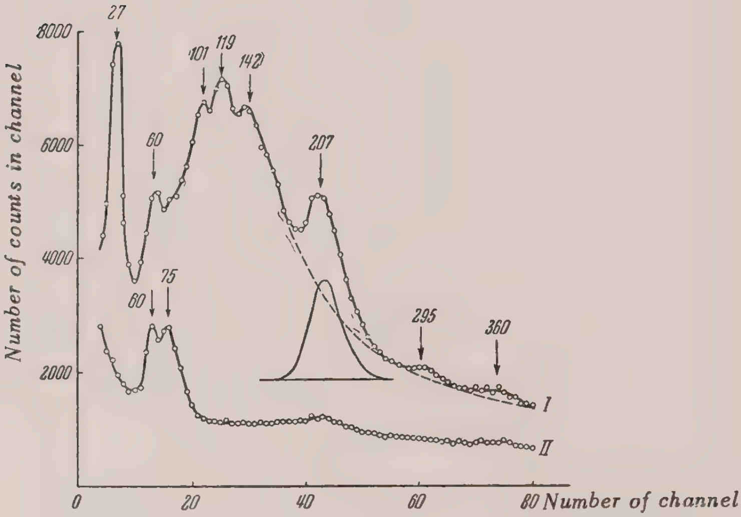

FIG. 4. The numbers on the peaks are given in kev.

determine the background of accidental coincidences the fission pulses were delayed by 0.9 μ sec. This background of accidental coincidences did not exceed 3% in any channel of the analyzer. The experimental results were completely reproducible upon numerous repetitions of the measurements.

Fig. 4 (curve 1) shows the pulse height distribution from γ-rays coincident with fission pulses and having energies between 15 and 400 kev. (5 kev per channel). The numbers have all been normalized to 10^7 fissions. The statistical errors of the measurements are 0.5 –1.5%. The photopeaks correspond to energies of 27, 60, 101, 119, 142, 207, 295 and 360 kev. The calibration points used for this region were obtained from the radiations of Hg^{203} , (279 and 71 kev) and Ce^{141} (145 and 35 kev). Some of the lines in the spectrum (60, 207 kev) may have arisen from the inelastic scattering of fission neutrons in iodine.[6]

Measurements carried out with a 5 mm sheet of lead between the chamber and the crystal made it possible to evaluate the contribution of this inelastic scattering. The spectrum obtained with the lead (Fig. 4, curve 2) does not have lines at 27, 101, 119, 142, and 295 kev and has the 360 kev line strongly absorbed. The line at 60 kev is not affected and there is present weak radiation at 207 kev. The pulse height distribution also

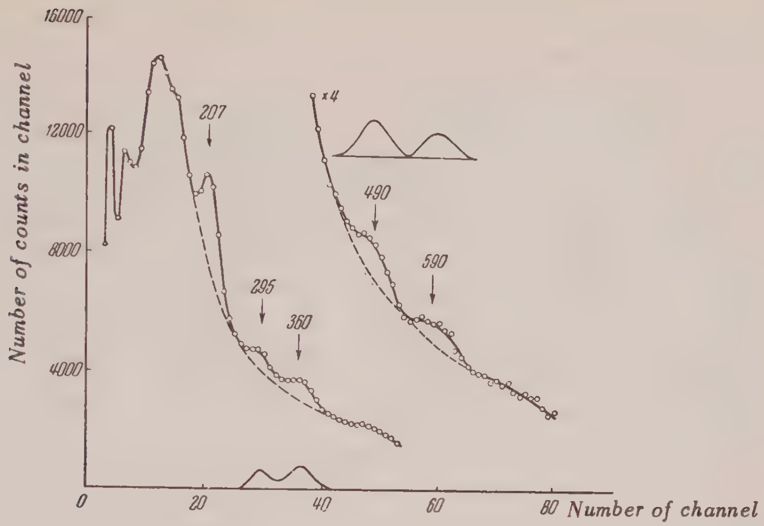

FIG. 5. The numbers on the peaks are given in kev.

shows a photo-peak from the x-rays of lead (75 kev).

The results of the experiment with the lead absorber allow us to conclude that the lines at 27, 101, 119, 142, 207, 295, and 360 kev correspond to γ-rays accompanying fission but that the lines at 60 kev and a small part of the 207 kev line are due to inelastic scattering of fission neutrons by the iodine of the crystal. A quantitative estimate of the probability of inelastic scattering agrees well with the experimental results.

The pulse height distribution in the energy region between 20 and 800 kev (10 kev per channel) shows additional photo-peaks from γ-rays having energies of 490 and 590 kev (Fig. 5; the curves are likewise normalized to 10^7 fissions). Here the calibration was made using the radiations from Cs^{137}, Hg^{203}, and Ce^{141}. Absorption measurements using 5 mm of lead (Fig. 6) (20 kev per channel) ruled out the possibility that the 490 and 590 kev peaks are due to inelastic scattering of fission neutrons by iodine (490 kev) or lead (590 kev).[6]

The data on the energies and intensities for the γ-ray lines accompanying fission are presented in the table.

The possibility of intense radiation of soft γ-rays by uranium nuclei during fission does not appear likely. The intensity of the lines in the soft part of the spectrum is comparable to the yield of fragments. It would appear that these radiations are emitted by excited fragments after neutron emission. This conclusion is supported by the results in work in Ref. 7. The energies of these soft γ-rays are characteristic of rotational levels. It may be that the residual excitation of the fragments is connected with collective motion of the nucleons.

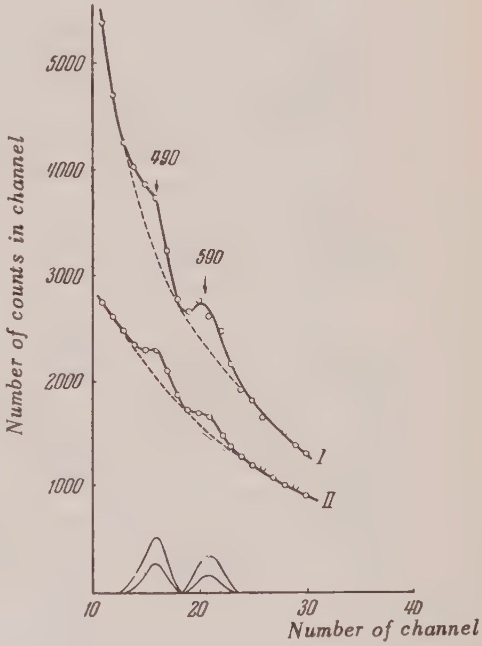

FIG. 6. I-without lead; II—with lead

The x-rays from the heavy fragments of fission lie in the region 25–30 kev. It may be assumed that the intense radiation having an energy of 27 kev is not monochromatic, but consists of the characteristic x-rays of these heavy fission fragments.

The authors are thankful to I. V. Kurchatov for his interest in the work, to B. T. Geilikman, and to V. M. Strutinskii for discussion of the results,

Energy	Intensity (quanta per fission)
27±3	0.45±0.15
101±3	—
119±3	—
142±5	—
207±5	0.107±0.052
295±5	0.026±0.020
360±10	0.085±0.050
490±10	0.071±0.037
590±15	0.101±0.047

and to G. N. Sofiev who helped in the construction of the pulse height analyzer.

---

1 Kinsey, Hanna and Van Patter, Can. J. Res. 26A, 79 (1948).

2 Progress in Nuclear Physics, II, London, 1952, pp. 150, 152.

3 R. B. Leachman, Paper presented at the International Conference on the Peaceful Uses of Atomic Energy, Geneva (1955).

4 Voitovetskii, Levin, and Marchenko, Report Institute of Atomic Energy, USSR (1955).

5 Artemenkov, Markov, Melnikov, Sofiev, Report Institute of Atomic Energy, USSR (1954).

6 R. B. Day, Paper presented at the International Conference on the Peaceful Uses of Atomic Energy, Geneva (1955).

7 Skliarevsky, Stepanov, Fomenkov, J. Exptl. Theoret. Phys. (U.S.S.R.) 32, 256 (1957); Soviet Phys. JETP 5, 220 (1957).

Translated by A. Turkevich
58

SOVIET PHYSICS JETP VOLUME 5, NUMBER 2 SEPTEMBER, 1957

Investigation of Slow Electron Emission Induced by High Energy Protons

E. S. MIRONOV AND L. M. NEMENOV
Institute of Atomic Energy, Academy of Sciences, USSR

(Submitted to JETP editor September 24, 1956)
J. Exptl. Theoret. Phys. (U.S.S.R.) 32, 269–273 (February, 1957)

An investigation has been carried out of the electron emission produced by high energy protons. The method is described. Values of the emission coefficients, γ_1 and γ_2 for aluminum and nickel in the energy range from 2 to 7.3 mev are presented.

INTRODUCTION

THE question of the interaction of positive ions with a metallic surface is not a new one. Most of the published work devoted to the dependence of the coefficient of emission γ on the energy of the impinging ions has involved relatively low energy ions. Thus for hydrogen and helium, the energy has not exceeded 400 kev[1]. Only in one investigation[2] has electron emission been observed using mercury ions having an energy of the order of 2.2 mev.

The present authors posed themselves the problem of studying the emission of electrons from thin foils both in the direction of the motion of protons (coefficient γ_1) and in the opposite direction (coefficient γ_2) At the same time it was proposed to determine the dependence of the coefficients γ_1 and γ_2 on the impinging proton energy in the interval from 2 to 7.3 mev. Aluminum and nickel were chosen to be the substances to be studied.

The source of the protons was a 1½ meter cyclotron having an external focused beam. The proton beam was obtained from hydrogen molecule ion acceleration up to approximately 14.7 mev with subsequent break-up of the molecule upon going through a thin aluminum foil. The beam of charged particles was taken to a distance of 12 m from the shielding wall of the cyclotron.

Work on measuring the beam strength of protons of the order of 7 mev showed that electron emission from the usual conducting materials amounted to 20–30% of the proton beam current. Calculations evaluating the expected magnitude of γ indicated values of the order of 30–40%. These facts determined to a certain extent the method used in the investigation.

1. METHOD OF MEASUREMENT

Fig. 1 shows the six principal methods used in measuring all the required quantities.

Method 1 is used to measure the total current,

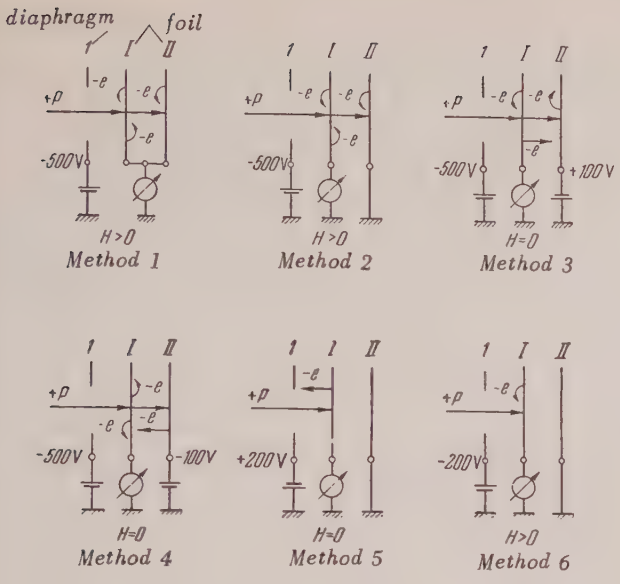

Method 1 Method 2 Method 3

Method 4 Method 5 Method 6

FIG. 1. Principal systems of measurement.

$I_1 = I_p'' + I_p''$, where I_p' is proton current entering the foil *I* and I_p'' is the proton current entering the foil *II*.

Method 2 is used to measure the current $I_2 = I_p'$ where I_p' is the proton current entering the foil *II*. The quantities measured in methods 1 and 2 are needed in order to establish the energy of the impinging protons.

Method 3 is used to measure the electron current i' from the foil *I* in the direction of motion of the proton beam.

Method 4 determines the electron current i'' from the foil *II* in the direction opposite to the proton beam motion.

Methods 5 and 6 are used to measure γ at the full energy of the proton beam. Foil *I* is chosen of such a thickness as to completely stop the proton beam.

The average energy of the incoming protons was determined by a range measurement in aluminum for which the range energy relation is known with high accuracy. Figure 2 shows schematically the arrangement used for the investigation. The fixed diaphragm *1* having a 20 × 30 mm opening defines the proton beam. Diaphragm *2* is also fixed and has a rectangular opening 25 × 35 mm in size and an insulated electrical lead for producing the necessary retarding potential. A series of metallic foils 44 × 44 mm can be placed successively into the insulated moveable frame *3*. Further on in the direction of the motion of the beam there is an insulated beam catcher *4*, into which a thick foil of the metal being studied can be placed. Before insertion of these foils they are carefully freed from grease. A special cold trap diminishes the possibility of oil vapors from the oil pumps reaching the foils. The pressure in the apparatus is of the order 1×10^{-5} mm Hg. A special clamp, not shown in the Figure, attached to the body of the apparatus makes possible the attachment of a small electromagnet for the production of a magnetic field. The main apparatus and all the parts are made from nonmagnetic materials.

All operations with the apparatus are carried out at a distance in view of the radiation hazards.

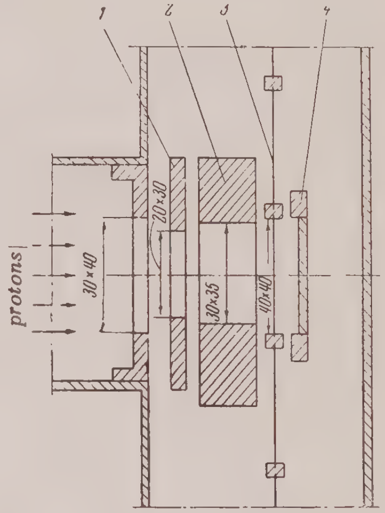

FIG. 2. Diagram of apparatus: Arrows at left indicate incoming protons.

2. ELECTRON–MEASURING APPARATUS

Figure 3 shows the electronics used in the measurements. A vacuum rectifier *2* furnishes a negative potential of 500 V with the help of a potentiometer R_{11} to the diaphragm 3. Foil *1* can be grounded by means of the switch Π_1 through one of the resistors having resistances between 5×10^4 and 10^6 Ω. The voltage drop across the resistor was measured using a direct current amplifier with a mechanical modulator. The output of the amplifier was fed into an indicating instrument.

In order to establish the sensitivity of the amplifier there was assembled an apparatus giving calibrated output which consisted of the dividers R_6, R_7, and the rectifier *3*. Using the switch Π_2 it was possible to pick out any one of the six principal schemes of measurement illustrated in Fig. 1.

The electromagnet pictured in Fig. 3 was powered from a direct current circuit through a variable resistor R_{13}. The capacitator C_4 served to remove residual magnetism. On opening the switch P_1 there starts a transient consisting of the exchange of energy between the capacitator C_4 and the inductance of the electromagnet windings. During this process the current in the magnet windings has a damped sinusoidal character. The result of this process is the complete demagnetization of the iron of the electromagnet.

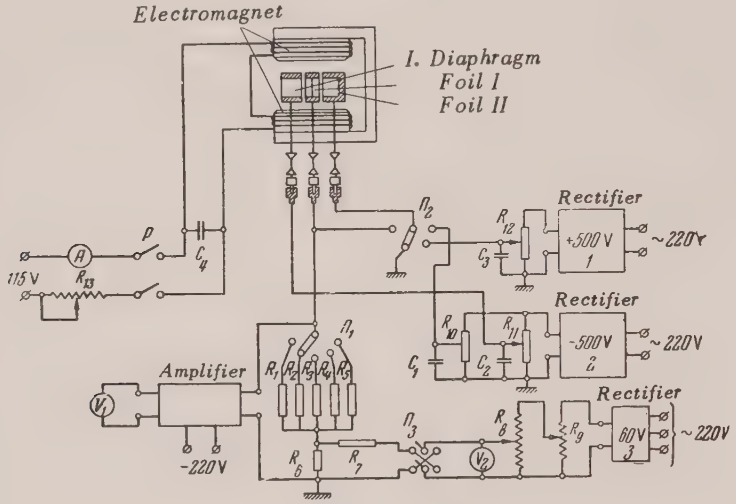

FIG. 3. Electron-measuring circuit.

3. RESULTS OF THE MEASUREMENTS

Preliminary experiments showed that even at magnetic fields H of the order of 200 Oe there was practically no electronic component to the current. In the final experiments the field had values up to 800 Oe. It was likewise shown that, in the measurement of the electronic current according to schemes 3 and 4, it was sufficient to have foil *II* at a potential of the proper sign of the order of 25 V. In practice 100 V was applied. In order to repel the electrons flying out from foil *I* in the direction opposite to the motion to the protons toward diaphragm *3*, it was sufficient to apply a potential of the order of –50 V. In practice foil *III* was placed at –500 V. The measurements were repeated three times; moreover, each measurement carried out according to schemes 2, 3, and 4 leads to a measurement of the current according to scheme 1 (the measurement of the total proton current impinging on the two foils). After each experiment the amplifier was calibrated with the generating equipment.

Figures 4 and 5 show the dependence of the coefficients γ_1 and γ_2 on the energy of the incoming protons for aluminum and nickel.* The results obtained show that, in the proton energy range from 2–7.3 mev, the coefficients of electron emission for aluminum and nickel do not differ much and change on the average from 1.8 to 0.5. The number of electrons knocked out in the beam direction is larger than the number knocked out in the direction opposite to the beam motion. This difference is observed for both aluminum and nickel and amounts to about 20%. The energy of the protons coming from the cyclotron was determined from the average range in aluminum. The accuracy of this measurement is ± 200 kev. Evaluation of the errors in measurement of the coefficients γ lead to maximum possible errors not exceeding ± 10%.

All these experiments were carried out in 1953.

In conclusion the authors thank Academician L. A. Artsimovich for discussions of the experiment and the results. At the same time, the authors take this opportunity to express their gratitude to V. I. Bernashevsky and to K. N. Petrov* who constructed the apparatus for this investigation.

---

*The range energy curve for nickel was kindly furnished us by B. V. Rybakov.

*Deceased.

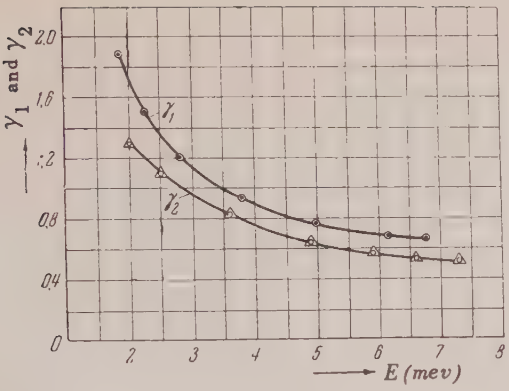

FIG. 4. Proton energy dependence of the coefficients of electron emission γ_1 and γ_2 for aluminum.

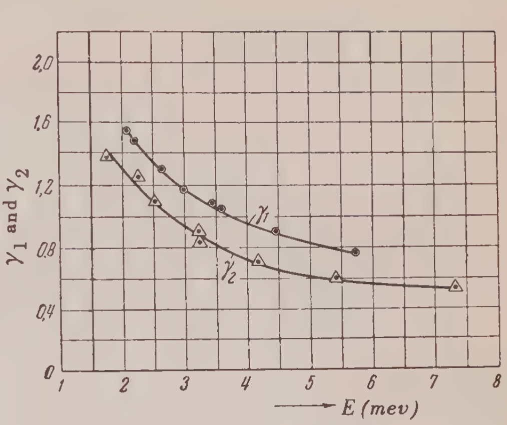

FIG. 5. Proton energy dependence of the coefficients of electron emission γ_1 and γ_2 for nickel.

---

[1] Hill, Buechner, Clark and Fisk, Phys. Rev. 55,463 (1939).

[2] A. Linford, Phys. Rev. 47, 279 (1935).

Translated by A. Turkevich
59

SOVIET PHYSICS JETP VOLUME 5, NUMBER 2 SEPTEMBER, 1957

Level Shifts in Helium. Three Body Forces

G. F. Filimonov
Moscow State University

(Submitted to JETP editor November 13, 1955)
J. Exptl. Theoret. Phys. (U.S.S.R.) 32, 311–315 (February, 1957)

A fourth order expression containing three-body forces is obtained for a two-field interaction Hamiltonian. An expression is obtained for the energy matrix element of triple collisions between two electrons and an α-particle, and computations are performed for the 1^1S state of helium. The resulting shift is found to be 1.02 ± 0.15 cm^{-1} and does not remove the discrepancy between theory and experiment. Some effects which might be invoked to bring the theory into agreement with experiment are discussed.

THE presence of a three-body interaction in a system of three particles does not lead to divergences and the Hamiltonian is conveniently written in the Schrödinger representation. In order to do this, let us apply Eq. (1.8) of a previous article* for $N = 4$ [2].

$$(i\partial/\partial t + \mathscr{H}_3)\psi(\mathbf{r}, t) = 0; \qquad (1)$$

$$\mathscr{H}_3 = e^{-iS_3}[e^{-iS_2}(e^{-iS_1}\mathscr{H}e^{iS_1})e^{iS_2}]e^{iS_3}.$$

As in Ref. 1, the resulting Hamiltonian for the system

$$\mathscr{H} = H_0 + H_1^{tr} + H_2^l,$$

contains the Hamiltonians for the free fields (H_0), the interaction of the particles with transverse photons (H_1^{tr}), and the Coulomb interaction (H_2^l). In the case of helium, these terms (excluding their operators S_k (see reference 1) consist of the following parts:

$$H_0 = H_{0e} + H_{0\alpha} + H_{0\gamma}, \quad H_1^{tr} = H_{1e}^{tr} + H_{1\alpha}^{tr};$$

$$S_1 = S_{1e} + S_{1\alpha}, \quad H_2^l = H_{2ee}^l + H_{2\alpha\alpha}^l + H_{2e\alpha}^l;$$

$$S_2 = S_{2ee} + S_{2\alpha\alpha} + S_{2e\alpha},$$

where H_{0e}, $H_{0\alpha}$, $H_{0\gamma}$, are respectively the Hamiltonians for free electrons, α-particles, and photons; H_{1e}^{tr}, $H_{1\alpha}^{tr}$ and H_{2ee}^l, $H_{2\alpha\alpha}^l$, $h_{2e\alpha}^l$ are the Hamiltonian interactions for electrons and α-particles with transverse photons, and the Coulomb interaction between electrons, between α-particles, and between electrons and α-particles.

It follows from Eq. (2) that the 1st and 2nd order Hamiltonians, even for two fields interacting through a third, consist of physically different types of terms. Thus, expanding the phase factors in $\mathscr{H}_3$ into S_1, S_2, . . . , leads to a complicated expression in which the same processes are denoted by terms of different structure. For example, the transverse part of the two-body interaction between electrons and α-particles consists in this case of two terms.

$$-\frac{i}{2}[S_{1e}, H_{1\alpha}^{tr}] - \frac{i}{2}[S_{1\alpha}, H_{1e}^{tr}].$$

The expression for the 4th order Hamiltonian may be rid of redundant terms and thereby simplified in the following manner; instead of expanding Eq. (1) in terms of S_1, S_2 . . . , expand it first in terms of S_{1e} for example, then $S_{1\alpha}$, $S_{2e\alpha}$, $S_{2\alpha\alpha}$ and so on. The transverse part of the two body interaction then becomes

$$-i[S_{1e}, H_{1\alpha}^{tr}].$$

Carrying out such an expansion of the phase factors in Eq. (1), leads to the following expression for H_4

$$H_4 = H_{4ee} + H_{4\alpha\alpha} + H_{4e\alpha}, \qquad (3)$$

where

$$H_{4ee} = \frac{(-i)^2}{2!}\left[S_{1e}, \left[S_{1e}, H_{2ee}^l - \frac{i}{4}[S_{1e}, H_{1e}^{tr}]\right]\right] \qquad (4)$$

$$-\frac{i}{2}[S_{2ee}, H_{2ee}],$$

$$H_{4\alpha\alpha} = \frac{(-i)^2}{2!}\left[S_{1\alpha}, \left[S_{1\alpha}, H_{2\alpha\alpha}^l - \frac{i}{4}\left[S_{1\alpha}, H_{1\alpha}^{tr}\right]\right]\right]$$

$$-\frac{i}{2}[S_{2\alpha\alpha}, H_{2\alpha\alpha}] \qquad (5)$$

describe the interactions of electrons and α-particles among themselves and with transverse photons (H_{4ee} and $H_{4\alpha\alpha}$ differ only in their indices); the term quired matrix element

---

*Here and below, we use the notation of Ref. 1, without further comment.

$$\Delta^3 E_n = \langle n | : H'_{4e\alpha} : | n \rangle, \tag{10}$$

which represents the correction to the nth energy level of a helium atom due to three-body forces. Expression (3) is too complex and cannot be solved exactly. Therefore we shall take advantage of the smallness of the effect we are investigating, and we shall simplify (10) by replacing $: H'_{4e\alpha} :$ by its nonrelativistic approximation. It is convenient to use the diagonal representation of the field operators, wherein the Hamiltonian for the free photons is in diagonal form.*

Carrying out the required transformation, we find

$$\begin{aligned}\Delta^3 E_n = {} & \frac{-Zq^4}{(4\pi)^3 m} \int d\mathbf{x}_1\, d\mathbf{x}_2\, d\mathbf{x}_4 \\ & \times \Big\{ 4 \frac{\partial}{\partial x_{4i}} \psi^*_{ab}(\mathbf{x}_2, \mathbf{x}_{41}) \frac{\partial}{\partial x_{2j}} \psi_{ab}(\mathbf{x}_{21}, \mathbf{x}_4) \\ & \times \left(\frac{1}{x_4} - \frac{1}{x_2}\right) \varepsilon\,(\mathbf{x}_{24}\mathbf{x}^0_1)\, \frac{\delta_{ij} - x^0_{1i} x^0_{1j}}{x^2_1} \\ & - 2i \Big[\frac{\partial}{\partial \mathbf{x}_4} \psi^*_{ab}(\mathbf{x}_2, \mathbf{x}_{41}) \left(\frac{[\mathbf{x}^0_1 \sigma_a]}{x_4} - \frac{[\mathbf{x}^0_1 \sigma_b]}{x_2} \right) \\ & + \psi^*_{ab}(\mathbf{x}_2, \mathbf{x}_{41}) \left(\frac{[\mathbf{x}^0_1 \sigma_b]}{x_4} - \frac{[\mathbf{x}^0_1 \sigma_a]}{x_2} \right) \frac{\partial}{\partial \mathbf{x}_2} \Big] \\ & \times \psi_{ab}(\mathbf{x}_{21}, \mathbf{x}_4)\, \frac{\delta\,(\mathbf{x}_{24}\mathbf{x}^0_1)}{x^2_1} \\ & + \frac{\partial}{\partial \mathbf{x}_2} (\psi^*_{ab}(\mathbf{x}_2, \mathbf{x}_{41}) [\sigma_a [\mathbf{x}^0_1 \sigma_b]] \psi_{ab}(\mathbf{x}_{21}, \mathbf{x}_4)) \\ & \times \left(\frac{1}{x_4} - \frac{1}{x_{41}}\right) \frac{\delta\,(\mathbf{x}_{24}\mathbf{x}^0_1)}{x^2_1} \Big\}, \end{aligned} \tag{11}$$

where $\delta\,(a)$ is a delta function, $\epsilon\,(a)$ is a sign function, and $\psi_{ab}(\mathbf{x}_2, \mathbf{x}_4)$ is the wave function for a three particle system in the center of mass coordinates. Its space part may be identified for the 1^1S state of helium with the Hylleraas function or with the screened wave function. There is no sense in using Hartree's method in Eq. (11), for although this method yields the best value to the zero approximation E^0_n, it leads to nonorthogonal wave functions and various potentials for the electrons thus excluding a consistent application of perturbation theory.

The integrals in (11) are very complicated and can only be evaluated approximately. They were computed graphically for the 1^1S state of helium making use of the three-term Hylleraas functions and it was found that

$$\Delta^3 E = (1.02 \pm 0.15)\ \text{cm}^{-1}, \tag{12}$$

which is beyond the present limits of experimental uncertainty.

The main contribution to this quantity arises from the third term of (11), and is due to the spin-spin part of the interaction. It contributes 1.1 ±0.13 cm^{-1} to $\Delta^3 E$.

The first term in (11) represents the orbit-orbital part of the interaction, and yields a small correction to this quantity, viz., –0.09 ± 0.03 cm.^{-1} The second term of (11) represents the spin-orbital part of the interaction and cannot contribute to a shift of the stationary levels.

The experimental value of the ionization potential for the 1^1S level of helium is $I_0 = 198313 \pm 5\ \text{cm}^{-1}$, while latest computations[8,9] lead to theoretical value $I_0' = 198304\ \text{cm}^{-1}$ if one uses the best value of E^0_n obtained from an eight-term Hylleraas wave function.

The correction (12) computed in the present article decreases the value of I_0' to

$$I''_0 = I'_0 - \Delta^3 E_{1^1S} = 198303\ \text{cm}^{-1} \tag{13}$$

and cannot bring theory in accord with experiment.

It should be noted that (13) does not by any means contain all 4th order relativistic corrections: Thus, we have not included the effect of the interaction of the atomic electrons through vacuum polarization [see Eq. (4a)] which partly explains discrepancy with experiment. A second important reason for the difference between experimental and theoretical values of I_0, is that while the Ritz variational method which was used for finding E^0_n leads to an increase in the absolute value of E^0_n, there is at present no way of estimating the degree of discrepancy between the value found for E^0_n and the actual minimum of the Ritz functional. Thus, when comparing the theoretical and experimental values of the 1^1S energy level of helium, it seems in order to use the results obtained with the eight-term function and the corresponding minimal $|E^0_n|$.

In connection with this, there is another important effect which may be responsible for the difference between the experimental and theoretical values of I_0. It consists in the fact that the relativistic

---

*As is well known, the transition to this representation can be made in the case of spinors with the aid of the unitary transformation.

$$H_{4e\alpha} = \frac{(-i)^2}{2!}\left[S_{1e}, \left[S_{1e}, H^{l}_{2e\alpha} - \frac{i}{3}[S_{1e}, H^{tr}_{1\alpha}]\right]\right] \tag{6}$$

$$+ (-i)^2\left[S_{1\alpha}, \left[S_{1e}, H^{l}_{2} - \frac{i}{2}\left[S_{1e}, \frac{2}{3}H^{tr}_{1e} + H^{tr}_{1\alpha}\right]\right]\right]$$

$$+ \frac{(-i)^2}{2!}[S_{1\alpha}, [S_{1\alpha}, H_{2ee} + H_{2e\alpha}]]$$

$$- i\,[S_{2ee}, H_{2e\alpha} + H_{2\alpha\alpha}]$$

$$- i\left[S_{2e\alpha}, \frac{1}{2}H_{2e\alpha} + H_{2\alpha\alpha}\right]$$

describes the interaction between electrons and α-particles, and free photons among themselves. Note that the particular nature of the fields e, α, γ have not yet been specified in equations (3) to (6), and these expressions may be used for describing the general interaction of two fields in the 4th order.

We shall now make use of the Hamiltonian H_4 to obtain the relativistic corrections to the terms of the helium atom. As is well known, the wave functions for He and the zero-order approximation eigenvalues E_n^0 of the Hamiltonian operator are obtained in the Coulomb interaction approximation (see for example Ref. 3). We must therefore omit from Eqs. (3) to (6) all the terms which include only longitudinal components as these have already been included in the zero order approximation. This may be achieved by replacing everywhere S_2 by S_2^{tr}. The Hamiltonian H_4' obtained in this fashion represents a small correction to $(H_0 + H_2^l)$ and is of the same order of magnitude ($\sim 1\ \text{cm}^{-1}$) as the experimental uncertainty. In computing the matrix elements $< n \mid H_4 \mid n >$, it is justified to keep only the largest terms in H_4', specifically those terms which contain the time component of the current of α-particle, in as much as the terms containing the space components of the current of α-particles lead to a correction ΔE_n which is far below the limits of experimental detection.

Accordingly, we can write the following approximate expression for the component of H_4' capable of producing in helium a measurable change in E_n°:

$$H'_{4ee} \approx \frac{(-i)^2}{2!}\left[S_{1e}, [S_{1e}, H^{l}_{2ee}]\right] - \frac{i}{2}[S^{tr}_{2ee}, H^{l}_{2ee}]; \tag{4a}$$

$$H'_{4\alpha\alpha} \approx 0; \tag{5a}$$

$$H'_{4e\alpha} \approx \frac{(-i)^2}{2!}[S_{1e}, [S_{1e}, H^{l}_{2e\alpha}]] - i[S^{tr}_{2ee}, H^{l}_{2e\alpha}]. \tag{6a}$$

The effect of triple collisions of an α-particle and two electrons will be included in $H'_{4e\alpha}$. As already stated, it does not lead to an "ultraviolet catastrophe" and can conveniently be written in the Schrödinger representation. The operators which appear in it have the following explicit form (see Refs. (1) and (4):

$$S_{1e} = \frac{-q}{4i\pi^{3/2}} \tag{7}$$

$$\times \int \frac{d\mathbf{p}_1 d\mathbf{p}_2 d\mathbf{k}}{\sqrt{k}}\,\delta(\mathbf{k} - \mathbf{p}_{12})\,\frac{a_i(\mathbf{k})\,\psi_1^*\alpha_i\psi_2 - a_i^*(\mathbf{k})\,\psi_2^*\alpha_i\psi_1}{k - \varepsilon_1 + \varepsilon_2},$$

$$S^{tr}_{2ee} = \frac{-q^2}{4\iota(2\pi)^3}\int \frac{d\mathbf{p}_1 d\mathbf{p}_2 d\mathbf{p}_3 d\mathbf{p}_4}{p_{12}}\,\delta(\mathbf{p}_{12} + \mathbf{p}_{34}) \tag{8}$$

$$\times\ :\frac{\psi_1^*\alpha_i\psi_2\psi_3^*\alpha_j\psi_4 - \psi_4^*\alpha_j\psi_3\psi_2^*\alpha_i\psi_1}{\varepsilon_2 + \varepsilon_4 - \varepsilon_1 - \varepsilon_3}:\ \frac{\delta_{ij} - p^0_{12i}p^0_{12j}}{p_{12} - \varepsilon_1 + \varepsilon_2} + A;$$

$$H^{l}_{2e\alpha} = \frac{-Zq^2}{(2\pi)^3} \tag{9}$$

$$\times \int \frac{d\mathbf{p}_1 d\mathbf{p}_2 d\mathbf{P}_1 d\mathbf{P}_2}{p^2_{12}}\,\delta(\mathbf{p}_{12} + \mathbf{P}_{12}) : \psi_1^*\psi_2\Phi_1^*\Phi_2 : \frac{E_1 + E_2}{2\sqrt{E_1E_2}}.$$

Here and from now on, $a_i(\mathbf{k})$ denotes an annihilation operator for transverse photons with momentum $\mathbf{k}$, polarized in the i direction ($i = 1,2,3$); $\psi_{k\alpha} = \psi_\alpha(\mathbf{p}_k)$ ($\Phi_{k\alpha} = \Phi_\alpha(\mathbf{P}_k)$) denote annihilation operators for electrons (α-particles) with momentum $\mathbf{p}_k$ ($\mathbf{P}_k$); A which appears in S^{tr}_{2ee} contains the photon operators; the two dot symbols denotes a normal product of field operators;

$$\mathbf{p}_{ab} = \mathbf{p}_a - \mathbf{p}_b,\quad \mathbf{p}^0_\alpha = \mathbf{p}_\alpha / p_\alpha;$$

$$E_k = \sqrt{\mathbf{P}_k^2 + M^2},\quad \varepsilon_k = \pm\sqrt{\mathbf{p}_k^2 + m^2};$$

M, m are the masses of the α-particles and the electrons; α, β are Dirac matrices; ab, [ab]', [abc] denote respectively scalar vector, and triple scalar products; the units are such that $c = \hbar = 1$, $q = \sqrt{4\pi}$.

Substituting operators (7) to (9) into Equation (6a), and keeping only normal products, we find the re-corrections contained in (13), were computed with a simple Hylleraas function instead of the eight–term function; thus there is no guarantee that the value of some of these terms would not change if they were evaluated with an eight–term function. This is especially true of the orbit–orbital part of the 2nd order relativistic correction,[8] where not only the magnitude, but even the sign depends on the choice of wave function. Furthermore, one should evaluate more correctly the Lamb shift in the electric field of the nucleus; this has been done so far using screened wave functions.

As for the relativistic corrections whose sign does not depend on the choice of wave function, for example the spin–spin part of the two and three–body interactions, it may be expected that the use of an eight–term Hylleraas function instead of the simpler one will not produce a noticeable change in the numerical values of these small quantities; this is indicated, for example, by the fact that in computing E_n^0 with various Hylleraas functions, the results were found to differ only in the fourth place.

On the basis of this analysis it may be expected that including the effects discussed above will lead to agreement between theoretical and experimental value for l_0 within the limits of experimental accuracy.

In conclusion the author wishes to express his gratitude to Iu. M. Shirokov for his continued interest in this analysis and to V. N. Ts'itovich for checking the formula.

---

[1] G. F. Filimonov and Iu. M. Shirokov, J. Exptl. Theoret. Phys. (U.S.S.R.) 32, 99 (1957); Soviet Phys. JETP 5, 84 (1957).

[2] Here and below we use the notation of Ref. 1 without further explanation.

[3] H. Bethe, *Handbuch der physik* (J. Springer, Berlin, 1933), Vol. 24, No. 1.

[4] G. Wentzel, *Quantum Theory of Fields* (Intersciences Publishers, Inc., New York, 1949).

[5] H. S. Snyder, Phys. Rev. 78, 98 (1950).

[6] As is well known, this may be realized in the case of spinors by means of a unitary transformation [see L. L. Fouldy and S. A. Wouthuysen, Phys. Rev. 78, 29 (1950)].

[7] J. Hopfield, Astrophys. J. 72, 133 (1930).

[8] A. M. Sessler and H. M. Foley, Phys. Rev. 92, 1321, 1322 (1953).

[9] H. A. S. Eriksson, Z. Physik 109, 762 (1938).

[10] Chandrasekhar, Elbert, and Herzberg, Phys. Rev. 91, 1172 (1953).

Translated by M. A. Melkanoff
65

SOVIET PHYSICS JETP VOLUME 5, NUMBER 2 SEPTEMBER, 1957

Non-Linear Theory of Betatron Oscillations in a Strong Focusing Synchrotron

IU. F. ORLOV

(Submitted to JETP editor November 15, 1955)
J. Exptl. Theoret. Phys. (U.S.S.R.) 32, 316–322 (February, 1957)

A new method has been developed for investigating betatron resonances. Parametric resonances are investigated.

1. EQUATIONS OF MOTION

THE equations describing betatron oscillations about some plane periodic orbit in a strong focussing synchrotron[1] have the following form:

$$\frac{d^2r}{d\theta^2}+\frac{1}{P}\left(\frac{l}{2\pi}\right)^2\frac{\partial H}{\partial r}r =\frac{1}{P}\left(\frac{l}{2\pi}\right)^2\left\{\frac{1}{\rho}(P-\rho H_0)-\delta\left(\frac{\partial H}{\partial r}\right)r -\frac{\partial H}{\partial z}z -\sum_{n\geqslant 2}\frac{\partial^n H}{\partial r^n}\left[\frac{r^n}{n!}-\frac{r^{n-2}z^2}{2!\cdot(n-2)!}+\frac{r^{n-4}z^4}{4!\,(n-4)!}-\cdots\right]\right\}; \tag{1}$$

$$\frac{d^2z}{d\theta^2}-\frac{1}{P}\left(\frac{l}{2\pi}\right)^2\frac{\partial H}{\partial r}z=\frac{1}{P}\left(\frac{l}{2\pi}\right)^2\left\{H_{\rho_0}+\delta\left(\frac{\partial H}{\partial r}\right)z -\frac{\partial H}{\partial z}r+\sum_{n\geqslant 2}\frac{\partial^n H}{\partial r^n}\left[\frac{r^{n-1}z}{(n-1)!}-\frac{r^{n-3}z^3}{3!\,(n-3)!}+\cdots\right]\right\}, \tag{2}$$

where r denotes the radial and z the vertical deviation of the particles from their periodic orbit; $\rho(\theta)$ is the radius of the orbit. The "angle" θ changes by 2π over a period length l; $\partial H/\partial r$ is the gradient of the magnetic field, $\delta(\partial H/\partial r)$ is the error in the gradient; $1/P = e/cp$, where p is the momentum of the particles. The series of unessential terms in (1) and (2) are discarded; we neglect H_θ in the frequency.

Let us set

$$r = x(\theta)\Phi_r^*(\theta)\exp(i\nu_r\theta) + x^*(\theta)\Phi_r(\theta)\exp(-i\nu_r\theta), \tag{3}$$

$$r'_\theta = x(\theta)\frac{d\Phi_r^*}{d\theta}\exp(i\nu_r\theta) + x^*(\theta)\frac{d\Phi_r}{d\theta}\exp(-i\nu_r\theta);$$

$$z = y(\theta)\Phi_z^*(\theta)\exp(j\nu_z\theta) + y^*(\theta)\Phi_z(\theta)\exp(-i\nu_z\theta), \tag{4}$$

$$z'_\theta = x(\theta)\frac{d\Phi_z^*}{d\theta}\exp(i\nu_z\theta) + y^*(\theta)\frac{d\Phi_z}{d\theta}\exp(-i\nu_z\theta),$$

where $\Phi_{r,z}$ are the Floquet functions with well-known properties

$$\Phi_{r,z}(\theta + 2\pi) = \Phi_{r,z}(\theta)\exp(2\pi i\nu_{r,z}),$$

$\nu_{r,z}$ is equal to the number of betatron oscillations in the length l. This yields

$$\frac{dx}{d\theta} + i\nu_r x = i\left(\frac{l}{2\pi}\right)^2\frac{1}{P\varpi_r}f_r(\theta) \tag{5}$$

$$\times\left\{\frac{1}{\rho}(P - \rho H_0) - \delta\left(\frac{\partial H}{\partial r}\right)(xf_r^* + x^*f_r)\right.$$

$$\left. - \frac{\partial H}{\partial z}(yf_z^* + y^*f_z) - \sum_{n\geqslant 2}\frac{\partial^n H}{\partial r^n}\left[\frac{(xf_r^* + x^*f_r)^n}{n!}\ \cdots\right]\right\};$$

$$\frac{dy}{d\theta} + i\nu_z y \tag{6}$$

$$= i\left(\frac{l}{2\pi}\right)^2\frac{1}{P\varpi_z}f_z(\theta)\left\{H_{\rho_0} + \delta\left(\frac{\partial H}{\partial r}\right)(yf_z^* + y^*f_z)\right.$$

$$\times\frac{\partial H}{\partial z}(xf_r^* + x^*f_r)$$

$$\left. + \sum_{n\geqslant 2}\frac{\partial^n H}{\partial r^n}\left[\frac{(xf_r^* + x^*f_r)^{n-1}(yf_z^* + y^*f_z)}{(n-1)!} - \cdots\right]\right\},$$

$$-i\varpi_{r,z} = \Phi_{r,z}\frac{d\Phi_{r,z}^*}{d\theta} - \Phi_{r,z}^*\frac{d\Phi_{r,z}}{d\theta}, \tag{7}$$

$$\Phi_{r,z}(\theta) = f_{r,z}(\theta)\exp(i\nu_{r,z}\theta); \tag{8}$$

$$f_{r,z}(\theta) = f_{r,z}(\theta + 2\pi).$$

It is important to note that Eqs. (5) and (6) have periodic coefficients with maximum period $2\pi M$, where M is the number of periodic elements.

2. FIRST RESONANCE APPROXIMATION

The distance between linear resonances is equal to $1/2M$ in the $\nu_r\,\nu_z$ plane. One of the main problems of the theory is to locate the boundaries of the so-called safe region between these resonances, i.e., a region where the amplitude does not exceed a certain given value. It is therefore of the greatest interest to know the values of ν_r, ν_z which lie on the boundaries of the safe region, i.e., sufficiently near to the exact resonance values. This allows us to single out the resonance harmonics in a disturbance and to neglect non-resonance ones in the first approximation. Since the disturbance is generally small, this operation gives a good approximation. We shall show in Sec. 4 how the non-resonance harmonics of a disturbance must be treated. The resonance equations obtained in this simple fashion in the first approximation coincide with the so-called "abbreviated" equations obtained by the method of Kryslov and Bogoliubov.[2]

An important advance can be made in the method. Specifically, it may be noted that with the proper choice of variables the resonance equation may be written in the form of Hamilton's equation. In all cases of practical interest, these variables turn out to be the squares of the amplitudes, A_r^2, A_z^2, and some phase variables φ_r, φ_z which usually appear in the "abbreviated" equations. This is especially useful for finding an integral of the motion in the difficult case of many simultaneous resonances. A remarkable property of the Hamiltonian is that it is independent of the angular variable θ; $\mathcal{H} = \mathcal{H}(A_r^2, A_z^2, \varphi_r, \varphi_z)$. This opens up wide possibilities for analysis.

3. PARAMETRIC RESONANCE

On the left and the lower boundaries of the safe region (Fig. 1), one can neglect the effect of all resonances except the parametric one. Let us consider, for instance, the left boundary. In that case the resonace equations in the first "resonance approximation" take the following form (leaving out everywhere the index r):

$$dA^2/d\theta = 2gA^2\cos\varphi = -\partial\mathcal{H}/\partial\varphi, \tag{9}$$

$$d\varphi/d\theta = 2(\varepsilon + \alpha A^2 - g\sin\varphi) = \partial\mathcal{H}/\partial A^2, \tag{10}$$

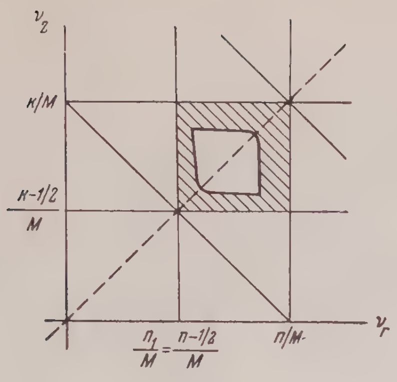

FIG. 1.

where, by definition,

$$x = \frac{A}{2\,|\Phi|_{\max}} \exp\left[-i\left(\frac{\varphi}{2} - \frac{n\theta}{2M} + \frac{\gamma}{2}\right)\right], \quad (11)$$

$$A = 2\,|\Phi|_{\max}\,|x|,$$

$$\varepsilon = \nu^{(1)} - \frac{n}{2M}, \quad (12)$$

$$\nu^{(1)} = \nu + \frac{l^2}{8\pi^3 M\varpi} \int_0^{2\pi M} |\Phi|^2 \delta\left(\frac{\partial H/\partial r}{H_0\rho_0}\right) d\theta,$$

$$g e^{i\gamma} = -\frac{il^2}{8\pi^3 M\varpi} \int_0^{2\pi M} \delta\left(\frac{\partial H/\partial r}{H_0\rho_0}\right) f^2 e^{in\theta/M}\, d\theta \quad (13)$$

$$\approx -\frac{il^2}{8\pi^3 M\varpi} \int_0^{2\pi M} \delta\left(\frac{\partial H/\partial r}{H_0\rho_0}\right) \Phi^2 d\theta,$$

$$\alpha = \frac{l^2}{16\pi^3\varpi} \frac{1}{4\,|\Phi|^2_{\max}} \frac{1}{P} \int_0^{2\pi} \frac{\partial^3 H}{\partial r^3} |\Phi|^4\, d\theta. \quad (14)$$

It should be stated that we have made use here of the general non-linear property of a strong focussing accelerator

$$\partial^3 H(\theta)/\partial r^3 \approx -\partial^3 H(\theta+\pi)\partial r^3. \quad (15)$$

This is related to the fact that the frequencies ν_r and ν_z are generally chosen near to each other

$$|\nu_r - \nu_z| \ll \nu_{r,z}. \quad (16)$$

Therefore,

$$\int_0^{\pi} |\Phi_r\Phi_z|^2\, d\theta \approx \int_{\pi}^{2\pi} |\Phi_r\Phi_z|^2\, d\theta, \quad (17)$$

$$\int_0^{2\pi} |\Phi_r\Phi_z|^2 \frac{\partial^3 H}{\partial r^3}\, d\theta \approx 0. \quad (18)$$

For this reason, in case of parametric resonance (and also for the case of the simultaneous action of parametric and external resonance for the same degrees of freedom) the variables may be separated in spite of the non-linearity of the equations. If ν_r differs considerably from ν_z, then we must use

$$\varepsilon + \alpha_1 A_r^2 + \alpha_2 A_z^2$$

instead of $\epsilon + \alpha A^2$ in Eq. (10), where

$$\alpha_2 = -\frac{l^2}{8\pi^3\varpi} \frac{1}{4\,|\Phi|^2_{\max}} \times \frac{1}{P} \int_0^{2\pi} \frac{\partial^3 H}{\partial r^3} |\Phi_r\Phi_z|^2\, d\theta, \quad (19)$$

and the canonical variables are now $\alpha_1 A_r{}^2$, $\alpha_2 A_z^2$. A is chosen such that it coincides with the amplitude of betatron oscillation. We have discarded in (9) and (10) non-linear terms which arise from derivatives $\partial^n H/\partial r^n$ of higher order than the third. Computations show that such an approximation is permissible as a rule.

According to (9) and (10), amplitude A sustains beats of a much longer period than the period of free oscillation $2\pi/\nu$. Thus the derivative $1/2\,d\varphi/d\theta$ which may be considered constant during the course of a few periods of free oscillations) may be considered as the difference between some effective "instantaneous" frequency

$$\nu_\theta = \nu^{(1)} + \alpha A^2 - g\sin\varphi$$

and its resonance value $n/2M$.

Equations (9) and (10) yield an integral of the motion (20)

$$\mathscr{H} = 2(\varepsilon - g\sin\varphi)A^2 + \alpha A^4 = \text{const.}$$

Note that the equations $dA^2/d\theta = 0$ and $d\varphi/d\theta = 0$ determine a periodic solution for x since according to (11) x is a periodic function of θ if A and φ are constant.

Substituting these periodic solutions into Eq. (20), we obtain formulas relating $\mathscr{H}$ and ϵ:

$$\text{a)}\quad -\frac{\alpha\mathscr{H}}{g^2} = \left(1 + \frac{\varepsilon}{g}\right)^2 \quad (21)$$

$$\text{b)}\quad -\frac{\alpha\mathscr{H}}{g^2} = \left(1 - \frac{\varepsilon}{g}\right)^2,$$

$$\text{c)}\quad \mathscr{H} = 0.$$

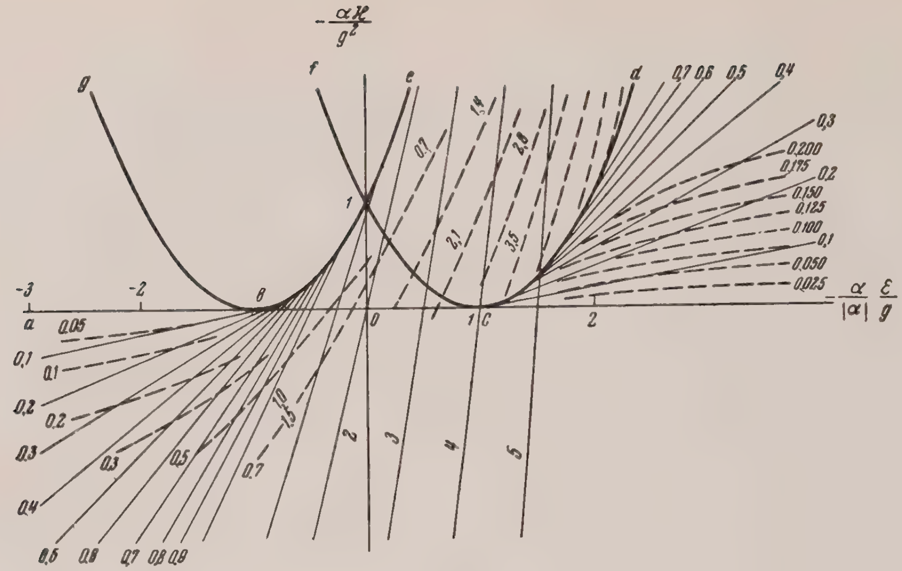

FIG. 2

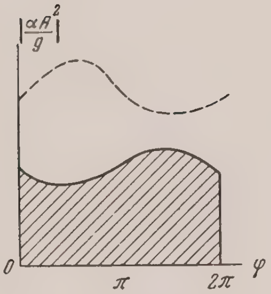

FIG. 3

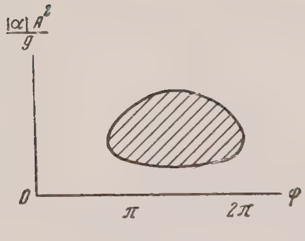

FIG. 4

Equations (21) obviously define curves on the plane $(-\alpha\mathcal{H}/g^2, \epsilon/g)$ which divide it into regions which yield different types of phase diagrams, $A^2 = A^2(\varphi, \mathcal{H}, \epsilon)$. A simple analysis which we shall not carry out here, shows that in the region below *abcd* (Fig. 2) the phase diagrams are unbounded (Fig. 3), while in the region inside *ebcd*, the phase diagrams are bounded (Fig. 4). Motion is impossible above *abc*. As for the curves given by (21), and which divide out the region, the situation is as follows: The phase diagrams for the points which lie on *eb* are simply points (which just correspond to periodic solutions); however characteristic asymptotic motions appear on *bc* and *cd*. Specifically

$$A\to 0 \quad \text{for} \quad \mathcal{H}\equiv 0, \ -1<\varepsilon/g<1; \tag{22}$$

$$-\frac{\alpha A^2}{g}\to\frac{\varepsilon}{g}-1, \tag{23}$$

$$\sin\varphi\to+1 \quad \text{for} \quad -\frac{\alpha\mathcal{H}}{g^2}=\left(\frac{\varepsilon}{g}-1\right)^2,$$

$$\frac{\varepsilon}{g}>1, \ \alpha<0;$$

$$\frac{\alpha A^2}{g}\to-\left(1+\frac{\varepsilon}{g}\right), \tag{24}$$

$$\sin\varphi\to-1 \quad \text{for} \quad -\frac{\alpha\mathcal{H}}{g^2}=\left(\frac{\varepsilon}{g}+1\right)^2,$$

$$\frac{\varepsilon}{g}<-1, \ \alpha>0.$$

If the form of the phase diagram is known, it is easy to compute $A_{\max}$ Besides the parabolas (21), Fig. 2 shows the lines $|\alpha A^2/g|_{\max} = \text{const}$ (solid lines). These lines may be obtained in the regions of practical importance from the formulas

$$\left.\begin{aligned}-\frac{\alpha\mathcal{H}}{g^2} &= 2\left|\frac{\alpha A^2}{g}\right|_{\max}\left(-\frac{\alpha\varepsilon}{|\alpha|g}-1\right)-\left(\frac{\alpha A^2}{g^2}\right)^2_{\max}\\ -\frac{\alpha\mathcal{H}}{g^2} &= 2\left|\frac{\alpha A^2}{g}\right|_{\min}\left(-\frac{\alpha\varepsilon}{|\alpha|g}+1\right)-\left(\frac{\alpha A^2}{g}\right)^2_{\min}\end{aligned}\right\}\begin{aligned}&0<-\frac{\alpha\mathcal{H}}{g^2}<\left(1-\frac{\varepsilon}{g}\right)^2,\\ &-\alpha\varepsilon>0;\end{aligned}\tag{25}$$

$$\left.\begin{aligned}-\frac{\alpha\mathcal{H}}{g^2} &= 2\left|\frac{\alpha A^2}{g}\right|_{\max}\left(-\frac{\alpha\varepsilon}{|\alpha|g}+1\right)-\left(\frac{\alpha A^2}{g}\right)^2_{\max}\\ -\frac{\alpha\mathcal{H}}{g^2} &= 2\left|\frac{\alpha A^2}{g}\right|_{\min}\left(-\frac{\alpha\varepsilon}{|\alpha|g}-1\right)-\left(\frac{\alpha A^2}{g}\right)^2_{\min}\end{aligned}\right\}\begin{aligned}&-\frac{\alpha\mathcal{H}}{g^2}<0,\\ &-\alpha\varepsilon<0.\end{aligned}\tag{26}$$

It should be noted at this point that in addition to the main solution given by formula (25) in the region $-\alpha\epsilon > 0$, there exists a second solution which has considerably larger amplitude (dotted lines in Fig. 3). If (25) corresponds to $d\varphi/d\theta \gtrless 0$, then this second solution corresponds to $d\varphi/d\theta \lessgtr 0$. For this solution the lines $|\alpha A^2/g|_{\min}$ = const have the form:

$$-\frac{\alpha\mathcal{H}}{g^2} = 2\left|\frac{\alpha A^2}{g}\right|_{\min}\left(-\frac{\alpha\varepsilon}{|\alpha|g}-1\right) -\left(\frac{\alpha A^2}{g}\right)^2_{\min}, \qquad -\alpha\varepsilon>0,$$

$$0<-\frac{\alpha\mathcal{H}}{g^2}<\left(1-\left|\frac{\varepsilon}{g}\right|\right)^2, \tag{27}$$

i.e., they are just like (25) for $A_{\max}$ in the fundamental solution. This $A_{\min}$, however, does not coinincide with $A_{\max}$ of the main solution. It may be easily verified that the line $A_{\max}$ = const of the main solution must stop at the point of tangency with the parabola. Its downward continuation turns out to be the line $A_{\min}$ = const. of the second solution. This fact becomes more evident if one considers for example the curve (Fig. 5)

$$-\frac{\alpha\mathcal{H}}{g^2} = 2\left(\frac{\varepsilon}{g}-1\right)\left|\frac{\alpha A^2}{g}\right|-\left(\frac{\alpha A^2}{g}\right)^2, \tag{28}$$

$$\alpha<0, \quad \varepsilon>0.$$

The intersection of this parabola with the line $-\alpha\mathcal{H}/g^2$ = const yields two solutions. The larger one on the right gives $A = A_{\min}$ for the second solution, while the smaller one on the left gives $A = A_{\max}$ for the main solution. They only coincide at the point $|\alpha A^2/g| = (\epsilon/g) - 1$, i.e. on the line cd. It follows that if one draws the line $A_{\max}$ = const for the largest possible amplitude and continues it downward until it intersects the abscissa, then the region to the left of this line (for $-\alpha\epsilon > 0$) must be forbidden. Indeed a large number of particles will be lost in the shaded region of Fig. 6 as they reach the second solution during the start of the acceleration (and also during scattering).

The range of the beat amplitude may be characterized by the quantity $\xi = A^2_{\max}/A^2_{\min}$. The following relation between ϵ/g and ξ can be obtained from Eqs. (25) and (26):

$$\left|\frac{\varepsilon}{g}\right| = \frac{\xi+1}{\xi-1}+\frac{\xi+1}{2\xi}\left|\frac{\alpha A^2}{g}\right|_{\max}; \tag{29}$$

$$-\alpha\varepsilon>0, \quad 0<-\frac{\alpha\mathcal{H}}{g^2}<\left(1-\left|\frac{\varepsilon}{g}\right|\right)^2,$$

$$\left|\frac{\varepsilon}{g}\right| = \frac{\xi+1}{\xi-1}-\frac{\xi+1}{2\xi}\left|\frac{\alpha A^2}{g}\right|_{\max}; \tag{30}$$

$$-\alpha\varepsilon<0; \quad -\frac{\alpha\mathcal{H}}{g^2}<0.$$

Another criterion for determining the boundaries of the safe region arises from the fact that the quantity $<\mathcal{H}^2>^{1/2}$ must not correspond to an amplitude which exceeds some given limiting value. In computing $<\mathcal{H}^2>$, one must take account of scattering by the residual gas.

The Hamiltonian form of Eqs. (9) and (10) permits one to calculate the change in amplitude resulting from a slow (adiabatic) change in the parameters. The dotted lines in Fig. 2 are adiabatic invariants; more exactly, they are defined by

$$I = \frac{|\alpha|}{g}\int A^2 d\varphi = \text{const}. \tag{31}$$

The integral appearing in (31) is numerically equal to the shaded area of Fig. 3 or 4. Figure 2 clearly shows the behavior of the amplitude for slowly varying parameters. In particular, the oscillations due to synchrotron oscillations in the momentum may be assumed adiabatic even at the start of the acceleration.

Evidently passage through resonance can only occur if $\alpha \, (d\epsilon/d\theta) > 0$.

4. THE RESONANCE THEORY OF DISTURBANCES

The effects of non-resonance harmonics can be analyzed by the so-called resonance theory of disturbance. This theory is based on a substitution suggested by Liuponov[3,4] Assume for example that the equation

$$(dx/d\theta) + i\nu x = F(\theta, x, x^*) \qquad (32)$$

has on its right hand side free, linear, quadratic, etc., terms with periodic coefficients. We shall seek solutions of the form

$$x = \Phi(\theta) + s + a_1(\theta)s + a_2(\theta)s^* \qquad (33)$$

$$+ b_1(\theta)s^2 + b_2(\theta)ss^* + b_3(\theta)s^{*2} + \cdots,$$

where Φ, a_i, b_i are periodic functions of θ to be determined. As for s, this new variable must satisfy a first approximation resonance equation accurate to terms which are quadratic in the disturbance on the right side of (32). This requirement, together with the periodicity condition, uniquely defines the substitution (33).

The procedure in the next approximation is clear. The practical second order effects in the resonance equations amount to corrections in the coefficients of the equation in the first approximation. This is essentially the effect of simultaneous oscillation in the momentum $\Delta p/p$ and other disturbances.

Non-resonance harmonics produce new resonances in higher approximation because of the non-linearity of the equation. In practice, however, they generally do not play any role.

The author wishes to express his profound gratitude to professor V. B. Berestetskii, V. V. Vladimirski and L.L. Gol'din for most helpful advice and discussions.

---

[1] Courant, Livingston and Snyder, Phys. Rev. 88, 1190 (1952).

[2] N. M. Krylov and N. N. Bogoliubov, *Introduction to Non-linear Mechanics* (Kiev, 1937).

[3] A. M. Liapunov, *The General Problem of the Stability of Motion* (Gostekhizdat, 1950).

[4] I. G. Malkin, *Theory of the Stability of Motion*, (GITTL, 1952).

Translated by M. A. Melkanoff
66

Measurement of the $C^{12}(p, \gamma)$ and $C^{12}(d, n)$ Effective Cross Sections for Low Energy Bombarding Particles

A. S. DEINEKO, A. IA. TARANOV AND A. K. VAL'TER
Physico-Technical Institute, Academy of Sciences, Ukrainian SSR

(Submitted to JETP editor July 5, 1956)
J. Exptl. Theoret. Phys. (U.S.S.R.) **32**, 251-255 (February, 1957)

In this experiment a tube electrometer capable of measuring effective cross sections down to $\sim 10^{-31}$ cm^2 was used. This instrument is only slightly sensitive to the shape of the energy spectrum of the emitted particles. It yields absolute values directly and permits one to determine the sign of the radioactive emission. It can moreover be used to measure small as well as large radiation intensities without alteration of the geometry or the recording apparatus.

The values of the yields for the reactions $C^{12}(p, \gamma)$ and $C^{12}(d, n)$ in thick targets in the energy range 300-400 kev agree satisfactorily with the shape of the analogous curves at energies above 400 kev as presented in Refs. 7 and 8. The measured cross section for the $C^{12}(p, \gamma)$ reaction in the 300 kev range is in good agreement with the value computed for this energy from the extrapolation formula.

WHEN carbon is bombarded with protons and deuterons, radioactive nitrogen is formed as a result of the following reactions:

$$C^{12} + H^1 \rightarrow N^{13} + Q\,(\gamma); \qquad (1)$$

$$N^{13} \rightarrow C^{13} + \beta^+ + \nu; \qquad (1a)$$

$$C^{12} + H^2 \rightarrow N^{13} + n + Q; \qquad (2)$$

$$N^{13} \rightarrow C^{13} + \beta^+ + \nu. \qquad (2a)$$

Many experimenters have studied reaction (1) as to the yield of N^{13} and γ-rays. It has been established that two resonance peaks exist in the energy range 0.380 to 1.700 mev. The first resonance occurs at $E_p = 456 \pm 2$ kev[1]. The width of the resonance is $\Delta E_p = 35$ kev. For the second peak, E_p 1.697 ± 0.012 mev[2] and $\Delta E_p = 74 \pm 94$ kev. In Ref. 2, furthermore, two excitation levels for N^{13} were determined from the resonances in the proton energies, these being at 2.83 ± 0.018 and 3.53 ± 0.027 mev.

Measurements of the upper limit of the β^+-spectrum[3] indicated that $E_\beta = 1.202 \pm 0.005$ mev. The positron spectrum has a simple Fermi distribution[4]. According to many sources, the half-life period of N^{13} (reaction 1a) is about 10 minutes.

As Bethe has shown[5], reaction (1) is the first stage in the carbon cycle, and the results of research on it have great importance for astrophysical applications. It is especially important to obtain experimental cross sections near $E_p \sim 30$ kev.

On the basis of the Breit-Wigner dispersion equation for a single level the resonance data given above may be used for computing cross sections at low energies. However, in this case the results may prove questionable because of the considerable extrapolation from the resonance energy, since resonances at higher energy may greatly increase the cross section, and the simple dispersion equation for one level may not hold true in regions far from resonance. On the other hand, this extrapolation will simply be ruled out if resonances exist in the energy region of 10-40 kev.

To check these possibilities, Hall and Fowler[6] have investigated reaction (1) at proton energies of the order of 100 kev. The measured cross section is about two times smaller than the calculated one. It is equal to 1.0×10^{-34} cm^2 for an energy of 96 kev, and increases to $(8.5 \pm 1) \times 10^{-34}$ cm^2 at 128 kev. The excitation curves of activity in carbon bombarded with deuterons with energies ranging from 380 to 900 kev, which are presented in Refs. 7 and 8, indicate that as the deuteron energy increases there is a steady increase in N^{13} emission. For deuterons in the energy range from 0.7 -1.9 mev[9] measurement of the positron yield from N^{13} disintegration revealed five resonance maxima at 0.92, 1.16, 1.30, 1.74 and 1.82 mev. These resonances were also obtained in measurements of the neutron yield.

The purpose of the present investigation was to determine the effective cross sections of reactions (1) and (2) for bombarding particles in the 300-400 kev energy region by measuring the positrons emitted in the disintegration of N^{13} nuclei. The study of reaction (1) permits an interesting comparison of the effective cross sections obtained in the experiment with those computed from the extrapolation formula. One may consider the measurement of the absolute yield and cross section of reaction (2) in an energy region close to the threshold as another important result.

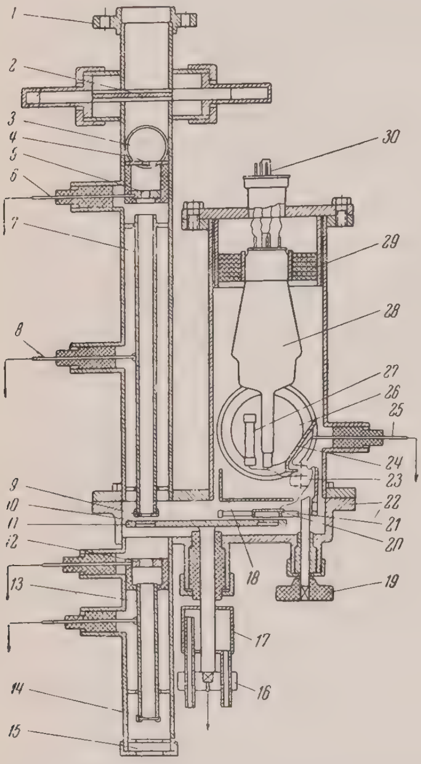

FIG. 1. Diagram of the apparatus. *1* – flange, *2* – gate diaphragm, *3* – window for observing the beam, *4,9* – diaphragms, *5, 12* – retaining diaphragms, *6* – outlet for tapping diaphragms, *7* – upper cylinder, *8* – outlet for measuring the current to the cylinder, *10* – target, *11* – disc with twelve targets, *13* – lower cylinder, *14* – screen, *15, 26* – windows, *16* – knob for turning the disc, *17* – tank for cooling the disc, *18, 24* – shields, *19* – switch knob, *20* – collecting electrode, *21* – amber insulation, *22* – apparatus housing, *23* – switch contacts, *25* – outlet for circuit calibration, *27* – (R_0) leakage resistor, *28* – EM-3 tube, *29* – rubber shock absorber, *30* – socket for cable tapping.

APPARATUS

The protons and deuterons were accelerated in the electrostatic generator of the Physico-Technical Institute, Academy of Sciences, Ukrainian SSR. A rotor voltmeter, calibrated with the resonance peaks of the $F(p, \gamma)$ reaction ,was used to measure the voltage to an accuracy of 0.5%.

The experiments were conducted with atomic and molecular beams of hydrogen and deuterium. Before the experiments were undertaken, the beams were analyzed. The current was measured with a current integrator.

The method used in the investigation was based on the quantitative determination of the β-activity of the reaction products accumulated in the target. At the present time this method is the only one that allows the measurement of very small effective reaction cross sections (in principle down to 10^{-35} cm^2). Thick targets of natural carbon were used in the experiments. The positrons were recorded with a tube electrometer, assembled with an EM-3 electronic tube, which was placed in a vacuum.

A diagram of the apparatus is shown in Fig. 1. The basic parts of the apparatus are the following: a) Faraday cylinder – *7*, which was used in a dual capacity: first, to measure the current passing through it to make sure it was not entering through the side walls of the cylinder; secondly, to permit the introduction through lead *8* of a retarding potential for stopping the electrons knocked out of the target by the beam; b) collecting electrode (collector) – *20*, which was used to collect the positrons emitted by the target; c) disc with twelve targets – *11*, which could be revolved with the aid of turning knob *16* to place the targets under the beam. The same device was used to move the targets under the collector. All of these operations were performed from outside , without disturbing the vacuum; d) electrometer switch – *23*, used for connecting the collector to the grid of the tube, for grounding the collector and grid, and also for admitting the voltage from its source to the collector during calibration of the circuit.

In this same apparatus there was an electronic tube, which was connected by a cable to a balance circuit (Fig. 2). Power for the circuit was supplied by acid batteries with a capacity of 120 amp-hr. Zero displacement in the circuit was practically non-existent. Before starting an experiment the circuit was calibrated; after the completion of the experiment this calibration was checked. The circuit sensitivity was $\sim 5 \times 10^{-5}$ V/fission. The indicator used was a mirror galvanometer of the *M*-21 type with a sensitivity of 5×10^{-10} A/mm/m. The charge sensitivity of the circuit was 7×10^{-16} coulomb/fission.

Given the capacity of the collector, the ballistic sensitivity of the circuit, and the measured galvanometer deflection, one can find the quantity of charge that was collected by the collector. From the charge determined in this manner it is possible to find the cross section of the reaction under investigation.

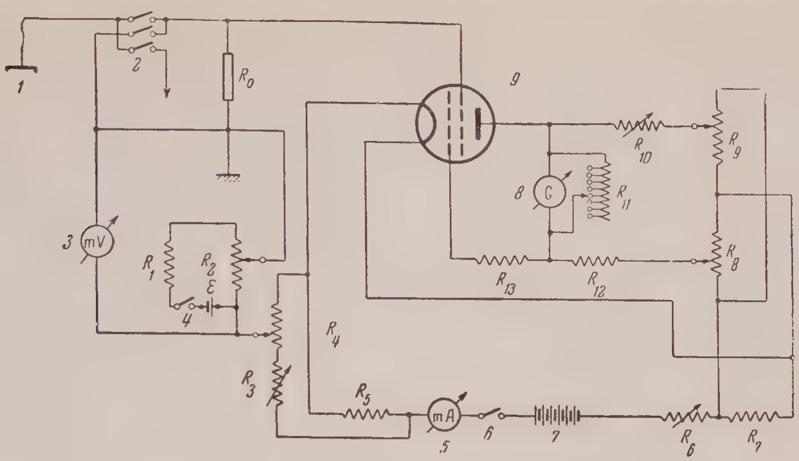

FIG. 2. The balance circuit. *1* – collecting electrode, *2* – electrometer switch, *3* – mV-meter, model 0.5, type M-15; *4* – calibration switch; *5* – mA-meter, max. 150 mA, type M-15; *6* – switch for circuit power supply; *7* – 12-volt accumulator battery; *8* – mirror galvanometer; *9* – EM-3 electronic tube; $\mathcal{E}$ – 1.5-volt dry cell; R_1 – 100 Ω; R_2, R_6 – 10 Ω; R_3 – 20 Ω; R_4, R_8, R_9 – 1000 Ω; R_5 – 30 Ω; R_7 – 45 Ω; R_{10} – resistance box to 10,000 Ω; R_{11} – galvanometer shunt (0.1; 1; 10; 100; 1000; 2500; 4000Ω); R_{12} – 2000 Ω; R_{13} – 4000 Ω; R_0 – 5×10^{10} Ω.

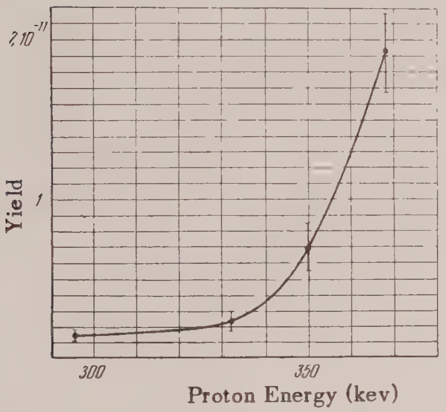

FIG. 3. N^{13} yield from the $C^{12}(p, \gamma)$ reaction.

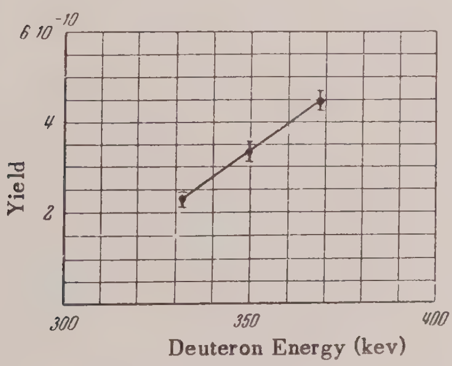

FIG. 4. N^{13} yield from the $C^{12}(d, n)$ reaction.

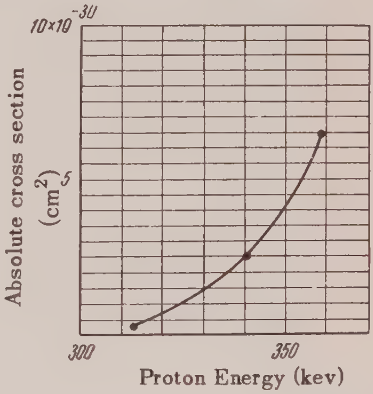

FIG. 5. $C^{12}(p, \gamma)$ cross section curve.

CROSS SECTION MEASUREMENTS

To determine the dependence of the cross sections of the $C^{12}(p, \gamma)$ and $C^{12}(d, n)$ reactions on the energy of the bombarding protons and deuterons, the β^+-activity of thick targets was measured.

The reaction yield for a given energy of the bombarding particles can be presented in the following form:

$$y = Ckn\lambda / N \cdot 1.6 \cdot 10^{-19} \dot{f} (1 - e^{-\lambda t_1}) (e^{-\lambda t_2} - e^{-\lambda t_3}),$$

where C is the capacity of the collector, k is the sensitivity of the circuit, n is the number of fissions from the galvanometer scale, λ is the disintegration constant, N is the number of particles bombarding the target during irradiation, f is the geometric factor, t_1 is the irradiation time of the target by the beam, t_2 is the time of onset of charge accumulation in the collecting electrode, and t_3 is the time of the cessation of accumulation. Before the yield was measured, the disintegration constant λ was determined, and the decay period of N^{13} was computed which, according to our data, proved to be 10.02 ± 0.1 min, in agreement with the findings of other authors.

Figures 3 and 4 show the yield curves for reactions (1) and (2). The ordinate indicates the yield, i.e., the number of positrons per particle bombarding the target, and the abscissa the energy of the bombarding particles in kilo-electron-volts.

From the yield curves one can determine the cross section by the familiar equation

$$\sigma = (dy / dE)(dE / dx) / n,$$

where dE/dx is the loss of energy by the bombarding particles in the target, y is the reaction yield and n is the number of nuclei per 1 cm^3. The quantities dy and dE are determined from the yield curve. Specific energy losses by the bombarding particles in the target are computed from the familiar Bethe formula.

Figure 5 shows the $C^{12}(p, \gamma)$ cross section curve. The value of the $C^{12}(p, \gamma)$ effective cross section is 0.30×10^{-30} cm^2 for an energy of 313 kev and grows to 6.4×10^{-30} cm^2 at 358 kev. The value of the $C^{12}(d, n)$ effective cross section is 0.8×10^{-28} cm^2 for an energy of 340 kev. The absolute errors in the determined cross sections do not exceed ±10%.

---

[1] W. A. Fowler and C. C. Lauritsen, Phys. Rev. **76**, 314 (1949).

[2] D. M. Van Patter, Phys. Rev. **76**, 1264 (1949).

[3] W. F. Hornyak and T. Lauritsen, Phys. Rev. **77**, 160 (1950).

[4] A. M. Feingold, Rev. Mod. Phys. **23**, 10 (1951).

[5] H. A. Bethe, Phys. Rev. **55**, 103, 434 (1939).

[6] R. N. Hall and W. A. Fowler, Phys. Rev. **77**, 197 (1950).

[7] L. R. Halfstad and M. A. Tuve, Phys. Rev. **48**, 306 (1935).

[8] R. B. Roberts and N. P. Heydenburg, Phys. Rev. **53**, 374 (1938).

[9] Bennet, Bonner, Hudspeth, Richards and Watt, Phys. Rev. **59**, 781 (1941).

Translated by A. Skumanich
56

SOVIET PHYSICS JETP VOLUME 5, NUMBER 2 SEPTEMBER, 1957

Equilibrium Spectrum of Electrons and Photons with Account of Scattering

I. P. IVANENKO
Moscow State University

(Submitted to JETP editor December 2, 1955)
J. Exptl. Theoret. Phys. (U.S.S.R.) 32, 333–337 (February, 1957)

An exact solution of the equation for the equilibrium spectrum of electrons and photons has been found with account of scattering, i.e., an expression is obtained for the angular and energetic distributions of particles at the shower maximum in heavy elements.

An analytical expression for the "equilibrium" spectrum (integrated over the depth t *) of photons and electrons, which is valid for any dependence of the absorption coefficient of the photons $\sigma(E)$ on the energy, was first obtained in the work of Tamm and Belen'kii.[1] An analytical expression for the "equilibrium" spectrum, with account of the Rutherford scattering of the charged particles, was found by Belen'kii and Maksimov.[2] However, the equations in Ref. 2 for the equilibrium spectrum with account of scattering were solved approximately; making use of the method of adjoint equations,[3] it is possible to find their exact solution.

Let us write the basic equations of cascade theory with account of scattering:

$$\cos\vartheta \frac{\partial P}{\partial t} = L_1 [P(E_0, t, E, \vartheta), \quad (1)$$

$$\Gamma(E_0, t, E, \vartheta)] + \frac{E_k^2}{4E^2} \Delta_\vartheta P(E_0, t, E, \vartheta),$$

$$\cos\vartheta \frac{\partial \Gamma}{\partial t} = L_2 [P(E_0, t, E, \vartheta), \Gamma(E_0, t, E, \vartheta)].$$

---

* The depth t is measured in atomic units.

Here P and Γ are the distribution functions of the electrons and photons at the depth t, energy E and angles ϑ in the shower, produced by primary particles of energy E_0; L_1 and L_2 are integro–differential operators which act on the variable E and take into account pair formation by photons, bremsstrahlung and ionization losses of the electrons; Δ_ϑ is the Laplace operator, $E_k = 21$ mev.

We apply the following boundary conditions:

$$P(E_0, 0, E, \vartheta) = \delta(E - E_0)\,\delta(\vartheta); \qquad \Gamma(E_0, 0, E, \vartheta) = 0. \tag{2}$$

Integrating Eq. (1) over t from 0 to ∞ with account of the boundary conditions (2), and excluding from the second equation the function $\Gamma_p(E_0, E, \vartheta)$, we get for the function $P_p(E_0, E, \vartheta)$ an equation of the following form:

$$-\cos\vartheta\,\delta(E - E_0)\,\delta(\vartheta) = \int_E^\infty P_p(E_0, E', \vartheta)\,\varphi(E', E)\,dE' - \mu_e(E)\,P_p(E_0, E, \vartheta) + \beta\frac{\partial P(E_0, E, \vartheta)}{\partial E} + \frac{E_k^2}{4E^2}\Delta_\vartheta P_p(E_0, E, \vartheta); \tag{3}$$

$$\varphi(E', E) = 2\varphi'(E', E) + W_e(E', E' - E);$$

$$\mu_e(E) = \int_0^\infty W_e(E, E')\,dE';$$

$$\varphi'(E', E) = \int_E^{E'} \frac{W_p(E'', E')\,W_e(E'', E)}{\sigma(E'')}\,dE'',$$

W_p and W_e are respectively the probability of processes of pair creation and the probability of bremsstrahlung.

Let us investigate the solution of Eq. (3) in the form of a series of Legendre polynomials:

$$P_p(E_0, E, \vartheta) = \sum_{n=0}^{\infty} \varphi_n(E_0, E)\,P_n(\cos\vartheta). \tag{4}$$

Substituting (4) in (3), multiplying (3) by $P_m(\cos\vartheta)$ and integrating over $\cos\vartheta$ from -1 to $+1$, we get the following equation for the function φ_n:

$$\left\{L + \beta\frac{\partial}{\partial E}\right\}\varphi_n(E_0, E) = -\frac{2n+1}{4\pi}\,\delta(E_0 - E), \tag{5}$$

where the operator L is given by the expression:

$$L\varphi_n(E_0, E) = \int_E^\infty \varphi_n(E_0, E')\,\varphi(E', E)\,dE' - \left\{\mu_e(E) + \frac{E_k^2}{4E^2}n(n+1)\right\}\varphi_n(E_0, E). \tag{6}$$

We determine the operator L^* so that

$$\int_{E_1}^\infty u_n(E, E_1)\,L\varphi_n(E_0, E)\,dE = \int_{E_1}^\infty \varphi_n(E_0, E)\,L^* u_n(E, E_1)\,dE, \tag{7}$$

where $u_n(E, E_1)$ is an arbitrary function satisfying the condition

$$u_n(E, E_1) = 0 \quad \text{for} \quad E < E_1. \tag{8}$$

The operator L^* operates on the variable E. Substituting (6) in (7) and changing the order of integration of E and E', we get

$$L^* u_n(E, E_1) = \int_{E_1}^{E} \varphi(E, E')\,u_n(E', E_1)\,dE' - \left\{\mu_e(E) + \frac{E_k^2}{4E^2}n(n+1)\right\}u_n(E, E_1).$$

Multiplying Eq. (5) by $u_n(E, E_1)$ and integrating over E from 0 to ∞, we get:

$$\int_0^\infty u_n(E, E_1)\left[L + \beta\frac{\partial}{\partial E}\right]\varphi_n(E_0, E) = -\frac{2n+1}{4\pi}\,u_n(E_0, E_1). \tag{9}$$

Taking (8) into account, and also the fact that $\varphi_n(E_0, E) = 0$ for $E > E_0$, we have

$$\int_0^\infty u_n(E, E_1)\,\beta\,\frac{\partial}{\partial E}\,\varphi_n(E_0, E)\,dE \tag{10}$$

$$= -\int_0^\infty \varphi_n(E_0, E)\,\beta\,\frac{\partial u_n(E, E_1)}{\partial E}\,dE.$$

Equation (10), together with (7) and (9), gives

$$\int_0^\infty \varphi_n(E_0, E)\Big[L^* - \beta\frac{\partial}{\partial E}\Big]u_n(E, E_1)\,dE \tag{11}$$

$$= -\frac{2n+1}{4\pi}\,u_n(E_0, E_1).$$

If the function $u_n(E, E_1)$ in Eq. (11) is given, then Eq. (11) can be regarded as an integral equation for the function $\varphi_n(E_0, E)$. One can make use of the arbitrariness of the selection of the function $u_n(E, E_1)$ in that (11) was solved more easily than (5). We assume that the $u_n(E,E_1)$ satisfy the equation

$$[L^* - \beta\partial/\partial E]\,u_n(E, E_1) \tag{12}$$

$$= -\delta(E - E_1)(2n+1)/4\pi.$$

It then follows from (11) that

$$u_n(E_0, E_1) = \varphi_n(E_0, E_1), \tag{13}$$

i.e., solution of the primary equation (5) is equivalent to a solution of (11). We make use of (12) so as to obtain an equation for the determination of the energy part of the integral distribution function

$$N_p(E_0, E, \vartheta) = \int_E^\infty P_p(E_0, E, \vartheta)\,dE.$$

For this purpose, we integrate (12) over E_1 from E_2 to ∞, taking it into account that the operator L^* acts only on the variable E, and that when (12) is satisfied, $u_n(E,E_1) = \varphi_n(E, E_1)$. Substituting E for E_2 and E_0 for E, we obtain as a result

$$\Big\{L^* - \beta\frac{\partial}{\partial E_0}\Big\}f_n(E_0, E) = -\frac{2n+1}{4\pi}, \tag{14}$$

$$f_n(E_0, E) = \int_E^\infty \varphi_n(E_0, E)\,dE.$$

Equation (12) is known as the associated equation to Eq. (5).

Let us consider the equation for the energy part of the nth component of the function N_p without account of the ionization loss:

$$L^* f_n(E, E_1) = -(2n+1)/4\pi. \tag{15}$$

The solution of (15) was given by Belen'kii:[5]

$$u_n(E, E_1) = 0 \quad \text{for } E < E_1; \tag{15 ´}$$

$$u_n(E, E_1) = [(2n+1)/4\pi]\,qE^2/[(q^2E^2$$

$$+ a_n^2\beta^2)(q^2E_1^2 + a_n^2\beta^2)]^{-1/2} \quad \text{for } E > E'$$

$$q = 2.29; \qquad a_n = {}^1/_2\,\varepsilon_k\sqrt{n(n+1)/q};$$

$$\varepsilon_k = E_k q/\beta.$$

This solution is exact for the value of $E \ll E_1$. The function $u_n(E, E_1)$ in Eq (11) depends on E; it satisfies the condition (8); in other respects, it is completely arbitrary. For u_n, we use the function (15 ´) and assume that it satisfies Eq. (15) exactly for arbitrary values of E.

The function $u_n(E, E_1)$ has a discontinuity for $E = E_1$. Consequently, for $E = E_1$, the following equation holds, (for $E^2q^2 > a_n^2\beta^2$):

$$\frac{\partial u_n(E, E_1)}{\partial E} = \frac{2n+1}{4\pi}\,\frac{1}{\sqrt{q^2E_1^2 + a_n^2\beta^2}} \tag{16}$$

$$+ \frac{2n+1}{4\pi}\,\frac{E_1}{\sqrt{q^2E_1^2 + a_n^2\beta^2}}\,\delta(E - E_1).$$

Transforming to the function $f_n(E_0, E)$ and replacing E_1 by E, we get Eq. (11) in the following form:

$$f_n^p(E_0, E)\Big\{1 + \beta\frac{1}{\sqrt{q^2E^2 + a_n^2\beta^2}}\Big\} \tag{17}$$

$$- \beta\frac{E}{\sqrt{q^2E^2 + a_n^2\beta^2}}\,\frac{\partial f_n^p(E_0, E)}{\partial E}$$

$$= \frac{2n+1}{4\pi}\,\frac{E_0}{\sqrt{q^2E^2 + a_n^2\beta^2}}.$$

For $a_n = 0$, it coincides with Eq. (77.4) of Ref.

3 for the "equilibrium" spectrum without account of scattering, obtained by the same method. Consequently,

$$f_0^p(E_0, E) = \frac{1}{4\pi}\,\frac{E_0}{\beta}\,\varepsilon e^{\varepsilon}\int_{\varepsilon}^{\varepsilon_0}\frac{e^{-x}}{x^2}\,dx. \tag{18}$$

It is not difficult to find the solution of Eq. (17):

$$f_n^p(E_0, E) = \frac{2n+1}{4\pi}\,\frac{\varepsilon_0}{q} \tag{18'}$$

$$\times \exp\left(\sqrt{\varepsilon^2 + a_n^2}\right)\varepsilon\left(\frac{\varepsilon}{a_n + \sqrt{\varepsilon^2 + a_n^2}}\right)^{a_n}$$

$$\times \int_{\varepsilon}^{\varepsilon_0}\exp\left(-\sqrt{x^2 + a_n^2}\right)\left(\frac{a_n + \sqrt{x^2 + a_n^2}}{x}\right)^{a_n}\frac{dx}{x^2}.$$

For $a_n = 0$, Eq. (18′) coincides with (18). For $\epsilon >> a_n$, Eq. (18′) transforms to

$$f_n^p(E_0, E) = \frac{2n+1}{4\pi}\,\frac{\varepsilon_0}{q}\,e^{\varepsilon}\,\varepsilon\int_{\varepsilon}^{\varepsilon_0}\frac{e^{-x}}{x^2}\,dx$$

$$n = 0,\ 1, 2, \ldots$$

and under the condition $\epsilon_0 >> \epsilon$, we get an asymptotic expansion identical with the expansion of the equilibrium spectrum without account of scattering:

$$f_n^p(E_0, E) = \frac{2n+1}{4\pi}\,\frac{E_0}{q}\,\frac{1}{E}\left(1 - \frac{2}{\varepsilon}\right)$$

$$n = 0,\ 1,\ 2, \ldots$$

For $\epsilon << a_n$, Eq. (18) becomes

$$f_n^p(E_0, E) = \frac{2n+1}{4\pi}\,\frac{\varepsilon_0}{q}\,\frac{1}{a_n + 1},$$

$$n = 1,\ 2,\ 3, \ldots$$

while for f_0^p we obtain the following asymptotic expansion for small ϵ:[1]

$$f_0^p(E_0, E) = (E_0/4\pi\beta)(1 + \varepsilon\ln\varepsilon + \varepsilon C + \ldots),$$

where $C =$ 0.5772 is Euler's constant.

For an estimate of the approximation of the equation for the "equilibrium" spectrum of Belen'kii and Maksimov[2], we compute the ratio $f_n^p(E_0 E)/f_n(\epsilon)$. The function f_n^p is determined by Eq. (18), while $f_n(\epsilon)$ is the corresponding function computed in Ref. 2. The results of the calculations of this ratio are given in the Table. It is seen from the Table that the functions $f_n^p(E_0, E)$ and $f_n(\epsilon)$ coincide within the limits of 6%. We note that the expression for the "equilibrium" spectrum (18) is still approximate, since the initial equations are approximate (in them we made use of simplified expressions for the cross section of elementary processes, taking the Compton effect approximately into account). However, in Ref. 1, an approximate "equilibrium" spectrum (without account of scattering) was obtained from these equations; this spectrum did not differ from the exact value by more than 4.5%. The equations (1) take multiple scattering accurately into account, so that, evidently, the "equilibrium" spectrum (18) differs from the exact also by no more than 4.5%.

TABLE

ε	0.0	0.2	0.5	1.0	2.0	5.0	10	25
$f_1^P(E_0,\ E)/f_1(\varepsilon)$	1.00	0.98	0.97	0.99	0.99	1.03	1.01	0.94
$f_2^P(E_0,\ E)/f_2(\varepsilon)$	1.00	1.00	1.01	1.03	0.99	1.00	1.02	1.06

In the completion of this research, the author made use of the valuable advice of Prof. S. Z.Belen'kii.

---

[1] I.Tamm and S. Belen'kii, J.Phys. (U.S.S.R.) 1, 177 (1939).

[2] S. Z.Belen'kii and B. I. Maksimov, J.Exptl. Theoret. Phys. (U.S.S.R.) 22, 102 (1952).

[3] B. Rossi, *High energy particles*.

[4] S. Z.Belen'kii, *Cascade processes in cosmic rays*, GITTL, Moscow, 1948.

[5] S. Z. Belen'kii, J. Exptl. Theoret. Phys. (U.S.S.R.) 15, 7 (1945).

[6] B. Rossi and S. J. Klapman, Phys. Rev. 61, 414 (1942).

Translated by R. T. Beyer
68

SOVIET PHYSICS JETP VOLUME 5, NUMBER 2 SEPTEMBER, 1957

Behavior of an Electron in a Periodic Electric and a Uniform Magnetic Field

G. E. ZIL'BERMAN

(Submitted to JETP editor November 27, 1955)
J. Exptl. Theoret. Phys. (U.S.S.R.) 32, 296–304 (February, 1957)

The general form of the eigenfunction of an electron in a periodic electric and a uniform magnetic field is derived. The equation of motion and the quasi-classical energy levels are found for an electron with an arbitrary dispersion law in a magnetic field. The broadening of the discrete energy levels of an electron in a crystal in a magnetic field is calculated.

THE magnetic properties of a metal are determined on the basis of the magnetic properties of the electron "gas." The latter is closely connected with the energy spectra of the electrons. To elucidate the magnetic properties of metals, we can go by either of two paths. We can make an assumption on the concrete form of the dispersion law and on the basis of this assumption construct a theory, in the comparison of which with experiment several numerical parameters are determined. The approximations of weakly bound[1,2] or very strongly bound[2–4] electrons apply to such a type of assumption. The second path consists of a search for the connection of the magnetic properties of the electrons with the law of their dispersion in the general form. In this case the concrete form of the dispersion law which holds in each separate case can be determined from a comparison of theory with experiment (in particular, with experiments on the de Haas–van Alphen effect), although such a comparison is considerably more difficult than is shown above.

Such a course of action was first pointed out by I. Lifshitz and Kosevich,[5] who determined the energy levels of the electron and the magnetic susceptibility of an electron gas in the quasi-classical approximation.

In this research, a central assumption is that the Hamiltonian of an electron with an arbitrary dispersion law $E\,(p_x, p_y, p_z)$ in a magnetic field can be determined by replacing p_x, p_y, p_z by the components of the linear momentum operator $\hat{P}_x, \hat{P}_y, \hat{P}_z$.

The present paper is a continuation and development of the work reported in Ref. 5.

The first Section gives the general form of the exact eigenfunction of the electron in a uniform magnetic and a periodic electric field. Later, we give an approximate equation of motion of the electrons, which is shown to be identical to the Hamiltonian constructed by I. Lifshitz and Kosevich.[5] A quasi-classical solution of this equation and the energy levels of the electron have been found.

In the last Section, we consider the effect of broadening of the discrete energy levels of an electron (in a magnetic field) into narrow bands under the action of the periodic field of the lattice. The author has pointed out this broadening in previous papers.[1,2] In these researches, a calculation of the broadening of the levels was carried out in the approximations of weakly coupled and strongly coupled electrons. In the present work, this broadening is calculated outside the framework of the approximations pointed out; the results of the researches of Refs. 1 and 2 are entirely substantiated.

2. EIGENFUNCTIONS OF THE ELECTRONS

Let us write out the Schrödinger equation for an electron in a periodic electric potential V_p and a uniform magnetic field $H = H_z$ [the vector potential $A = (-Hy, 0, 0)$]:

$$\hat{H}\psi = -(\hbar^2/2m)\,\Delta\psi - (i\mu Hy\partial\psi/\partial x) + (e^2H^2y^2/2mc^2 + V_p)\,\psi = E\psi. \qquad (1)$$

We introduce the translation operator of the electron $\hat{T}_{\mathbf{m}}$, $\mathbf{m} = (m_1a_1,\ 0,\ m_3a_3)$ is the vector of the lattice, which lies in the plane x, z. It is evident from the form of the operator $\hat{H}$ that $\hat{T}_m$ and $\hat{H}$ commute:

$$\hat{T}_m \hat{H} = \hat{H} \hat{T}_m, \tag{2}$$

and therefore the eigenfunctions of the operator $\hat{H}$ are also eigenfunctions for the operator $\hat{T}_m$. Application of $\hat{T}_m$ to such a function gives $\hat{T}_m \psi = e^{ikm} \psi$. It follows therefore that the eigenfunctions of the operator $\hat{H}$ have the form:

$$\psi = e^{i(k_1 x + k_3 z)} u(x, y, z),$$

where the functions u are periodic with the period of the lattice along the x and z axes, but are non-periodic in y. Equation (7) for the function u shows that the third quantum number ought to be discrete. Thus the function ψ can finally be written in the form

$$\psi_{k_1 n k_3 s} = e^{i(k_1 x + k_3 z)} u_{k_1 n k_3 s}(x, y, z), \tag{3}$$

(s is the number of the band). In the absence of a magnetic field,the solution (Bloch function) can also be represented in the form (3), where, however,

$$u_s = u_{0s} = e^{ik_2 y} v_s(x, y, z), \tag{4}$$

and $v_s(x,y,z)$ are periodic in x,y,z. In the absence of a periodic field,

$$u = \varphi_n\left(\frac{y + \alpha_0^2 k_1}{\alpha_0}\right), \tag{5}$$

where $\varphi_n(x)$ is the Hermite function and

$$\alpha_0 = \sqrt{\hbar c / eH}. \tag{6}$$

2. TRANSFORMATION OF THE EQUATION OF MOTION OF THE ELECTRON

If Eq. (3) is substituted in Eq.(1), then we get for the function u the equation

$$\hat{L}u = -\frac{\hbar^2}{2m}\Delta u - i\frac{\hbar^2}{m}\left(k_1 + \frac{y}{\alpha_0^2}\right)\frac{\partial u}{\partial x} - i\frac{\hbar^2}{m}k_3\frac{\partial u}{\partial z} + \left[\sum_g V_g e^{2\pi i g r} + \frac{\hbar^2 k_3^2}{2m} + \frac{\hbar^2}{2m}\left(k_1 + \frac{y}{\alpha_0^2}\right)^2\right]u - Eu = 0; \tag{7}$$

at the time when $H = 0$, the equation for the function (4) is

$$-\frac{\hbar^2}{2m}\Delta u_0 - i\frac{\hbar^2}{m}k_1\frac{\partial u_0}{\partial x} - i\frac{\hbar^2}{m}k_3\frac{\partial u_0}{\partial z} + \left[\sum_g V_g e^{2\pi i g r} + \frac{\hbar^2 k_3^2}{2m} + \frac{\hbar^2 k_1^2}{2m}\right]u_0 - E^0(k_1, k_2, k_3)\,u_0 = 0. \tag{8}$$

Below we shall omit the dependence on the coordinates and write the solution of this equation in the form

$$u_0 = u_0(k_1, k_2, k_3). \tag{9}$$

We shall consider further the limiting case of a weak magnetic field. As a criterion of weakness of the field we use the relation

$$\varepsilon = a / \alpha_0 \ll 1, \tag{10}$$

where a is the lattice constant. Conditions (10) are satisfied in practice down to fields of $H \sim 10^5 - 10^6$ Oe (for $H = 10^4$ Oe and $a = 2.5 \times 10^{-8}$ cm, $\epsilon = 10^{-2}$).

In Eq. (9), we make the formal substitution

$$k_1 \to k_1 + y / \alpha_0^2$$

and seek a solution of Eq. (7) in the form

$$u = \sum_s \int g_s(k_1, k_2, k_3) \times u_{0s}(k_1 + y/\alpha_0^2, k_2, k_3)\,dk_2. \tag{11}$$

Subsituting (11) in (7), we multiply by

$$u_{0r}^*(k_1 + y/\alpha_0^2, k_2', k_3)$$

and integrate over all space. Equation (7) has the following form (see Appendix A1).

$$\sum_s \int g_s(k_1, k_2', k_3) \times \left[\int \left(E_s^0(k_1 + y/\alpha_0^2, k_2', k_3) - E\right) u_{0r}^*(k_2)\, u_{0s}(k_2')\, d\tau - \frac{\hbar^2}{m\alpha_0^2}\int u_{0r}^*(k_2)\frac{\partial^2}{\partial k_1 \partial y} u_{0s}(k_2')\, d\tau\right] dk_2' = 0. \tag{12}$$

Here

$$E_s^0(k_1, k_2, k_3) \tag{13}$$

$$= \sum_{\mathbf{n}} A_{\mathbf{n}s} \exp(ik_1n_1)\exp(ik_2n_2)\exp(ik_3n_3).$$

Equation (12) was obtained by neglecting terms of order $\epsilon^4 = (a/\alpha_0)^4$ [see Appendix, Eq. (A–1)]. Below we shall neglect such terms everywhere. The distance between levels is (in corresponding dimensionless units) a quantity of order ϵ^2; therefore, neglect of quantities of higher order of magnitude is legitimate (in our case, such a neglect does not change the character of the equation).

As shown in the Appendix, Eqs. (A2), (A3), transitions between bands in (12) give terms of order not greater than ϵ^3; generally speaking, they will be of order ϵ^4. With accuracy up to terms of such an order of smallness, Eq. (12) can be written in the form

$$\sum_{\mathbf{n}} A_{\mathbf{n}r} \exp\{i\mathbf{kn} - in_1n_2/2\alpha_0^2\} \tag{14}$$

$$\times g_2(k_1, k_2 - n_1/\alpha_0^2, k_3) = E_r g_r(k_1, k_2, k_3).$$

Introducing the operator

$$\hat{Q}_{n_1} = \exp in_1(k_1 - (1/i\alpha_0^2)\,\partial/\partial k_2), \tag{15}$$

we can write (14) also in the form

$$E_r^0(k_1 - (1/i\alpha_0^2)\,\partial/\partial k_2, k_2, k_3) \tag{16}$$

$$\times g_r(k_1, k_2, k_3) = E_r g_r(k_1, k_2, k_3).$$

Here, by the product of the operators $\hat{Q}_n$ and $\exp(ik_2n_2)$ [see Eq. (13)], one understands the symmetrized expression

$$^1/_2\,[\hat{Q}_{n_1}e^{ik_2n_2} + e^{ik_2n_2}\hat{Q}_{n_1}].$$

Thus, the equation of motion of the electron in the magnetic field is obtained by substitution in Eq. (13) (which is for the energy of the electron in the absence of a magnetic field) of the quantum number k_1 for the operator $k_1 - (1/i\alpha_0^2)\partial/\partial k_2$ (under conditions of application of the order of operation pointed out for non-commutative multipliers).

3. SOLUTION OF THE EQUATION OF MOTION OF THE ELECTRON

Let us transform Eq. (14) to the form (17), omitting the band index:

$$\sum_{\mathbf{n}} A_{\mathbf{n}} \exp\{i\mathbf{kn} - in_1n_2/2\alpha_0^2\} \tag{17}$$

$$\times g(k_1, k_2 - n_1/\alpha_0^2, k_3) = Eg(k_1, k_2, k_3).$$

The solution of this equation will be sought in the form

$$g(k_1, k_2, k_3) \tag{18}$$

$$= \exp\{i\alpha_0^2 k_1 k_2 - i\psi(k_1, k_2, k_3)\}.$$

The function ψ has a real and an imaginary part

$$\psi = \varphi + i\varphi_1.$$

Here the imaginary part is small (of the order ϵ^2) in comparison with the real. Considering the function ψ to be slowly changing in a change of k_2 by a/α_0^2, we expand $\psi(k_2 - n_1/\alpha_0^2)$ in a series and, neglecting terms of order $(a/\alpha_0)^4$, we get, after substitution of Eq. (18) in Eq. (17):

$$E^0\left(\frac{\varphi'(k_2)}{\alpha_0^2}, k_2, k_3\right) + i\frac{\varphi_1'(k_2)}{\alpha_0^2}\frac{\partial E^0}{\partial \varkappa_1} \tag{19}$$

$$+ \frac{i}{2\alpha_0^2}\left(\frac{\partial^2 E^0}{\partial \varkappa_1 \partial k_2} + \frac{\partial^2 E^0}{\partial k_1^2}\frac{\partial \varkappa_1}{\partial k_2}\right) = E.$$

Here the prime denotes differentiation with respect to k_2, $\varkappa_1 = \varphi'(k_2)/\alpha_0^2$.

We so choose the function φ_1 that the terms in Eq. (19) which are of order $(a/\alpha_0)^2$ (the second and third terms on the left) cancel each other. This gives for the function φ_1

$$\varphi_1 = -{}^1/_2 \ln|\partial E^0/\partial \varkappa_1|. \tag{20}$$

For the function φ we get a differential equation of first order:

$$E^0(\varkappa_1, k_2, k_3) = E. \tag{21}$$

Solving this equation for $\varkappa_1$, we get (because of its parity) two* roots: $\pm|\varkappa_1|$ and therefore,

---

*We consider only the case in which the simply connected curve $\varkappa_1 = \varkappa_1(k_2)$ is double–valued.

$$\varphi(k_2) = \pm \alpha_0^2 \int \varkappa_1 dk_2. \tag{22}$$

Consequently, we can write the total eigenfunction $g(k_1, k_2, k_3)$ in the form of a linear combination

$$g(k_1, k_2, k_3) = |\partial E^0/\partial \varkappa_1|^{-1/2} e^{i\alpha_0^2 k_1 k_2} \left(A \exp\left\{i\alpha_0^2 \int \varkappa_1 dk_2\right\} + B \exp\left\{-i\alpha_0^2 \int \varkappa_1 dk_2\right\}\right)$$

or in the form

$$g(k_1, k_2, k_3) = |\partial E^0/\partial \varkappa_1|^{-1/2} e^{i\alpha_0^2 k_1 k_2} \sin\left(\alpha_0^2 \int \varkappa_1 dk_2 + \gamma\right). \tag{23}$$

The function (23) differs from the usual quasi-classical function of one-dimensional motion (the coordinate in the given case is k_2) only by the factor

$$\exp(i\alpha_0^2 k_1 k_2).$$

The quantity $\alpha_0^2 \varkappa_1$ plays the role of the momentum as was noted by I. Lifshitz and Kosevich.[5]

The turning points of the classical motion are those points of the phase plane $(\varkappa_1, k_2)$ in which the derivative $\partial E^0/\partial \varkappa_1 = 0$. In particular, such points are always points for which $\varkappa_1 = 0$ or $\pm \pi/a_1$ (for $\varkappa_1 = 0, \pm\pi/a_1$, the derivative $\partial E^0/\partial \varkappa_1$ is necessarily equal to zero).

Let us consider the case in which the curve $\varkappa_1 = \varkappa_1(k_2)$ is closed and double-valued, and lies wholly inside a single cell of the reciprocal lattice, while at the turning point, $\varkappa_1 = 0$. In order to find the phase γ of the wave function (23), we expand E^0 about the turning point in a series in powers of $\varkappa_1 - \varkappa_1^0$ and $k_2 - k_2^0$.

Since

$$\partial E^0/\partial \varkappa_1 = 0 \text{ and } \partial^2 E^0/\partial \varkappa_1 \partial k_2 = 0$$

at $\varkappa_1 = 0$, Eq. (21) in the vicinity of the turning point will be

$$E^0(\varkappa_1, k_2, k_3) = E_0^0 + \frac{\partial E_0^0}{\partial k_2}(k_2 - k_2^0) + \frac{1}{2}\frac{\partial^2 E_0^0}{\partial \varkappa_1^2}\varkappa_1^2 = E. \tag{24}$$

Hence

$$\varkappa_1 = \pm[-(\partial E_0^0/\partial k_2)(k_2 - k_2^0)/{}^1/_2(\partial^2 E_0^0/\partial \varkappa_1^{02})]^{1/2}, \tag{25}$$

which must be substituted in Eq. (23),

The exact equation [by exact is meant Eq. (17) or Eq. (16)] near the turning point has, as is easy to show, the solution

$$e^{i\alpha_0^2 k_1 k_2} \sin\left[\alpha_0^2 \int \varkappa_1 dk_2 + \pi/4\right], \tag{26}$$

where by $\varkappa_1$ is meant Eq (25).

Thus if the curve $\varkappa_1 = \varkappa_1(k_2)$ is closed, double-valued, and located in a single cell of the reciprocal lattice, then $\gamma = \pi/4$.

The rules of quasi-classical quantization are based on the coincidence of the wave functions (23), written in such form which guarantees the correct value of the phase at the turning point. The factor

$$\exp(i\alpha_0^2 k_1 k_2)$$

here falls out from the condition of quasi-classical quantization and has the usual form

$$\alpha_0^2 \int_a^b \varkappa_1 dk_2 = \pi\left(n + \frac{2}{\pi}\gamma\right). \tag{27}$$

The quantity

$$2\hbar^2 \int_a^b \varkappa_1 dk_2$$

for the case of a closed, double-valued curve in a single cell represents the area of the intersection of the surface of constant energy (in the momentum space $\hbar\varkappa_1, \hbar k_2, \hbar k_3$), with the plane $k_3 = \text{const}$; therefore, Eq. (27) can be written in the form

$$cS(E, k_3)/h|e|H = n + 2\gamma/\pi, \tag{28}$$

which was obtained earlier by I. Lifshitz and Kosevich.[5] This condition also determines in implicit form the energy levels of the electron $E = E(n, k_3)$.

We note that upon the introduction of the phase

y, in addition to the double-valuedness of the curve

$$\varkappa_1 = \varkappa_1(k_2),$$

we have implicitly assumed the fulfillment of the following inequalities (in the neighborhood of the turning point b):

$$\alpha_0^2 \varkappa_1 (b - k_2) \gg 1 \tag{29}$$

[which is necessary for writing out the Airy function in asymptotic form],

$$d\varkappa_1 / dk_2 \ll \alpha_0^2 \varkappa_1 / a \tag{30}$$

(quasi-classical condition), which has, in the neighborhood of the turning point, the form

$$b - k_2 \gg a / \alpha_0^2 \tag{30 ′}$$

and, finally,

$$\frac{\partial E_0^0}{\partial k_2}(b - k_2) \gg \frac{1}{2}\frac{\partial^2 E_0^0}{\partial k_2^2}(b - k_2)^2 \tag{31}$$

which was used in the expansion of Eq. (24).

The first and second inequalities do not contradict each other. However, (29) and (30) or (31) are contradictory if $\partial E^0{}_0/\partial k_2$ is small. For strongly coupled electrons, for example, it takes place within 1/3 of the zone. The inequalities that have been shown are also contradictory for the lower levels of the zone.

The function (23) takes place in the limits of the region of classical motion. Outside of the limits of this region, the eigenfunctions decay exponentially and have the form

$$g(k_1 k_2 k_3) = e^{i\alpha_0^2 k_1 k_2} f(k_2) \tag{32}$$

$$= e^{i\alpha_0^2 k_1 k_2} \frac{1}{2}\left|\frac{\partial E^0}{\partial \varkappa_1}\right|^{-1/2} \exp\left\{-\alpha_0^2 \int |\varkappa_1| dk_2\right\}.$$

The functions are discussed by us in a subsequent section.

For sufficiently large filling of the band, curves of constant energy have the form of closed trajectories surrounding the points $\pm\pi/a_1$ and $\pm\pi/a_2$.

In this case we can also obtain the energy levels from Eq. (28), if we make the transformation

$$\varkappa_1 = \varkappa_1' \pm \pi/a_1; \; k_2 = k_2' \pm \pi/a_2,$$

in (6) and then write

$$E^0(\varkappa_1' \pm \pi/a_1, k_2' \pm \pi/a_2, k_3) = E^{0\prime}(\varkappa_2', k_2', k_3).$$

If the curve in the new coordinates lies in a single cell of the reciprocal lattice, then the equation of I. Lifshitz and Kosevich (28) is valid. In that equation we must understand by $S(E, k_3)$ the cross section of the plane k_2 = const, not with the surface $E^0 = E$, but with the surface $E^{0\prime} = E$ (the dispersion law

$$E^{0\prime}(\varkappa_1', k_2', k_3')$$

differs from the dispersion $E^0(\varkappa_1, k_2, k_3)$ by the fact that the coefficients A_{n_1, n_2, n_3} in Eq. (13) are substituted for the coefficients $(-1)^{n_1+n_2} A_{n_1 n_2 n_3}$).

If the curve $\varkappa_1 = \varkappa_1(k_2)$ is multiply connected and consists of closed contours which have the $\varkappa_1$ and k_2 axes as axes of symmetry [where the individual contours do not abut on one another, but intersect, and the function $\varkappa_1(k_2)$ is doubly valued in the limits of each contour], then, shifting the origin to the center of each curve $(\varkappa_1^0, k_2^0)$ we get the quantization condition in the form (28), in which S denotes the cross section of the surface

$$E^0(\varkappa_1' + \varkappa_1^0, k_2' + k_2^0, k_3) = E^0(\varkappa_1', k_2', k_3) = E$$

with the plane k_3 = constant.

4. DISTRIBUTION OF THE ENERGY LEVELS OF THE ELECTRON

In the preceding Sections, it was shown that the eigenfunction of the electron in k space, $g(k_1, k_2 k_3)$, is determined by the equation $\hat{E}^0 g = Eg$ [Eq. (17)]. The energy E was shown to be dependent on the two quantum numbers n and k_3. It had been shown earlier[2] that the electron's energy should depend on all three quantum numbers k_1, n, k_3, where the dependence on k_1 leads to a broadening of the discrete energy levels of the electron in a narrow band. This broadening has, generally speaking, the order of magnitude ϵ^4. However, there are special cases when the broadening becomes appreciable. This takes place when the energy surfaces in neighboring cells of the reciprocal lattice are almost in contact, and also for open trajectories (which will be considered in later research). A penetration is then possible from one region of quasi-classical motion* into another through the "potential barrier," by virute of which the discrete energy levels merge into narrow bands.

The eigenfunction of the electron in periodically arranged regions can be written in the form

$$\psi_{k_1} = \sum_m \exp\left\{i\alpha_0^2 k_1 \left(k_2 - \frac{2\pi}{a_2} m\right)\right\} f\left(k_2 - \frac{2\pi}{a_2} m\right)$$
$$= \sum_m g\left(k_1,\ k_2 - \frac{2\pi}{a_2} m,\ k_3\right). \qquad (33)$$

Substituting (33) in Eq. (17), multiplying by

$$g^*(k_1,\ k_2,\ k_3)$$

and integrating over k_2, we get an expression for the energy levels of the electron with their broadening taken into account:

$$E_{k_1 n k_3} = E_{nk_3} + E''_{nk_3} J_{nk_3} \cos\frac{2\pi\alpha_0^2 k_1}{a_2}. \qquad (34)$$

Here E_{nk_3} are the levels obtained from Eq. (28),

$$E''_{nk_3} = \partial^2 E_{nk_3} / \partial k_2^2$$

is the second derivative at the point $k_2 = \pi / a_2$,

and

$$J_{nk_3} = \int f_{nk_3}(k_2)\, f_{nk_3}\left(k_2 - \frac{2\pi}{a_2}\right) \qquad (35)$$
$$\times \left(k_2 - \frac{2\pi}{a_2}\right)^2 dk_2.$$

Here $f_{nk_3}(k_2)$ is defined by Eq. (32).

Let us carry out an estimate of this integral. We can write down the following expansion about the turning point k_{20}:

$$k_2 = k_{20} + \frac{1}{2}\frac{\partial^2 k_{20}}{\partial \varkappa_1^2}\varkappa_1^2 = k_{20} - \frac{a_2}{2R}\varkappa_1^2, \qquad (36)$$

where R is a dimensionless radius of curvature of the curve $\varkappa_1 = \varkappa_1(k_2)$ at the point $(0, k_{20})$. We also introduce the small parameter x_0 as the distance between neighboring trajectories (in units of $1/a$).

Making use of the Eq. (32), we get

$$J \sim \exp\{-4\sqrt{2R}\, x_0^{3/2} / 3\varepsilon^2\} a_2^{-2} x_0^2 \sqrt{x_0/R} \quad (37)$$

For a fixed energy level, determined by the parameters R and x_0 at $\epsilon \to 0$, $J \to 0$. However, for each ϵ there are other values of the small parameters x_0 and R for which $J \sim x_0^2$. Usually, as $x_0 \to 0$, R also $\to 0$. If $R \sim x_0$, then $J \sim x_0^2$ means $x_0 \approx \epsilon$ (just as the quasi-classical approximation is invalid only in the region $\sim \epsilon^2$ around the turning point, so our calculation is valid).

The author expresses his sincere gratitude to I. M. Lifshitz for his interest in the present work and for discussions.

APPENDIX

1. Application of the operator $\hat{L}$ of Eq. (7) to the function $u_{0s}(k_1 + y/\alpha_0^2,\ k_2,\ k_3)$ gives

$$\hat{L} u_{0s} = \left(E_s^0\left(k_1 + \frac{y}{\alpha_0^2},\ k_2,\ k_3\right) - E\right) u_{0s} \qquad (A-1)$$
$$- \frac{\hbar^2}{2m\alpha_0^4}\frac{\partial^2 u_{0s}}{\partial k_1^2} - \frac{\hbar^2}{m\alpha_0^2}\frac{\partial^2 u_{0s}}{\partial y \partial k_1}.$$

We discard the second term since its value $\sim \hbar^2 a^2 / 2m\alpha_0^4$.

The last term $\sim \hbar^2 / m\alpha_0^2$, and we take it into account.

2. The function (9), as is well known, can be written in the form

$$u_{0s}(k_1,\ k_2,\ k_3) \qquad (A-2)$$
$$= e^{ik_2 y} \sum_{\mathbf{h}} e^{2\pi i \mathbf{hr}} b_{\mathbf{h}s}(k_1,\ k_2,\ k_3).$$

The properties of (9) of interest to us, according to which the expansion (11) is carried out, are based on the following properties of the coefficients

$$b_{\mathbf{h}s}(k_1,\ k_2,\ k_3)$$

(these properties do not change under the substitution $k_1 \to k_1 + y/\alpha_0^2$):

a) $b_{\mathbf{h}s}(k_1 k_2 k_3)$ are real and even functions of the arguments $k_i + 2\pi h_i$; ;

b) for identical k, the coefficients $b_{\mathbf{h}s}$ are orthogonal. We shall consider them to be normalized:

$$\sum_{\mathbf{h}} b_{\mathbf{h}s}(k_1 k_2 k_3)\, b_{\mathbf{h}r}(k_1 k_2 k_3) = \delta_{rs}; \qquad (A-3)$$

---

*If such regions have such cells, then everything pointed out below refers in equal measure to them.

c) Proceeding directly from the equation which is satisfied by the coefficients $b_{\mathbf{h}s}$,

$$b_{\mathbf{h}s}\left[\frac{\hbar^2}{2m}(\mathbf{k}+2\pi\mathbf{h})^2-E_s^0\right]+\sum_{\mathbf{g}}V_{\mathbf{g}}b_{\mathbf{h}-\mathbf{g},s}=0 \qquad \text{(A–4)}$$

we can obtain the well known connection between the current and the energy:

$$\sum_{\mathbf{h}}(k_2+2\pi h_2)\,b_{\mathbf{h}s}^2(k_1k_2k_2)=\frac{m}{\hbar^2}\partial E_s^0/\partial k_2; \qquad \text{(A–5)}$$

e) from this same equation for $b_{\mathbf{h}s}$ we can obtain a much more general relation

$$(2m/\hbar^2)\,[E_r^0(k_2')-E_s^0(k_2)]\sum_{\mathbf{h}}b_{\mathbf{h}s}(k_2)\,b_{\mathbf{h}r}(k_2') \qquad \text{(A–6)}$$
$$+\sum_{\mathbf{h}}b_{\mathbf{h}s}(k_2)\,b_{\mathbf{h}r}(k_2')\,[(k_2+2\pi h_2)^2-(k_2'+2\pi h_2)^2]=0,$$

from which it follows, in particular, that for $k_2=k_2'$

$$(E_r^0-E_s^0)\sum_{\mathbf{h}}b_{\mathbf{h}s}\frac{\partial b_{\mathbf{h}r}}{\partial k_2}=-\frac{\hbar^2}{m}\sum_{\mathbf{h}}b_{\mathbf{h}s}b_{\mathbf{h}r}(k_2+2\pi h_2); \qquad \text{(A–7)}$$

$$\sum_{\mathbf{h}}\frac{\partial b_{\mathbf{h}s}}{\partial k_1}b_{\mathbf{h}r}(k_2+2\pi h_2)=-\frac{m}{\hbar^2}\frac{\partial E_s^0}{\partial k_1}\sum_{\mathbf{h}}b_{\mathbf{h}s}\frac{\partial b_{\mathbf{h}r}}{\partial k_2}. \qquad \text{(A–8)}$$

To obtain Eq. (14) and what follows it, use is made of the properties that have been pointed out, and of the expansion

$$\sum_{\mathbf{h}}b_{\mathbf{h}s}(k_2')\,b_{\mathbf{h}r}(k_2)=\delta_{rs}+(k_2'-k_2)\sum_{\mathbf{h}}\frac{\partial b_{\mathbf{h}s}}{\partial k_2}b_{\mathbf{h}r}+\cdots \qquad \text{(A–9)}$$

3. Making use of the properties of the coefficients $b_{\mathbf{h}s}$, we can compute the integrals in (12). Neglecting quantities of order ϵ^4, we obtain the following equation:

$$\sum_{\mathbf{n}}A_{\mathbf{n}r}\exp\{i\mathbf{k}\mathbf{n}-in_1n_2/2\alpha_0^2\} \qquad \text{(A–10)}$$
$$\times g_r(k_1,\ \ k_2-n_1/\alpha_0^2,\ \ k_3)-E_rg_r(k_1,\ \ k_2,\ \ k_3)$$
$$+\sum_{s\neq r}(E_s-E_r)$$
$$\times\int g_s(k_2')\,(k_2'-k_2)\,F_{sr}(\alpha_0^2(k_2'-k_2))\,d(k_2a_2)=0,$$

where g_r, g_s, E_r, E_s refer to different bands but to one and the same quantum number, and

$$F_{sr}(\alpha_0^2(k_2'-k_2))=e^{-i(k_2'-k_2)k_1\alpha_0^2} \qquad \text{(A–11)}$$
$$\times\int e^{i(k_2'-k_2)\alpha_0^2\xi/a_1}\sum_{\mathbf{h}}\frac{\partial b_{\mathbf{h}s}}{\partial k_2}b_{\mathbf{h}r}d\xi,$$
$$\xi=a_1(k_1+y/\alpha_0^2).$$

In Eq. (A–10), there are small non-diagonal terms in addition to the diagonal terms. Since the sum in the integrand is periodic in ξ (with period 2π), we can write:

$$\sum_{\mathbf{h}}b_{\mathbf{h}r}\partial b_{\mathbf{h}s}/\partial k_2=\sum_m B_me^{-im\xi}. \qquad \text{(A–12)}$$

Then F_{sr} will be the sum of δ-functions:

$$F_{sr}=\sum_m B_me^{-i(k_2'-k_2)k_1\alpha_0^2}\delta\left(\frac{\alpha_0^2}{a_1}(k_2'-k_2)-m\right), \qquad \text{(A–13)}$$

and the non–diagonal terms in (A–10) are written as

$$\sum_m\sum_{s\neq r}(E_s-E_r)\,mB_m\frac{a_1}{\alpha_0^2}e^{-ik_1a_1m}g_s\left(k_2+\frac{ma_1}{\alpha_0^2}\right). \qquad \text{(A–14)}$$

In view of the smallness of these terms, we can regard them as a perturbation. Inasmuch as this perturbation is of order ϵ^2, it is necessary to compute only the diagonal matrix element

$$\sum_m\sum_{s\neq r}(E_s-E_r)\frac{a_1}{\alpha_0^2}mB_me^{-ik_1a_1m} \qquad \text{(A–15)}$$
$$\times\int g_s\left(k_2+\frac{ma_1}{\alpha_0^2}\right)g_r^*(k_2)\,dk_2.$$

Employing (18), we write the integral in the form

$$\int \exp\{-i\varphi_s(k_2+ma_1/\alpha_0^2)+i\varphi_r(k_2) + \varphi_{1s}(k_2+ma_1/\alpha_0^2)+\varphi_{1r}(k_2)\}\,dk_2 \qquad \text{(A–16)}$$

Since [see Eq. (22)]

$$\varphi_r(k_2)=\alpha_0^2\int_c^{k_2}\varkappa_{1r}dk_2,$$

$$\varphi_s\left(k_2+\frac{ma_1}{\alpha_0^2}\right)=\alpha_0^2\int_c^{k_2+ma_1/\alpha_0^2}\varkappa_{1s}dk_2,$$

then the imaginary part of the exponent is very large ($\alpha_0\to\infty$) and the integral can be solved by the method steepest descents. A saddle point will exist if there is a point of the plane ($\varkappa_1$, k_2) in which $\varkappa_{1r}(k_2)=\varkappa_{1s}(k_2+ma_1/\alpha_0^2)$. Since $a_1/\alpha_0^2 \ll \pi/a_2$, then the conditions given above will be satisfied only if the curves $\varkappa_{1r}(k_2)$ and $\varkappa_{1s}(k_2)$ intersect (more precisly, if they come very close to one another, or intersect). In this case we can employ the method of steepest descents. It is easy to convince oneself of the fact that the integral in this case will be of order ϵ while the entire matrix elements will be of order ϵ^3.

If $\varkappa_{12}$ and $\varkappa_{12}$ (which refer to states with identical n and k_3 in the bands r and s) do not intersect, the saddle points will not exist and the integral will be of order ϵ^2, while the matrix element will be of order ϵ^4.

---

[1] G. E. Zil'berman, J. Exptl. Theoret. Phys. (U.S.S.R.) 23, 49 (1952).

[2] G. E. Zil'berman, J. Exptl. Theoret. Phys. (U.S.S.R.) 30, 1092 (1956); Soviet Phys. JETP 3, 835 (1956).

[3] R. Peierls, Z. Physik 80, 763 (1933).

[4] G. E. Zil'berman, Uchenye zapiski Kharkov State Univ. No. 6, 1955.

[5] I. M. Lifshitz and A. M. Kosevich, Dokl. Akad. Nauk SSSR 96, 963 (1954)

Translated by R. T. Beyer
63

SOVIET PHYSICS JETP VOLUME 5, NUMBER 2 SEPTEMBER, 1957

The Acceleration of a Plasma by a Magnetic Field

A. I. Morozov
Moscow State University

(Submitted to JETP editor November 28, 1955)
J. Exptl. Theoret. Phys. (U.S.S.R.) 32, 305–310 (February, 1957)

Acceleration of a current–conducting plasma jet by a magnetic field is considered. The nature of the processes is preliminarily elucidated by examining the case of motion of conductors possessing some resistance and inductance. Furthermore, the motion of ions and electrons is studied under conditions where collisions, magnetic interaction of the particles and excitation of waves are negligible. The existence of a critical charge density in accelerators has been established for this case. Peculiarities of acceleration of very dense jets are also considered.

If a current is flowing in a plasma jet situated in a magnetic field, there will be a force of the volume density $f=[\mathrm{jH}]/c$ acting upon the jet and imparting to it an acceleration. As an example, we might consider the case of the motion of an electric arc, burning between two electrodes connected to a current source, in a magnetic field. Such a process was experimentally studied by Bron[1,2] at atmospheric pressure. In his experiments, the velocity of the arc attained several hundred meters per second despite air resistance.

It is of interest to consider the motion of the arc in the absence of the resistance of the surrounding medium, i.e., in a vacuum. In that case, the process of divergence of the jet can be prevented by several means. In particular, we shall assume that the time during which the jet is accelerated is sufficiently small, or that the jet is contracted by its proper magnetic field. We shall not consider the processes of jet formation (consult, for instance, Ref. 3)

1. ON THE MOTION OF CONDUCTORS

We can obtain a rudimentary picture of the motion of a current–conducting plasma jet in a magnetic field if we consider it as a conductor with resistance R and inductance L. We shall examine the simplest case of a straight conductor of length l, which makes contact with conducting rails and moves perpendicularly to a homogeneous magnetic field $H(t)$. A voltage $U(t)$ is applied to the rails. The equations for this case are

$$m\frac{dv}{dt} = \frac{1}{c}IHl, \tag{1}$$

$$\frac{1}{c^2}\frac{dLI}{dt} = -\frac{1}{c}lHv - IR + U,$$

where I is the current intensity in the circuit.*

Let R, L, m, H, and U be constant. For these conditions, and for a relatively small resistance of the circuit, i.e., for $Q = \omega L/R >> 1$, we have

$$I = I_0 \sin\omega t; \tag{2}$$

$$I_0 = c^2U/L\omega = cu\sqrt{m/L}; \quad u = cU/lH;$$

$$x = u(t - \omega^{-1}\sin\omega t); \tag{2a}$$

$$v = u(1 - \cos\omega t); \quad \omega = Hl/\sqrt{Lm}.$$

We shall call u the drift velocity and shall assume it to be much smaller than the velocity of light. Formula (2a) indicates that the motion of the conductor can be represented as a drift with a constant velocity u, upon which oscillations with the amplitude u/ω are superimposed. The maximum velocity $V = 2u$ will be attained by the conductor after the time $T_0 = \pi/\omega$, which we shall call the acceleration time. The path traversed during this time is $a = uT_0$.

In the second extreme case, where the inductance is small ($Q << 1$), we have

$$x = ut - T_0u(1 - e^{-t/T_0}); \tag{3}$$

$$I = (U/R)e^{-t/T_0}; \quad T_0 = c^2Rm/H^2l^2,$$

that is, the velocity asymptotically approaches the drift velocity.

It is useful to note that, for $R = 0$, the system of equations (1) is analogous to the equations of motion of a single charged particle in mutually perpendicular electric and magnetic fields. If the fields E and H are constant, the motion of the particle, as is well known,[9] consists of a drift with the velocity $u = cE/H$ with superimposed uniform circular motion with the angular velocity $\omega = eH/mc$.

Apart from the case of the direct contact coupling between the conductor and the current source, inductive coupling is of considerable interest. This case can be realized if a closed ring is placed within within a changing magnetic field. In this case, an induced current flows in the ring and under the influence of the magnetic field, the ring will start moving.

A similar case of gas discharge, the so-called ring electrodeless discharge, is known. It is conspicuous by the fact that, due to the absence of any electrodes, the current in such discharge can attain a very large value, even at quite low pressures. For instance, at a pressure of 1.7×10^{-4} mm Hg and for an EMF of the rotor field in the circuit equal to 8V, the current in the experiments of Smith[4] using mercury vapors attained 450A. The generator frequency was of the order of 900 c/s.

If we assume the jet to be sufficiently thin and axially symmetric, then we can write the system of equations, describing the displacement of the ring permeated by the flux Φ perpendicularly to its plane (along the z-axis) and the expansion of its radius, making use of the Lagrangian

$$\mathscr{L} = (m/2)(\dot{r}^2 + \dot{z}^2) \tag{4}$$

$$+ (LI^2/2c^2) + (\Phi I/c) - W(r),$$

where $W(r)$ is the potential of the elastic stresses acting in the cross-section of the jet, and I can be regarded as a generalized velocity q. It should be noted that, for the densities encountered in modern accelerators, $W(r) = 0$ and $L = c^2 l^2 m_1^2/e^2 m$, a case which we shall treat in greater detail below [see Eq. (14)].

It can be seen from Eq. (4) that, for the case where both the resistance and $W(r)$ are small, the kinetic energy of the ring leaving the field will be of the order of $\Phi_0^2/2L$, under the obvious condition that the current intensity at this moment will drop to zero. Φ_0 and L_0 denote certain values of the magnetic flux and of the inductance, characteristic for the process. The mean current will be of the order of $c\Phi_0/L_0$. In the simplest case, for example, where an ideally conducting ring of a constant radius and inductance moves in the direction of the z-axis, with the ring permeated by the flux

$$\Phi = \Phi_0(t/T)(1 - z/a), \tag{5}$$

the velocity of ejection and the current are, respectively,

---

*U includes the EMF induced by the changing magnetic field.

$$V = 2\Phi_0 / 3\sqrt{Lm}, \qquad (6)$$

$$I = (c\Phi_0 t / LT_0)(1 - z/a).$$

The initial velocity and current are assumed to be zero.* The acceleration time and the corresponding ing path a are connected by the relation

$$T_0 = 4a\sqrt{mL}/\Phi_0. \qquad (7)$$

In the second extreme case of practical interest, namely that of plane motion of a ring that contracts to a point, the results obtained correspond to the estimate given above.

Similarly to the fact that the equations of motion for a particle in a homogeneous field are identical with the equations of motion for a straight conductor, the Lagrangian (4) is identical with the Lagrangian describing the motion of a charged particle in an axially-symmetric magnetic field.

2. MOTION OF E-CONNECTED PARTICLES

We shall consider a neutral jet of ions and electrons of sufficiently low density that we can neglect the collisions between the particles as well as their magnetic field, and we shall account for the electric interaction between the particles only. Such a cloud of particles we shall call an E- plasma, and the particles, E-connected.

The behavior of the plasma can be described by the system of two kinetic equations of Vlasov,[6] written for the electrons and the ions respectively, taking into account the self-consistent field. For simplicity, we shall consider the plane case, and assume that the plasma jet has the shape of an infinite (in y and z) layer of finite thickness, perpendicular to the x-axis. In order to avoid the necessity of having to account for the divergence of the plasma, we shall assume that the thickness of the layer is much larger than $v_T^i\ T_0$, where v_T^i denotes the mean thermal velocity of ions. In addition, in the present treatment we shall limit ourselves to the solutions with constant density, which correspond to $R = 0$, being equivalent to neglecting the terms proportional to $\partial f/\partial r$ in the kinetic equations.

Under these conditions, the above-mentioned system of equations can, by averaging over the velocities, be written in the following way, valid for the whole region of constant concentration:

$$m_e d\mathbf{v}_e / dt = -e(\mathbf{E}_0 + \mathbf{E}') - \frac{e}{c}[\mathbf{v}_e\mathbf{H}]; \qquad (8)$$

$$m_i d\mathbf{v}_i / dt = e(\mathbf{E}_0 + \mathbf{E}') + \frac{e}{c}[\mathbf{v}_i\mathbf{H}]. \qquad (8a)$$

where $\mathbf{v}_i$ and $\mathbf{v}_e$ denote the velocities of the ordered motion of ions and electrons respectively. In the following discussion, we shall call $\mathbf{v}$ simply the particle velocity and, correspondingly, talk about its trajectory and coordinates, having in mind the line of current and the coordinates of a point on it. It can be assumed that, if the displacement of particles with respect to each other will be sufficiently small compared to the layer thickness, then the solution of the above system of equations will correctly describe the behavior of the cloud.

Since the plasma as a whole is neutral and the problem is one-dimensional, we have, in the region under consideration,

$$E' = 4\pi e \int\limits_{-\infty}^{x} (n_e - n_i)\, dx = 4\pi e n (x_e - x_i) \qquad (9)$$

independently of the state of the plasma on the surface (Fig. 1).* x_i and x_e are the coordinates of two fixed particles which coincided at the initial moment when the plasma was non-polarized.

Substituting (9) into (8), we obtain a system of ordinary linear equations. For convenience, we shall introduce the notation

$$\omega_0^2 = 4\pi e^2 n / m_e, \ \mu = m_e / m_i,$$

$$\omega_e = eH / m_e c, \ \lambda^2 = \omega_e^2 / \omega_0^2$$

and assume the fields to be constant, and the plasma to be at rest and $x_i = x_e = 0$ for $t = 0$.

a) We shall consider the motion of particles in the direction of the x-axis. The characteristic equation of the system (8) has two roots

$$\Omega_1^2 \approx \mu\omega_e^2(1 + \mu\lambda^2)/(1 + \lambda^2), \ \Omega_2^2 \approx \omega_e^2 + \omega_0^2. \qquad (10)$$

---

*The expression for z, under the condition (5) and for $z(0) = 0$, $z(0) = 0$, $I(0) = 0$ is of the following form:[5]

$$z = a\left[\frac{\alpha}{3\cdot 4}\left(\frac{t}{T_0}\right)^4 - \frac{\alpha^2}{3\cdot 4\cdot 7\cdot 8}\left(\frac{t}{T_0}\right)^8 + \cdots\right],$$

$$\alpha = \frac{c^2\Phi_0^2 T_0^2}{mLa^2}.$$

*We shall obtain a formula analogous to (9) also in the case where the cross-section of the jet is, and remains in the process of acceleration, of the form of an ellipse or a circle.

In these formulas, we neglected those of the terms $\sim \mu^2$ which do not qualitatively change the relation between Ω and λ. The root Ω_1 equals the angular frequency of ion rotation in a magnetic field for $\lambda \to \infty$, that is, for diminishing concentration of particles, and for $\lambda \to 0$ tends to $\omega_e \sqrt{\mu}$. The root Ω_2 gives the electron rotation frequency for $\lambda \to \infty$, and equals the Langmuir frequency for $\lambda \to 0$. Evidently, the root Ω_1 for $\lambda \to 0$ pertains to the movement of the jet as a whole, while Ω_2 characterizes its polarization vibration.

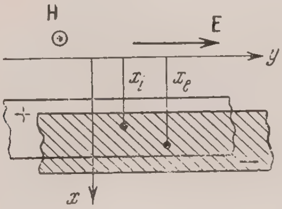

FIG. 1

The motion of particles in the x direction, for our initial conditions, will be as follows:

$$x_e = u\left[t - \frac{1}{\Omega_1^2(1+\lambda^2)}\sin\Omega_1 t - \frac{\lambda^2}{\Omega_2(1+\lambda^2)}\sin\Omega_2 t\right]; \tag{11}$$

$$x_i = u\left[t - \frac{1}{\Omega_1^2}\sin\Omega_1 t + \frac{\lambda^2\mu}{\Omega_2(1+\lambda^2)}\sin\Omega_2 t\right]. \tag{11a}$$

From these formulas it is clear that, for small λ, the electrons lead the ions for the first half of the acceleration time (that is, for $t < \pi/2\Omega_1$), while during the second half of that period the ions catch up with them.

The maximum displacement of the one type of particles with respect to the other equals, in the central region of the layer,

$$\Delta = u\lambda^2/\Omega_1 = E/4\pi en\sqrt{\mu}. \tag{12}$$

Of the same order of magnitude is the region of the diffuse boundary of the plasma, due to the difference in the motion of ions and electrons. Consequently, it is necessary for the validity of our laws that the layer thickness be $<< \Delta$. For instance, for an external field of 3000 V/cm and $n \sim 10^{12}$ cm^{-3}, we have $\Delta \sim 0.1$ cm. It is interesting to note that the maximum value of the polarization field is $1/\sqrt{\mu}$ times larger than the external field,

b) we shall now consider the displacement of particles in the direction of the y-axis. From (8) and (11), we have, for $\lambda \to 0$,

$$(v_i)_y \approx \sqrt{\mu}\, u \sin(\sqrt{\mu}\,\omega_e t); \tag{13}$$

$$(v_e)_y \approx (u/\sqrt{\mu}) \sin(\sqrt{\mu}\,\omega_e t).$$

Integrating over t, we find that the displacement of ions in the y-direction is smaller by a factor of $1/\mu$ than that of electrons. This is exactly the opposite of what takes place for free particles, and resembles the situation in metals. Ions in an E-connected jet accelerate because of the electron current. The trajectories of the particles are shown schematically in Fig. 2.

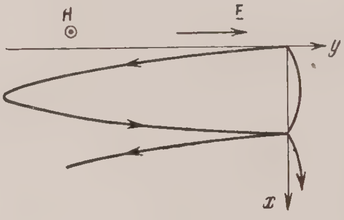

FIG. 2

It is important to mention that the above calculation does not take into account the abrupt stopping of particles on the electrodes and, therefore, pertains in fact to a ring-shaped jet.

It can be shown, making use of the conservation of energy, that the character of the results obtained for the idealized one-dimensional case, including formula (12), will not change for the case of a ring-shaped jet of finite cross-section, if the magnetic field safeguards the stability of the cloud in the direction perpendicular to the direction of motion [see, for instance, (19)].

c) it is not difficult to find the coefficient of self-induction for a jet of E-connected particles, under some limiting conditions fulfilled for $\lambda \to 0$, making use of the equations of motion of the particles, containing the interaction forces acting between the particles. This coefficient of self-induction L_I arises due to the inertia of particles, and therefore we denote it as inertial. For a cloud of similar particles with mass m_1 it equals

$$L_{\mathrm{I}} = c^2 l^2 m_1^2 / e^2 m,$$

and for a cloud consisting of ions and electrons (see Ref. 10)

$$L_{\mathrm{I}} = c^2 l^2 m_i m_e / e^2 m, \qquad (14)$$

where m is the total mass of the jet and l its length. Taking into account that $m_e << m_i$, we come to the conclusion that in this case L_{I} is determined by the inertia of electrons. Formula (14) is correct for thecase of a ring-shaped plasma as well.

It can be seen from (14) that L_{I} decreases without limits for increasing concentration and, therefore, for a considerable value of concentration the coefficient of self–induction of the jet will not any more equal L_{I} but L_{E} – the electromagnetic coefficient of self–induction of the jet,* which may be calculated from the distribution of currents according to well known rules of electrodynamics.

Since, in the absence of magnetic materials in the immediate vicinity of the jet, L_{E} for a straight conductor or a ring equals, in Gaussian system of units,

$$L_{\mathrm{E}} = \Lambda l, \qquad (15)$$

where Λ is a value of the order of unity,[7] then the concentration n_L for which $L_{\mathrm{I}} = L_{\mathrm{E}}$, is given by the formula

$$n_L = (4 / \Lambda S) \cdot 10^{12} \ \text{см}^{-3}, \qquad (16)$$

where S is the cross-section of the jet.

d) The influence of the proper magnetic field of the jet is not limited only to the change of the coefficient of self–induction, but causes a contradiction of the jet as well. This takes place because the forward motion of the front particles is decelerated by the proper magnetic field of the jet, while the motion of the rear particles is accelerated.

In orderto neglect this effect, as it has been done in the preceding calculation, it is necessary that the jet density be smaller than or of the order of

$$n_m = \alpha n_L \Lambda (b / a)^2 \qquad (17)$$

(see reference 11), where α is a value of the order of unity depending on the field structure, the form of the jet cross–section etc. and b is the half–width of the jet. If the jet density is much larger than n_m, then the jet will be strongly contracted in the process of acceleration under the influence of the proper magnetic field. As a result, the velocity of ejection may be considerably decreased. This is connected both with the increase in the resistance of the ring and the increase of the influence of the electromagnetic inductance.

Consequently, the largest velocities of ejection are attainable for thecase of an E-plasma. Since for that case $L \approx L_{\mathrm{I}}$, it follows from (6) that

$$V \approx 2\Phi_0 / 3\sqrt{Lm} \approx 2{,}7 \cdot 10^5 \, \Phi_0 / \sqrt{A}\,(2\pi r_0), \qquad (18)$$

where A is the atomic weight of the ion. It follows that the ejection velocity will is, in this case, independent of the total mass of the ring.

For $n >> n_L$, the ejection velocity will decrease as $\sim m^{-1/2}$ even in the absence of resistance if the external flux Φ_0 remains constant. Something similar takes place for an induction accelerator with immobile jet of the betatron type if we take into account that the current intensity is Φ_0 / L and the beam energy equals $\Phi_0^2 / 2L$.

Finally, in connection with all that was said above, we want to make two additional comments:

1) Condition (17) indicates that the concentrations for which the magnetic interaction between the particles can be neglected are relatively low, and it can be therefore assumed that, in this region, the resistance of the jet will be relatively low.

2) It is necessary for the existence of a ring of E-plasma that the magnetic field safeguards its stability in the direction perpendicular to the acceleration. The necessary conditions for that, which have to be imposed on the field, can be obtained from equation (4). The stability conditions both for the ions and the electrons are then fulfilled.* As an example of such a field for which the radius r_0 of the ring remains constant we may take

$$A_\varphi = {}^1\!/_2 \, H_0(t)\,(a - z)\,(r / r_0 + r_0 / r). \qquad (19)$$

3. EJECTION VELOCITY OF A DENSE JET

Let us consider a dense jet, prevented from diverging by its proper magnetic field. Let the state of the plasma in it be stationary, so that the condition $\rho = \gamma p / c_T^2$, where C_T is the sound velocity in the plasma, be fulfilled. Assuming $p \sim H^2 / 4\pi$ and taking into the account that for the absence of resistance we have $I \sim V\sqrt{m/L}$, we obtain, after a simple calculation, the following expression:

---

*This corresponds to taking into account the magnetic interaction between the particles.

*With the exception, possibly, of the initial moment, since the depth of the potential well[8] in which the oscillations of particles take place is of the order of $\sim 1/m$ and the progressing plasma can be in a state of thermal equilibrium.

$$V = kc_T \sqrt{\Lambda},$$

Λ has been determined above [see Eq.(15)] and $k \sim 1$. The ejection velocity, therefore, is found to be of the order of the maximum velocity of sound in the jet during the acceleration stage. The formula is independent of the nature of the coupling with the current source (contact or induction) but since the flux Φ_0 in the ring is known and $V \sim \Phi_0 / \sqrt{Lm}$, the relation between m and c_T follows.

The author wishes to express his gratitude to Prof. A. A. Sokolov for the interest shown in the present work, and to G. M. Strakhovskii for the discussion of problems connected with it.

---

1 O. Bron, *Motion of the Electric Arc in a Magnetic Field*, Gosenergoizdat Moscow–Leningrad 1944.

2 O. Bron, *Electric Arc in Control Apparatus*, Gosenergoizdat, Moscow–Leningrad 1954.

3 R. Weiss, Z. Physik **138**, 170 (1954).

4 C. G. Smith, Phys. Rev. **59**, 991 (1941).

5 I. M. Ryzhik and I. S. Gradshtein, *Tables of Integrals* etc. GITTL, Moscow–Leningrad 1951.

6 A. A. Vlasov, *Theory of Many Particles*, GITTL, Moscow Leningrad 1950.

7 W. Smythe, *Electrostatics and Electrodynamics*, IIL, Moscow, 1954.(Russian translation).

8 J. A. Rajchmann and W.H. Cherry, J. Franklin Inst. **243**, 4, 1947.

9 L. Landau and E. Lifshitz, *Classical Theory of Fields*.

10 H. Alfvén, *Cosmical Electrodynamics*, IIL, Moscow (1952) (Russian translation)

11 W. Bennett, Phys.Rev. **98**, 1584 (1955).

Translated by H.Kasha
64

SOVIET PHYSICS JETP VOLUME 5, NUMBER 2 SEPTEMBER, 1957

Investigation of U^{235} Fission γ Rays in the Energy Region up to 250 kev

V. V. SKLIAREVSKII, D. E. FOMENKO AND E. P. STEPANOV
Atomic Energy Institute, Academy of Sciences, USSR

(Submitted to JETP editor September 24, 1956)
J. Exptl. Theoret. Phys. (U.S.S.R.) **32**, 256-262 (February, 1957)

A scintillation spectrometer with a NaI(Tl) crystal and a proportional counter connected in coincidence with a fission chamber was used to measure the U^{235} fission γ spectrum in the energy range up to 250 kev. Gamma rays with energies of 30 ± 1.5 and 210 ± 10 kev were detected, as well as a broad distribution in the 110 to 150 kev region, which apparently consists of several lines. It has been found that in the investigated energy region most of the fission γ rays are emitted by fission fragments with life times between 0.5×10^{-9} and 2.5×10^{-9} sec.

The measurements made with the proportional counter showed that the line at 30 kev is not monochromatic and apparently corresponds to x radiation (K line) from heavy fission fragments with different Z.

1. INTRODUCTION

FISSION γ rays have thus far been the subject of very few investigations, and there have been only brief reports on the results of these. Rose and Wilson[1] have measured the angular distribution of fission γ rays relative to the direction in which the fission fragments emerge. Voitovetskii, Levin, and Marchenko[2] have discovered several monochromatic γ rays in the low energy region. Other papers[3-5] deal with measurements of either the average energy of fission γ rays or their spectrum.

The measurement of a fission γ ray spectrum by itself furnishes no basis for any conclusions as to the mechanism of the radiation. Theoretically one cannot rule out the possibility that some or all fission γ rays are connected with the processes that occur at the moment of fission. On the other hand they may be emitted by fission fragments in excited states.

In this investigation the geometric distribution method, consisting of making separate measurements of the γ rays emitted by fission fragments was used. This method has made it possible to establish that the principal part of fission γ rays in the energy region up to 250 kev is emitted by fission fragments.

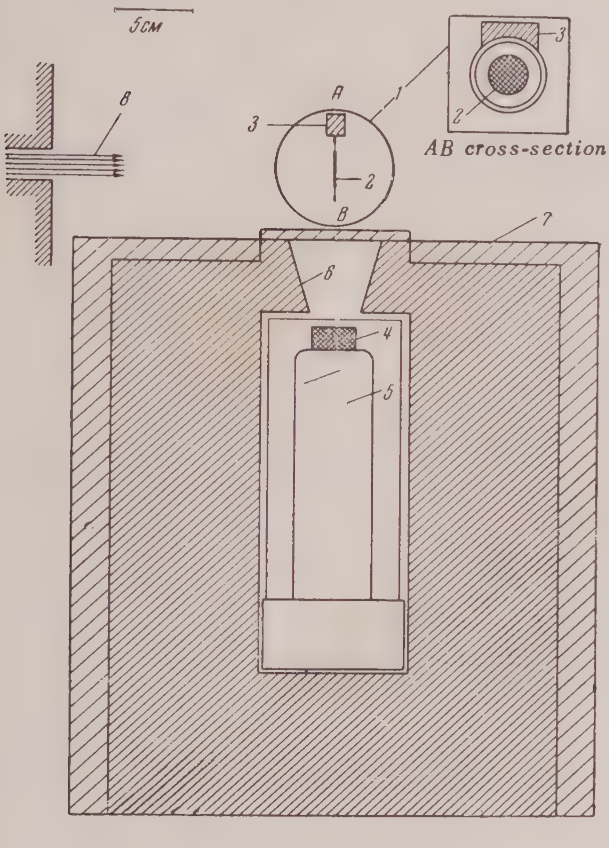

FIG. 1. Experimental Setup. *1* – fission chamber, *2* – layer of U^{235}, *3* – lead screen, *4* – NaI(Tl) crystal, *5* – photomultiplier, *6* – lead shield, *7* – boron, *8* – neutron beam.

2. EXPERIMENTAL APPARATUS

Figure 1 shows the experimental arrangement. The ionization chamber with a layer of U^{235} was located in a beam of thermal neutrons from the RFT reactor. The beam was 2.3 cm in diameter. The layer of U^{235} used had a density of about 1 mg/cm^2 and was spread on a nylon film*. This layer was covered by a thin conductive layer of silver which served as the collecting electrode for the chamber. The total pulse from both fragments was obtained from this electrode; furthermore, the high voltage was supplied to it. The chamber housing was the other electrode. The chamber was filled with a mixture of argon and methane (30%) to a pressure of 10 cm. At this pressure practically all the fission fragments emitted by the layer reached the walls of the chamber housing.

A scintillation spectrometer with a crystal of NaI(Tl) was used to measure the γ ray spectrum. The crystal was cylindrical in form and had a diameter of 3.0 cm and a height of 1.4 cm. A type "C" spectrometric photomultiplier was used. The crystal and photomultiplier were surrounded by a lead shield with a conical opening through which γ rays from the fission chamber irradiated the crystal. The distance between the center of the layer and the surface of the crystal was 11.5 cm. The scintillation spectrometer was calibrated by γ rays with energies of 661 kev (Cs^{137}), 102 and 41.7 kev (Gd^{153}). The resolution for photopeaks from these radiations was respectively 8, 20 and 30%.

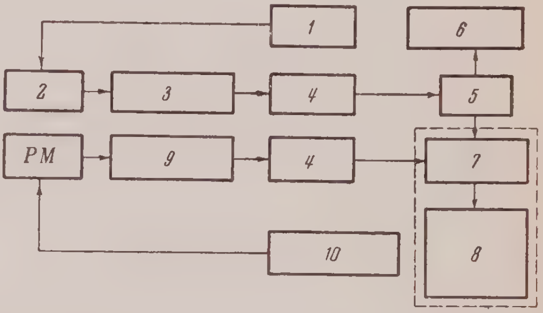

FIG. 2. Block diagram of the electronic apparatus. *1* – supply battery, *2* – fission chamber, *3* – pre-amplifier, *4* – linear amplifier, *5* – delay line, *6* – counter, to 10,000, *7* – coincidence circuit, *8* – channel amplitude analyzer, *9* – cathode follower, *10* – high-voltage rectifier.

Figure 2 is a block diagram of the electronic apparatus. Pulses from the photomultiplier were amplified by the linear amplifier and entered the coincidence circuit together with the amplified pulses from the fission chamber. Those pulses from the photomultiplier which coincide with the fission chamber pulses entered the 30-channel amplitude analyzer. In the fission chamber channel there was a variable delay, which made it possible to obtain the time resolution of the equipment. The resolving time used for the coincidence circuit was $2t = 0.4$ microseconds. Measurements of the resolution curve at different times showed that for $2t = 0.4$ microseconds, the counting efficiency for true coincidences was close to unity. The rate of counting fission fragments was $\sim 2 \times 10^4$ counts/sec.

---

* This layer was graciously presented by V. I. Mostov, to whom the author expresses his gratitude.

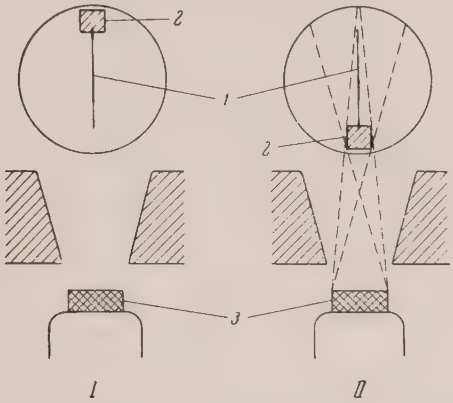

FIG. 3. Measurement geometry. *I* – measurement of the total intensity of the fission γ rays; *II* – measurement of γ rays emitted by fission fragments. *1* – layer of U^{235}, *2* – lead screen, *3* – NaI(Tl) crystal.

3. THE METHOD OF MEASUREMENT

The fission γ ray spectra were measured with the fission chamber in two different positions in relation to the crystal (positions I and II), as shown in Fig. 3. As is apparent from this figure, in position I the crystal records γ rays emitted by the layer of U^{235}, i.e., formed during the fission process, and γ rays emitted by fission fragments. In position II the layer and the area of space adjacent to it are closed off from the crystal by the lead screen, 1.5 cm thick. Such a screen absorbs practically all γ rays up to 250 kev. Therefore in position II the crystal records only γ rays emitted by fission fragments. In order to enter the chamber region "seen" by the crystal, the fission fragments must cover an average distance of $l = 1.5$ cm.

This method permits one to isolate the gamma radiation from fission fragments emitted after $t = l/v_{\text{frag}} \approx 1.3 \times 10^{-9}$ sec. after the act of fission. It is also possible to arrive at a quantitative evaluation of the life time of the excited states of the fission fragments which emit these γ rays.

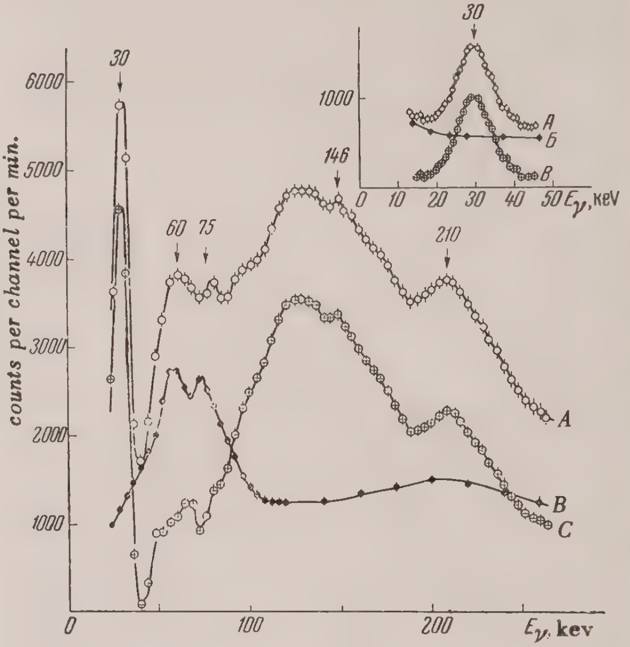

FIG. 4. Fission γ ray spectra obtained in position *I*.

4. RESULTS OF THE MEASUREMENTS

The results of the measurements made in position I are shown in Fig. 4, and the results of those made in position II are shown in Fig. 5. The A curves in these graphs represent the spectra of true coincidences, which were obtained by subtracting the spectra of random coincidences. The number of random coincidences for position I amounted to 2-4% and for position II, 6-10% of the total number of coincidences.

The B curves represent the spectra of true coincidences obtained when the chamber was separated from the crystal by a lead absorber whose thickness was sufficient for total absorption of the measured γ rays (0.16 mm for the 30 kev region and 2.5 mm for the rest of the spectrum). Thus, the B curves give the background of true coincidences created in the measured portion of the spectrum by hard fission γ rays and neutrons. The difference between the A and B curves (the C curve) gives the spectrum of pulses solely from fission γ rays in the measured energy region.

The fission chamber served as the monitor for all the measurements. The measurement time in position I (~ 30 min) corresponded to $N_f = 3 \times 10^7$, total number of recorded fission fragments, and in position II (~ 60 min) to $N_f = 6 \times 10^7$.

As can be seen from Figs. 4 and 5, the radiation intensity at energy peaks of 60 and 75 kev is but slightly reduced by the lead absorber, which would have completely absorbed γ rays with these energies. Therefore, these peaks must be attributed mainly to secondary effects. Actually, the peak at 60 kev is produced by inelastic scattering of fission neutrons by the iodine nuclei in the crystal of NaI(Tl). The peak at 75 kev represents X radiation (*K* line) from the lead and is formed by fission γ rays and neutrons in the shield surrounding the crystal.

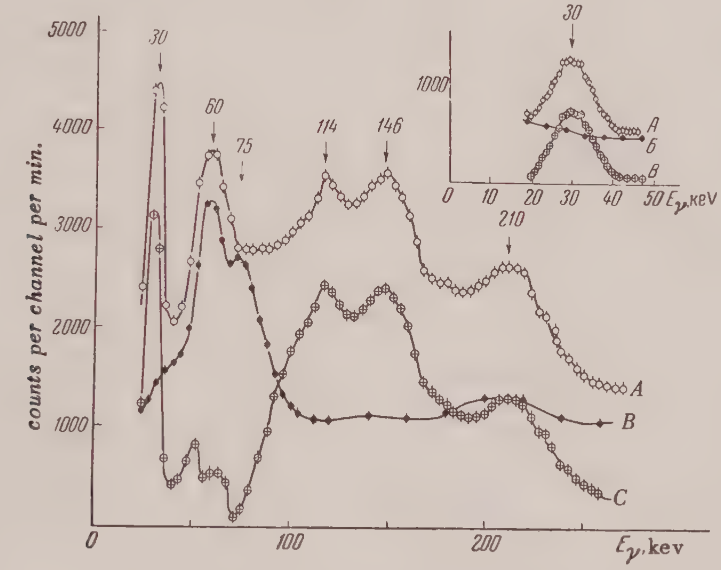

FIG. 5. Fission γ ray spectra obtained in position *II*.

The fission γ ray spectra measured in positions I and II (the C curves in Fig. 4 and 5) are plotted together in Fig. 6 for comparison ,and they coincide at an energy of 114 kev. As can be seen

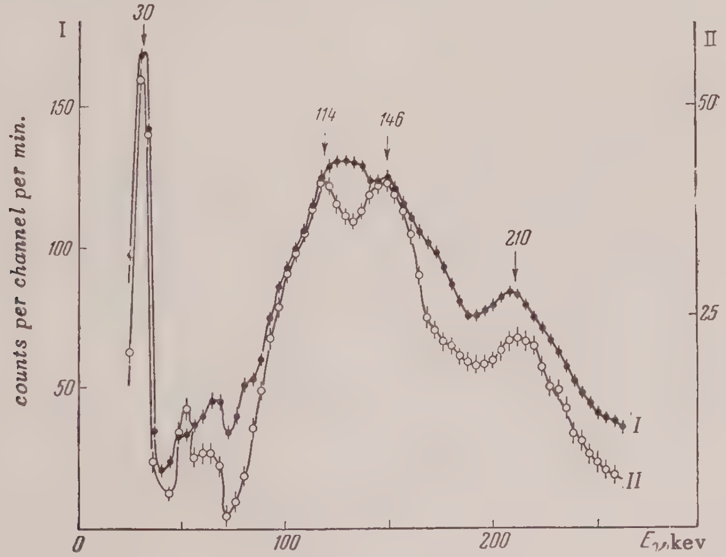

FIG. 6. Comparison of fission γ ray spectra obtained in positions *I* and *II*.

from Fig. 6, the spectra for I and II are almost identical in form, while the intensity of the spectrum for II is approximately 3 times less than that for I. In both spectra there are γ ray lines at 30 and 210 kev. Moreover, in the energy region 110-150 kev, there is an intense broad distribution whose form differs somewhat in the spectra for I and II. In the spectrum for II this distribution consists of two distinctly separate maxima at energies of 114 and 146 kev. Apparently the spectrum for I contains the greater number of unresolved lines. It should be remarked that this portion of the spectrum was investigated with special care, and the difference in the forms of the spectra for I and II was securely established for this region. The spectrum for I was also measured when screen 3 (see Fig. 1) was absent, and it was found that the screen does not distort the form of the spectrum.

γ ray energy	Number of γ quanta per fission, ν_I, measured in position *I*.	The ratio of the γ intensity measured in positions *I* and *II* ν_I/ν_{II}.
30 ± 1.5 kev	0.42 ± 0.12	3.1 ± 0.15
Group of lines in 110-150 kev region.	0.94 ± 0.2	3.2 ± 0.2
Single line or a group of lines in 210 kev region.	0.5 ± 0.10	3.8 ± 0.2

Our results with regard to the spectrum for I are in agreement with the results described in Ref. 7. The first data on the presence of several lines in the fission γ ray spectrum are reported in Ref. 2.

The table presents the energies of the fission γ rays and their absolute intensities.

When ν_I was determined, allowance was made for γ ray absorption by all substances located between the chamber and crystal. The solid angle was determined from the control measurements on γ rays from a Am^{241} source (60 kev), which is an alpha emittor. These measurements were made in the same geometry and with the same apparatus as the measurements of the fission γ rays. The values for ν_I/ν_{II} were determined from the ratios of the areas of the spectra for I and II. Therefore, the error in determining ν_I/ν_{II} was less than the error in ν_I.

5. MEASUREMENTS WITH THE PROPORTIONAL COUNTER

The fission γ ray spectrum for the energy region up to 100 kev had already been measured by us[6] with a proportional counter filled with a mixture of krypton or xenon and methane (10%) under pressure of 800 mm of mercury. The measurements with the proportional counter were also made in two positions, one of which measured only γ rays from fission fragments and the other of which measured all fission γ rays. These measurements are in good agreement with the measurements made with the scintillation spectrometer, both as to the forms of the spectrum and its identity when measured in the two positions.

It is interesting that in the measurements made with the proportional counter the half-width of the 30 kev line (≈ 30%) proved to be considerably greater than the half-width that should have characterized a monochromatic line of this energy (for example, the half-width for the 24 kev x-ray line from In^{114m} measured 15%). This may be explained by the fact that the 30 kev line represents x-radiation due to internal conversion of γ radiation from fission fragments with different Z. It is also noteworthy that a 30 kev line is likewise present in the spectra of U^{233} and Pu^{239} fission γ rays.

6. DISCUSSION OF THE RESULTS. AN EVALUATION OF THE LIFE TIME FOR FISSION γ RAY EMISSION

The results obtained can be summarized as follows: 1) the spectra measured in positions I and II have approximately the same form; 2) for the measured energy region ν_I/ν_{II} lies within the range 3.1-3.8. On the basis of these results it is possible to make alternate assumptions regarding the origin of fission γ rays.

1. The γ rays measured in positions I and II are attributable to a single process – γ ray emission by fission fragments in excited states.
2. The γ rays measured in positions I and II were emitted as the result of different processes with different life times, one process consisting of γ ray emission during fission and the other of γ ray emission by fission fragments. In this case almost all the coincidence in the forms of the spectra in the two circumstances would be accidental.

The second assumption would be unnatural for the main portion of the measured γ ray spectrum. Using the first assumption, one can evaluate the lifetime of the excited states of the fission fragments that emit γ rays. Assuming that the γ rays measured in positions I and II were emitted with identical lifetime τ, we can easily derive (by elementary reasoning) the equation: $\tau = t/\ln(\nu_I/\nu_{II})$, where t is the average transit time of fragments through the region "unseen" in position II and is equal to $\sim 1.3 \times 10^{-9}$ sec, and ν_I/ν_{II} is the ratio of the intensity of γ rays with the given τ, emitted during the time from 0 to ∞, to the intensity of those γ rays emitted during the time from t to ∞. However, it must be noted that ν_{II} must be less than ν_I, not merely on account of disintegration but also because of the fact that some of the fission particles do not emerge at all beyond the limit of the "unseen" region in position II. Computation has shown that the contribution of these fission fragments is 20-25%, while the experimental value for ν_I/ν_{II} lies within the range 3.1-3.8. Therefore, the indicated correction can be neglected and then from $\nu_I/\nu_{II} = 3.1 - 3.8$ we obtain $\tau \approx (1.0\text{-}1.2) \times 10^{-9}$ sec. The true life time for the main portion of fission γ rays in the measured energy region can vary by no more than a factor two from this value, i.e., τ lies within the range $(0.5\text{-}2.5) \times 10^{-9}$ sec. The major error in the determination of τ is due to the indefiniteness in the value of t, which is caused both by inaccuracy in determining the distance crossed by the fragments in the "unseen" region and by the difference in the velocity of heavy and light fragments, $(0.9\text{-}1.4) \times 10^9$ cm/sec. To obtain more accurate results it would be necessary to collimate the fission fragments and sort them energy wise.

We should point out that some difference in the forms of the spectra for I and II, which appears especially clear near 120 kev, indicates the presence of γ rays either emitted by fission fragments, though with a life time far less than 10^{-9} sec, or directly released in the process of fission. The last possibility is especially interesting but requires more detailed investigation.

The results obtained can be explained in the following manner. The spectrum of fission γ rays in the energy region of 100-250 kev consists of many γ ray lines from emissions by various fission fragments in excited states. These states arise after the fission fragments emit neutrons and harder γ rays. The value of the life time of these states ($\sim 10^{-9}$ sec) appears to indicate that transitions from them are of a dipole nature. A quadrupole nuclear moment of the order of 2.5×10^{-24} cm^2 corresponds to a quadrupole transition with a life time of 10^{-9} sec. These quadrupole moments are possessed by greatly deformed nuclei in the rare earth region. However, fission fragments with $A > 145$, i.e., corresponding to these nuclei, have small yields, too small to explain the observed γ ray intensity.

The multichannel analyzer used in this investigation was operated by Engineer G. P. Mel'nikov to whom the authors are deeply grateful.

The authors express their obligation to Academician I. V. Kurchatov for his interest in the investigation and for his help in conducting it and also to L. V. Groshev and V. M. Strutinskii for reviewing the results.

---

[1] W. I. Whitehouse, Prog. Nuclear Physics **2**, 151 (1952).

[2] Voitovetskii, Levin and Marchenko, Report of the Atomic Energy Institute, Akad. Nauk SSSR (1955).

[3] Kinsey, Hanna and Van Patter, Canad. J. Res. **26A**, 79 (1948).

[4] H. Goldstein, Nucleonics **11**, 41 (1953).

[5] R. B. Leachman, Determinations of Fission Quantities of Importance to Reactors. Report at the International Conference on the Peaceful use of Atomic Energy at Geneva, 1955.

[6] Skliarevskii, Fomenko and Stepanov, Report of the Atomic Energy Institute, Akad. Nauk SSSR (1955).

[7] Voitovetskii, Levin and Marchenko, J. Exptl. Theoret. Phys. USSR **32**, 263 (1957); Soviet Phys. JETP **5**, 184 (1957).

Translated by A. Skumanich
57

SOVIET PHYSICS JETP VOLUME 5, NUMBER 2 SEPTEMBER, 1957

Quantum States and Optical Transitions of the F_2^+ Center Electron

M. F. Deigen, V. L. Vinetskii
Kiev State University

(Received by JETP editor November 19, 1955)
J. Exptl. Theoret. Phys. (U.S.S.R.) 32, 289–295 (1957)

The quantum states of a system consisting of two negative vacancies and an electron in an ionic crystal (F_2^+ center) are considered. The thermal dissociation and ground state energies of the system are computed by quantum mechanical consideration of the motion of lattice ions. The parameters of the optical absorption band—its position and half–width—have been determined. For illustration the numerical values have been obtained using this theory for KCl and KBr crystals; the results are in a satisfactory agreement with the experimental results.

An intensive experimental study of impurity absorption in ionic crystals now makes it possible at least for a part of the spectrum, to construct models of several absorbing centers (color centers). This discussion will concern the *R* and *M* absorption bands found at wavelengths longer than the *F* band.

Seitz[1] has attempted the foundation of a model of the absorbing centers which correspond to those bands with the aid of an analysis of the experimental data on the kinetics of their production, and both thermal and optical dissociation. In particular, one of the two *R* bands (R_2 band) was identified with the absorption band of F_2 centers, i.e., a system consisting of two negative vacancies and two electrons. The second band (R_1 band) was identified as an absorption band of F_2^+ centers. It is natural that, without a quantitative calculation of the parameters of these bands, it was not possible to carry out such identification at all reliably.

In the previous works [2,3] one of the authors calculated the quantum states and parameters of the F_2 center absorption band. These calculations showed that the parameters of an F_2 absorption band are indeed very close to the corresponding parameters of an R_2 band.

In recent works[4,5] the absorption of light by F_2 and F_2^+ centers was studied in two approximations: the approximation of crystal–continuum which was earlier employed by Pekar and Deigen[2,3], and the molecular orbital method.[5] In the molecular orbital approximation, the authors entirely ignored the interaction of the electron with the optical vibration modes of the crystal (the polarization of the crystal by the field of the electron), calculated incorrectly the overlap integrals, and took into account only the first sphere of ions surrounding the vacancy. Such rough approximation did not lead to an agreement of the theory with the experiment. In calculating the frequency of the optical transition by the first technique the following material errors were made: 1. the periodic crystal potential was igonored; 2. to determine the parameters of the ground and excited states in the Franck–Condon approximation the authors calculated the energy of the "self–consistent" state [6,2] instead of solving the Schrö–dinger equation for the system in a fixed potential well.

Calculations show that every one of the errors enumerated above can cause errors of the order of magnitude of the calculated quantity. Therefore the results of Nagamiya et al [4,5] are in sharp disagreement with experiment.

The quantum states and optical transitions of F_2^+ center are considered in the present work by a method developed previously[2,3] which does not contain the above errors.

1. THE GROUND STATE OF THE SYSTEM

In a complete analogy with the previously published results[6,2] the parameters of the ground state of an F_2^+ center are determined from the condition of an absolute minimum of the function

$$I_0[\psi] = \frac{\hbar^2}{2\mu}\int|\nabla\psi|^2 d\tau - \frac{e^2}{\varepsilon}\int|\psi|^2\left(\frac{1}{r_a}+\frac{1}{r_b}\right)d\tau - \frac{c}{8\pi}\int D^2[\psi, \mathbf{r}]\,d\tau \qquad (1)$$

with the additional normalization condition

$$\int|\psi|^2 d\tau = 1, \qquad (2)$$

where μ is the effective mass of an electron, ϵ

is the dielectric constant, $c = 1/n^2 - 1/\epsilon$, n is the index of refraction, ψ the electronic part of the system's wave function, D $[\psi, \mathbf{r}]$ the electrostatic field density produced by the electron cloud, r_a and r_b are the distances from the a and b vacancies. Direct variational method was used to find the minimum $I_0\,[\psi]$. The approximate wave function was chosen as

$$\psi(\mathbf{r}) = A(\psi_a + \gamma\psi_b); \tag{3}$$

in which ψ_a and ψ_b were given by the expressions

$$\psi_a = \alpha^{3/2} e^{-\alpha r_a} / \sqrt{\pi}; \quad \psi_b = \alpha^{3/2} e^{-\beta r_b} / \sqrt{\pi}; \tag{4}$$

Here A is the normalizing constant, α and γ the variational parameters.

It will be shown below that the wave function of Eq. (3) approaches infinity as F_2^+ center changes into F center and isolated vacancy at R.

Substituting Eq. (3) into the functional (1), we obtain

$$I[\alpha, \gamma] = \frac{e^2}{\varepsilon} A^2 \Big\{ \frac{\hbar^2 \varepsilon}{2\mu e^2} [(1+\gamma\gamma^*) I_2 \tag{5}$$

$$-(\gamma+\gamma^*) I_3] - [(I_4 + I_5)(1+\gamma\gamma^*) + 2(\gamma+\gamma^*) I_6]$$

$$-\frac{\varepsilon c}{2} A^2 [(1+\gamma^2\gamma^{*2}) u_1 + 2(\gamma+\gamma^*)(1+\gamma\gamma^*) u_3$$

$$+ (\gamma+\gamma^*)^2 u_4 + 2\gamma\gamma^* u_2] \Big\},$$

where I_k and u_k are integrals dependent on wave-functions ψ_a and ψ_b. The extremum condition

$$\partial I / \partial\gamma = 0, \quad \partial I / \partial\gamma^* = 0$$

leads to a system of equations for determination of γ. Two complex and four real roots are obtained as a final solution. The real roots are:

$$\gamma_1 = 1; \quad \gamma_2 = -1; \tag{6}$$

$$\gamma_{3,4} = (b_3/2b_4) \pm \sqrt{(b_3/2b_4)^2 - 1};$$

where b_k are complicated functions of the parameters of the crystal and of the integrals I_k and u_k. The roots $\gamma_{3,4}$ yield identical values for the functional (5). Following the usual procedure of the variation method, the solution of the problem is the root which yields the lowest value on substitution into the variation functional.

Minimizing over α was carried out graphically for each of the obtained values of γ. The quantities α and γ obtained in this manner determine the electronic part of the ground state wave–function of the system.

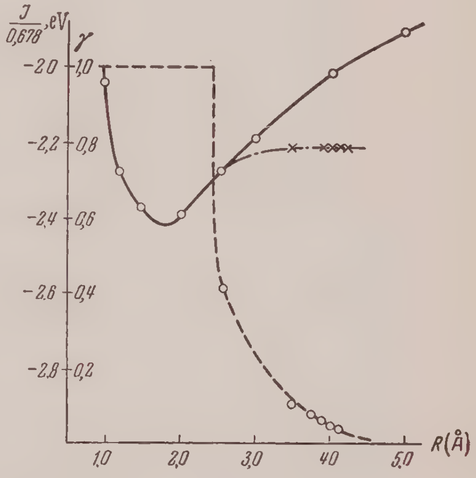

FIG. 1. Solid curve shows I for $\gamma = 1$, dotted curve for $\gamma = \gamma_{\text{ext.}}$ and dash–dotted curve for $\gamma = \gamma_{3,4}$.

Investigation of the dependence on R of the functional (5) showed that for sufficiently large R the lowest value of the functional $I\,[\alpha, \gamma]$ is obtained with the roots $\gamma = \gamma_{3,4}$. These roots approach zero as $R \to \infty$. It follows from Eq. (3) that the wave–function of the system then changes into a wave–function of the F center type and from Eq. (5) that the functional $I\,[\alpha, \gamma]$ goes into a functional for an F center . For small R, the extrema of the functional are given by the root $\gamma = 1$. It is interesting to note the existence of a continuous transition from the extreme value of the functional for $\gamma = \gamma_{3,4}$ to the extremum for $\gamma = 1$ as R decreases.

The results of a numerical calculation for the crystal KCl are shown in Fig. 1. It is evident from the Figure that the minimum $I_0 = I_0\,(R)$ corresponds to a separation $R = 1.8$ Å between vacancies. The difference in energies of the systems with F_2^+ and F centers turns out to be considerable. However, in real crystals with the NaCl type lattice, the minimum possible separation between two identical isolated vacancies is approximately $d\sqrt{2}$, where d is the separation between two nearest neighbors oppositely charged ions. At this separation, the derivative $\partial I_0 / \partial R$, which determines the attractive force between two vacancies in an F_2^+ center, is nearly zero and in any case is considerably smaller than other forces in the lattice. Therefore, separations approximately equal to $d\sqrt{2}$ should be considered as equilibrium separations rather than those that correspond to the minimum $I_0(R)$. For these same separations, it is evident from Fig. 1 that the energy gain due to creation of an F_2^+ center from an F center and vacancy is negligible for KCl crystal (as well as other alkali-halide crystals). Therefore the thermal equilibrium of an F_2^+ center is evidently connected mainly with large activation energy of diffusion of vacancies, rather than the energy gain in creation of F_2^+ centers.

Comparatively small radii of the electron cloud in the ground state of an F_2^+ center and large separations between vacancies allow a second approximation of an F_2^+ center as an F center in an approximately uniform field of a vacancy. To determine the energy of such a system one can use the results of Perlin,[7] according to which the energy gain in creation of an F_2^+ center from an F center and a vacancy is determined by the expression

$$\Delta I_0 = \eta E^2 / 2, \tag{7}$$

where η is the polarizability of the F center, $E = e/\epsilon R^2$ is the field of a vacancy at the position of the F center. For KCl, for example,

$$\eta = 8.7\,(m/\mu)^3 \cdot 10^{-23}\ \text{cm}^3,$$

$$\varepsilon = 4.78,\quad R = 4.44\ \text{Å}.$$

With these values of the parameters, we obtain $\Delta I_0 \sim 0.01$ ev. Therefore a calculation in this approximation leads to a negligible energy gain.

2. EXCITED STATE OF AN F_2^+ CENTER

As pointed out above, the parameters will be calculated for : a) the lowest excited state in a fixed polarization potential well, determined by the ground state wave–function; b) the lowest–lying self-consistent excited state.

a) The quantum states of the system are determined in this case by the solution of the wave equation:

$$\left(-\frac{\hbar^2}{2\mu}\Delta - \frac{e^2}{\varepsilon r_a} - \frac{e^2}{\varepsilon r_b} + V_p\right)\varphi(\mathbf{r}) = E_1\varphi(\mathbf{r}). \tag{8}$$

Here V_p is the polarization potential well produced by the ground state electron cloud:

$$V_p = -e^2 c \int \frac{\psi^2(\mathbf{r}_1)}{|\mathbf{r} - \mathbf{r}_1|}\, d\tau_1. \tag{9}$$

Equations (3) and (9) allow a determination of the explicit form of V_p. Substituting Eq. (9) into Eq. (8) and solving the latter, one obtains the parameters of the quantum states of the system.

The problem is simplified considerably for those crystals whose extreme value of γ is very small. In particular, such crystals include alkali-halides. For these crystals the polarization potential well practically coincides with the polarization well produced by an electron in the ground state of an isolated F center.

The Eq. (8) is solved in this case by perturbation theory, taking as a small perturbation $-e^2/\epsilon r_b$. The zero order equation represents the wave function of an F center with an electron localized at a vacancy a. As a zero order wave–function, a linear combination of functions corresponding to two unperturbed $2s$ and $2p$ wavefunctions of an F center is selected. The symmetry of the problem shows that $2p$ states with quantum number $m = \pm 1$ need not be taken into account. Therefore,

$$\varphi_0 = c_1\varphi_{a1} + c_2\varphi_{a2}, \tag{10}$$

$$\varphi_{a1} = K_1 e^{-\beta r_a} r_a \cos\vartheta_a, \tag{11}$$

$$\varphi_{a2} = K_2 e^{-\delta r_a}(1 - s r_a),$$

where K_1 and K_2 are normalization constants. The parameters of the non–self-consistent $2p$ state of an F–center were determined by Deigen,[8] the parameters of the $2s$ state were especially calculated.

The calculations could be carried out to a numerical result. In particular, for crystals KCl and KBr the energy of the excited state to the first order perturbation treatment turns out to be:

$$E_1(\text{KCl}) = -2.17\ \text{ev};\quad E_1(\text{KBr}) = -1.93\ \text{ev}$$

Calculations to the higher order of perturbation theory show that the error in the above results does not exceed one percent.

Replacement of Eq. (8) by an equivalent variation principle permits a calculation of the parameters of a non-self-consistent excited state by the variation method. The appropriate variation function has the following form:

$$\bar{E}_1[\varphi] = \frac{\hbar^2}{2\mu}\int |\nabla\varphi|^2 d\tau \tag{12}$$

$$-\frac{e^2}{\varepsilon}\int |\varphi|^2\left(\frac{1}{r_a}+\frac{1}{r_b}\right)d\tau - e^2 c\int \frac{\psi^2(1)\,\varphi^2(2)}{|\mathbf{r}_1-\mathbf{r}_2|}d\tau_1 d\tau_2.$$

The approximate wave function is chosen in the form

$$\varphi = N(\varphi_{a1} + k\varphi_{a2}), \tag{13}$$

where φ_{a1} and φ_{a2} are given by Eq. (11), N is the normalizing constant, β, δ, k the variation parameters. Such selection of approximate wave-functions is motivated by the results of the perturbation theory. We note that such choice is good only in the case when γ is close to zero in Eq. (3), since only then is the orthogonality condition of Eqs. (13) and (3) fulfilled (with an appropriate choice of the parameter s). If γ is close to unity in Eq. (3), the approximate wave function should be chosen as a linear combination of the corresponding wave function of the centers a and b. Substituting Eq. (13) into Eq. (12) and performing the variation over k results in a relationship for k. After substituting the values for k into the variation functional and numerically minimizing it over β and δ one can carry out a calculation of the energy term of the excited state. In particular, for KCl and KBr crystals:

$$E(\text{KCl}) = -2.17\ \text{ev}; \qquad E(\text{KBr}) = -1.94\ \text{ev}.$$

It should be noted that the results of the variation and perturbation methods agree very well.

b). The parameters of the self-consistent excited state of an F_2^+ center are obtained by seeking the minimum of the functional

$$I_1[\varphi] = \frac{\hbar^2}{2\mu}\int |\nabla\varphi|^2 d\tau \tag{14}$$

$$-\frac{e^2}{\varepsilon}\int |\varphi|^2\left(\frac{1}{r_a}+\frac{1}{r_b}\right)d\tau - \frac{e^2 c}{2}\int \frac{\varphi^2(1)\,\varphi^2(2)}{|\mathbf{r}_1-\mathbf{r}_2|}d\tau_1 d\tau_2.$$

The wave function φ must satisfy the normalization conditions and must be orthogonal to the ground state wave function.

It is natural to try a wave function of the excited state similarly to Eq. (3) in the form:

$$\varphi = B(\varphi_a + \rho\varphi_b); \tag{15}$$

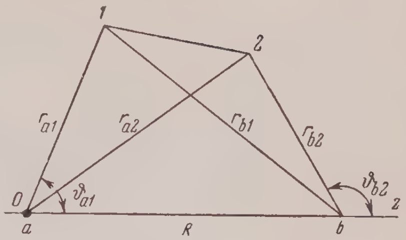

FIG. 2.

$$\varphi_a = \pi^{-1/2}\beta^{5/2}e^{-\beta r_a}r_a\cos\vartheta_a; \tag{16}$$

$$\varphi_b = \pi^{-1/2}\beta^{5/2}e^{-\beta r_b}r_b\cos\vartheta_b$$

Figure 2 shows the coordinates used; ρ and β are the variation parameters.

Substitution of Eq. (15) into (14) and subsequent variation over ρ leads to a relationship for ρ. Depending on the crystal parameters, the lowest value of the function of Eq. (14) is determined by one of the roots $\rho = -1$ or $\rho = \rho_{3,4}$. The quantities $\rho_{3,4}$ are determined in the same manner as $\gamma_{3,4}$ of Eq. (6), except that the integrals I_k and u_k depend on the functions φ_a and φ_b of Eq. (16).

The resulting solution will be good only if the orthogonality condition is fulfilled for the wave-functions of Eq. (3) and (15). This condition is satisfied under two conditions: 1) if the extreme values of γ and ρ for a fixed R are equal to 1 and -1 respectively; 2) if the extreme values of γ and ρ for a fixed R are simultaneously close to zero.

Under these conditions, one can obtain a defnite energy value of the self-consistent excited state by substituting the extreme values of ρ into the functional and minimizing it with respect to β. In all other cases the wave function must be selected in a different form. In particular, if γ is close to zero in Eq. (3), the wave function of the excited state should be taken in the form

$$\varphi = M(\varphi_a + \nu\varphi_b + \lambda\psi_a), \tag{17}$$

where ψ_a is given by Eq. (4) and M is a normalization constant.

The parameter λ is determined from the condition of orthogonality of the ψ wave functions of the ground and excited states, β and ν are the variation parameters.

The selection of the wave functions in the form of Eqs. (15) and (17) is also justified by the fact that these wave functions go into the ψ wave-function of an isolated F center as $R \to \infty$, in accordance with the physical formulation of the problem. Substitution of Eq. (17) into Eq. (14) and minimizing over ν and β also allows a calculation of the energy of the excited self-consistent state.

In numerical calculations, we have limited ourselves to approximate methods, setting β approximately equal to the corresponding parameter of an isolated F center and carrying out the variation procedure only for ν. Therefore the values I_1 are somewhat higher than they should be. The numerical calculations carried out for two crystals yielded the following values

$$I_1(\mathrm{KCl}) = -0.78\ \mathrm{ev};\ I_1(\mathrm{KBr}) = -0.77\ \mathrm{ev}.$$

3. PARAMETERS OF THE ABSORPTION BAND OF F_2^+ CENTERS

Illumination of a crystal containing F_2^+ centers by light can lead to a transition of an electron from ground state into an excited state or to a photodissociation of an F_2^+ center with simultaneous absorption of light. The energy of the photodissociation of an F_2^+ center is determined by the expression

$$E_0 = I_0[\psi_{\mathrm{ext}}] - \frac{e^2c}{2}\int \frac{\psi^2_{\mathrm{ext}}(1)\,\psi^2_{\mathrm{ext}}(2)}{|\mathbf{r}_1 - \mathbf{r}_2|}\,d\tau_1 d\tau_2, \quad (18)$$

where ψ_{ext} is the value of ψ wave function in the ground state corresponding to the minimum I_0. The frequency of the band absorption peak by an F_2^+ center is determined by the expression

$$\hbar\Omega_{\max} = |E_0 - E_1|. \quad (19)$$

Numerical calculations yielded the following values for crystals KCl and KBr (in ev):

$$E_0(\mathrm{KCl}) = -4.07;\ E_0(\mathrm{KBr}) = -3.62;$$

$$\hbar\Omega(\mathrm{KCl}) = 1.90;\ \hbar\Omega(\mathrm{KBr}) = 1.68.$$

Using the results of Pekar[9] in a way similar to the theory of F centers,[6] it is possible to obtain the following expressions for the frequency of the band absorption peak of an F_2^+ center and the half-width δ_0 of the absorption band at low temperatures:

$$\hbar\Omega_{\max} = |I_0 - I_1| + a\hbar\omega/2, \quad (20)$$

$$\delta_0 = 2\hbar\omega\sqrt{a\ln 2},$$

$$a = \frac{c}{4\pi\hbar\omega}\int (\mathbf{D}_0 - \mathbf{D}_1)^2\,d\tau. \quad (21)$$

Here ω is the limiting vibration frequency of the ions in the lattice, $\mathbf{D}_0$ and $\mathbf{D}_1$ are the electrostatic field densities produced by the ψ electron cloud in the ground and excited states.

The expression for a can be written in a somewhat different form:

$$a = e^2c\left\{\int \frac{\psi^2(1)\,\psi^2(2)}{|\mathbf{r}_1 - \mathbf{r}_2|}\,d\tau_1 d\tau_2 + \int \frac{\varphi^2(1)\,\varphi^2(2)}{|\mathbf{r}_1 - \mathbf{r}_2|}\,d\tau_1 d\tau_2 - 2\int \frac{\psi^2(1)\,\varphi^2(2)}{|\mathbf{r}_1 - \mathbf{r}_2|}\,d\tau_1 d\tau_2\right\}. \quad (22)$$

Substitution of Eqs. (3) and (17) into Eq. (22) and performance of the calculations for KCl and KBr crystals results in the values 0.63 and 0.57 ev, respectively, for $a\hbar\omega/2$. Using the above values of I_0, I_1 and $a\hbar\omega/2$, we obtain (in ev):

$$\hbar\Omega_{\max}(\mathrm{KCl}) = 2.0;\ \hbar\Omega_{\max}(\mathrm{KBr}) = 1.8; \quad (23)$$

$$\delta_0(\mathrm{KCl}) = 0.30;\ \delta_0(\mathrm{KBr}) = 0.25.$$

The discrepancy of the numerical values of $\hbar\Omega_{\max}$ in Eq. (23) from the ones obtained earlier can be explained by the fact that the values of Eq. (23) were obtained by an approximate calculation in which the absolute magnitude of I_1 was somewhat lower. The latter circumstance has only a small effect on the numerical value of the half-width of the absorption band because δ_0 is proportional to $\sqrt{a}$. Furthermore, any error in the evaluation of a caused by some inaccuracy in the calculation of β was found to be very small in more detailed calculations.

A comparison of the above values of $\hbar\Omega_{\max}$ and δ_0 with the corresponding parameters of the R_1 band is shown in the following table:

	$\hbar\Omega_{\mathrm{exp}}$	$\hbar\Omega_{\mathrm{th.}}$	$\delta_{0\,\mathrm{exp}}$	$\delta_{0\,\mathrm{th.}}$
KCl	1.85[10]	1.91	~0.25[10]	0.30
KBr	1.7[11]	1.68	—	0.25

---

[1] F. Seitz, Rev. Mod. Phys. 18, 384 (1946).

[2] M. F. Deigen, J. Exptl. Theoret. Phys. (U.S.S.R.) 21, 992 (1951).

[3] M. F. Diegen, J. Exptl. Theoret. Phys. (U.S.S.R.) 24, 631 (1953).

[4] T. Nagamiya and N. Tatsuuma, J. Phys. Soc. Jap. 9, 307 (1954).

[5] Nagamiya, Kojima and Kondoh, J. Phys. Soc. Jap. 9, 307 (1954).

[6] S. I. Pekar, *Investigations of the electron theory of crystals* (GITTL), (1951).

[7] Iu. E. Perlin, J. Exptl. Theoret. Phys. (U.S.S.R.) 20, 274 (1950).

[8] M. F. Deigen, Progress Report, Kiev State University 5, 21 (1950).

[9] S. I. Pekar, J. Exptl. Theoret. Phys. (U.S.S.R.) 22, 641 (1952).

[10] St. Petroff, Z. Physik 127, 443 (1950).

[11] L. S. Druskina, J. Exptl. Theoret. Phys. (U.S.S.R.) 12, 54 (1942).

Translated by M. J. Stevenson
62

SOVIET PHYSICS JETP VOLUME 5, NUMBER 2 SEPTEMBER, 1957

Investigation of the Energy Levels of the F^{20} Nucleus by Magnetic Analysis

L. M. KHROMCHENKO
Radiation Institute, Academy of Sciences, USSR

(Submitted to JETP editor July 11, 1956)
J. Exptl. Theoret. Phys. (U.S.S.R.) 32, 194–198 (February, 1957)

The products of the reaction $F^{19}(d,p)F^{20}$ were studied by applying the magnetic analysis method. In the investigated excitation energy range (up to 6.75 mev) 24 proton groups were recorded which determine the ground state and 23 excitation levels of the F^{20} nucleus. Six of these levels, with excitation energies 4.55, 4.86, 5.41, 5.54, 6.07 and 6.36 mev, have not been observed previously. The $E^* = 6.74$ mev level in the (d,p) reaction has likewise been observed previously, but the relatively close F^{20} level has been detected in investigations on resonance scattering of neutrons.

ONE of the most effective means of investigating the levels of the nucleus F^{20} is analysis of the products of the reaction $F^{19}(d,p)F.^{20}$ This reaction has been investigated in a series of experiments.[1–6] The results of the most recent of these can be summarized as follows.

Burrows, Powell and Rotblat investigated the energy spectrum of protons from the indicated reaction by measuring their range in photo plates. Notwithstanding the comparatively high energy of the bombarding deuterons (8 mev), the authors studied only a relatively narrow band of excitation energies of the F^{20} nucleus, up to 4.73 mev. In this interval the authors observed ten levels of the F^{20} nucleus. 8 proton groups with excitation energy less than 4.01 mev were reported by Allen and Rall[4] In their work, the proton energy was determined by range in aluminum, that is, under circumstances giving poor accuracy and resolution.

In a subsequent short communication of Shull,[5] the proton energy was studied by a more exact method, with the aid of magnetic analysis. However, notwithstanding the bombardment by deuterons of energy greater than 10 mev in this work, the author investigated an energy range of excitation only to 4.4 mev and observed only seven levels of the F^{20} nucleus.

In 1952 Watson and Buchner[6] gave more exact and complete information about the energy levels of the F^{20} nucleus in the excitation interval up to 4.3 mev. The target was bombarded by deuterons of comparatively small energy (up to 2.1 mev) and the authors were able to observe, with the aid of a magnetic spectrometer, 19 proton groups characterizing the ground state of the F^{20} nucleus and 18 excited levels.

At the beginning of the present work (May, 1955) a collection of the data on the levels of the F^{20} nucleus given in the survey of Ajzenberg and Lauritsen[7] gave an incomplete picture. There was an excitation energy region up to 4.3 mev which had been sufficiently thoroughly studied by analysis of the reaction $F^{19}(d,p)F^{20}$. There were also data in the region of higher excitation energy (6.6 to 8.5 mev) obtained by study of the resonance scattering of neutrons by F^{19}. The interval between these two regions remained practically uninvestigated.

The present work had the aim of investigating the levels of F^{20} in the region of higher excitation energy and a filling of the uninvestigated gap between two series of data which existed till then.

METHOD AND CONDITIONS OF THE EXPERIMENT

The levels of the F^{20} nucleus were determined in the present work by analysis of the reaction F^{19} (*d, p*) F^{20}. Proton groups of various energies were separated with the aid of a magnetic field. The analyzer was the magnetic field of the same cyclotron which served as the source of the accelerated deuterons which bombarded the target. For this purpose, a specially constructed box described by us in Refs. 8,9 was put into the cyclotron vacuum in the space between the dees. The target which was located inside the box was hit by a beam of deuterons passing through a system of two collimating slits. Because of this a comparatively monoenergetic part of the initial deuteron beam was selected. Outgoing particles arising from the target as the result of nuclear reactions described a part of their circular trajectory inside the box, and passing through a narrow slit fell upon a photographic plate which was coated with a thin layer of nuclear emulsion.

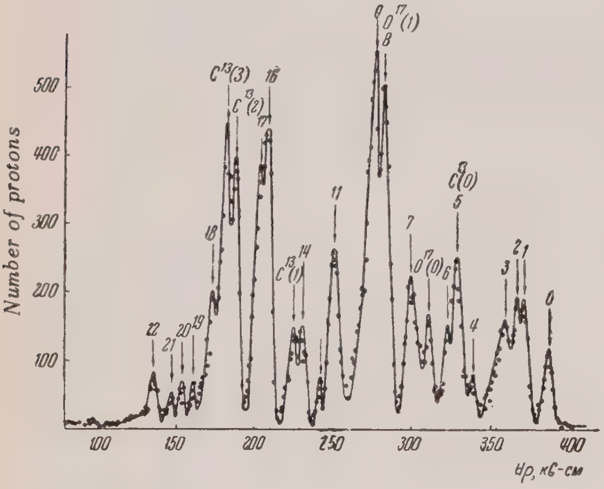

As in previous experiments involving the (*d, p*) reaction, an aluminum filter lay along the entire photographic plate, covering half its width. The filter increased in thickness with distance from the target in such a way that at any point deuterons and particles of still shorter range were filtered out and only protons were able to reach the plate. The plate half without the filter showed visible lines from deuterons elastically scattered from the target material. These lines were investigated with the aid of a microphotometer; the energy of the incident deuterons bombarding the target was thus determined.

The half plate which was covered by the filter contained mainly protons from the reaction (*d*,*p*) and was investigated under a microscope. A count of proton tracks was made with intervals of 200 μ along the entire length of the plate. Thus the energy of a group was determined by its position on the plate, and its intensity by the number of tracks in the group. These measurements were repeated at 10 locations across the width of the plate. For each plate the proton energy spectrum was obtained by summing these 10 measurements.

The target in our experiments was a thin silver foil on which a thin layer of finely powdered CeF_3 was deposited. This fluorine compound was selected because of its temperature stability and also because the second component (cerium) is a sufficiently heavy element to prevent a (*d,p*) reaction. The latter, incidentally, was checked by a special control experiment. A proton spectrum was investigated from a target of BaF_2. The identity of these spectra made completely sure the identification of protons from the F^{19} (*d, p*) F^{20} reaction.

In addition, another type of check was performed. The proton spectrum from the deuteron bombardment of a silver foil was investigated. This showed the presence of two contaminations which were unavoidable under the conditions of the experiment: carbon and oxygen. The CeF_3 target was bombarded by deuterons of various energies in the interval 3.0 to 4.0 mev. This also served as the control on the identification of the proton groups.

To determine the levels of the F^{20} nucleus, we investigated six plates. The results presented here are weighted averages of these six determinations.

DISCUSSION OF THE RESULTS

Study of the F^{19}(*d,p*) F^{20} reaction under the experimental conditions described above allowed us to register 24 proton groups in the excitation energy up to 6.75 mev. These characterize the ground state of the F^{20} nucleus and 23 excited levels.

The figure shows a proton spectrum obtained with bombarding deuteron energy 3.7 mev. The successive numbers indicate the proton groups from the F^{19} (*d, p*) F^{20} reaction. These same indices have corresponding levels of the F^{20} nucleus. Proton groups from (*d,p*) reactions with carbon and oxygen are indicated in the curve by the symbol of the final nucleus and number of the group. Two proton groups on this curve have double indices: C^{13} (0) and 5, and also O^{17} (1) and 8. In these cases, there is a superposition of the proton groups from the impurities and the fluorine itself. This conclusion is reached by comparison of the relative intensities of proton groups from control spectra (only carbon and oxygen) with spectra from a fluorine target.

Excited levels of the F^{20} nucleus, in mev

Group number	present work	data of other authors					
		[3]	[4]	[5]	[6]	[7]	[10]
1	0.66	0.63	0,64	0.69	0,652	—	—
2	0,81	0,83	—	—	0,828	—	—
3	1,08	1,0	0,97	0,98	0,988 1,059	— —	—
4	1.34	1.37	1,31	—	1.309	—	—
—	—	—	1,91	—	1.970	—	—
5	2.15	—	—	2,20	2,048 2,195	— —	—
(6)	(2.54)	2,55	2,52	—	—	—	—
—	$O^{17}(0)$	2,91	2.83	2,70	2.870	—	—
—	—	—	—	—	2,966	—	—
7	3.11	—	—	3,12	—	—	—
8	3.58	3,49	3,45	—	3,491 3,528 3.586	— — —	—
—	—	—	—	—	3.681	—	
9	3.77	—	—	3,74	—	—	—
—	—	—	—	—	3,961	—	—
10	4.09	4,06	4,01	—	4,079	—	—
11	4.37	4,31	—	4.41	4,275 4,310	— —	—
12	4,55	—	—	—	—	—	—
(13)	(4.73)	4,73	—	—	—	—	—
14	4.86	—	—	—	—	—	—
—	$C^{13}(1)$	—	—	—	(5,063)	—	5.04
15	5.16	—	—	—	—	—	5,19
—	—	—	—	—	—	—	5,27
16	5.41	—	—	—	—	—	—
17	5,54	—	—	—	—	—	—
—	$C^{13}(2)$	—	—	—	—	—	5,72
—	—	—	—	—	—	—	5,87
—	$C^{13}(3)$	—	—	—	—	—	5,95
18	6,07	—	—	—	—	—	—
19	6.17	—	—	—	—	—	6,25
20	6,36	—	—	—	—	—	—
21	6,47	—	—	—	—	—	6,52
22	6,65	—	—	—	— —	6.63 6.65	6,63
23	6,74	—	—	—	—	6.70	—
—	—	—	—	—	—	6.86	6,81
—	—	—	—	—	—	6.92	6,98
—	—	—	—	—	—	7,0	—
—	—	—	—	—	—	7.08	—
—	—	—	—	—	—	7.17	7.20
—	—	—	—	—	—	7,50	—
—	—	—	—	—	—	8,18	—
—	—	—	—	—	—	8.54	—

The proton group number 23, corresponding to an excitation energy of 6.74 mev is not seen in the Figure. It appears on plates obtained from deuteron bombardment of the target at higher energies. The energy levels of F^{20} obtained in our experiments are given below in the Table. Our results are compared with those of four other authors which were also based on a study of the F^{19} (d, p) F^{20} reaction. Besides this the table shows levels of the F^{20} nucleus at higher excitation energies taken from work which investigated the F^{19} (n, n) F^{20} reaction. The last column gives data from the work of El Bedewi [10]. In that article which was delivered to us as we were submitting for publication, the author describes experiments on the magnetic analysis of the F^{19} (d, p) F^{20} reaction. These were carried out with deuterons of 8.9 mev. The author investigated the levels of F^{20} up to an excitation energy of 7.2 mev. For a majority of the groups the angular distribution of the protons was also studied. Since in the region previously studied by Watson and Buchner, El Bedewi used their values for the energy levels of F^{20}, we have included only the data for higher levels which the author determined independently.

For the reaction $F^{19}(d,p)F^{20}$ we obtained the value for the reaction energy $Q_0 = 4.383 \pm 0.015$ mev. Watson and Buchner give for this quantity $Q_0 = 4.373 \pm 0.10$ mev. The energy of the reaction obtained from the mass difference is $Q_0 = 4.375$ mev. All three values are in sufficiently close agreement.

For the majority of levels our experimental uncertainty was 20–25 kev. Only some values were determined with greater accuracy. Comparison of our results with those of other authors shows a good degree of agreement for the values of most excited levels of F^{20}. There are however some differences which are outside the limit of error in our measurements. We will discuss these.

In our experiment we did not observe the F^{20} level with $E^* = 1.970$ mev which was shown by Watson and Buchner and earlier by Allen and Rall ($E^* = 1.91$ mev).

The energy level with $E^* = 2.54$ mev was observed in our experiments only in three out of six plates. The corresponding value is less certain and is shown in parentheses in the table. The level of F^{20} analogous to this was observed in Refs. 3 and 4, but not in Refs. 6 and 10. In the experiment of El Bedewi it is true that the group could have been masked by a proton group from the $O^{16}(d,p)O^{17}$ reaction.

In our experiment there is no level with $E^* = 2.966$ mev, as was found by Watson and Buchner. The closest level to this which we observed was $E^* = 3.11$ mev. These can probably not be compared because they fall outside the errors of both measurements. A value close to ours $E^* = 3.12$ mev. was observed by Shull.

We did not observe two weak levels at $E^* = 3.681$ and $E^* = 3.961$ mev which were observed by Watson and Buchner. Our curves however show a strong group 9 with $E^* = 3.77$ mev, that is an excitation energy lying between the indicated two levels. A level similar to ours is reported by Shull ($E^* = 3.74$ mev).

Although we have identified the 6.17 mev level which we have observed with the 6.25 mev level observed by El Bedewi this identification is not definite since the spread of data is too large. In a number of cases we did not observe levels determined by the work of El Bedewi and registered others which did not appear in his experiments.

As can be seen from the Table, seven levels of the F^{20} nucleus with indices 12, 14, 16, 17, 18 20 and 23 have not been observed in any of the preceding work. Level 23 can, however, be identified with the relatively close value $E^* = 6.70$ mev which was observed in a study of resonance scattering of neutrons.

The author would like to express his indebtedness to Professor Iu. A. Nemilov for his attention to the work and for the opportunity to perform the experiments.

---

[1] J. C. Bower and W. E. Burcham. Proc. Roy. Soc. (London), 173A, 379 (1939).

[2] Yu. A. Nemilov and L. I. Gedeonov, Dokl. Akad. Nauk SSSR 70, 219 (1950).

[3] Burrows, Powell and Rotblat, Proc . Roy. Soc. (London) A209, 478 (1951).

[4] R. C. Allen and W. R. Rall, Phys. Rev. 81, 60 (1951).

[5] F. B. Shull, Phys. Rev. 83, 875 (1951).

[6] H. A. Watson and W. W. Buechner, Phys. Rev. 88, 1324 (1952).

[7] F. Ajzenberg and T. Laurtisen, Rev. Mod. Phys. 27, 77 (1955).

[8] L. M. Khromchenko, Dokl. Akad. Nauk SSSR 93, 451 (1953).

[9] L. M. Khromchenko, Izv. Akad. Nauk SSSR Fiz. Ser. 19, 277 (1955).

[10] F. A. El Bedewi, Proc. Phys. Soc . (London) A69, 221 (1956).

Translated by G. L. Gerstein
48

SOVIET PHYSICS JETP VOLUME 5, NUMBER 2 SEPTEMBER, 1957

Optical Contact of Polished Glass Surfaces

I. V. Obreimov and E. S. Trekhov
Moscow Engineering-Physics Institute

(Submitted to JETP editor September 25, 1956)
J. Exptl. Theoret. Phys. (U.S.S.R.) 32, 185–193 (February, 1957)

It is shown that the specific work required to separate two surfaces in optical contact is fairly constant and that the forces between two surfaces are effective at a very small distance, on the order of 10^{-7} cm.

1. CONCEPT OF OPTICAL CONTACT

THE word "contact" is frequently used in physical and technical literature as a self-evident concept. However, the fact that it is usually accompanied by the adjective "electrical," "mechanical," or "optical" shows that the concept "contact" requires a definition.

The term optical contact signifies the following phenomenon: two well-ground and polished plane glass surfaces adhere so strongly when placed on top of each other, that it becomes difficult to separate them. If the two glass surfaces have the same index of refraction, the optical contact reflects almost no light (the reflection coefficient from the hypotenuse faces of two total–internal–reflection prisms made of BK–10 glass, placed in optical contact, was measured by us to be roughly from 1×10^{-4} to 1×10^{-7}).

To separate two glass surfaces placed in optical contact, they are slightly heated (with a match or with a burner). The resultant elastic stresses create forces that are sufficient to break the contact. If the break has not been completed, both surfaces again make contact after cooling.

If the contact is placed in a liquid (water, alcohol or ethyl ether), the liquid penetrates into the contact zone and the contact-making surfaces may separate after a few hours. However, if the contact is removed from the liquid before separation, the liquid will evaporate gradually and the surfaces will adhere again. Such an experiment can be repeated several times with a single pair of surfaces placed in contact.

Surfaces in optical contact can be separated only by application of normal forces; they cannot be slid apart. Before the contact is completed, while a layer of air remains between the surfaces, they slide readily on each other. A pronounced symptom of the contact is that the surfaces stop sliding on each other, and attempts to slide them apart result at best case in only stripping (and usually scratching when two glass surfaces are placed in contact.

The condition of the surface plays a certain role in the establishment of an optical contact.

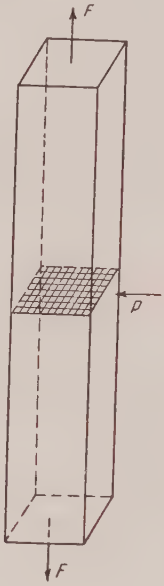

FIG. 1. Glass bars, placed in optical contact. *FF*—tension force, *P*—surface of optical contact.

Glass surfaces freshly polished with tar and rouge are very easy to place in contact, requiring only primitive surface cleaning—rubbing with alcohol and a clean rag and brushing the dust off. It is equally easy to establish contact between two silvered (wet method) glass surfaces. Thin laminae of anthracene, phenantrene and naphthalene crystals also produce an optical contact with glass, so strong that they must be scraped off or dissolved before they can be removed. Fire-polished glass surfaces, if they remain in air, are readily placed in contact, and if they are thin, they adhere so tightly, that they cannot be removed by neither scraping nor immersion in liquid. Surfaces cleaned by corona discharge lose their contact–making ability but regain it if the surfaces are left in the air for a while.

In spite of the fact that optical contact is a phenomenon well known to a large circle of physicists and technicians, it has been little investigated up to recently (disregarding many optical–engineering investigations devoted primarily to special technological problems). Optical contact is attributed to three causes: (1) pressure of the atmospheric air, (2) capillary pressure (adhesion) due to small traces of oil remaining on the surface of the glass, and (3) direct molecular attraction with the aid of molecular forces. Atmospheric pressure must be discarded: experiments on the separation of two glass bars placed in contact (Figure 1) have shown that the separation force always exceeds the atmospheric pressure, sometimes by a factor of several (up to seven) times. The choice lies between adhesion and the Van–der–Waals forces.

2. OBJECTS OF INVESTIGATION

To test optical contacts for strength, special specimens were prepared of a glass of nearly the same composition as K–8 glass (Figure 2). Each specimen comprises one thick and one thin plate. The thick plate was rectangular, measuring 50 × 40 mm with a thickness of 10 mm. Both wide faces and the two longer side faces of the thick plate were thoroughly polished for optical contact.

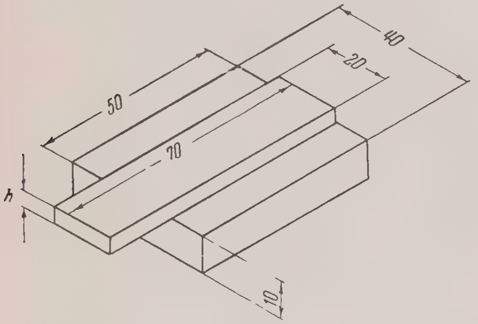

FIG. 2. Sketch of glass plates, placed in optical contact; $h = 0.5$, 1.0, and 2.0 mm. All dimensions are given in millimeters.

The thin plates came in three thicknesses: $h = 0.5$, 1.0, and 2.0 mm; all were 20 mm wide. The thin plate was placed in contact on the wide surface of the thick one. The thin plate projected 20 mm beyond the edge of the thick plate, polished with tar and rouge until bright, and the plates were placed in optical contact immediately after polishing was completed.*

The only cleaning done before establishing contact was to rub the contact–making surfaces first with a pad soaked in ethyl alcohol and then with a dry clean cloth napkin. This manner of establishing optical contact between our surfaces did not differ from the conventional manufacturing procedure.

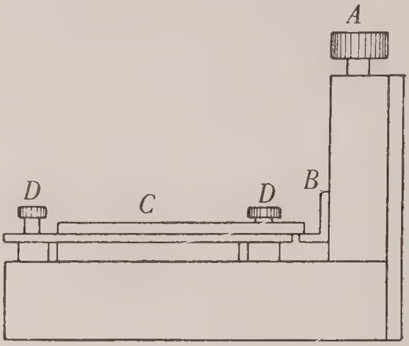

FIG. 3. Diagram of fixture for separating the optical contact. *A*–knob of lifting screw, *B*–hook used to separate the glass plate, *C*–glass plate, *D*–clamping screws.

3. METHOD OF OBSERVATION AND MEASUREMENT

The separation of an optical contact is usually difficult to observe because of the fact that the separation is very rapid and cannot be stopped at any intermediate phase. It is possible, however, to eliminate this shortcoming in the following manner: the specimen described in the preceding section is clamped in a special fixture (Figure 3) with the thin plate on top. A metal hook engages the projecting plate and is attached to the nut of a lead screw. The latter permits fine adjustment of the vertical motion of the tooth. When the nut moves up, the hook engages the projecting end of the upper plate and pulls it upwards. The resultant bending moment strips a portion of the upper plate. If the rise of the hook is stopped, the curvature of the plate and consequently also the stripping moment will diminish toward the contact zone until equilibrium is established between the stripping moment and the forces that bring the contact surfaces together. By regulating the rise of the stripping hook it is possible to set the boundary of the contact region in any location.

An air wedge is formed between the separated surfaces. If the separation region is examined in monochromatic light one sees pronounced interference fringes of equal thickness. From the thickness of these fringes it is possible to judge the shape of the bent upper surface, which turns out to be , as called for by the theory of elasticity, strictly parabolic. This is proven by the fact that the distance between the first and fourth interference fringes equals the distance between the fourth and ninth fringes and between the ninth and sixteenth fringes. Thus, it is possible to obtain the position of the zero fringe by extrapolation, i.e., to determine the place where the two plates come in contact. From the curvature of the upper plate one can also calculate the work required to strip the contact; in fact, the work required to strip the contact, calculated for one surface is

---

* Close contact of optical surfaces is used extensively by optical workers in those cases when cementing deforms the glass part or does not yield a dependable bond. In that case the part ground with carborundum is not polished to full brightness.

$$\alpha = K / 4\rho^2. \qquad (1)$$

here α is one quarter of the work required to strip one square centimeter of the contact surface, ρ the radius of curvature of the separated plate along the line of separation, and K is the stiffness, which for an isotropic rectangular plate is

$$K = Eh^3 / 12(1 - \sigma^2), \qquad (2)$$

where E is Young's modulus and σ is the Poisson coefficient.* Since the shape of the bent plate is parabolic, we have

$$y = x^2/2\rho, \qquad (3)$$

$$1/\rho = 2y/x^2 \text{ and } \alpha = Eh^3 y^2 / 12x^4(1 - \sigma^2).$$

here x is the distance between the zero and the n'th interference fringe, y the thickness of the air layer, equal to $2n\lambda$, where λ is the wavelength of the light.

4. MEASURING THE WORK OF SEPARATION

As follows from Eqs. (1) and (2), to determine the work of separation of the optical contact it is necessary to know either the modulus of flexure of the glass plate, or the elastic constant of its material. Both were determined in this investigation. Since the glass plate bends along a parabola, the distances between the first and fourth, fourth and ninth, etc. interference fringes should all have an equal value, x_0 for normal incidence of the light and Eq. (1) becomes:

$$\alpha = Kn^2\lambda^2 / 4x_0^4. \qquad (4)$$

We used this equation to calculate α for the separation of the optical contact of all three thicknesses of plates. The results are given in Tables 1–3.

TABLE I

$h = 0.5$ mm, $\alpha_{av} = 36$ erg/cm^2

Number of experiment	α, erg/cm^2	Number of experiment	α, erg/cm^2
1	4.7	22	27.7
2	27.5	136	52.2
3	26.3	136	68.4
4	20.6	137	50.0
5	19.4	138	47.9
6	26.5	138	65.3
19	23.3	139	46.1
21	20.6	140	46.1

What attracts attention in these tables is not the large dispersion in the values of α, but the fact that in spite of the huge dispersion, one can still obtain average values for the work of separation of the optical contact.

The results of measurements on a plate 0.5 mm thick are given in Table I. The first column gives the number of the measurement; if several measurements bear the same number, this means that the experiment was performed in succession with the same specimen, but with a continuously lengthening separation region. The second column gives the values of α.

Table II gives the results for a plate made of the same glass but 1.0 mm thick. The results for the 2.0 mm plates are given in Table III.

5. REPRODUCIBILITY OF CONTACT

Anyone working with optical contacts knows that occasionally it takes time to establish contact between two glass surfaces. Thus, for example, in one of our experiments two plates, each 4 cm^2 in area and 5 mm thick, were first placed in contact, and separated by slight heating, upon which it became impossible to reestablish the contact. Two days later, however, without any action on the experimenter's part, the optical contact was restored spontaneously. Many such experiments lead us to believe that the possibility of a spontaneous repeated optical contact depends on its freshness. The fresher the contact, the less time elapsed since the first contact, the easier will it be restored, spontaneously, but this is not a law; the contact cannot be restored if the work of the primary separation is large.

It is easiest to restore a contact if the stripping was not carried out to the end and the two glass plates are not yet completely apart. In that case the contact moves back several millimeters when the stripping separating force is removed. The contact can always be restored by applying added pressure to the plates. Table IV illustrates one such experiment, which the specimen was kept in contact in a machine shop for 45 days. The following are the results of an experiment with repeated stripping of the contact (Table IV).

---

*It can be proven that when the contact is stripped half the work is consumed in bending the plate. The surface formed is 2 cm.^{2}

TABLE II

$h = 1.0$ mm, $\alpha_{av} = 28$ erg/cm^2

No. of experiment	α, erg/cm^2	No. of experiment	α, erg/cm^2	No. of experiment	α, erg/cm^2
23	39.7	51	19.5	63	67.2
25	30.6	52	21.2	64	22.4
26	21.6	53	14.2	65	24.9
27	47.7	54	31.2	65	29.0
28	32.5	55	33.1	66	29.0
31	26.1	57	31.1	67	31.3
32	24.4	58	48.7	68	31.2
43	21.4	59	35.3	69	29.0
45	13.6	60	23.4	131	36.6
46	8.4	60	29.0	132	35.8
47	11.9	61	22.4	134	21.2
48	12.1	62	24.9	135	43.8
49	3.7	62	29.6	135	55.7
50	21.4	63	22.4		

The first stripping (1) gives a rather high value of work of separation, usually not varying much from one section of the contact to another. The contact-making surfaces were not fully separated and after the stripping force was removed, the broken contact was spontaneously restored. Nevertheless, the contact boundary did not return to its initial position. After experiment (2) strong pressure was applied to the contact–making surfaces, a click was heard, and the contact was restored fully in its initial area. The work of separation then returned to its initial value.

TABLE III

$h = 2.0$ mm, $\alpha_{av} = 27.0$ erg/cm^2

No. of experiment	α, erg/cm^2	No. of experiment	α, erg/cm^2
36	7.3	87	36.2
37	8.5	88	36.2
38	8.3	89	38.3
39	7.1	90	38.3
40	6.9	91	37.0
41	5.8	100	10.2
81	43.6	101	29.6
82	41.1	102	36.3
83	41.7	103	69.2
84	45.0	105	9.2
85	37.3	106	9.0
86	40.6	107	8.7
86	44.2	108	8.3

Many experiments of the type reported in Table IV were performed; the full restoration of the contact by pressure is typical.

Table V gives the results of another series of experiments in which the contact was stripped and reestablished many times. The specimen was heated to 100° C in a muffle furnace prior to the experiment, but not again. The contact was restored spontaneously each time. The table lists the work of separation for the repeated strippings, and the constant value of this quantity is quite striking.

6. ELASTIC STRESSES IN THE REGION OF THE CONTACT

Viewing the specimens in contact through crossed Nicol prisms discloses slight brightening of the field, evidencing the presence of stresses. The bright regions are distributed unevenly over the surface of the contact.

When the specimen is viewed from the side a solid bright band is seen in the plane of the contact over the entire contact region. This gives an idea not only of the magnitude of the stresses but also of the large area of the stressed layer along the line of sight (Figure 4). Since the stressed layers on the two sides of the contact surface are not more than 0.1 mm thick, photographs magnified 5–12 diameters were taken with an MP–1 polarization microscope. The stressed regions which look solid when viewed with the naked eye, are actually broken up into individual sections and attenuate rapidly with depth. The region adjacent to the con-

TABLE IV

No. of experiment	Stripping conditions	α, erg/cm^2
1	a) First stripping	55.6
	b) First stripping (continued)	44.2
2	After spontaneous restoration of contact	21.4
3	Separation after restoration of contact under strong pressure	51.5

tact is therefore characterized by the presence of stresses perpendicular to the surface of the contact unevenly distributed in the plane of the contact, and attenuating rapidly with depth. The contact-making surfaces are thus subject in addition to adhesion forces also to elastic tension produced in the glass, when the contact is made. These stresses reduce the resistance of the contact to stripping and may be the cause of the fluctuations of α. These tensions in the glass become relieved after long time intervals (months), evidencing the plasticity of glass. This may be the cause of the increasing contact strength with time.

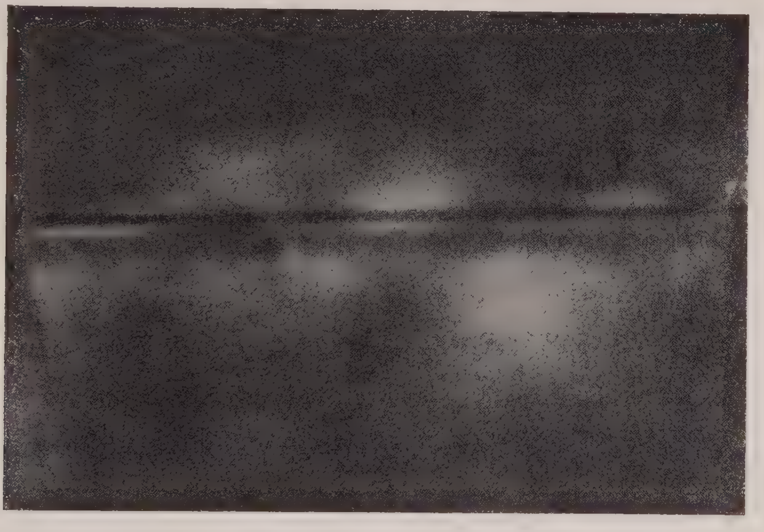

FIG. 4. Region of optical contact seen in crossed Nicol prisms. Magnification approximately 5 ×. *1—1*—contact line between two glass plates.

The stresses in the contact region are analogous to some extent to the stresses occurring near a surface crack in glass. Examination of a crack immediately after its formation shows that the stresses concentrate principally near the end of the crack and are perpendicular to its plane. After a relatively long time (several days), the stresses are no longer concentrated near the end of the crack.

Analogously, optical contact involves the appearance of local stresses in the immediate vicinity in the plane of contact. Upon stripping, the stresses completely disappear from the free surface of the plate, but the region adjacent to the contact line can be readily identified by the high stress concentration of stresses. A magnified micro-

TABLE V

Specimen No. 2, h=1.0mm

No. of stripping	α, erg/cm^2	No. of stripping	α, erg/cm^2
1*	141	10	29,7
2	25.6	15	20,3
7	21.6	25	26.0
9	22,9	50	20.3

---

*An accidental quantity. May be due to aging.

photograph of the contact line is given in Fig. 5, which is turned through 45° to save space.

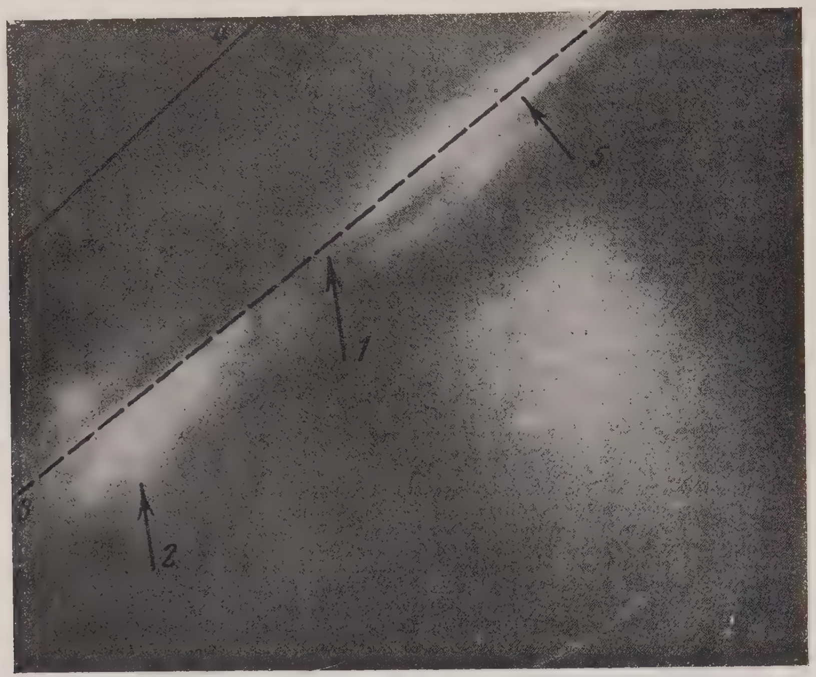

FIG. 5. Region of separation of contact as seen in crossed Nicol prisms. *1*—contact line; *2*—region of unbroken contact; *3*—contact boundary between two plates (thicker below, thinner above) with thickness of 0.5 mm; *4*—outer edge of thin plate; *5*—there is no more tension to the right of the arrow in the thick plate (below).

It is particularly interesting to view between crossed Nicol prisms the spontaneous restoration of contact upon reduction of the stripping force. One can see well under the microscope how the contact line moves over the specimen together with the stresses and how new local stresses appear again on the surface of the restored contact. These stresses are also indicative of the character of the adhesion forces in the optical contact. The stresses at the contact line are large and localized stresses, as shown in Fig. 5. They extend for 0.05 cm, and for this plate $2\rho = 4.5 \times 10^2$ cm. Consequently, assuming $y = 0$ at the start of the stressed region, we have at its boundary

$$y = \frac{x^2}{2\rho} = \left(\frac{2.5\cdot 10^{-3}}{4.5\cdot 10^{2}}\right)\ \text{cm} = 5.6\cdot 10^{-6}\ \text{cm}.$$

This is the upper limit for y. The region of strongly-localized stresses may become indistinct if the axis of the polarization microscope is not directed along the contact line or else if the line itself is curved, as occurs frequently. Actually, the region of the localized stresses is sometimes much more pronounced. We once succeeded in observing stresses at the contact line in a region 0.1 mm in size, giving for y a value of 2.2×10^{-7} cm, i.e., on the order of the effective radius of the molecular forces. Thus, all data indicate that optical contact is sometimes accompanied by direct molecular forces between glass surfaces covered by adsorbed gas.

7. SINTERING OF OPTICAL CONTACT

It is known[5] that if surfaces in optical contact are carefully heated to a temperature even below the softening temperature of the glass, the two surfaces may sinter together, and can no longer be separated. A crack produced in the upper glass will pass through the lower one, and even if one succeeded somehow in separating the two sintered contact surfaces, they would be substantially damaged, parts of the lower surface stripping together with the upper one.

These results were confirmed in our experiments.

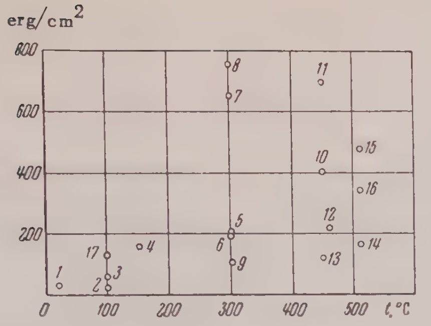

FIG. 6. Work of separation of optical contact as a function of the sintering temperature.

The specimens were heated in a muffle furnace. The temperature distribution in the furnace was first measured and the specimens were then located in the furnace in a region having a practically zero temperature gradient.

After many experiments we established a heating schedule resulting consistently in a fixed hot spot in the specimen. As a rule, this schedule left no temperature stresses in the heated specimen. Nothing happens to glass surfaces in optical contact heated to 100° C, the work of separation remaining almost unchanged. Upon carefully heating to 150° C and higher, occluded gas is liberated between the surfaces and separates them partially or totally (the contact is broken). Sometimes one plate floats above the other and unless they are perfectly horizontal, the upper plate may slide. When all the gas is liberated, the contact between the plates is spontaneously restored, with a sharp increase in the work of separation. Finally, at higher heating temperatures, the strength of the sintered contact increases to a value commensurate with the strength of the solid glass.

The behavior of one of the specimens is quite characteristic. Prior to heating, the average value of the work of separation fluctuated between 22.4 and 33.0 erg/cm.^{2} A specimen with an incompletely restored contact region was heated in a muffle furnace to 450 °±10° C and tested after slow cooling in the furnace to room temperature. The exterior surfaces, although retaining their optical properties, were changed. Where a wooden stick could previously glide easily over the glass, it now stuck to the surface and scratched it. The measured work of separation were high, from 113 to 400 erg/cm^2. The contact line became highly irregular and serrated. When the stripping moment was reduced to zero, the contact line did not return spontaneously to its previous location, and the contact was not restored. In the new separation region, when viewed in reflected light, one could see almost a uniform, gray, structureless field. The optical contact could not be restored by external pressure on the contact surfaces. A sharp boundary was formed between the old contact line (prior to sintering) and the new separation region; this

TABLE VI

Temperature, °C	Work of separation after sintering erg/cm^2	Thickness, mm	Remarks
20	30	—	Average of numbers obtained prior to sintering
100	17.4	1	
100	58.4	1	
150	156	1	
300	205	2	Region of multiple stripping
300	195	2	
300	650	2	
300	753	2	
450	113	1	Region of multiple stripping
450	400	1	
450	690	1	
460	216	0.5	Broke when stripped
300	100	2	Repeated sintering (after stripping
510	156	1	Region of multiple stripping
510	472	1	
510	339	1	
100	140	1	

boundary can be attributed to permanent flexure and bending of a previously flat surface.

The maximum reliably–measured value of the work of separation in a specimen heated to 450° was 400 erg/cm^2. However, this is not the limit, and apparently the work of separation may even be higher.

Table VI and Figure 6 give a summary of typical values of the work of separation for two different sintering temperatures.

The measured work of separation is accurate to within ± 10%. Surfaces separated from a sintered contact contain pinpoints. The local nature of these pinpoints is evidence that the contact, even the optical one, fuses together only at isolated points on the contact–making surface. As a rule, strong stresses are observed in the sintered–contact region.

---

[1] Lord Rayleigh, Proc. Roy. Soc. (London) **156A**, 326 (1936).

[2] L. D. Landau and E. M. Lifshitz, *Mechanics of Continuous Media*, GTTI, Moscow, 1954.

[3] I. V. Obreimov, Proc. Roy. Soc. (London) A127,390 (1930).

[4] D. Kuznetsov, *Physics of Solids*, Tomsk, 1949.

[5] Parker and Dalladay, Proc. Farad. Soc. 12, 305 (1937).

Translated by J. G. Adashko
47

SOVIET PHYSICS JETP VOLUME 5, NUMBER 2 SEPTEMBER, 1957

Explosion of a Metal by an Electric Current

S. V. LEBEDEV

P. N. Lebedev Physical Institute, Academy of Sciences, USSR

(Submitted to JETP editor March 20, 1956)

J. Exptl. Theoret. Phys. (U.S.S.R.) 32, 199–207 (February, 1957)

The destruction of metal wire at currents of 5×10^5 5×10^6 amp/cm^2 was investigated. Two different types of processes were observed: rupture of the melted wire into macroscopic fragments by surface tension forces, and explosion of the melted wire caused by changes in its volume properties. The abrupt change in the electrical conductivity of melting tungsten, molybdenum, platinum, or nickel was measured. A previous conclusion, that the energy of the metal at which its electric conductivity vanishes depends on the current density, is confirmed.

THE physical mechanism by which metal wires explode when heated by electric current has not yet been clarified and even the external aspect of this phenomenon is differently presented by various investigators.*

We established a relationship between the explosion of the wire and the jump increase in its total electric resistance R', observed at current densities approximately greater than 5×10^6 amp/cm.^{2} We concluded[2,3] that this increase in R' is caused by a jump in the specific resistivity R of the metal, and that energy E_j delivered to the metal prior to the instant of the jump in R is a function of the current density j. The dependence of E_j on j seemed inexplicable, and led to the assumption that high values of j produce an anomalous state in the metal. In contradiction to this assumption, it is usually stated that the explosion is due to macrosopic processes in the wires, and any talk of a special state of the metal itself is unfounded.

It is the purpose of this work to investigate the destruction of wire at currents of various densities and to check the assumption concerning the anomalous state of the metal at the instant of explosion.

1. PROCEDURE

The destruction of the wire by a current i was investigated by correlating the photographs of the wire with oscillograms of $V_R(t)$ and $V_r(t)$, which make it possible to determine, for any instant of time and particularly for the exposure time t_e, the resistance of the wire $R'(t)$ and the energy $E'(t)$ delivered to the wire during the time $t - t_1$, (t_1 is the instant the current is switched on, taken to mean hereinafter the beginning of the time measurement, and $i = (\pi d^2/4)\, j$, where d is the diameter of the wire).

The procedure used to obtain and process oscillograms of the voltage across the wire, $V_R(t) = R'(t)\, i(t)$ and across a standard resistor $V_r(t) = ri(t)$ is discussed in Refs. 2 and 3. The electric circuit of the setup is shown in Fig. 1, where the path of the current i is shown by a heavy line.

The wires were photographed in all experiments with a 15 x magnification and a constant exposure of approximately 3 microseconds. In the photography we rotated the plane of polarization of the light with a magnetic field, and illuminated the wire with spark S. The photographic setup did not differ in principle from those given in Refs. 4 and 5.

To determine t_e, the light from the spark S was aimed on a vacuum photocell, the current i_{ph} of which was recorded with one beam of a cathode–ray oscillograph. The second beam of the oscillograph recorded the voltage $V_R(t)$. These oscillograms were used to determine the time of exposure relative to the various states of the metal as represented by the discontinuities in the curve $I = R(E)$.

2. DESTRUCTION OF WIRES AT APPROXIMATELY 5×10^5 AMP/CM^2

Figure 2 shows photographs of current–carrying wires at $j \approx 5 \times 10^5$ amp/cm^2. The current rises abruptly when the circuit is closed and is reduced gradually by 20% after 1×10^{-3} sec. Adjacent to each photograph is the oscillogram of $V_R(t)$ obtained in the same experiment. The instant of exposure t_e is determined from the start of the pip on the lower line of the oscillogram and is marked with a stroke (this pip is shown exaggerated in Fig. 2 compared with the actual duration of the exposure). In Figs. 2*a* and 2*b* the t_e marker is shown in the form of a dot under the $V_R(t)$ curve.

The photographs show that the jump in the total

---

*A detailed list of references on this problem is given in Ref. 1.

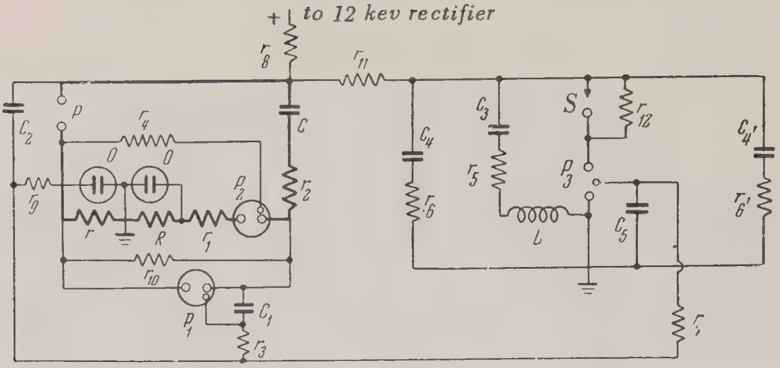

FIG. 1. Electric diagram of setup. Capacitator C— source of current i; R and r—tested wire and resistance standard; O— oscillograph; P_1, P_2, P_3 and P_4 – spark relays. Resistances r_1 and r_2 limit the current: r_3, C_1 and r_7, C_5 determine the instants the current i is shut off and the exposure is started, respectively: C_2 ($1 \mu F$) ignites P_1 and P_3 ; C_3 ($0.25\ \mu F$) is the current source ($i_3^{\max} = 1000$ amp) in the coil ($L = 5 \times 10^{-6}$ henry) of the Faraday shutter; $C_4 = c_4{}'$ ($0.25\ \mu F$) and C_3 are the current source for the spark S; r_8, r_9, r_{10}, r_{11}, and r_{12} insure the charging of C, C_2, C_3, C_4, and $C_4{}'$; $r_5 = 4.5$ ohm; $r_6 = r_6{}' = 7$ ohm; different values of r, r_1, r_2, r_3 and r_7 are used for each set of conditions.

wire resistance is caused by contraction and breaking. An arc flashed across the broken wire and therefore the current remains continuous (if $i \lesssim 30$ amp, the glow of this arc cannot be distinguished against the bright background, produced by the spark. The arc may evaporate part of the metal.)

Figures 2*g* and 2*h*, produced with wires of different diameter but at equal $j(t)$ show that at equal current densities a thin wire breaks sooner than a thick one.

The nature of the variation of the breaking instant t_c with d and the length of the period of the resulting chain of droplets indicate that the breaks are caused by capillary forces.* In fact, the period of the chain produced by the capillary forces was found theoretically to be $\lambda = 4.508\ d$ (see Ref. 7, p. 591). Measurements based on Fig. 2*g* also yield $\lambda = 4.5d$.

Let us summarize the results of experiments in which the current i is shut off prior to the instant t_c . If the current is shut off at the instant $t_d = t_4$ at which $E(t_d) = W_h + W_m$, a wire with $d = 0.008$ cm breaks up into droplets only 3×10^{-4} — 4×10^{-4} sec after t_d (t_d is the instant at which the current is disconnected**, W_h is the energy required to heat the metal to its melting point T_m , and W_m is the melting energy). If $t_d < t_4$, the wire will of course not be completely destroyed.

The nature of the remnants of the wire depends not only on $E(t_d)$ but also on the extent to which the wire becomes deformed before its surface hardens. For example, a time interval $t_d = t_4$ is enough to break a wire with $d = 0.0077$ cm into droplets, but merely melts a wire with d –0.01 cm. This difference is due to the longer time the capillary forces require to deform the wire surface with increasing d . If d is large enough, the capillary forces can probably no longer overcome the gravitational or electrodynamic forces.

3. DESTRUCTION OF WIRE AT APPROXIMATELY 5×10^6 AMP/CM.^{2}

Figures 3–4 show photographs of a nickel wire

---

*The destruction of wires by capillary forces was observed earlier. Se, forexample, Ref. 6.

**It takes about thesame time to destroy a current-carrying wire. Consequently in wires with $d \lesssim 0.008$ electrodynamic forces do not play a substantial role in the contraction.

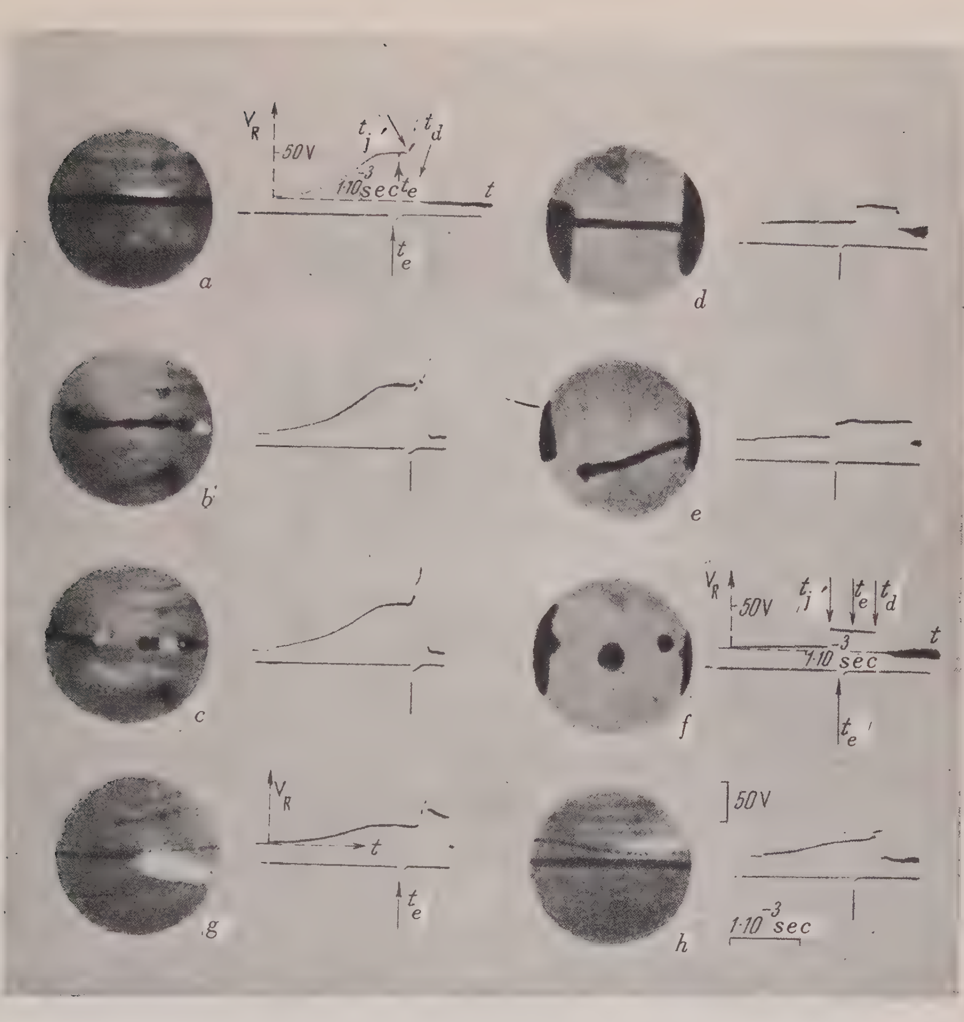

FIG. 2. Photographs (15×) and oscillograms $V_R(t)$ of wires l cm long and d cm in diameter in air at $j \approx 5 \times 10^5$ amp/cm^2; a, b, c— tungsten, $l \approx 1.5$; $d = 0.0077$; d, e, f— nickel, $l \approx 0.15$, $d = 0.008$; g, h—tungsten, $l = 0.5$, wires with $d = 0.0077$ and 0.0018 connected in parallel. In each oscillogram, the upper beam is shifted to the right by $\Delta x = 0.12$ relative to the lower beam. The scales marked on Fig. a, is common to Figs. a, b, and c; that on Fig. f is common to Figs. d, e, and f; and that on Fig. h is common to Figs. g and h. t_d, t_e and t_j' are the instant of current shutoff, exposure, and jump in V_r. (The bright spot of Fig. 2g is the drop into which the wire contracted. The tungsten drop remaining in the field of view illuminates the film through a pair of crossed polaroids).

carrying $j \approx 5 \times 10^6$ amp/cm.[2] The start of the exposure and its duration are seen from the pip on lower line of the oscillogram, the magnitude of which is proportional to the current i_{ph} (see Sec. 1). As can be seen from the photograph, the outline of the wire does not change prior to the instant ($t = t_j$)* of the jump in V_R, except for bending. At $t = t_j$, the wire suddenly begins to expand rapidly, and the metal is exploded.

Estimating the speed of the boundary between the material of the wire and the surrounding air from Figs. 3c and 3e we get

$$V_r = [d(t_e) - d(t_c)] / 2(t_e - t_c)$$
$$= 5\cdot10^3 - 1\cdot10^4 \text{ cm/sec.}$$

---

*At $j \gtrsim 5 \times 10^6$ amp/cm,^{2} the instant at which the jump in V_R occurs is independent of the wire dimensions.[3]

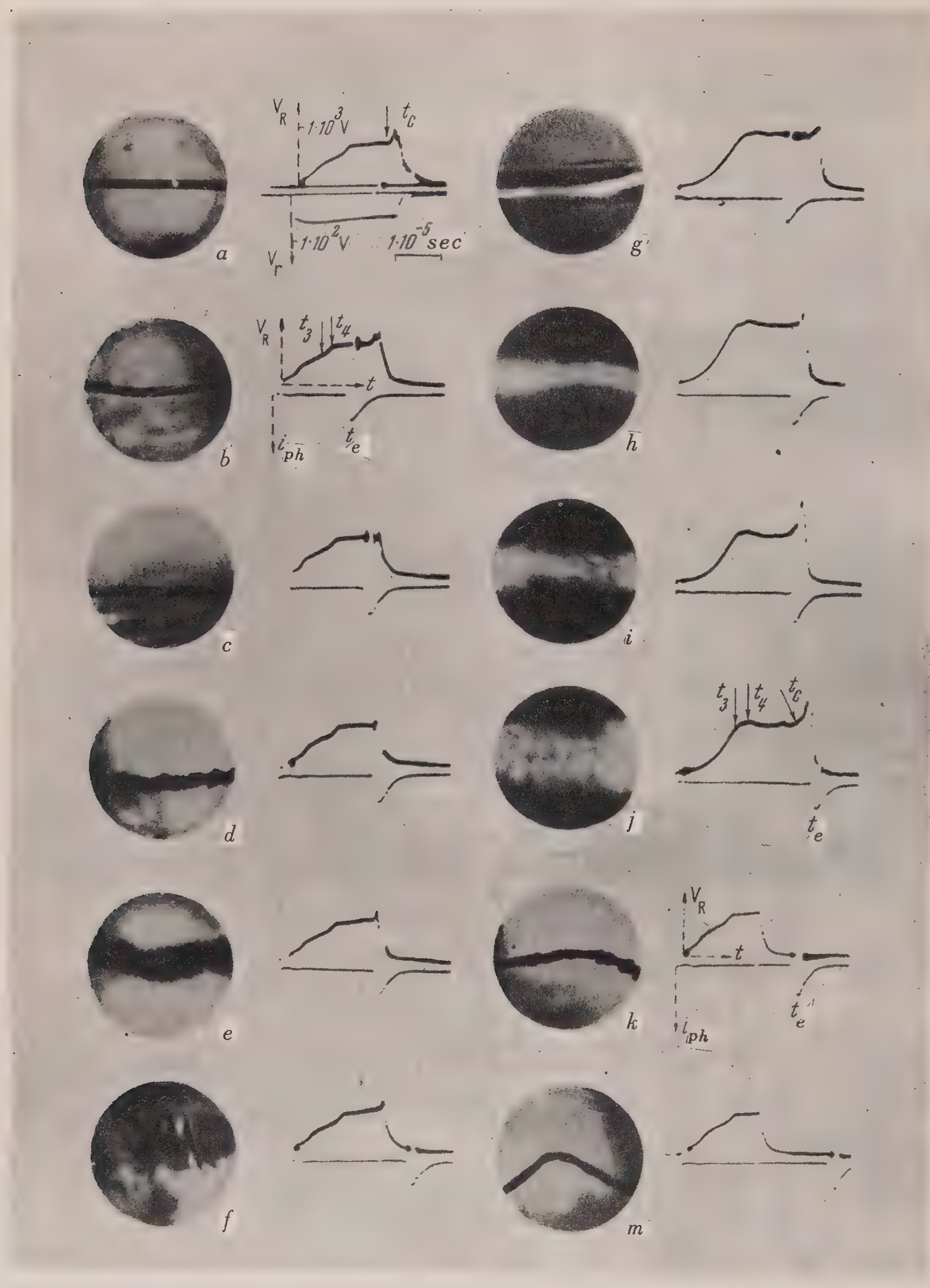

FIG. 3. Photographs (15×) and oscillograms $V_R(t)$ of nickel wire with $d = 0.008$ cm in air (*a* – *f*, *k*, *m*) and of tungsten wire with $d = 0.0077$ in glycerine (*g* – *j*) at $j = 5 \times 10^6$ amp/cm,^{2} $l \approx 2$ cm. An oscillogram of $V_r(t) = ri(t)$ ($r = 0.45$ ohm) is shown in photograph *a*; *a*– appearance of wire before turning the current on. The dark band on photograph *g* is the compression wave of the glycerine. The tungsten explosion products appear bright against the background produced by the spark *S*; *k*, *m* – current turned off at $t < t_j$ and no explosion takes place; $\Delta x = 0.12$ cm.

Figures 3g–3j show photographs of a tungsten wire in glycerine. (In experiments with $t_d \gtrsim t_j$, the tungsten wire was placed in glycerine because a flash discharge was produced over its surface in air[3] at $E \approx W_h + 2W_m$.)

If the current is turned off at a certain instant t_s somewhat earlier than t_j, the metal will no longer explode. For example, no symptoms of an explosion are seen in the experiments with $t_j < t_s$ (Figs. 3k, 3m) even though the exposure took place later than in the experiments with $t_d \approx t_j$ (Figs. 3e, 3f). (The volume of the explosion products is always considerably greater than the initial volume of the wire after the start of the exposure.) One can judge the character of the damage to the wire from its remnants: in experiments with $t_d \geq t_j$ the metal pulverizes (glass placed near the wire becomes coated with a deposited mirror surface, but experiments with $t_d < t_s$ leave droplets measuring $\sim d$. The fact that t_s and t_j are not exactly equal is apparently due to the inhomogeneity in the wire and to an insufficiently abrupt current shutoff.

Further reduction in t_d within the range $t_4 \leq t_d < t_s$ leaves the character of the wire destruction unchanged. Figure 4 shows photographs obtained at various time intervals after t_d in experiments with $t_4 < t_s$. These photographs show that if $t_d < t_s$, the wire is destroyed already after t_d, because it breaks by bending* and because drops are formed. The bending is apparently due to uneven distribution of pressure along the axis of the wire** caused by the rapid increase in its energy.

4. REMARKS ON THE INTERPRETATION OF PREVIOUS EXPERIMENTS WITH TUNGSTEN IN THE CASE OF SHORT PULSES, AND ON THE MELTING OF THE METAL.

From the appearance of the wire after the experiments, it was concluded in Ref. 9 that the state of the tungsten at the instant $t = t^*$, when the value of dR/dE drops*, is different for $j = 5 \times 10^6$ than for $j = 5 \times 10^6$ amp/cm^2, and that $e(t^*)$ increases and diminishes with j. However, measurements made on the oscil-

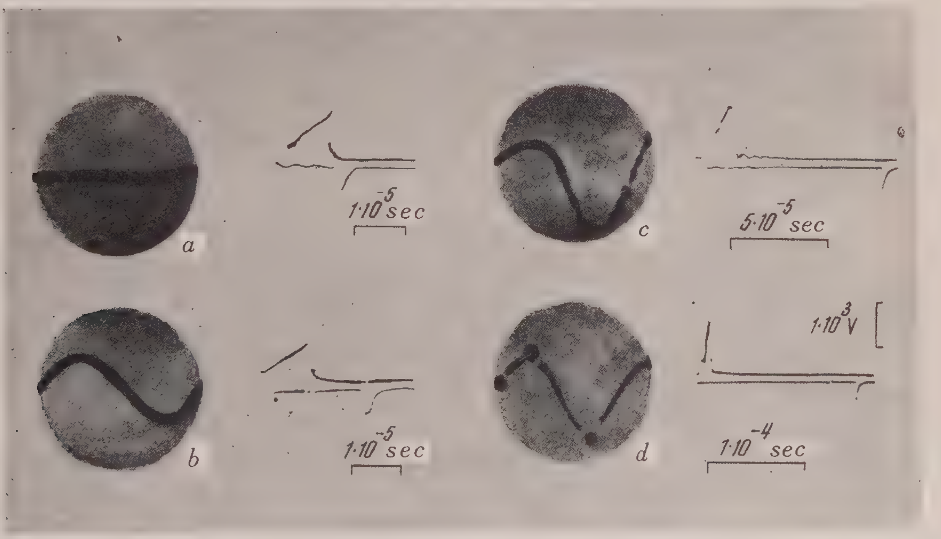

FIG. 4. Various stages of destruction of nickel wires with $d = 0.008$ cm and $l \approx 2.5$ cm in air at $t_e < t_d < t_s$; $j = 5 \times 10^6$ amp/cm^2; $\Delta x = 0.12$ cm; magnification 15×.

---

*Similar motion of the wire was investigated in Ref. 8.

**At $j \approx 5 \times 10^6$ amp/cm,^{2} the time required to expand the metal by heating is $\Delta t = t_3 - t_1 \approx 8 \times 10^{-6}$ sec. and the time needed to melt the metal is $\Delta t = t_4 - t_3 \approx 2 \times 10^{-6}$ sec. Therefore $u\Delta t > l$, where $u \approx 2 \times 10^5$ cm/sec is the speed of propagation of the disturbance of the metal and l is the length of the wire. At $j = 5 \times 10^5$ amp/cm,^{2} Δt is two orders of magnitude greater, add $u\,\Delta t >> l$. Consequently, the pressure along the wire will be uneven in the first case and uniform in the second case.

***The experiments in Ref. 9 were not accuaate enough to be able to distinguish the points t_3 and t_4 where the curve of $V_r(t)$ for tungsten breaks, or to determine the postion of t_d with respect to these two points.

lograms showed no dependence of $E\ (t^*)$ on j.[2,9] As was explained in Sections 2 and 3, the metal has a different microscopic motion** at $j = 5 \times 10^5$ amp/cm^2 than at $j = 5 \times 10^6$ amp/cm^2, and this determines the difference in the type of wire remnants at equal values of $E\ (t_d)$. There is consequently no indication that $E\ (t^*\ )$ depends on j.

In Reference 2 we were ableto locate*** the break points t_3 and t_4 on the curve $I = R\,(E)$ for tungsten (Fig. 3k) and to show that $E_3 = W_h$, $E_4 = W_h + W_m$, and $R_3 = R_m^s$ for all $j\ (t)$. The appearance of these points is naturally interpreted as the start and finish of the usual melting and we use here the following symbols: $E\,(t_{3,4}) = E_{3,4}$ $R\,(t_{3,4}) = R_{3,4}$. R_m^s and R_m^1 are thevalues of the resistance in the solid and liquid states at T_m). However, in Ref. 9 no melting was observed in a tungsten wire in experiments with $j = 5 \times 10^5$ amp/cm^2 at $E\ (t_d) > W_b$. This and the values of R_3 and R_4 would apparently indicate an anomaly in the melting (R_4 of tungsten differs from R_3 much less than R_m^1 differs from R_m^s of any metals, for which the values are known).

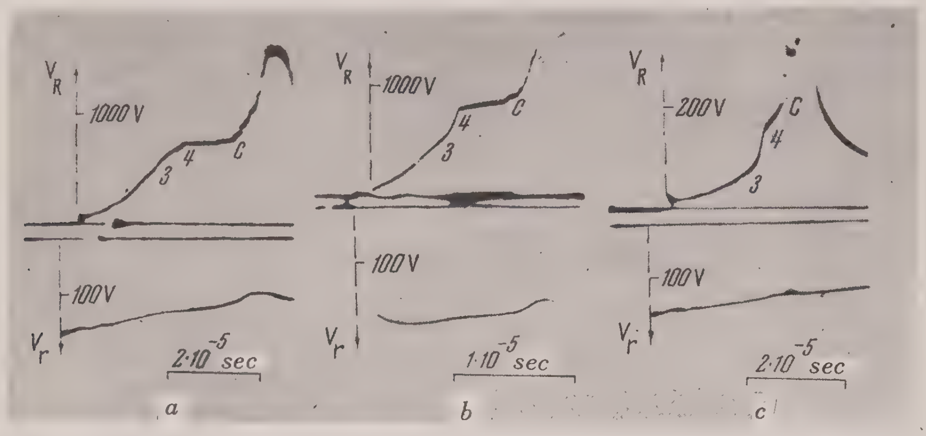

FIG. 5. Oscillograms of $V_R\ (t)$ and $V_r\ (t)$, $\Delta x = 0.2$ cm, a – Mo in glycerine, $d = 0.01$ cm, $1 = 2.05$ cm, $r = 0.5$ ohm, $j^{\max} = 4.6 \times 10^6$ amp/cm.^{2} b – Pt in glycerine, $d = 0.002$ cm, $1 = 1.55$ cm, $r = 12.3$ ohm, $j^{\max} = 6.2 \times 10^6$ amp/cm.^{2} c – Cu in air, $d = 0.008$ cm, $1 = 1.23$ cm, $r = 0.5$ ohm, $j^{\max} = 7 \times 10^6$ amp/cm.^{2}

As explained now, the wires were not observed to melt at $j = 5 \times 10^5$ amp/cm^2 in Ref. 9 because the immobile molten tungsten hardened before its surface had a chance to become sufficiently deformed.

There is therefore no reason for assuming the melting of metal at large values of j to be unusual. Since the melting proceeds normally, and no contraction occurs in the wire prior to t_4, the quantities W_h, W_m, R_m^s and R_m^1 can be measured from the oscillograms. Using the data of Ref . 2 for R_4 / R_3, we obtained R_m^s and R_m^l for tungsten, nickel and gold. In this investigation we performed experiments

---

**The kinetic energy of this motion, estimated from Figure 4b, is less than 1% of W_h.

***For metals with large ratios R_m^l / R_m^s, the points t_3 and t_4 were already compared with the melting point in Ref. 10. However, in Ref. 10, an increase in E_3 was observed with increasing j. In Ref. 11, these points were used to measure R_m^l / R_m^s for Au and Pt at $j = 1 \times 10^6$ amp/cm.^{2} But in Ref. 11, " a shift in the breaking points towards lower energy was observed for platinum" for $j = 4 \times 10^6$ amp/cm.^{2} These data indicate the peculiar melting behavior at large values of j.

with molybdenum, platinum* and copper (Fig. 5), and repeated the measurements for tungsten and nickel. We consider experiments with copper to be the control measurements, since the quantity R_4/R_3 for copper agrees with the tabular values for R_m^1/R_m^s. The values $R_4/R_3 = R_m^1/R_m^s$ for other metals are given in the Table.

5. VERIFICATION OF CONCLUSION CONCERNING THE ANOMALOUS STATE OF THE METAL

It was confirmed in Sec. 3 that what occurs at $j \gtrsim 5 \times 10^6$ amp/cm^2 at the instant t_j is a change in the volume properties of the metal and not a rupture of the wire into parts. Consequently, our measurements of R' and E' actually make it possible to find the specific resistivity R and the internal energy E of the metal.

The dependence of E_j on j was investigated in this work over a wider range of j than in Reference 2. Here the current varied little prior to the instant t_j at $j \lesssim 5 \times 10^6$ amp/cm^2 (Figs. 3*a* and 5). But at j greater than 1×10^7 amp/cm,^{2} the time $t_4 - t_1$ became shorter and approached the duration of the current buildup that occurred after the current was turned on. The current can therefore be assumed constant only at $t_4 < t < t_j$, and the measured values of $E(t)$ and $E(t_j) - E(t_4)$ are best examined separately. For $j_{\max} = 1.8 \times 10^7$ amp/cm^2 we observed, within the limits of the measurement accuracy (10%), that $E(t_4)$ equals $W_h + W_m$, and that $E(t_3)$ equals W_h. The measured values $E(t_j) - E(t_4)$ are shown in Figure 6. The maximum difference between values of $E(t_j) - E(t_4)$ for any one value of $j \gtrsim 5 \times 10^6$ amp/cm^2 does not exceed 8%. This difference increases as j drops below 5×10^6 amp/cm,^{2} owing to the increase in the dispersion of t_j (of the time $t_j - t_1$). The maximum and minimum values of $E_j - E_4$ obtained for a wire with $d = 0.008$ cm* at $j \approx 1.3 \times 10^6$ amp/cm^2 are plotted in Figure 6. The increased dispersion of t_j with diminishing j is explained by the rise in t_j to a value close to t_j, in other words, by the fact that the wire and time to become deformed by capillary forces during the time of the experiment. It is therefore impossible to estimate E_j from the jump in V_R at $j < 1 \times 10^6$ amp/cm^2 for $d \lesssim 0.008$ cm.

Thus, for $1.3 \times 10^6 < j < 18 \times 10^6$ amp/cm,^{2} according to Figure 6, the value of the internal energy of the metal E_j, at which the jump in dR/dE occurs, is a function of j.

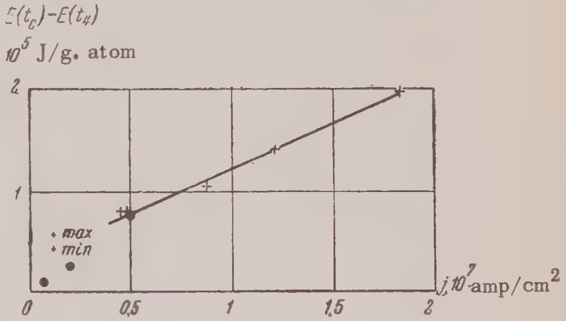

FIG. 6. Dependence of energy $E_j - E_4$ on j for nickel. Abscissas indicate the values of j at $t = t_4$; + – results of experiments with $d = 0.008$ cm and $l = 0.5 - 2$ cm; ● – results of earlier experiments [2] with defective wire 0.0015 cm in diameter.

---

*For Pt we obtained $R_1 = 10.2 \times 10^{-6}$ ohm. cm; $R_4 = R_m^1 = (75.6 \pm 2) \times 10^{-6}$ ohm. cm, $E_3 = W_h = (58.5 \pm 2) \times 10^3$ J/g-atom, $E_4 - E_3 = (23.2 \pm 3) \times 10^3$ J/g-atom and for $j = 6 \times 10^6$ amp/cm we obtained $E_j - E_4 = (130 \pm 3) \times 10^3$ J/g-atom. For tabular data we have for Pt at 18° C $R = 10.5 \times 10^{-6}$ ohm. cm and at 1500°C, $R = 52.6 \times 10^{-6}$ ohm. cm[12], $W_h = 53.4 \times 10^3$ J/g-atom[13] and $= W_h = 61.5 \times 10^3$ J/g-atom[12], $W_m = 22 \times 10^3$ J/g-atom[12,13], and $T_m = 1773°$ C.[12] For Mo we obtained $R_4 = R_m = (96 \pm 2) \times 10^{-6}$ ohm. cm, $E_4 = W_h + W_m = (115 \pm 8) \times 10^3$ and $E_4 - E_3 = W_m = (40 \pm 4) \times 10^3$ J/g-atom. According to Ref. 14, we have for Mo at 2000° C, $R = 60 \times 10^{-6}$ ohm. cm, $W_m \sim 20 \times 10^3$ J/g-atom and $T_m = 2622°$ C.

*A sharp reduction in $E_j - E_4$ (black dots on Fig. 6) was observed for small j in experiments with a wire having ing $d = 0.015$ cm and containing defects; this increase is explained as follows: at large values of j, premature destruction of the wire at the defective points is concealed by the arc that is produced and produces only small dents in the oscillograms of $V_r(t)$. At small values of j, $V_r = ir$ is small and the individual wire defects cause greater jumps in V_r at $t < t_j$, i.e., at $E < E_j$.

An attempt was made to attribute the dependence of E_j on j to changes in the external conditions, by suggesting, for example, that t_j is the instant at which the metal begins to boil, and that the increase in E_j with increasing j is due to an increase in the electrodynamic pressure. But were this so, the metal in experiments 3*k* and 3*m* should boil off as soon as this pressure was removed at the instant t_d, for the value of $E\ (t_d)$ in these experiments exceeds the value of E_j, measured when the wire was exploded by a current with $j \approx 1.3 \times 10^6$ amp/cm^2. In fact, according to Figures 3*k* and 3*m*, the metal does not explode at $t_d < t_s$. The fallacy of the above assumption is seen also from the fact that there is no electrodynamic pressure on the surface of the wire. The surface layer would therefore boil at the same value of E at all values of j.

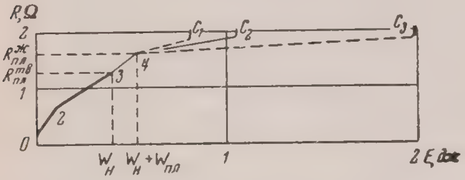

FIG. 7. Plot of $R = R\,(E)$ for nickel. The data were obtained for wires with $d = 0.015$ cm ($j \leq 5 \times 10^6$ amp/cm^2 and $d = 0.008$ cm (all values of j) of varying lengths and were recalculated for $d = 0.008$ cm and $l = 1$ cm. The dependence of R on E is regular up to a point 4 (heavy line). Sections $4 - c_1$, $4 - c_2$, and $4 - c_3$ correspond to $j = 1.4 \times 10^6$, 5×10^6, and 18×10^6 respectively.

6. COMPARISON OF OUR IDEAS CONCERNING THE EXPLOSION OF METAL WITH DEDUCTIONS MADE BY OTHER INVESTIGATORS

Explosion of wires was studied by many experimenters whose interpretation of this phenomenon differs substantially from ours. For example, according to Ref. 5, the "wire breaks down into individual sections" as a result of its inhomogeneity. "The occurrence of these breaks leads to an interruption of the current and to occurrence of pauses in the current. . . During the time of the current pause, the wire particles evaporate because of the heat received during the time of current flow". Our data show, however, that at $j \gtrsim 5 \times 10^6$ amp/cm^2 a well-calibrated wire breaks up into parts because of the velocity attained by the metal during its thermal expansion, and not because of any inhomogeneities. These pieces fly apart and cool in the form of macroscopic droplets, and do not evaporate. Rather than cause the current interruption, the breaks occur after the current is shut off. Were the current not shut off prior to the instant t_j the wire would tear before the breaks would occur. Breaks are therefore observed only at $t_d < t_j$, when no explosion occurs at all.

Reference 1 gives an interpretation of the first stage of the explosion, similar to that given in Ref. 5, but the causes of the inhomogeneities* of the wire are assumed to be wire deformations caused by capillary forces. In old,[10], as well as new (Ref. 18, p. 191) investigations, the explosion is considered to be a rapid evaporation of the metal. We, to the contrary, assume the explosion to be not evaporation, but expansion of the metal over its entire volume**. An explosion differs from ordinary evaporation in that there exists an instant t_j, at which the expansion of the metal changes abruptly, and dR/dE experiences a jump. (If an attempt is made to ascribe the expansion of the image of the wire in Fig. 3 to evaporation of the metal, one must assume that the velocity of evaporation experiences a jump of one order of magnitude at $t = t_j$.) That the explosion cannot be identified with rapid surface evaporation can also be seen from the fact that E_j may be less than the binding energy of the metal, as seen, for example, in experiments with nickel at $j \approx 5 \times 10^6$ amp/cm,^{2} in which the total energy delivered $E\ (t_d) \approx E_j = 0.43\ W_{\text{subl}}$, could not rate even half the mass of the wire (W_{subl} is the sublimation energy). Yet various photographs similar to 3*d* and 3*e*, obtained in similar experiments, show no remnants of the wire.

The mechanism of the metal explosion is still unexplained. Apparently, the increase in the thermal expansion at large values of E starts disturbing the metallic bond destroys the metallic conductivity. The energy E_j at which this occurs may

---

**No vapor is seen near the wire at $E\ (t_d) < E_j$ in Figs. 3*k* and 3*m*, but Fig. 3*e* shows for $E\ (t_d) = E_j$ a dense cloud with a sharp boundary, the character of which is important to the explanation of the "current pause" phenomenon[10,5,3]. Were the boundary indistinct, the cloud would be electrically weak and would immediately break down at a distance from the wire at which the density makes breakdown possible. Actually, however, if the conditions are right (Ref. 3, page 632), the cloud breakdown is noticeably later than the instant t_j, when the density in the cloud is reduced sufficiently by expansion.

be less than the binding energy of the metal. In fact, metallic conductivity disappears when the metal decomposes in particles that are smaller than the mean free path of the electron. This assumed phenomenon could also be produced by heating the metal at low current. But in our experiments heating by low current stops at a low value of E because the wire breaks by capillary forces.

Metal	$R_m^l/R_m^s = R_4/R_3$ Our data	R_m^l/R_m^s Literature data
Au	1.94±0.05*	2.28[15], 4, 335; 2**[11]
Pt	1.40±0.02	1,4[11]
Ni	1,30±0.02	1.94[16], p. 295; [15], 1, 129; 4, 335 1,3 [17]
Mo	1,23±0.01	—
W	1.08±0.01	—

*See Ref. 2, p. 107, concerning the purity of the Au.

**The authors of Ref. 11 attribute the deviation of this result from 2.28 to the measurement error.

The increase of E_j with j could be caused by a change in the state of the electrons and of the metal under the influence of a strong electrical field, thus causing a change in the metallic bond. According to Fig. 7, dR'/dE' decreases with increasing j for $E' > E'_{4'}$, apparently indicating a reduction in dR/dE. The drop in dR/dE could be interpreted as a symptom of the appearance of the "excess energy" $\mathcal{E}$ (Ref. 9, Sec. 4).

CONCLUSIONS

1. *Destruction of the Wire.* At currents $j \approx 5 \times 10^5$ amp/cm,^{2} surface tension causes the wires ($d < 0.01$ cm) break up into droplets after melting. At greater values of j, dE/dT ($\sim j^2$) becomes greater, and the surface tension σ does not change for a given value of E. The energy E therefore may rise enough to destroy the metal even prior to the instant (t_c) at which the breaks occur. For example, for nickel at $j \approx 5 \times 10^6$ amp/cm^2 and at $d = 0.008$ cm, the value of E ($p_{c'}$) would reach $30\ W_h \approx 4.6\ W_{\text{subl}}$, were R and σ to remain close to R_m^1 and σ_m^1. But actually, at $j \approx 5 \times 10^6$ amp/cm,^{2} the wire becomes destroyed at an instant $t_j < t_j$, when $E(t_j) = 2.7\ W_h$. The destruction of the wire at the instant t_j has the nature of an explosion: there is no substantial change in d prior to t; but at $t = t_j$ the metal starts expanding rapidly, and within several microseconds it already has the shape of a cloud (even if $t_d = t_j$).

No explosion will occur if the current is shut off prior to t_j ($t_4 \leq t_d < t'_s$) without changing the value of j. The destruction of the wire differs in this case from that occurring at low values of j only in the macroscopic motion: at $j \gtrsim 5 \times 10^6$ amp/cm,^{2} various portions of the wire acquire different velocities, causing the wire to bend and later on to break up into droplets. These velocities are apparently due to the expansion of the metal by the rapid increase in E even before the end of the melting. At $j < 5 \times 10^5$ amp-cm,^{2} dE/dt is small, the wire is not seen to bend but only to be torn by capillary forces.

Thus, the destruction of the melting wire may be of two types: *a*) a break up into macroscopic parts by external forces (if the energy has not reached the value E_j prior to the instant t_j, of this break); *b*) an explosion* due to the change in the state of the metal itself and to its pulverization (if E reaches the value E_j). The value of E_j increases with j, and at $j \leq 18 \times 10^6$ amp/cm^2 E_j is less than the sublimation energy for nickel.

2. *Dependence of R on E.* Figure 7 shows the curve $R = R(E)$ for nickel, taken from Reference 2 and supplemented by new data.

Region 1–3. As explained in Reference 2, no singularities are observed in the dependence of R on E at $j \leq 5 \times 10^6$ amp/cm^2 prior to the start of the melting point 3).** This conclusion was confirmed in our investigation up to $j = 18 \times 10^6$ amp/cm.^{2}

---

*Usually attention is paid in the study of wire explosions not so much to the explosion of the wire itself, as to the explosive phenomena produced in its destruction products by the continuing flow of current. For example, in Refs. 4 and 5 the speed of expansion of the explosion products in the air ($V_g = 1 \times 10^5 - 2 \times 10^5$ cm/sec) was apparently measured at $i \neq 0$. In our measurements, however, we obtained $V_g = 5 \times 10^3$ to 1×10^4 cm/sec after shutting the current off.

Region 3–4. The quantities R_3, E_3, R_4, and E_4 agree, within the limits of experimental accuracy, with R_m^s, W_h, R_m^1 and ($W_h + W_m$) respectively for all $j \leq 18 \times 10^6$ amp/cm.^{2}

Region 4 – j. It was confirmed that the form of the curve $R = R(E)$ depends on j for $E > E_4$: the value $E = E_j$, at which the jump in dR/dE occurs (points C_1, C_2, C_3 on Fig. 7) increases with increasing j. For example, a metal state with energy $E > E_{j2}$ is observed only at $j > 5 \times 10^6$ amp/cm.^{2} The state of the metal before the start of the explosion is different in experiments with $j = 5 \times 10^6$ amp/cm^2 (point C_2) from the state of metal with the same value of energy E_{j2} produced in experiments with $j = 1.8 \times 10^7$ amp/cm,^{2} since the explosion takes place at the latter density not at E_{j3} , but at E_{j2} . This difference in states is seen also from the difference in the slopes of the curves $R = R(E)$ past point 4 in Fig. 7. However, the data on the dependence of dR/dE on j prior to the start of the explosion still require verification.

The conclusion that the metal has an anomalous state at $E > E_{jl}$ is based on the following premises: the explosion of the wire is determined by the state of the metal; if the external conditions do not change, the value of the energy E_j at the instant of explosion depends on j. Both these premises were confirmed in this investigation.

I am indebted to L. N. Borodovskaia who participated in all the experiments at $j \approx 5 \times 10^6$ amp/cm,^{2} and in all the measurements of R_m^l / R_m^s.

Note added in proof. The latest work known to us[19] ascribes the explosion to inhomogeneous heating and melting of the wire.

**This result was confirmed in Ref. 18 for strongly-varying currents, reaching values $j^{\max} = 6 \times 10^7$ amp/cm^2 in Ag and Cu. The $R'(E')$ curves of Ref. 18, differ from ours. Thus, our data show dR'/dE' for Pt to drop sharply at the instant melting is ended (point *4* of Fig. 5*b*), but according to Ref. 18 (Fig. 5, point B, corresponding to the end of the melting), dR'/dE' remains large. If the correct instant, indicated in Fig. 5, is taken for the end of the melting in Ref. 18, the resultant value of W_m is too high by approximately a factor of 2. The $R'(E')$ curves of Fig. 6 of Ref. 18 do not show at all the breaking points *3* and *4* for tungsten at $j = 1.5 \times 10^7$ amp/cm.^{2}

1 W. M. Conn, Z. angew. Phys., 7, 539 (1955).
2 L. N. Borodovskaia and S. V. Lebedev, J. Exptl. Theoret. Phys. (U.S.S.R.) 28, 96 (1955). Soviet Phys. JETP 1, 71 (1955).
3 S. V. Lebedev and S. E. Khaikin, J. Exptl. Theoret. Phys. (U.S.S.R.) 26, 629 (1954).
4 J. A. Anderson and S. Smith, Astrophys. J. 64, 295 (1926).
5 N. N. Sobolev, J. Exptl. Theoret. Phys. (U.S.S.R.) 17, 986 (1947).
6 W. Kleen, Ann. Physik 11, 579 (1931).
7 H. Lamb, *Hydrodynamics* (Russian translation), OGIZ, 1947.
8 O. Bethge, Ann. Physik 8, 475 (1931).
9 S. V. Lebedev, J. Exptl. Theoret. Phys. (U.S.S.R.) 27, 605 (1954).
10 J. Wrana, Arch, Elektrotech, 33, 605 (1954).
11 L. A. Ignat'eva and S. G. Kalashnikov, J. Exptl. Theoret. Phys. (U.S.S.R.) 22, 385 (1952).
12 Boitsov, Boitsova and Avdonina, *Noble Metals*, Metallurgizdat, 1946.
13 Landolt–Börnstein, *Phys–chem*, Tabellen, 1923–1926, Berlin.
14 M. A. Filiand and E. I . Semenova, *Properties of Rare Metals, Handbook*, Ferrous and Nonferr. Met. Publ. House, Moscow, 1953.
15 Tech. Encyclopedia, Handbook of Physical, Chemical and Technological Quantities, OGIZ, 1931.
16 *Encylopedia of Metal Physics*, ed. by Mazing, 1, ONTI, 1937.
17 N. P. Mokrovskii and A. P. Regel', J. Tech. Phys. (U.S.S.R.) 23, 2121 (1953).
18 Bondarenko, Kvarkhtsava, Pliutto and Chernov, J. Exptl. Theoret. Phys. (U.S.S.R.) 28, 191 , 1955: Soviet Phys. JETP 1, 221 (1955).
19 Kvarkhtsava, Pliutto, Chernov, and Bondarenko, J. Exptl. Theoret . Phys. (U.S.S.R.) 30, 42, 1956 ; Soviet Phys. JETP 3, 40 (1956).

Translated by J. G. Adashko
49

SOVIET PHYSICS JETP VOLUME 5, NUMBER 2 SEPTEMBER, 1957

Fission of U, Th, Bi and Tl Induced by High Energy γ-Quanta

E. V. MINARIK AND V. A. NOVIKOV
The P. N. Lebedev Physical Institute, Academy of Sciences, USSR

(Submitted to JETP editor August 30, 1956)
J. Exptl. Theoret. Phys. (U.S.S.R.) 32, 241-246 (February, 1957)

The photofission yields of U^{238}, Th^{232}, Bi^{209} and $Tl^{204,206}$ have been measured with an ionization chamber at bremsstrahlung maximum energies from 80 to 250 mev. The photofission effective cross sections computed by the total spectrum method rapidly increase from ~80 mev and at 250 mev reach a value of (220 ±80) mb for U, (80 ±30) mb for Th, (4.7 ±0.6) mb for Bi and (1.6 ±0.2) mb for Tl. The energy dependence of the cross sections is the same for all four elements and, above 150 mev, is similar to the energy dependence of the total cross section for photoproduction of neutral and charged mesons.

INTRODUCTION

ALL the experimental results on photofission reactions attest to the fact that for photons with energies 10 to 30 mev, γ-ray absorption in nuclei takes place through a dipole mechanism. The measurement of photoneutron yields[1,2] and photostars[3,4] showed the rise in the effective cross section for photon energies greater than 100 mev. An attempt has been made[4] to explain the observed increase in the cross section for formation of stars above 150 mev by reabsorption of mesons in nuclei. On the basis of the concept of reabsorption, a conclusion has been reached[5] that within the nucleus mesons, because of their nature, must be absorbed as soon as they are created, and that virtual mesons must give an appreciable contribution, in consequence of which the "meson" part of the photofission cross section will extend in the region of photon energies less than the threshold for meson production.

The study of the dependence of the fission cross section of heavy nuclei on the photon energy up to $\hbar\nu \sim 300$ mev[6–10] has given in a general way analogous results. However, while in the region of the giant resonance the energy dependence of the photofission cross section has been studied sufficiently thoroughly, fairly complete information is not available for $\hbar\nu > 100$ mev. Because of this, there was interest in investigating this dependence more fully for a number of heavy nuclei at high photon energies. This work is devoted to this problem.

DESCRIPTION OF THE EXPERIMENT

In our experiments, carried out on the synchrotron of the Physics Institute of the Academy of Sciences, USSR, we measured the dependence of the photofission yield of the nuclei of U^{238}, Th^{232}, Bi^{209} and $Tl^{203,205}$, on the maximum energy of the bremssrahlung radiation. The geometry of the experiments is shown in Fig. 1.

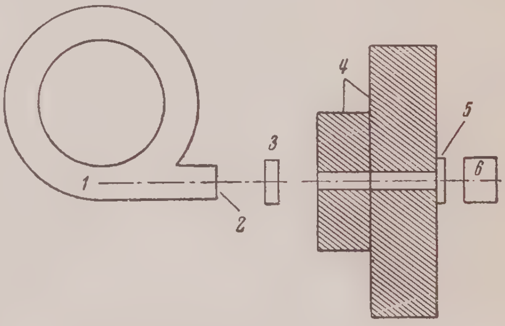

FIG. 1. Experimental Set-up. *1*—synchrotron target; *2*—aluminum disk covering the window in the vacuum chamber; *3*—thin-walled ionization chamber; *4*—lead shielding; *5*—holder for the copper foil; *6*—ionization-chamber registering fission events.

The beam of γ-quanta, leaving the vacuum chamber of the synchrotron through a window covered with a thin aluminum disk, passed through a lead collimator of 50 mm diameter behind which was placed a pulse ionization chamber, registering fission events. A thin-walled ionization chamber placed in front of the collimator was used for measurements of the relative intensity of the beam of γ-quanta.

The characteristic property of work with the accelerator is the presence of a strong electron background which, to a considerable extent, makes it more difficult to carry out the measurements. In order to decrease the background ionization, produced in the sensitive volume of the chamber by secondary electrons, the electrodes were made of thin aluminum foils and the windows in the housing of the chamber were closed with an organic layer of 30 μ thickness. Nevertheless, reliable compensation for the background was attained only when the duration of the photon beam was increased to 500 μ sec for maximum energies of 250 and 200 mev and to 300 μ sec for lower energies. The chamber was filled with chemically pure argon to a pressure of 250 mm of Hg.

The targets of the elements being investigated were prepared in the form of thin U_3O_8 and ThO_2 layers[7] and metallic (layers) of Bi and Tl[11] deposited on aluminum backings of 30 μ thickness and of 40 mm diameter. Since the diameters of the chamber electrodes were 75 mm, the fragments emitted from the edge of the target were not counted.

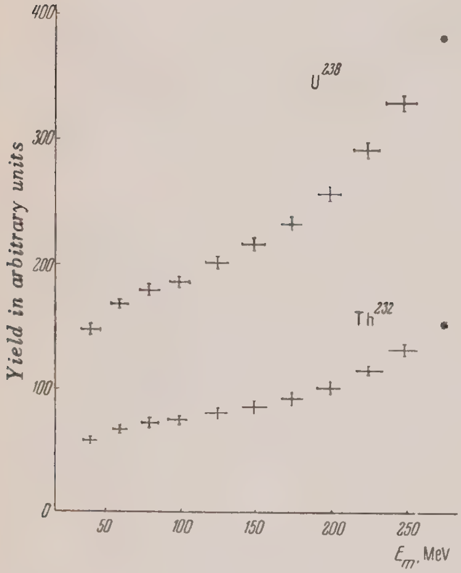

FIG. 2. Dependence of the photofission yield of U^{238} and Th^{232} on the maximum energy of the bremsstrahlung radiation (* are the values obtained by extrapolating the curves to E_m = 275 mev).

In the determination of the dependence of the photofission yield of thorium on the maximum energy of the bremsstrahlung radiation, the intensity of the γ-quanta beam was measured from the yield of the reaction $Cu^{63}(\gamma, n)Cu^{62}$ [12] in a copper target irradiated at the same time as the thorium target. Corrections dealing with non-uniform intensity during irradiation were introduced in the experimental value of the yield of the 10-minute activity of the Cu^{62} nuclei. The photofission yields of uranium, bismuth and thallium were measured relative to the yield for thorium. From the curves of the dependence of the photofission yields on the maximum energy of the bremsstrahlung radiation, the effective cross sections were calculated as a function of photon energy by the total spectrum method. Moreover the effective cross section for the reaction $Cu^{63}(\gamma,n)Cu^{62}$ for photon energies greater than 30 mev was taken to be zero. The agreement of the results on the photofission of Bi^{209} obtained in this work with the results obtained by Ref. 10, in which the intensity of the γ-quanta was measured with a threshold chamber, shows that it is possible to neglect the possible existence of the tail of the cross section of this reaction.

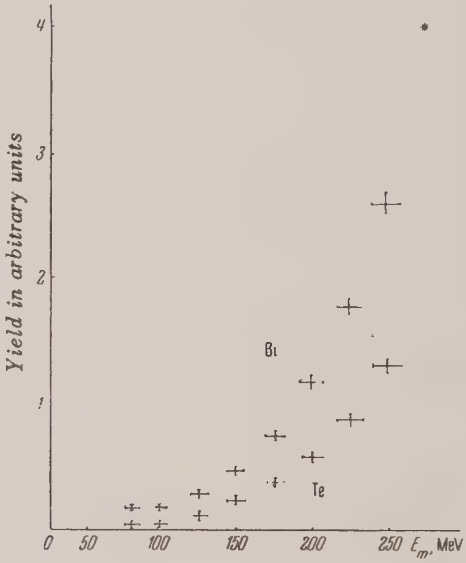

FIG. 3. Dependence of the photofission yield of Bi^{209} and $Tl^{203,205}$ on the maximum energy of the bremsstrahlung radiation.

Figures 2 and 3 show the dependence of the photofission yield, proportional to

$$\int_{E_p}^{E_m} \sigma_f(w)\,\eta(w, E_m)\,dw,$$

on the maximum energy of the bremsstrahlung radiation. The energy dependence of the photofission cross section is presented in Figs. 4–7.

The value of the average cross section

$$\int_{5}^{40} \sigma_f(w)\,\eta(w, 40)\,dw \Big/ \int_{5}^{40} \eta(w, 40)\,dw$$

in the 5 to 40 mev interval for U^{238} is equal to 38 mb which is not very different from the value of 44 mb which can be obtained from the results of Ref. 13.

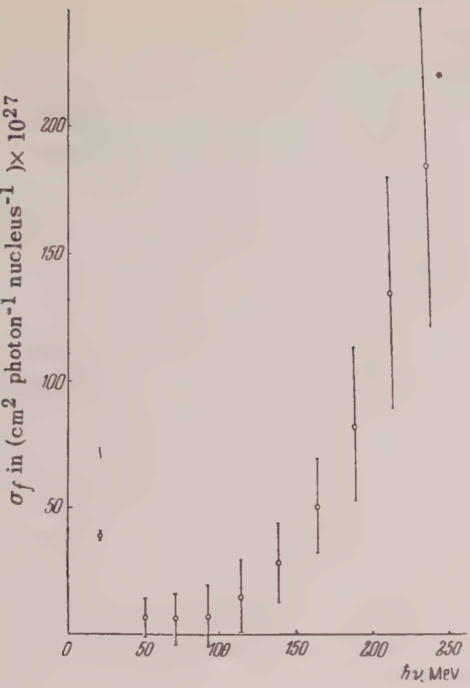

FIG. 4. Photofission cross section of U^{238} (*denotes the value obtained by extrapolating the curve to an energy $\hbar\nu = 250$ mev).

However it turns out to be for example one and a half times smaller than the values obtained from Refs. 8 and 14. The ratio of the photofission yields of Bi^{209} and U^{238} for a maximum energy of 85 mev, equal to 0.0009, coincides with the result of Ref. 15. The ratios of the photofission yields of U^{238}, Th^{232}, Bi^{209} and $Tl^{203,205}$ for a maximum energy of 275 mev[9] coincides with the ratios of the yields extrapolated to this energy from the present work. The energy dependence and the magnitude of the photofission cross section of Bi^{209} are in good agreement with the results of Ref. 10.

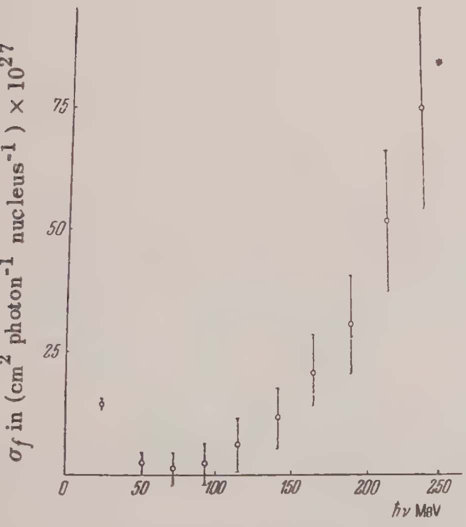

FIG. 5. Photofission cross section of Th^{232}.

While the errors in the cases of uranium and thorium are large, nevertheless it is clear that the photofission cross sections for all four elements rise quickly with an increase in the energy of the photons starting for example at 80 mev and attaining values of (220 ±80) mb for U^{238}, (80 ±30) mb for Th^{232}, (4.7 ±0.6) mb for Bi^{209} and (1.6 ±0.2) mb for $Tl^{203,205}$ by 250 mev. Figure 8 shows the course of the photofission cross sections of these nuclei as well as the sums $\sigma(\pi^{\circ}) + \sigma(\pi^{+})$ of the production cross section for neutral and charged mesons from free protons, normalized at a photon energy of 250 mev. As can be seen, the course of the photofission cross section in the region of 80 to 250 mev is the same for all four elements and above 150 mev coincides with the course of the total production cross section of neutral and charged mesons.

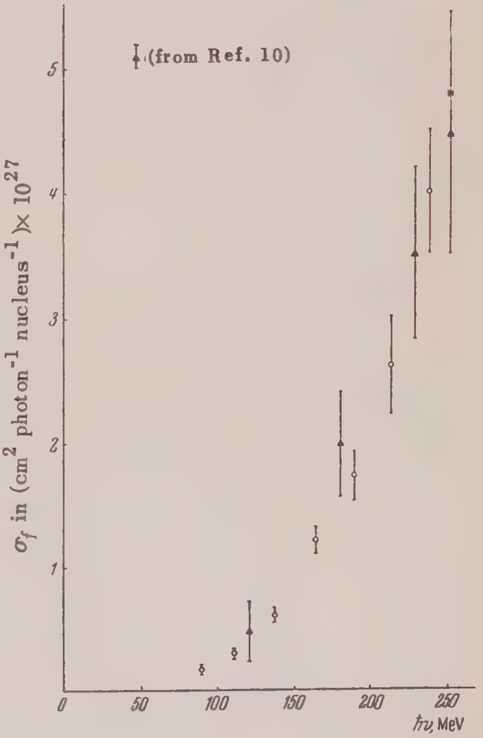

FIG. 6. Photofission cross section of Bi^{209}. ▲: data of Ref. 10

DISCUSSION OF THE RESULTS

The photofission cross section can be presented in the form

$$\sigma_f = \sigma_a \Gamma_{f,} \Sigma\Gamma,$$

where σ_a is the absorption cross section for the photon in the nucleus, and $\Gamma_f / \Sigma\Gamma$ is the relative fission probability which is equal to 0.2 to 0.4 for uranium[14,17] and which is 2.5 to 3 times smaller for thorium.[17] Because of this, the photofission cross section can rise because of the increase of $\Gamma_f / \Sigma\Gamma$ a maximum of 5 times in the case of uranium and of 10 times in the case of thorium.

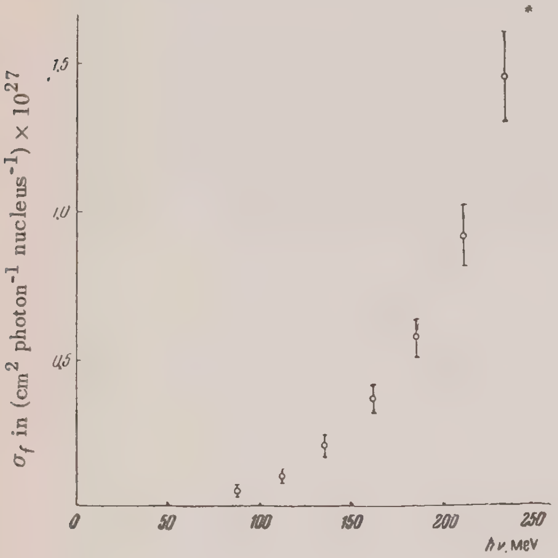

FIG. 7.Photofission cross section of $Tl^{203,205}$.

However, the experimental values of the photofission cross section of these elements increase more than 20 times from 80 to 250 mev. Moreover, a value of also ~ 0.4[18] was obtained for $\Gamma_f/\Sigma\Gamma$ in experiments on the fission of U^{238} by slow π^-–mesons. This shows that for a wide region of excitation energy the relative fission probability of U^{238} remains practically constant. The non–emissive character of the fission of U^{238} is confirmed by the results of experiments on the study of the mass spectra of fragments.[13,19] The curves obtained on the distribution of fragments as a function of mass testifies to the fact that for γ–quanta in the energy region of 10 to 300 mev, 3 to 4 neutrons are emitted in each fission event. Thus, at least in the case of U^{238}, the rise of σ_f in the interval of photon energy of 80 to 250 mev depends only on the increase of σ_a.

The fact that the photofission cross sections of all four elements start to rise at the same photon energy and change in the same way up to $h\nu$ = 250 mev shows, in our opinion, that for Th^{232}, Bi^{209} and $Tl^{203,205}$ the rise of σ_f depends also on the increase in σ_a. The emissive character of fission,observed when Bi^{209} was irradiated with neutrons[11,20] and γ–quanta[15,21] with energies of up to 85 mev, can be reconciled with the observed rise of the photofission cross section of Th^{232}, Bi^{209} and $Tl^{203,205}$ if the relative fission widths of these nuclei increase with increasing photon energy in the same way. From this, one can make the deduction that the rise in the photofission cross section of U^{238}, Th^{232}, Bi^{209} and $Tl^{203,205}$, observed for γ–quanta energies greater than 80 mev, depends on the rise of the absorption cross section for photons in nuclei. This is verified by other experimental data.[1,3]

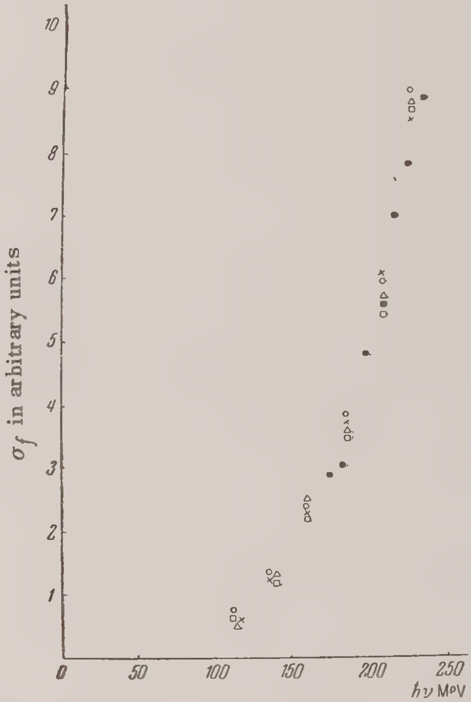

FIG. 8. Dependence of the photofission cross sections of U, Th, Bi and Tl, and of the total $\sigma(\pi^\circ) + \sigma(\pi+)$ production cross section of mesons, on the photon energy. The magnitudes of the cross sections were normalized to 10 for $h\nu$ = 250 mev. ×– U^{238} O–Th^{232}, Δ–Bi^{209}, □–$Tl^{203,205}$, ■–$\sigma(\pi^\circ) + \sigma(\pi^+)$.

An attempt was made[10] to estimate the photofission cross section of the Bi^{209} nucleus under the assumption that the rise in the photofission cross section above 150 mev is connected with the reabsorption of the mesons. Agreement with the experimental values σ_f was attained with $\Gamma_f/\Sigma\Gamma = 0.25$. However, experiments on the fission of Bi^{209} by slow π^--mesons[18] have given $\Gamma_f/\Sigma\Gamma$ a value one order of magnitude smaller which is confirmed by the results of this work. Therefore the rise observed above 150 mev and the magnitude of the photofission cross section cannot be explained only in terms of meson reabsorption. However, the similarity of the energy dependence of the photofission cross section and the photoproduction of mesons lead us to think that the very same interaction mechanism for γ-quanta with nuclei is responsible for the photoproduction of mesons and for the rise of the photofission cross section.

In conclusion we use this occasion to express our sincere acknowledgement to Professor P. A. Cerenkov for his constant attention to this work, to N.N.Novikov for help with carrying out the measurements, and also to I. V. Chuvilo for help in setting up the experiment and to Professor V. I. Goldanskii for discussion of the experimental results.

---

[1] L. W. Jones and K.M. Terwilliger, Phys. Rev. 91, 699 (1953).

[2] P. S. Baranov, Dissertation, Moscow, Physics Institute, Academy of Sciences, USSR (P.I. A. S.) (1955).

[3] Veksler, Pisarev, and Lebedev. Report to the P.I. A. S. (1951); R. M. Lebedev, Dissertation, Moscow, P. I. A. S. (1953).

[4] R. Miller, Phys. Rev. 82, 260 (1951), and S. Kikuchi, Phys. Rev. 86, 41 (1952).

[5] R. Wilson, Phys.Rev. 86, 125 (1952).

[6] G.C. Baldwin and G.S.Kleiber, Phys. Rev. 71, 3 (1947).

[7] I. V. Chuvilo, Dissertation, Moscow, P. I. A. S. (1951).

[8] Lazareva et al., Collection of papers presented at the session of the Academy of Sciences, USSR on the peaceful use of atomic energy (session of the Division of Physical and Mathematical Sciences), p. 306, Academy of Sciences of the USSR (1955).

[9] J. F. Gindler and R. B. Duffield, Bull. Am. Phys. Soc. 29, 13 (1954).

[10] Bernardini, Reitz and Segre, Phys. Rev. 90, 573 (1953).

[11] Goldanskii, Pen'kina and Tarumov, J. Exptl. Theoret. Phys. (U.S.S.R.) 29, 778 (1955); Soviet Phys. JETP 2, 677 (1956).

[12] L. Katz and A. G. W. Cameron, Canad. J. Phys. 29, 518 (1951).

[13] L. Katz et al., Phys. Rev. 99, 98 (1955).

[14] R. B. Duffield, J. R. Huizenga, et al., Phys. Rev. 89, 1042 (1953).

[15] N. Sugarman, Phys. Rev. 79, 532 (1950).

[16] G. Goldschmidt-Clermont et al., Phys. Rev. 97, 188 (1955); D. C. Oakley and R. L. Walker, Phys. Rev. 97, 1283 (1955); A. V. Tollestrup et al., Phys. Rev. 99, 220 (1955).

[17] J. R. Huizenga et al., Phys. Rev. 95, 1009 (1954), Valuev, Gavrilov, Zatsepina and Lazareva, J. Exptl. Theoret. Phys. (U.S.S.R.) 29, 280 (1955); Soviet Phys. JETP 2, 106 (1956).

[18] W. John and W. F. Fry, Phys. Rev. 91, 1234 (1953); Belovitskii, Romanova, Sukhov and Frank, J. Exptl. Theoret. Phys. (U.S.S.R.) 29, 537 (1955); Soviet Phys. JETP 2, 493 (1956); Perfilov, Lozhkin and Shamov, J. Exptl. Theoret. Phys. (U.S.S.R.) 28, 655 (1955); Soviet Phys. JETP 1, 439 (1955); N. A. Perfilov and N. S. Ivanova, J. Exptl. Theoret. Phys. (U.S.S.R.) 29, 551 (1955); Soviet Phys. JETP 2, 433 (1956).

[19] R. A. Schmitt and N. Sugarman, Phys. Rev. 95, 1260 (1954).

[20] E. Kelly and C. Wiegand, Phys. Rev. 73, 1135 (1948).

[21] N. Sugarman and K. Peters, Phys. Rev. 81, 951 (1951).

Translated by Fay Ajzenberg-Selove
55

SOVIET PHYSICS JETP VOLUME 5, NUMBER 2 SEPTEMBER, 1957

A New Method for Measuring the Polarization of Medium Energy Neutrons and the Phase Shift Analysis of n – He^4 Scattering

I. I. LEVINTOV, A. V. MILLER AND V. N. SHAMSHEV

(Submitted to JETP editor October 1, 1956).
J. Exptl. Theoret. Phys. (U.S.S.R.) 32, 274–283 (February, 1957)

A helium analyzer to measure the polarization of neutrons in the 1-18 mev energy range is described. The efficiency of the analyzer is about 100% in this range, and a typical counting rate is $\sim$ 20 counts/min at a current of 10^5 neutrons/cm^2 sec. The background is practically zero.

The azimuthal asymmetry in the scattering of (D + D) neutrons from He^4 has been measured at neutron energies of 2.4 and 3.4 mev. Analysis of the results agrees with the experimental phase shifts given by Seagrave and disagrees with those of Huber and Baldinger.

1. INTRODUCTION

MOST nucleons produced in nuclear reactions appear to be partially polarized, as is to be expected from the strong spin dependence of nuclear forces. It would be interesting to study these polarizations systematically, both in order to obtain further information on nuclear processes and to find a source of strongly polarized particles.

The presently available data on neutron polarization are sparce and limited to the reactions $D(d, n)$ (E_d = 600 kev and Li (p, n) (E_p = 2.262 mev). It is hard to do more with the presently available methods, which use C^{12} or O^{16} as analyzers.

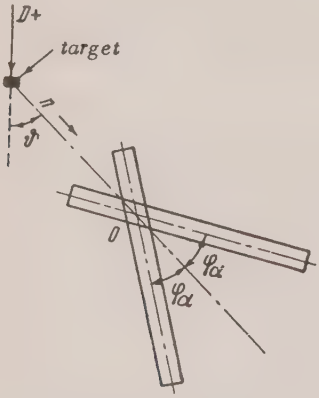

FIG. 1. Schematic drawing of apparatus.

In order to study neutron polarization systematically, an analyzer is needed which will give a large and accurately known polarization over a wide range of incident neutron energies. The levels of C^{13} and O^{17} are widely spaced in the energy range 1-20 mev and have widths of about 100 kev. Hence the polarization of neutrons scattered from C^{12} and O^{16} fluctuates, and an exact phase shift analysis is difficult because there are many levels corresponding to various states. Hence C^{12} or O^{16} are not very suitable for use as analyzers over a wide range of neutron energies and in any case demand a difficult phase shift analysis for each energy region.

A second fundamental disadvantage of these methods is the high neutron background due to neutrons reaching the detector directly from the target without passing through the analyzer. Even with elaborate shielding and collimation, the background is $\sim$ 80% of the total effect, while the presence of the shielding no doubt complicates measurements on the angular dependence of the polarization.

In the present paper we describe a method for measuring neutron polarization which has an efficiency of $\sim$ 1 at energies between 1 and 20 mev and which is practically free of background*. In addition, we have cleared up some points in the phase shift analysis for the scattering of neutrons by He^4 and measured the polarization of (D + D) neutrons using both thick and thin targets and deuterons of energies 400-1800 kev (cf Ref. 6).

Our analyzer uses He^4 as scatterer. Let us consider the polarization properties of this nucleus in more detail. Since the levels of He^4, if any exist, lie above 25 mev, neutrons incident with energies up to 20 mev can lead only to elastic scattering. Hence at these energies the states of He^5 can to a good approximation be derived from the motion of a neutron in an effective potential due to an unexcited alpha particle. The potential is equivalent to a well of depth $V_{eff} \approx 40$ mev, $r \approx 2 \times 10^{-13}$ cm, the well depth being strongly spin dependent[7]. As is well known, such an interaction gives scattering phase shifts which vary smoothly with energy. On the other hand, the small radius limits the orbital angular momentum of the scattered waves to

---

* The principle of the method and preliminary results on the phase shifts in n-He^4 scattering are given in Ref. 5.

P states for $E_n \lesssim 10$ mev and to D states for $E_n \lesssim 20$ mev. The phase analysis is simple because there are few phase shifts and they vary slowly with energy*. The strong spin orbit splitting gives a large and smoothly varying polarization, which, for convenient scattering angles, turns out to be about one in the whole energy range 1-20 mev.

The second advantage of He^4 as an analyzer is that we can detect the recoil nuclei rather than the scattered neutrons, thus eliminating background problems.

As detectors we used thin proportional counters filled with helium (Fig. 1). The apparatus was set up to detect He^4 nuclei recoiling at that angle φ_α with the incident beam which gave the largest azimuthal asymmetry in the scattering of polarized neutrons with given energy from He^4. To do this, the counters were placed along the direction φ_α; then the helium pressure and discriminator settings were chosen so that only the nuclei recoiling along the counter axis were detected. The azimuthal asymmetry R was measured by comparing the counting rate I_1 when the counter was in position φ_α with the counting rate I_2 in the position $-\varphi_\alpha$:

$$R = I_1 / I_2 = (1 + \overline{P}_x \cdot \overline{P}_{\mathrm{He}}) / (1 - \overline{P}_x \cdot \overline{P}_{\mathrm{He}}).$$

Here $\overline{P}_x$ is the polarization of the incident neutrons, averaged over the volume in which the recoil nuclei were formed (the working volume), while $\overline{P}_{\mathrm{He}}$ is the polarization resulting from neutron scattering on He^4, averaged over the scattering angles.

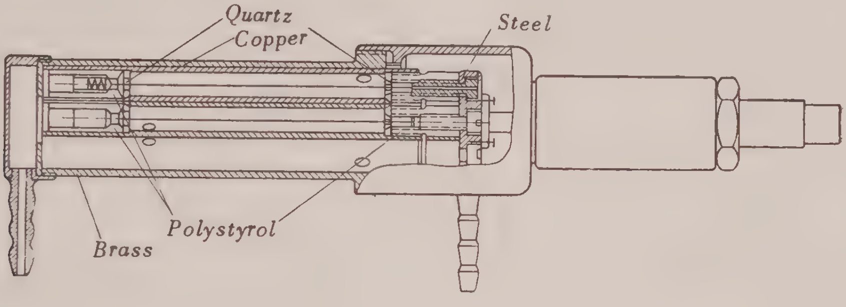

FIG. 2. Construction of the proportional counter.

In order to find P_x, it is necessary to know the phase shifts for n-He^4 scattering. At the present time, two phase shift analyses have been carried out, using the angular distribution of the scattered neutrons. These are the analyses of Huber and Baldinger[11] and Seagrave[8]. They do not agree with each other, especially for $P_{1/2}$. The discrepancy is apparently fundamentally due to the fact that it is difficult to obtain phase splits, arising from spin-dependent forces, using only the differential cross section $\sigma_0(\theta)$ for unpolarized neutrons. This is because the spin-orbit splitting appears in $\sigma_0(\theta)$ as a correction proportional to $\sin^2(\delta_l^+ - \delta_l^-)$. Hence for fixed $(1 + l)\delta_l^+ + l\delta_l^-$, $\sigma_0(\theta)$ is often quite insensitive to changes in $(\delta_l^+ - \delta_l^-)$.

On the other hand, the polarization is directly proportional to $\sin(\delta_l^+ - \delta_l^-)$ and hence is sensitive to the magnitude of the spin orbit splitting. Thus even if the incident beam is not very polarized, a measurement of the angular dependence of the axial asymmetry in n-He^4 scattering, using the method described above, can lead to a more exact phase analysis.

We used the (D + D) reaction as a source of polarized neutrons. Since this is not a resonance reaction, it is reasonable to expect that P_n varies smoothly with deuteron energy. This makes the neutrons from the (D + D) reaction especially suitable to use in carrying out a phase shift analysis on n-He^4. It was immaterial that the polarization of the neutrons from the (D + D) reaction was known at only one energy ($E_d = 600$ kev), since measurements of the azimuthal asymmetry at various scattering angles in n-He^4 allowed us to obtain both the n-He^4 phase shifts and, at the same time, obtain the polarization of the (D + D) neutrons.

2. MEASUREMENTS ON THE AZIMUTHAL ASYMMETRY IN n-He^4 SCATTERING

The detector is shown in Fig. 2. Seven copper tubes, each of inner diameter 7 mm, were soldered together into one block and placed in an airtight container. The tungsten wires in the counters were 0.07 mm in diameter. They were centered through openings in the polystyrene insulators by brass screws. High voltage from a battery was applied simultaneously to all the counters. The quartz washers shielded the working volume from recoil protons produced in the polystyrene insulators. The centering was to 150μ, which limited that part of the uncertainty in the gas multiplication factor which arose from lack of centering to ±1%.

---

* The results of the analysis can also be compared with the measured phase shifts for elastic proton scattering on He^4 [8-10].

Figure 3 shows a general view of the apparatus. Two groups of counters were used, one on each side of the target. The counter supports could be moved around on a light brass ring whose center was at the target. The counters could be rotated individually on their own supports, their angle of rotation φ_α being read off on a graduated scale. The angle of emission of the neutrons detected was fixed by a scale on the brass ring.

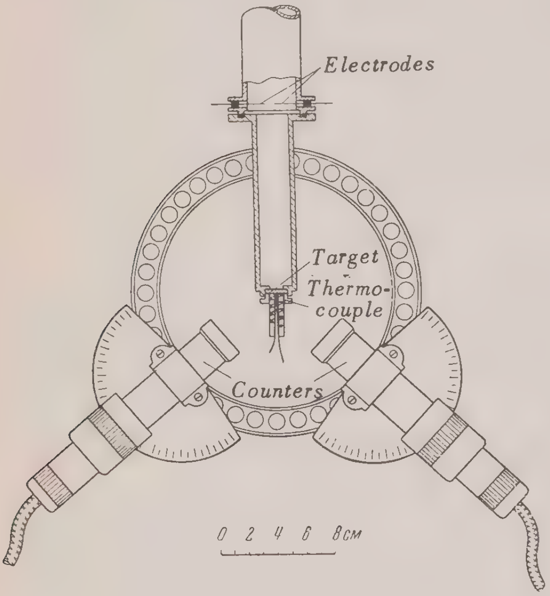

FIG. 3. General view of the experiment.

The geometry of the experiment was such that the position of the neutron source had to be precisely known. To achieve this, electrodes were placed in the tube with the target and connected to a null reading galvanometer. This, together with small correcting magnets, allowed us to determine the position of the ion beam on the target to within 0.2 mm.

Measurements were made using thick and thin zirconium targets saturated with deuterium. The temperature of the target was controlled by a thermocouple and maintained at ~ 200° C. This was to prevent the formation of a carbon film, which can arise from breakdown of adsorbed oil under the action of the beam. A uranium fission chamber 10 cm from the target served as monitor. Less than 1% of the neutrons counted in the chamber were formed outside the target (on the diaphragms, electrodes etc). In all the experiments the helium pressure was chosen so that the recoil He^4 nuclei going down the counter axis had a range of 44 mm. The energy of the recoil nuclei was $E_\alpha = 0.64 E_n \times \cos^2 \varphi_\alpha$ (where E_n is the neutron energy). Data on the slowing down of alpha particles in helium were taken from Ref. 12. The solid angle into which the helium recoil nuclei had to go in order to be counted depended on the discriminator setting and was adjusted to be 10 to 18°, depending on the intensity available.

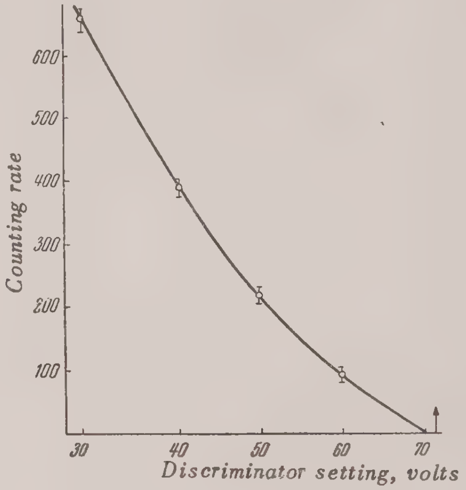

FIG. 4. Spectrum of pulses produced by recoil He^4 nuclei when the counter is in the position $\varphi_\alpha = 0°$. The solid line gives the spectrum calculated from the cross section $\sigma_{n\alpha}(\theta)$ and geometrical factors.

A constant helium current was passed through the counters in order to keep the composition of the gas the same. The current was 30-40 cm^3/min and was controlled by a rheometer at the output of the gas system. In setting the helium pressure, on which the gas multiplication of the counters depends critically, variations in atmospheric pressure were taken into account. Special automatic equipment kept the pressure constant to 0.1%.

Our set up used type DB linear amplifiers feeding five-channel integral discriminators. The scales of the latter were calibrated as follows:

The counters were set to $\varphi_\alpha = 0°$ and the pulse height spectrum taken near its upper boundary. In this case the largest pulses come from head on collisions between neutrons and He^4. Using five discriminator channels the upper limit of the spectrum could be determined to 2% and hence the discriminator scale calibrated in terms of the energy with which the helium nuclei recoiled (Fig. 4)*.

The following points were checked:

1) linearity of the gas multiplication and of the electronics,

2) sensitivity of the apparatus to background neutrons,

3) effect of neutron scattering from the counter walls on the measured asymmetry,

4) dependence of the gas multiplication on helium pressure and current,

5) distortion of the results due to superposition of pulses.

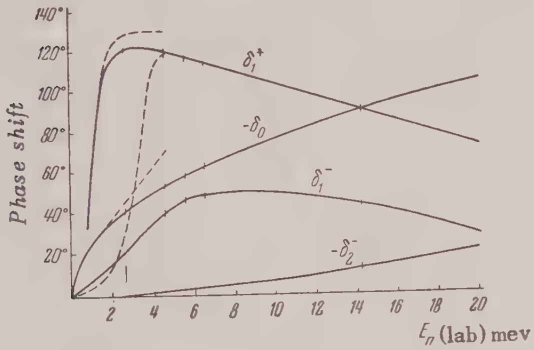

FIG. 5. Energy dependence of the phase shifts in n-He^4 scattering. Dotted curves: from Huber and Baldinger[11]; solid curves: calculated from p-He^4 phase shifts. The experimental points are Seagrave's data[8].

In order to check on the linearity of the amplification, the observed pulse height spectrum was compared with one calculated from data on $\sigma_{n\alpha}(\theta)$ and geometrical considerations. The good agreement between the two spectra (Fig. 4) indicates that departures from linearity are negligible.

The sensitivity of the apparatus to a background of scattered neutrons was estimated by bringing up a heavy (70 kg) lead scatterer close (20 cm) to the counters. No change was observed in the counting rate.

To check on whether neutron scattering from the counter walls was affecting the measured asymmetry, the wall thickness was trebled for one run by adding a lead covering. This led to a slight decrease in counting rate (~ 10%) but had no effect on the measured asymmetry within the statistical error (~ 3%).

The gas ~~amplification~~ depends critically on the pressure of helium and on contaminants. The helium used in the measurements was 99.8% pure. The variation in gas amplification with pressure is 0.017 mm Hg^{-1} (the amplification at 1100 mm Hg being taken to be 1). At speeds < 10 cm^3/min, the gas amplification is particularly sensitive to the helium flow which kept the gas composition constant. At speeds > 30 cm^3/min, the amplification scarcely changed at all with changing helium current.

No distortion due to superposition of pulses was detected at the highest counting rate (1500 pulses/sec) used. The asymmetry measurements were made to 3% at ion currents of 20 and 5 μamp.

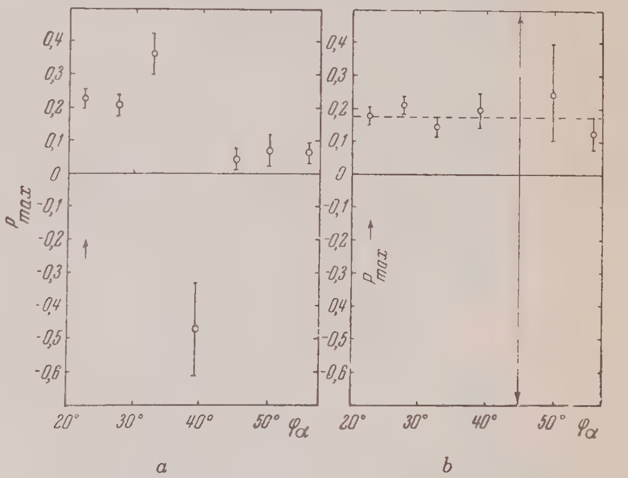

a

b

FIG. 6. Values of P_{max} obtained from the experimental data at various counter positions φ_α. a – using the phase shift from Huber and Baldinger[11], b – using Seagrave's phase shift[8].

The sensitivity of the apparatus to neutrons was as follows: at a neutron current of 3×10^5 neutrons/cm^2 sec ($E_n \approx 3.5$ mev) and angle $\varphi_\alpha = 22°$, the discriminator channels set at 0.4, 0.5, 0.6, 0.7 and 0.8 registered about 180, 125, 75, 35 and 17 counts/min respectively.

3. PHASE SHIFT ANALYSIS OF NEUTRON SCATTERING FROM He^4

Since the geometry of the analyzer was rather

---

* In the following, discriminator settings are given in units such that one corresponds to the pulse height from head on collisions.

"bad", it would have been difficult to carry out a complete phase analysis from the asymmetry measurements. Hence we limited ourselves to investigating two points on the most doubtful phase shift, δ_1^-, and took the other phases δ_0 and δ_1^+ to be sufficiently well known. This choice was made on the basis of the following considerations: 1) The experimental data of Huber and Baldinger[11] and Seagrave[8] on the phases δ_0 and δ_1^+ agree quite well, but disagree strongly on δ_1^- (cf Fig. 5). 2) Charge symmetry implies a definite relation between the phases for n-He^4 and p-He^4. Since the p-He^4 phase shifts have been measured much more accurately than those of n-He^4, analysis of the proton data gives independent information on the n-He^4 phase shifts. Adair[9] and Dodder and Gammel[10] carried out an approximate calculation of the n-He^4 phase shifts from the p-He^4 ones using the method of Wigner and Eisenbud. The results were in satisfactory agreement with experiment (Fig. 5) for the phases δ_0 and δ_1^+. The δ_1^- phase differs appreciably from the δ_1^- obtained by Huber, but, except for one point at 2.61 mev[*], agrees with the δ_1^- given by Seagrave.

3) A large peak in the total cross section occurs at around 1 mev neutron energy. This is due to the $P_{3/2}$ level in He^5. Since the $P_{3/2}$ state accounts for about 90% of the total cross section at these energies, Γ and E_{res} can be obtained from the shape of the peak, and from them

$$\delta_1 = \operatorname{arc\,tg}\,[{}^1/_2\Gamma/(E_{\text{res}} - E_n)].$$

calculated. The δ_1^+ so obtained agrees with that cbtained from the analysis of $\sigma(\theta)$ for n-He^4 scattering.

We measured δ_1^- for neutron energies of 2.45 and 3.4 mev. The 3.4 mev point is interesting because according to the data of Huber and Baldinger, δ_1^- passes through $\pi/2$ here, which indicates a $P_{1/2}$ state in He^5.

Energy $E_n = 3.4$ mev.

Neutrons of this energy were emitted at $\theta_n = 49°$ when 800 kev deuterons bombarded the target. The asymmetry in the scattering was measured at 7 angles φ_α. The results are shown in the following table.

TABLE

Counter position	22,5°	27,5°	32,5°	39°	45°	50°	56°
Helium pressure (atm.)	1,340	1.213	1.100	0.935	0,790	0.680	0,540
Discriminator setting	0.75	0.67	0.60	0,49	0.40	0.33	0.25
Solid angle $\Delta\Omega$	10°25′	10°35′	10°40′	11°05′	11°30′	12°00′	12°35′
Measured asymmetry	1.259 ±0.037	1.250 ±0.039	1,105 ±0.033	1,033 ±0.042	0,835 ±0.020	0,807 ±0.032	0,780 ±0.022

Before obtaining $P_{n\alpha}$ and $P_{\text{D}(dn)}$ from the data, several corrections have to be made for the poor geometry. The measured asymmetry can be written

$$R = \int \sigma_{\text{DD}}\sigma_{n-\alpha}\Delta\Omega r^{-2}\,(1 + P_x P_{n-\alpha})\,dv \Big/ \int \sigma_{\text{DD}}\sigma_{n-\alpha}\Delta\Omega r^{-2}\,(1 - P_x P_{n-\alpha})\,dv. \tag{1}$$

where σ_{DD} is the differential cross section of the (D + D) reaction, $\sigma_{n\alpha}$ is the differential scattering cross section, P_x the polarization of the neutrons, $P_{n\alpha}$ the polarization of neutrons scattered from helium, $\Delta\Omega$ the solid angle in which the recoil nuclei were counted and r the distance from the target to an elementary counter volume. We can regard P_x and $P_{n\alpha}$ as known functions of $P_{\max}$ and δ_1^-, where $P_{\max}$ is the maximal polarization of D(dn) for a given E_d (cf Ref. 13):

$$P_x = P_{\max}\frac{\sin 2\theta}{\sigma(\theta)}\,K(E_d),$$

$K(E_d)$ is a normalization constant. The connection between P_n and the phase δ_1^- is given by Lepore[14]. Thus formula (1) reduces to an equation with two unknowns:

---

[*] The fact that this discrepancy is real was pointed out to us by Sigrein (private communication).

$$R = f(\delta_1^-, P_{\max}).$$

For a fixed δ_1^-, and each of the seven measured values of R, $P_{\max}$ can be calculated. The calculation was carried out graphically: two values of $P_{\max}$ were chosen, one making $f(\delta_1^-, P_{\max})$ a little larger than the measured asymmetry R, the other a little smaller. The value of $P_{\max}$ corresponding to the measured asymmetry (taking its errors into account) was then found by interpolation. Values of the function $f(\delta_1^-, P_{\max})$ were found by numerical integration, the working volume of each counter being subdivided into 20 parts for this purpose.

A proposed value for δ_1^- was checked in the following way:

1) The asymmetry was measured at seven angles φ_α (cf the table above).

2) The maximal polarization $P_{\max}$ of neutrons from the (D + D) reaction was calculated for each of the seven angles, and two values of δ_1^-: 30° (Seagrave) and 90° (Huber and Baldinger).

3) The seven values of $P_{\max}$ obtained for each value of δ_1^- were compared with each other. Good agreement supported whichever value of δ_1^- had been used.

The results are shown in Fig. 6. Clearly the scatter in the values of $P_{\max}$ obtained using $\delta_1^- = 90°$ (Huber and Baldinger) is more than experimental error, while the scatter of those obtained with $\delta_1^- = 30°$ (Seagrave) is within experimental error. The polarization of neutrons from the (D + D) reaction is $P_{\max} = 0.17$ in this case.

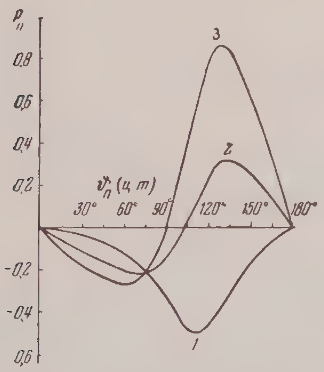

FIG. 7. Polarization of 2.45 mev neutrons scattered from He^4, as calculated for three values of δ_1^-: 1 – 0°, 2 – 10°, 3 – 10°10′ ($\delta_0 = -39°\,10'$, $\delta_1^+ = 121°\,10'$)

Energy $E_n = 2.45$ mev

δ_1^- was obtained by comparing the experimental asymmetry in the scattering of neutrons with a known polarization with the asymmetry calculated using various values for δ_1^-. Such a measurement depends critically on the value of δ_1^-. This is shown by Fig. 7, in which polarization is plotted against angle for the scattering of 2.45 mev neutrons from He^4. The calculations were carried out using Seagrave's values for δ_0 and δ_1^+ and for three values of δ_1^-: 0°, 10° and 19° 10′.

2.45 mev neutrons were obtained at an angle $\theta_n = 106°$ (121° in c.m.) with 1800 kev deuterons. At this angle, the polarization of the D + D neutrons is close to maximal. Since, in the D + D reaction, the collision is between two identical particles, $P(\pi - \theta_{c.m.}) = -P(\theta_{c.m.})$. Therefore the polarization of neutrons going "back" at an angle $\theta_{c.m.} = 121°$ can be found directly from the data on the asymmetry in the scattering of neutrons going "forward" at an angle $\theta_{c.m.} = 59°$, since for the latter neutrons we can take the value for δ_1^- given by Seagrave. Indeed, the energy of the neutrons going "forward" is 4.11 mev, i.e., close to where our measurements confirmed Seagrave's analysis. Furthermore, at this energy Seagrave's analysis agrees with the proton one.

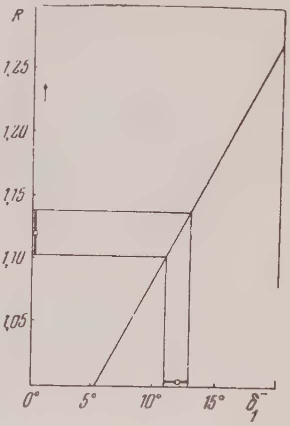

FIG. 8. The expected asymmetry R in the scattering of 2.45 mev neutrons as a function of the phase δ_1^-. The measured value of R, 1.120 ± 0.18, corresponds to $\delta_1^- = 12 \pm 1°$.

The asymmetry in the scattering of neutrons emitted "forward" at $\theta_{n(c.m.)} = 59°$ from a thin

(~ 150 kev) target (for details, see Ref. 6) when bombarded by 1800 kev deuterons was measured and yielded a neutron polarization $P_{max} = 0.170 \pm 0.010$. The asymmetry in the scattering of neutrons emitted "backward" from the same target was measured with the counter rotated to $\varphi_\alpha = 26°$.

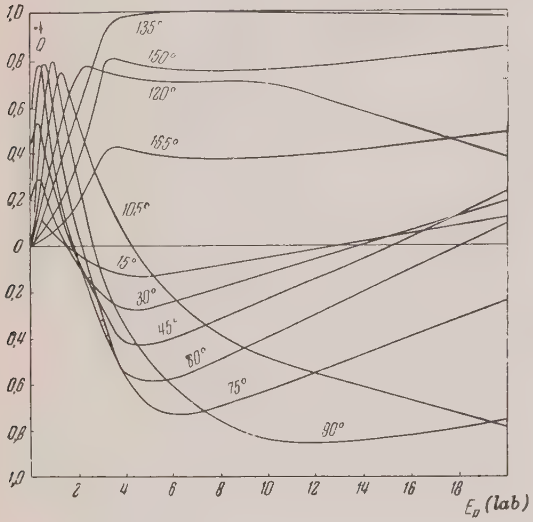

FIG. 9. The polarization of neutrons scattered from He^4 as a function of neutron energy E_n for various scattering angles in the center of mass frame. The curves are calculated from the phase shifts given by Seagrave[8]. The angle at which the He^4 nucleus recoils is $\varphi_\alpha = (\pi - \theta_n)/2$ in the laboratory frame.

With a discriminator setting 0.4 and helium pressure 0.87 atm., the asymmetry turned out to be 1.120 ±0.018. Figure 8 shows how the expected asymmetry in these measurements depends on the phase δ_1^-. This curve was calculated by the same method used for $E_n = 3.5$ mev. From Fig. 8 we can conclude that the measured asymmetry corresponds to $\delta_1^- = 12 \pm 1°$, i.e., δ_1^- differs considerably from the value obtained from the proton data, but agrees with the experimental data of Seagrave.

Our confirmation of Seagrave's phases clears the way to using helium as a convenient and well calibrated analyzer for polarized neutrons. Figure 9 shows the polarization of neutrons scattered from He^4 as a function of neutron energy and for various scattering angles in the center of mass system.

Our results confirm Seagrave's values for the phase shift δ_1^- at $E_n = 2.61$ mev. The discrepancy between δ_1^- as obtained from the proton data by Dodder and Gammel[10] and the measured value should be attributed to the inadequacy of the Wigner-Eisenbud formalism in this case. The assumption that the logarithmic derivative is linear over such a wide energy range is particularly doubtful.

We should like to thank S. N. Malyshko and E. Z. Tarumov for their help in carrying out the experiment, and to Prof. A. I. Shal'nikov for preparing important parts of the apparatus.

---

1 Meier, Scherrer and Trumpy, Helv. Phys. Acta **27**, 577 (1954).

2 Adair, Darden and Fields, Phys. Rev. **96**, 503 (1954).

3 R. Ricamo, Helv. Phys. Acta **26**, 423 (1953).

4 P. Huber and E. Baumgartner, Helv. Phys. Acta **26**, 420 (1953).

5 Levintov, Miller and Shamshev, Dokl. Akad. Nauk SSSR **103**, 803 (1955).

6 Levintov, Miller, Tarumov and Shamshev, J. Exptl. Theoret. Phys. (U.S.S.R.) **32**, 375 (1957); Soviet Phys. JETP **5**, 310 (1957).

7 Sack, Biedenharn and Breit, Phys. Rev. **93**, 321 (1954).

8 J. D. Seagrave, Phys. Rev. **92**, 1222 (1953).

9 R. K. Adair, Phys. Rev. **86**, 155 (1952).

10 D. C. Dodder and J. L. Gammel, Phys. Rev. **88**, 520 (1952).

11 P. Huber and E. Baldinger, Helv. Phys. Acta **25**, 435 (1952).

12 R. W. Gurney, Proc. Roy. Soc. (London) **A107**, 340 (1925).

13 R. J. Blin-Stoyl, Proc. Phys. Soc. (London) **A65**, 949 (1951).

14 J. Lepore, Phys. Rev. **79**, 137 (1950).

Translated by R. Krotkov
60

SOVIET PHYSICS JETP VOLUME 5, NUMBER 2 SEPTEMBER, 1957

Decay of the τ Meson

I. N. MIKHAILOV

(Submitted to JETP editor November 15, 1955)
J. Exptl. Theoret. Phys. (U.S.S.R.) 32, 284-288 (February, 1957)

The energy spectrum of the π mesons resulting from the decay of the τ meson is calculated on the assumption that the isotopic spin of the τ meson is one.

DALITZ[1] and Fabri[2] have considered the decay of the τ meson into 3 π's:

$$\tau^{\pm} \rightarrow 2\pi^{\pm} + \pi^{\mp}. \tag{1}$$

They computed the energy distribution of the π mesons on the basis of various assumptions about the spin and parity of the τ, and also on the assumption that in the expansion of the matrix element for the process into the orbital angular momenta of the π's, only the lowest momenta need be considered. No assumptions were made about the isotopic spin of the τ. The fact that the τ meson has almost the same mass as the θ particles (966 electron masses for both) suggested that the τ meson and the θ particles form an isotopic spin triplet, i.e., that the τ meson has isotopic spin 1 (see Ref. 3)*

The present paper describes a calculation which takes isotopic spin into account. It turns out that, in certain cases, if the π mesons are emitted with minimal orbital angular momentum, the distributions considered by Dalitz and Fabri are still valid. Furthermore, if the τ meson is a pseudoscalar particle (see Ref. 4) then the ratio of the probability dw_1 for decay into charged π's to the probability dw_2 for decay according to

$$\tau^{\pm} \rightarrow \pi^{\pm} + 2\pi^0 \tag{2}$$

is 4, while if the τ is vector, pseudovector or tensor it is 1. If dw_1/dw_2 is neither 4 nor 1, then higher orbital angular momenta must enter into the matrix element for the process. We shall give below the simplest matrix elements for the decay of a τ into 3 π's such that the ratio dw_1/dw_2 is one if the decaying particle is pseudoscalar and four if it is vector, pseudovector or tensor.

Consider the decay of a particle with spin J_τ, parity P_τ, mass m_τ and isotopic spin $I_\tau = 1$, (which we call the τ meson), into 3π mesons, i.e., into three particles with spin $J_\pi = 0$, parity $P_\pi = -1$, mass m_π and isotopic spin $I_\pi = 1$.

Let the momentum, total energy and kinetic energy of the ith π-meson ($i = 1, 2, 3$) be $\mathbf{p}_i$, $E_i = \sqrt{m_\pi^2 + p_i^2}$, and $\epsilon_i = E_i - m_\pi$ respectively, and $\mathbf{t}_{\alpha_i}$, $\mathbf{t}_\beta$ (α_i, $\beta = +, -, 0$) be the isotopic spin vectors, in the canonical basis, for the ith π meson and the τ meson:

$$\mathbf{t}_+ = \begin{pmatrix}1\\0\\0\end{pmatrix}, \quad \mathbf{t}_- = \begin{pmatrix}0\\0\\1\end{pmatrix}, \tag{3}$$

$$\mathbf{t}_0 = \left.\begin{pmatrix}0\\1\\0\end{pmatrix}\right\} \begin{matrix}\nu = 1\\ \nu = 0\\ \nu = -1\end{matrix}$$

All quantities are referred to the system where the meson is at rest:

$$\mathbf{p}_1 + \mathbf{p}_2 + \mathbf{p}_3 = 0. \tag{4}$$

Consider now the matrix element $\langle V \rangle$ corresponding to the decay of a τ meson with charge β, and the projection of whose spin in some direction is μ, into 3π mesons with charges $\alpha_1, \alpha_2, \alpha_3$ and momenta $\mathbf{p}_1$, $\mathbf{p}_2$ and $\mathbf{p}_3$. In the momentum space of the π mesons, this is the μth component of an irreducible tensor of order J_τ relative to the rotation group, while it is a scalar in the isotopic spin space formed by the vectors $\mathbf{t}_\beta$, $\mathbf{t}_{\alpha_1}^+$, $\mathbf{t}_{\alpha_2}^+$, $\mathbf{t}_{\alpha_3}^+$ + here means the Hermitian conjugate:

$$(t^+)_\nu = (-1)^\nu t_{-\nu}; \tag{5}$$

$$\langle V \rangle = (E_1 E_2 E_3)^{-1/2} v_\mu^{J_\tau} (\mathbf{p}_1, \mathbf{t}_{\alpha_1}^+; \mathbf{p}_2, \mathbf{t}_{\alpha_2}^+; \mathbf{p}_3, \mathbf{t}_{\alpha_3}^+; \mathbf{t}_\beta) \times \delta(m_\tau - E_1 - E_2 - E_3)\, \delta(\mathbf{p}_1 + \mathbf{p}_2 + \mathbf{p}_3). \tag{6}$$

---

* Note added in proof: Several authors[6-8] have recently proposed schemes in which the isotopic spin of various K mesons is half integral. In such schemes the τ and θ mesons do not form an isotopic spin multiplet and the equality of their masses receives no interpretation. However, all the results of the present work will remain valid, no matter what the isotopic spin of the τ meson is, if it decays into 3π mesons which have total isotopic spin one.

[The factor $(E_1 E_2 E_3)^{-\frac{1}{2}}$ in the expression for the matrix element comes from the normalization of the wave functions for the particles].

Up to a constant, the probability per unit time for decay of an unpolarized τ meson is then

$$dw = (1 / E_1 E_2 E_3) \sum_{\mu} | v_{\mu}^{J_\tau} |^2 \delta (m_\tau - E_1 - E_2 - E_3) \delta (\mathrm{p}_1 + \mathrm{p}_2 + \mathrm{p}_3) \, d\mathrm{p}_1 \, d\mathrm{p}_2 \, d\mathrm{p}_3. \tag{7}$$

The expression above can be put into the following form, which is more suited to calculation,

$$dw = W (\xi, E_3) \, d\xi \, dE_3, \tag{8}$$

$$W (\xi, E_3) = \sum_{\mu} | v_{\mu}^{J_\tau} |^2 ,$$

where $\xi = E_1 - E_2$. In what follows we take the index 3 in $W(\xi, E_3)$ to refer to the $\pi^\pm$ meson in reaction (1) or to $\pi^\pm$ in reaction (2). Then (8) gives the probability for decay into a state where the difference in energy $E_1 - E_2$ of the identical π mesons lies in the interval $\xi \leq E_1 - E_2 \leq \xi + d\xi$ and the energy of the third π meson is between E_3 and $E_3 + dE_3$. Integrating (8) with respect to ξ over the interval $| \xi | \leq |E_1 - E_2|_{\mathrm{max}} = y(E_3)$* will give the energy spectrum of the third π meson.

Since the π mesons are Bose particles, $v_{\mu}^{J_\tau} (\mathrm{p}_i, \mathrm{t}_{\alpha_i}^+ ; \mathrm{t}_\beta)$ must be symmetric in the indices 1, 2, 3. From (4), it follows that $v_{\mu}^{J_\tau} (\mathrm{p}_i; \mathrm{t}_{\alpha_i}^+; \mathrm{t}_\beta)$ can be written

$$v_{\mu}^{J_\tau} (\mathrm{p}_i, \mathrm{t}_{\alpha_i}^+; \mathrm{t}_\beta) = f_\mu (\mathrm{p}_1, \mathrm{p}_2, \mathrm{p}_3) X_0 \tag{9}$$

$$+ \varphi_\mu (\mathrm{p}_3, \mathrm{p}_1 - \mathrm{p}_2) X_{12}$$

$$+ \varphi_\mu (\mathrm{p}_1, \mathrm{p}_2 - \mathrm{p}_3) X_{23} + \varphi_\mu (\mathrm{p}_2, \mathrm{p}_3 - \mathrm{p}_1) X_{31}.$$

Here

$$X_0 (\mathrm{t}_{\alpha_i}^+, \mathrm{t}_\beta) = (\mathrm{t}_{\alpha_1}^+, \mathrm{t}_{\alpha_2}^+) (\mathrm{t}_{\alpha_3}^+, \mathrm{t}_\beta) \tag{10}$$

$$+ (\mathrm{t}_{\alpha_2}^+, \mathrm{t}_{\alpha_3}^+) (\mathrm{t}_{\alpha_1}^+, \mathrm{t}_\beta) + (\mathrm{t}_{\alpha_3}^+, \mathrm{t}_{\alpha_1}^+) (\mathrm{t}_{\alpha_2}^+, \mathrm{t}_\beta);$$

$$X_{12} = (\mathrm{t}_{\alpha_1}^+, \mathrm{t}_{\alpha_3}^+) (\mathrm{t}_{\alpha_2}^+, \mathrm{t}_\beta) - (\mathrm{t}_{\alpha_2}^+, \mathrm{t}_{\alpha_3}^+) (\mathrm{t}_{\alpha_1}^+, \mathrm{t}_\beta),$$

$$X_{23} = (\mathrm{t}_{\alpha_2}^+, \mathrm{t}_{\alpha_1}^+) (\mathrm{t}_{\alpha_3}^+, \mathrm{t}_\beta) - (\mathrm{t}_{\alpha_3}^+, \mathrm{t}_{\alpha_1}^+) (\mathrm{t}_{\alpha_2}^+, \mathrm{t}_\beta); \tag{11}$$

$$X_{31} = (\mathrm{t}_{\alpha_3}^+, \mathrm{t}_{\alpha_2}^+) (\mathrm{t}_{\alpha_1}^+, \mathrm{t}_\beta)$$

$$- (\mathrm{t}_{\alpha_1}^+, \mathrm{t}_{\alpha_2}^+) (\mathrm{t}_{\alpha_3}^+, \mathrm{t}_\beta) = - X_{12} - X_{23},$$

$$(\mathrm{t}_\alpha, \mathrm{t}_\beta) = \sum (-1)^{\nu} (t_\alpha)_\nu (t_\beta)_{-\nu},$$

$f_\mu(\mathrm{p}_1, \mathrm{p}_2, \mathrm{p}_3)$ is a symmetric function of the π meson momenta;

$$\varphi_\mu (\mathrm{p}_1, \mathrm{p}_2 - \mathrm{p}_3) = - \varphi_\mu (\mathrm{p}_1, \mathrm{p}_3 - \mathrm{p}_2).$$

In the case that the τ meson decays into three charged π's (reaction (1)). then $\alpha_1 = \alpha_2 = \beta = \pm$, $\alpha_3 = \pm$ (where 1 and 2 refer to the two identical π mesons). Then

$$W (\xi, E_3) = W_1 (\xi, E_3) \tag{12}$$

$$= 4 \sum_{\mu} | f_\mu |^2 + \sum_{\mu} | \varphi_\mu (\mathrm{p}_1, \mathrm{p}_2 - \mathrm{p}_3)$$

$$- \varphi_\mu (\mathrm{p}_2, \mathrm{p}_3 - \mathrm{p}_1) |^2 - 4 \sum_{\mu} \mathrm{Re} \{ f_\mu^* [\varphi_\mu (\mathrm{p}_1, \mathrm{p}_2 - \mathrm{p}_3)$$

$$- \varphi_\mu (\mathrm{p}_2, \mathrm{p}_3 - \mathrm{p}_1)] \}.$$

If the τ meson decays according to (2), $\alpha_1 = \alpha_2 = 0$, $\alpha_3 = \beta = \pm n$,

$$W (\xi, E_3) = W_2 (\xi, E_3) \tag{13}$$

$$= \sum_{\mu} | f_\mu |^2 + \sum_{\mu} | \varphi_\mu (\mathrm{p}_1, \mathrm{p}_2 - \mathrm{p}_3) - \varphi_\mu (\mathrm{p}_2, \mathrm{p}_3 - \mathrm{p}_1) |^2$$

$$+ 2 \sum_{\mu} \mathrm{Re} \{ f_\mu^* [\varphi_\mu (\mathrm{p}_1, \mathrm{p}_2 - \mathrm{p}_3) - \varphi_\mu (\mathrm{p}_2, \mathrm{p}_3 - \mathrm{p}_1)] \}.$$

---

* Using Fabri's results[2] it is easy to show that

$$y = | E_1 - E_2 |_{\mathrm{max}}$$

$$= (m_\tau - 3m_\pi) \sqrt{\frac{1 - x^2 - \alpha (1 + x) x^2}{3 [1 + \alpha (1 - 3x)]}} ;$$

$$x = 3\varepsilon_3 / (m_\tau - 3m_\pi) - 1;$$

$$\alpha = \frac{(m_\tau - 3m_\pi) / m_\tau}{2 [1 - (m_\tau - 3m_\pi) / 2m_\tau]^2} = 0.089.$$

Upon integrating (12) and (13) over ξ and E_3, and denoting the total cross sections for (1) and (2) by W_1 and W_2, while

$$\int\sum_{\mu} |f_\mu|^2 \, d\xi \, dE_3 \tag{14}$$

$$= \int F(\xi, E_3) \, d\xi \, dE_3 = F,$$

$$\int\sum_{\mu} |\varphi_\mu(\mathbf{p}_1, \mathbf{p}_2 - \mathbf{p}_3) - \varphi_\mu(\mathbf{p}_2, \mathbf{p}_3 - \mathbf{p}_1)|^3 \, d\xi \, dE_3$$

$$= \int \Phi(\xi, E_3) \, d\xi \, dE_3 = \Phi,$$

we obtain the ratio of the reactions (1) and (2) (cf Refs. 4 and 5)

$$1 \leqslant W_1 / W_2 = (4F + \Phi)/(F + \Phi) \leqslant 4. \tag{15}$$

From (12) and (13) it follows that

$$W_1(\xi, E_3) + 2W_2(\xi, E_3) \tag{16}$$

$$= 6F(\xi, E_3) + 3\Phi(\xi, E_3).$$

Having (16) and (15), we can consider separately the matrix elements

$$f^\mu(\mathbf{p}_1, \mathbf{p}_2, \mathbf{p}_3) X_0 \quad \text{and} \quad \sum_{i \neq j \neq k} \varphi_\mu(\mathbf{p}_i, \mathbf{p}_j - \mathbf{p}_k) X_{jk}.$$

$f_\mu(\mathbf{p}_1, \mathbf{p}_2, \mathbf{p}_3)$ and $\varphi_\mu(\mathbf{p}_1, \mathbf{p}_2 - \mathbf{p}_3)$ can be expanded in the following series:

$$f_\mu(\mathbf{p}_1, \mathbf{p}_2, \mathbf{p}_3) \tag{17}$$

$$= \sum_{i \neq j \neq k} \sum_{ll'} A_{ll'}(p_i, |\mathbf{p}_j - \mathbf{p}_k|) Z_{ll'}^{J_\tau, \mu}(\mathbf{p}_i, \mathbf{p}_j - \mathbf{p}_k),$$

$$\varphi_\mu(\mathbf{p}_1, \mathbf{p}_2 - \mathbf{p}_3)$$

$$= \sum_{ll'} B_{ll'}(\mathbf{p}_1, |\mathbf{p}_2 - \mathbf{p}_3|) Z_{ll'}^{J_\tau, \mu}(\mathbf{p}_1, \mathbf{p}_2 - \mathbf{p}_3),$$

where

$$Z_{ll'}^{J_\tau, \mu}(\mathbf{p}, \mathbf{p}')$$

$$= p^l p'^{l'} \sum_{\alpha, \beta} C_{l, \alpha; l'\beta}^{J_\tau, \mu} Y_{l;\alpha}(\mathbf{p}/p) Y_{l', \beta}(\mathbf{p}'/p'),$$

$C_{l, \alpha; l', \beta}^{J_\tau, \mu}$ are the Clebsch-Gordon coefficients and $Y_{l\alpha}(\mathbf{p}/p)$ the spherical harmonics of order l.

Matrix elements for the decay of a τ meson into three π mesons which have minimum possible orbital angular momenta. l and l' are the orbital angular momenta entering into (17); $\mu, \nu = 1, 2, 3$. Expressions underlined are considered in Refs. 1 and 2. In $F(p_i)$ and $\Phi(p_i)$ the indices 1, 2 refer to the identical π mesons.

J_τ, P	l, l'	$f_\mu(\mathbf{p}_1, \mathbf{p}_2, \mathbf{p}_3)$	$F(\mathbf{p}_1, \mathbf{p}_2, \mathbf{p}_3)$	l, l'	$\varphi_\mu(\mathbf{p}_1, \mathbf{p}_2 - \mathbf{p}_3)$	$\Phi(\mathbf{p}_1, \mathbf{p}_2, \mathbf{p}_3)$
0—	0,0	$\underline{1}$	$\underline{1}$	2,2	$2\mathbf{p}_1\mathbf{p}_2 + p_3^2$	$(p_1^2 + p_2^2 - 2p_3^2)^2$
1+	1,0 2,1	$p_1^2\mathbf{p}_1 + p_2^2\mathbf{p}_2 + p_3^2\mathbf{p}_3$	$\{p_1^2\mathbf{p}_1 + p_2^2\mathbf{p}_2 + p_3^2\mathbf{p}_3\}^2$	0,1	$\underline{\mathbf{p}_3}$	$\underline{p_3^2}$
1—	2,2 4,4	$\sum_{i,j=1}^{3} [\mathbf{p}_i\mathbf{p}_j](p_i^2 - p_j^2)^3$	$[\mathbf{p}_1\mathbf{p}_2]^2 \{(p_1^2 - p_2^2)^3 + (p_2^2 - p_3^2)^3 + (p_3^2 - p_1^2)^3\}^2$	2,2	$\underline{[\mathbf{p}_1\mathbf{p}_2](p_1^2 - p_2^2)}$	$\underline{[\mathbf{p}_1\mathbf{p}_2]^2 (p_1^2 - p_2^2)^2}$
2+	2,1 2,3	$\sum_{i \neq j \neq k} p_i^2 [\mathbf{p}_j\mathbf{p}_k]_\mu (\mathbf{p}_j - \mathbf{p}_k)_\nu$	$[\mathbf{p}_1\mathbf{p}_2]^2 \{p_1^2(\mathbf{p}_2 - \mathbf{p}_3) + p_2^2(\mathbf{p}_3 - \mathbf{p}_1)^2 + p_3^2(\mathbf{p}_1 - \mathbf{p}_2)^2\}$	2,1	$\underline{[\mathbf{p}_1\mathbf{p}_2]_\nu (\mathbf{p}_1 - \mathbf{p}_2)_\mu}$	$\underline{[\mathbf{p}_1\mathbf{p}_2]^2 (\mathbf{p}_1 - \mathbf{p}_2)^2}$

Suppose that $A_{ll'}$ and $B_{ll'}$ as functions of p and p' can be written

$$A_{ll'} = a_0 + a_1 p^2 + a_2 p'^2 - \ldots,$$
$$B_{ll'} = b_0 + b_1 p^2 + b_2 p'^2 + \ldots$$

and that only the non vanishing terms of lowest order are important (this is equivalent to neglecting higher momenta l and l'). Certain simple expressions for f_μ and φ_μ then result. These are shown in the table for the cases where the decaying particle is pseudoscalar, pseudovector, vector and tensor. The case that τ is scalar is eliminated by the requirement that parity be conserved (see Ref. 3).

From the above it follows that if the π mesons from τ decay are emitted into states with minimum orbital angular momentum, then

$$W_1(E_3) + 2W_2(E_3) = \\ = aF_0(E_3) + b\Phi_0(E_3), \qquad (18)$$

$$F_0(E_3) = \\ = \int F(\xi, E_3)\, d\xi \Big/ \int F(\xi, E_3)\, d\xi\, dE_3,$$

$$\Phi_0(E_3) = \\ = \int \Phi(\xi, E_3)\, d\xi \Big/ \int \Phi(\xi, E_3)\, d\xi\, dE_3,$$

[$W_1(E_3)$ is the probability that in reaction (1) a $\pi^\pm$ meson will appear with energy between E_3 and $E_3 + dE_3$, while $W_2(E_3)$ is defined similarly for a $\pi^\pm$ meson in reaction (2)].

The weights a and b in formula (18) are found from(15):

$$a = 2(W_1 - W_2), \\ b = 4W_2 - W_1. \qquad (19)$$

We note that the Lagrangian for the interaction between the τ and π meson fields can be written

$$\mathscr{L}_{\text{int}} = \Big\{ \sum_{\mu, \lambda} D^{J_\tau, \mu, \lambda} [\psi^+_{\alpha_1}(x_1)\, \psi^+_{\alpha_2}(x_2)\, \psi^+_{\alpha_3}(x_3)\, \Psi^\mu_\beta(x_\tau)] \\ \times X_\lambda(\mathrm{t}^+_{\alpha_i}, \mathrm{t}_\beta) + \text{c. c.} \Big\},$$

where $\psi^+_{\alpha_i}(x_i)$ is the creation operator for a π^{α_i}-meson at x_i, $\Psi^\mu_\beta(x_\tau)$is the destruction operator of a τ^β meson at x_τ whose spin projection along some axis is μ and $D^{J_\tau,\mu,\lambda}$ are certain differential operators containing the minimal number of derivatives for given J_τ, p, λ and evaluated at the point $x_1 = x_2 = x_3 = x_\tau = x$. The matrix elements obtained from this agree, up to relativistic corrections, with those in the table.

In conclusion, I should like to express my sincere thanks to I. S. Shapiro, under whose guidance this work was carried out.

---

1 R. H. Dalitz, Phil. Mag. **44**, 1068 (1953).

2 E. Fabri, Nuovo Cim. **11**, 479 (1954).

3 I. S. Shapiro, J. Exptl. Theoret. Phys. (U.S.S.R.) **27**, 257 (1954).

4 V. B. Berestetskii, Dokl. Akad. Nauk SSSR **92**, 519 (1953).

5 R. H. Dalitz, Proc. Phys. Soc. (London) **A66**, 710 (1953).

6 M. Gellmann,Pisa conference, 1955.

7 A. Salam, and J. Polkinghorne, Nuovo Cim. **2**, 686 (1955).

8 M. A. Markov, *The Systematics of Elementary Particles*. Academy of Sciences Press, Moscow, 1955.

Translated by R. Krotkov
61

SOVIET PHYSICS JETP VOLUME 5, NUMBER 2 SEPTEMBER, 1957

The Theory of Ferromagnetism of Metals and Alloys at Low Temperatures

E. S. KONDORSKII AND A. S. PAKHOMOV
Moscow State University

(Submitted to JETP editor November 28, 1955)
J. Exptl. Theoret. Phys. (U.S.S.R.) 32, 323–332 (February, 1957)

Formulas are obtained for the temperature dependence of spontaneous magnetization near absolute zero for a ferromagnetic lattice consisting of one kind of atoms in the case which in the number of electrons with uncompensated spins is greater than the number of atoms, and for lattices of binary ordered alloys of various structure. In the calculation, use is made of the method of approximate second quantization. It is shown that, in all cases considered, the theory leads to the temperature dependence of spontaneous magnetization of the form of a 3/2 power law.

---

1. INTRODUCTION

ONE of the problems of the theory of ferromagnetism is the deduction of a formula for the temperature dependence of spontaneous magnetization. This formula has been obtained for the ideal case, namely, for the ferromagnetic lattice of weakly interaction hydrogen–like atoms in the low temperature region. In this case,[1] the specific spontaneous magnetization is equal to

$$\sigma_s = n\mu_0 [1 - (T/\theta')^{3/2}], \qquad (1.1)$$

where n is the number of atoms and the number of electrons per unit mass, μ_0 is the Bohr magneton, $\theta' = 4.17(2c)^{2/3} J/k_0$, $c = 1/2, 1, 2$ for the simple, space-centered and face-centered cubic lattices, respectively, J = exchange integral, k_0 is Boltzmann's constant.

Real crystals of ferromagnetic elements have: 1) siginificant electrical conductivity, 2, a number of electrons with uncompensated magnetic moments that is not equal to the number of ions in the lattice. The theory of ferromagnetism with account of the state of polarization and the effect of the conductivity of the electrons on the spontaneous magnetization was developed in the researches of Vonsovskii,[2] and Turov.[3] In the most general form, the theory of the polar model of the metal was recently developed by Bogoliubov and Tiablikov.[4,5]

Möller[6] made an attempt to generalize the theory of the nonconducting ferromagnetic lattice to the case in which the number of electrons with uncompensated moments is greater than the number of atoms, and obtained a formula, similar to Eq. (1.1), but with this difference, that $\theta' = 4.17\,(2cz)^{2/3}\, zJ/k_0$, where z is the number of electrons with uncompensated spins per atom. Later, Holstein and Primakoff deduced a formula for the temperature dependence of spontaneous magnetization with account of magnetic interaction. When the interaction terms are discarded, the formula of Holstein and Primakoff reduces to that of Möller.

In the researches of Refs. 6 and 7, the exchange integrals between the electrons of neighboring atoms did not differ, but the exchange integrals between the electrons of one and the same atom did not enter into the calculation. This corresponded to an implicit assumption that the states of the electrons belonging to one atom differ only in the spin function. As a result, a series of terms fall out in the calculation of the lowest energy levels, as will be shown.

However, we can also begin from another, more consequential assumption, namely that the unperturbed wave functions of the electrons belonging to any atom differ not only in their spin functions, but also in the functions of the coordinates of the electrons. In this case it is necessary to take it into account that the exchange integrals between electrons of corresponding atoms differ in their dependence on whether electrons are exchanged which are found in identical states, or electrons which are found in different states. Moreover, we must take into account the exchange integrals between the electrons of one and the same atom.

Our problems are then the following: 1) to obtain the theoretical dependence of the spontaneous magnetization on the temperature, near absolute zero, in the case in which the number of electrons with uncompensated magnetic moments is larger than the number of atoms; 2) to derive formulas for the temperature dependence of spontaneous magnetization in the region of low temperatures for binary ferromagnetic ordered alloys of different crystalline structure and different composition.

2. GENERAL FORM OF THE HAMILTONIAN OF THE PROBLEM AND ITS DIAGONALIZATION

Let us consider the general case of a multicomponent crystal, consisting of N atoms of h different types, located at the points of the lattice; each of the atoms has z_h ferromagnetic electrons which differ in state one from another. Altogether, there are $n = \Sigma N_h z_h$ electrons in the lattice, where N_h is the number of atoms of type h and $\Sigma N_h = N$. (It must be noted that the type of atom is also determined here by what neighbors surround it. Two identical atoms can belong to different types h.)

The Hamiltonian of such a system, in the case in which only electrostatic interactions are taken into account, can be described in the following form:

$$\hat{H} = U_0 - \frac{\hbar^2}{2m} \sum_{(f,g)} \Delta q_{f,g} \tag{2.1}$$

$$+ \sum_{(f,f',g')} U_f (q_{f'g'}) + \sum_{(f,f',g,g')} \Phi (q_{fg}, q_{f'g'}).$$

Each electron of the system is characterized by two indices f and g: the index f defines the number of the lattice point at which the electron is located, and the index g defines the quantum state of the given electron in the atom. Inasmuch as only a single atom of any type can be located at a given lattice point f, we can neglect the indices h (which characterize the type of atom at the point f) in Eq. (2.1) and in subsequent expressions. The quantity U_0 is the constant potential energy of electrostatic interaction of the ions. These ions are assumed to be fixed at the points of the lattice, The quantity m is the electronic mass, Δq_{bg} is the Laplace operator in the coordinates of the electron f, g; U^f is the interaction potential of the electron with any ion; Φ is the interaction energy of the electrons.

Transforming to the representation of second quantization, the Hamiltonian (2.1) can be written in the form

$$\hat{H} = U_0 + \sum L (f, g, f', g') \hat{a}^+_{fg\sigma} \hat{a}_{f'g'\sigma} \tag{2.2}$$

$$+ \frac{1}{2} \sum F (f_1, g_1, f_2, g_2; \;\; f'_1, g'_1, f'_2, g'_2)$$

$$\times \; \hat{a}^+_{f_1 g_1 \sigma_1} \hat{a}^+_{f_2 g_2 \sigma_2} \hat{a}_{f_2' g_2' \sigma_2} \hat{a}_{f_1' g_1' \sigma_1},$$

where L and F are the matrix elements of the additive and binary parts of the operator (2.1) in the system of single particle functions, $\hat{a}^+$ and $\hat{a}$ are the second quantization operators in Fermi statistics; the summation is carried out over all indices.

The unexcited wave function in the second quantization representation $c_0(\ldots N_{fg\sigma})$ is defined by a system of unitary occupation numbers:

$$N_{fg\sigma} = \sum_{(\sigma)} n_{fg\sigma} = \sum_{(\sigma)} \hat{a}^+_{fg\sigma} \hat{a}_{fg\sigma} = 1. \tag{2.3}$$

Making use of the operator form of perturbation theory,[5] we can obtain the equivalent Hamiltonian of the secular equation of the third approximation in the following form:

$$\hat{\tilde{H}} \, \tilde{G}_0 \tag{2.4}$$

$$= - \frac{1}{2} \sum J (f, g, f', g') \hat{a}^+_{fg\sigma} \hat{a}^+_{f'g'\sigma'} \hat{a}_{f'g'\sigma} \hat{a}_{fg\sigma'},$$

where $J (f, g, f', g')$ is the exchange integral. The summation is carried out over all indices under the necessary conditions:

$$f \neq f', \quad \text{if} \quad g = g'; \tag{2.5}$$

$$g \neq g, \quad \text{if} \quad f = f'.$$

Finding the spectrum of the energy eigenvalues of the system of electrons under consideration requires diagonalization of the Hamiltonian (2.4). For this purpose, we make use of the method of approximate second quantization in the form developed by Bogoliubov and Tiablikov.[5] Applying this method to the general case, we can change Eq. (2.4) to the following form:

$$\hat{\tilde{H}} = E_0 + \sum_{(f,g)} \Big\{ \sum_{(f'g')} J(f,g,f',g') \Big\} \hat{b}^+_{fg} \hat{b}_{fg} \tag{2.6}$$

$$- \sum_{(f,g,f',g')} J (f,g, f', g') \hat{b}^+_{fg} \hat{b}_{f'g'},$$

where $\hat{\xi}^+_k$ and $\hat{\xi}^+_k$ are the operators of second quantization in Bose statistics.

Diagonalization of the appropriate quadratic form is brought about with the aid of the canonical transformation:

$$\hat{b}^{+}_{fg} = \sum_{(k)} U^{*}_{k}(f,\ g)\hat{\xi}^{+}_{k}, \tag{2.7}$$

$$\hat{b}_{fg} = \sum_{(k)} U_{k}(f,\ g)\,\hat{\xi}_{k},$$

where $\hat{\xi}^{+}_{k}$ and $\hat{\xi}^{+}_{k}$ are operators which are also subject to Bose statistics, and the eigenvalues E_k and $U_k\,(f,g)$ are determined by a set of n equations in terms of the number of possible values f and g:

$$E_k U_k(f,g) = \Big\{ \sum_{(f',g')} J(f,\ g,\ f',\ g') \Big\} U_k(f,g) \tag{2.8}$$

$$- \sum_{(f',\,g')} J(f,\ g, f', g')\, U_k(f',\ g') \quad (2.8)$$

and the normalization condition

$$\sum_{(f,g)} U^{*}_{k}(f,g)\, U_{k'}(f,g) = \delta(k - k'). \tag{2.9}$$

We shall seek the solution of the set (2.8) in the following form:

$$U_k(f_h,\ g) = N^{-1/2} U_k(g,\ h) \exp\{i(\mathbf{k}\mathbf{f}_h)\}. \tag{2.10}$$

Here h is an index characterizing the type of atom in lattice site f.

Then, after elementary transformations, a system of equations is obtained for the determination of the eigenvalues of the energy E_k. The number of these equations is equal to $\Sigma\, z_h$:

$$E_k U_k(g,\ h) = \sum_{(g'h')} I^{(k)}_{g,g',h,h'}\, U_k(g',\ h') \tag{2.11}$$

$$+ \Big\{ \sum_{(g',h')} I_{g,g',h,h'} \Big\} U_k(g,h) -$$

$$- \sum_{(g',\,h')} I_{g,g',h,h'}\, U_k(g',h'),$$

where the following notation is used:

$$I^{(k)}_{g,g',h,h'} \tag{2.12}$$

$$= \sum_{(f',h')} J(f_h, g,\ f'_{h'},\ g')\ \ \{1 - \exp[-ik(f'_{h'} - f_h)]\},$$

$$I_{g,g',h,h'} = \sum_{(f',h')} J(f_h, g, f'_{h'}, g'),$$

and the $U_k\ (f,g)$ satsifying the following normalization condition, as is easy to verify:

$$\sum_{(g,h)} U^{*}_{k}(g,\ h)\, U_{k'}(g,\ h) = \delta(k - k'). \tag{2.13}$$

We thus see that the problem of finding the energy spectrum of a system of electrons of a multi-component crystal reduces to the solution of the set $z = z_A + z_B + \ldots + z_h$ linear homogeneous equations (2.11) for the unknown functions $U_k\ (g, h)$.

In the general case, all the unknown functions $U_k\ (f,g)$ are different, and consequently, all the equations of the set are different. However, in particular cases, some equations (and sometimes, all of them) can, from the physical meaning of the problem, be shown to be identical, and therefore the order of the set is decreased, which permits us finally to develop the solution and find the spectrum E_k. For example, in the case of a pure metal, which has only a single ferromganetic electron per atom ($z_B = z_C = \ldots = z_h = 0,\ z_a = 1$), the solution of the problem reduces to the solution of a single equation.[5] If there were not one but z ferromagnetic electrons in each atom in the crystalline lattice of the pure metal, then finding the spectrum of the energy E_k would require the solution of a set of z equations.

In the lattice of a disordered alloy, the different atoms f will have a different number of nearest neighbors of different types and, consequently, their equations will be located in different conditions. The number of different equations of the system (2.11) can be shown to be sufficiently large and will be determined by the number of possible combinations of neighboring atoms of different types at each of the atoms of the alloy.

It therefore follows that the degree of the equation for obtaining E_k, which is obtained by equating the determinant of the system (2.11) to zero (and consequently, the number of possible energy levels E_k), will be larger the larger the number of electrons found in the lattice of the alloy under different conditions, in particular. as the ordering of the lattice becomes less. In the ordering, the number of possible values of E_k decreases, and therefore the formula for the dependence of the spontaneous magnetization on the temperature must change. Calculation in the general case of binary alloys cannot be carried through to completion, and we limit ourselves to a consideration only of a series of completely ordered structures of binary alloys.

3. TEMPERATURE DEPENDENCE OF THE SPONTANEOUS MAGNETIZATION OF A METAL WITH TWO FERROMAGNETIC ELECTRONS PER ATOM

Let there be two ferromagnetic electrons in each of N atoms of a crystal, located in two possible low energy states (we shall conditionally give the index g the values 1 and 2). Then, setting the determinant of the set (2.11) to zero, and taking it into consideration that $I_{21}^{(k)} = I_{12}^{(k)*}$ and $I_{21} = I_{12}$, we obtain a quadratic equation for the determination of E_k which gives the following two solutions:

$$E_k = \frac{1}{2}\{2\,|I_{12}| + I_{11}^{(k)} \tag{3.1}$$

$$+ I_{22}^{(k)} \pm \sqrt{[I_{11}^{(k)} - I_{22}^{(k)}]^2 + 4\,[|I_{12}^{(k)} - I_{12}|]^2}\}\,.$$

We are interested in the case of small values of the wave number k, which are had at low temperatures. Taking into consideration only the exchange interval between nearest neighbor atoms, expanding (2.12) in a series in k and considering only the first terms of the expansion, we obtain for the particular case of a simple cubic lattice

$$\begin{aligned} I_{11}^{(k)} &\approx a^2 J(f,\ 1,\ f',\ 1)\,k^2 = a^2 J_{11} k^2; \qquad (3.2)\\ I_{22}^{(k)} &\approx a^2 J(f,\ 2,\ f',\ 2)\,k^2 = a^2 J_{22} k^2;\\ I_{12}^{(k)} &\approx a^2 J(f,\ 1,\ f',\ 2)\,k^2 = a^2 J_{12} k^2;\\ I_{12} &= J(f,\ 1,\ f,\ 2) + 6J(f,\ 1,\ f',\ 2) = J_{12}^{0} + 6J_{12}, \end{aligned}$$

where a is a parameter of the crystalline lattice, J_{11}, J_{22} are the exchange integrals between the electrons of adjacent atoms, located at identical positions, J_{12}^{0} is the exchange integral between two electrons located in different states in the same atom, J_{12} is the analogous exchange integral for two nearest neighbors.

The following expressions are then obtained for the values $E_k^{(1)}$ and $E_k^{(2)}$:

$$E_k^{(1)} = \frac{a^2}{2}(J_{11} + J_{22} + 2J_{12})\,k^2, \tag{3.3}$$

$$E_k^{(2)} = 2\,(J_{12}^{0} + 6J_{12}) + \frac{a^2}{2}(J_{11} + J_{22} - 2J_{12})\,k^2,$$

and the Hamiltonian has the following diagonal form:

$$\hat{H} = E_0 + \sum_{(k)} E_k^{(1)}\,\hat{N}_k^{(1)} + \sum_{(k)} E_k^{(2)}\,\hat{N}_k^{(2)}, \tag{3.4}$$

$$\hat{N}_k^{(1)} = \hat{\xi}_k^{(1)+}\,\hat{\xi}_k^{(1)}, \quad \hat{N}_k^{(2)} = \hat{\xi}_k^{(2)+}\,\hat{\xi}_k^{(2)}.$$

If we take into account the effect on the electron of the external magnetic field H, then the eigenvalues of the energy operator can be written in the form

$$\hat{H} = E_0 - 2\mu_0 HN \tag{3.5}$$

$$+ \sum_{(k)}\{E_k^{(1)} + 2\mu_0 H\}\,N_k^{(1)}$$

$$+ \sum_{(k)}\{E_k^{(2)} + 2\mu_0 H\}\,N_k^{(2)},$$

where $N_k^{(1)}$ and $N_k^{(2)}$ are the occupation numbers, which take on all the integral values from zero.

Now, constructing the phase sum and carrying out standard calculations, we obtain the following relation for the mean magnetic moment M of the system of electrons under discussion:

$$M = \left(k_0 T\,\frac{\partial \ln Z}{\partial H}\right)_{H=0} \tag{3.6}$$

$$= 2\mu_0 H - \frac{\mu_0 G}{\pi^2}$$

$$\times \int_0^\infty \frac{k^2 dk}{\exp\{a^2 k^2 (J_{11} + J_{22} + 2J_{12})\,/\,2k_0 T\} - 1}$$

$$- \frac{\mu_0 G}{\pi^2}$$

$$\times \int_0^\infty \frac{k^2 dk}{\exp\{[a^2 k^2 (J_{11} + J_{22} - 2J_{12}) + 4\,(J_{12}^{0} + 6J_{12})]\,/\,2k_0 T\} - 1},$$

where $G = Na^3/2c$ and $c = 1/2$, 1,2 for simple, body-centered and face-centered lattices, respectively, k_0 = Boltzmann's constant.

The integrals entering into Eq. (3.6) are computed in elementary fashion, and the formula for the temperature dependence of the spontaneous magnetization of a ferromagnet possessing two electrons per atom takes the form:

$$M = M_0 \left\{ 1 - \frac{1{,}306}{4c\pi^2} \left(\frac{2k_0T}{J_{11} + J_{22} + 2J_{12}} \right)^{3/2} \right. \quad (3.7)$$

$$- \frac{0{,}4431}{4c\pi^2} \left(\frac{2k_0T}{J_{11} + J_{22} - 2J_{12}} \right)^{3/2}$$

$$\left. \times \exp \left[- \frac{2\,(J_{12}^0 + 6J_{12})}{k_0T} \right] \right\}.$$

At low temperatures, and for J°_{12} and J_{12} having the order of usual exchange integrals (10^{14} erg),[12] $J^{\circ}_{12} + 6J_{12} \gg k_0 T$, the third term in the curly brackets is small in comparison with the second, and Eq. (3.7) leads in practice to the same law of dependence of M on T as in the Bloch-Möller formula (1.1) for the case $z = 2$. Here

$$\theta' = 3.88\,(4c)^{2/3}\,(J_{11} + J_{22} + 2J_{12}) \,/\, 2k_0. \quad (3.8)$$

However, it should be noted that this dependence is obtained by us as the special case of a general formula. The general formula is derived with the aid of a method which differs essentially from the method used by Möller and by Holstein and Primakoff in deriving similar expressions.

Equation (3.17) permits us to carry out an estimate of the various exchange integrals from the temperature dependence of the spontaneous magnetization, known from experiment. The estimate from Eq. (3.8) gives, for iron, $J_{11} + J_{22} + 2J_{12} \approx 800\, k_0$. If both electrons are found in a single shell, we can set $J_{11} = J_{22} = J$, and then our estimate gives $J_{11} + J_{12} \approx 400\, k_0$, i.e., for $J_{12} > 0$, $J < 400\, k_0$ For $J_{12} \approx J_{11} = J$; $J \approx 200\, k_0$.

4. TEMPERATURE DEPENDENCE OF THE SPONTANEOUS MAGNETIZATION OF A METAL WITH z FERROMAGNETIC ELECTRONS PER ATOM

For the approximate solution of the problem of the determination of the energy spectrum of a ferromagnet with z ferromagnetic electrons per atom, and for the determination of the character of the temperture dependence of its spontaneous magnetization, we made use of a method similar to that used by Born[8] for the calculation of the frequency spectrum of the characteristic vibrations of a crystalline lattice. His method consisted of an expansion in powers of a small parameter of the k coefficients for the unknowns and the unknowns themselves in a system of linear homogeneous equations (2.11), and the consequent determination of the coefficients of these expansions.

Let us write (2.11) in the following form:

$$(A_g - E_k)\, U_k(g) + \sum_{(g' \neq g)} A_{gg'}\, U_k(g') = 0, \quad (4.1)$$

$$A_g = I_{gg}^{(k)} + \sum_{(g \neq g')} I_{gg'}, \quad (4.2)$$

$$A_{gg'} = I_{gg'}^{(k)} - I_{gg'} \quad (g, g' = 1, 2, \ldots, z).$$

The condition for the solvability of theset of equations (4.1) is the vanishing of its determination. This gives us an equation of degree z for the determine of the z eigenvalues of the energy E_k, wherein, inasmuch as the coefficients A are of Hermitian form, all the E_k will be real.

For the approximate determination of the eigenvalues of the energy just mentioned, we make use of thefact that as $T \to 0$, the wave number k is a small quantity and we expand the coefficients A_g, $A_{gg'}$, and also E_k and $U_k(g)$ in series in k. Limiting ourselves to the quadratic terms, we get

$$A_g = A_g^{(0)} + |k|^2 A_g^{(2)}, \quad (4.3)$$

$$E_k = E_k^{(0)} + |k|^2 E_k^{(2)},$$

$$A_{gg'} = A_{gg'}^{(0)} + |k|^2 A_{gg'}^{(2)},$$

$$U_k(g) = U_k^{(0)}(g) + |k|^2 U_k^{(2)}(g).$$

Here

$$A_g^{(0)} = \sum_{(g \neq g')} I_{gg'}, \quad A_{gg'}^{(0)} = - I_{gg'} - J_{gg'}^0,$$

$$A_g^{(2)} = a^2 J_{gg}, \quad A_{gg'}^{(2)} = a^2 J_{gg'},$$

and by J_{gg}, $J_{gg'}$ and $J^{\circ}_{gg'}$ we mean

$$J(f,\ g,\ f' \pm 1,\ g),$$

$$J(f,\ g,\ f \pm 1,\ g') \text{ и } J(f,\ g,\ f, g').$$

and $J(f,\ g,\ f, g')$.

Substituting the series (4.3) in Eq. (4.1) and equating coefficients for equal powers of k to zero, we get as a consequence the system of equations of the different approximations (we restrict ourselves to the second approximation):

$$(A_g^{(0)} - E_k^{(0)})\, U_k^{(0)}(g) + \sum_{(g \neq g')} A_{gg'}^{(0)} U_k^{(0)}(g') = 0, \tag{4.4}$$

$$(A_g^{(0)} - E_k^{(0)})\, U_k^{(2)}(g) + \sum_{(g \neq g')} A_{gg'}^{(0)} U_k^{(2)}(g') = -(A_g^{(2)} - E_k^{(2)})\, U_k^{(0)}(g) - \sum_{(g \neq g')} A_{gg'}^{(2)} U_k^{(0)}(g'). \tag{4.5}$$

It is easy to show that the equation of degree z, obtained by setting the determinant of the system (4.4) equal to zero, will always have one root equal to zero, $E_{k_1}^{(0)} = 0$, namely, for the condition that the unknown $U_k^{(0)}$ are equal to each other:

$$U_k^{(0)}(1) = U_k^{(0)}(2) = \ldots = U_k^{(0)}(z) = c, \tag{4.6}$$

where c is an arbitrary constant.

Now, substituting the value $E_{k_1}^{(0)} = 0$ and solving (4.6) in a system of equations of the second approximation (4.5), we get

$$A_g^{(0)} U_k^{(2)}(g) + \sum_{(g \neq g')} A_{gg'}^{(0)} U_k^{(2)}(g') = -\left[(A_g^{(2)} - E_k^{(2)}) - \sum_{(g \neq g')} A_{gg'}^{(2)}\right] c. \tag{4.7}$$

The system of inhomogeneous equations (4.7) is solvable only when the vector whose components are are the right sides of these equations, are orthogonal to all vectors whose components form the systems of partial solutions of the corresponding homogeneous equations. The homogeneous equations obtained from the left side of (4.7) coincide with the equations (4.4); consequently, they have a system of partial solutions (4.6). Taking this into account, and considering that $c \neq 0$, we get from the condition for the solvability of the system of equations (4.7) an equation for $E_k^{(2)}$. Solving this latter equation, and substituting the resultant expression for $E_k^{(2)}$ into (4.3), we get

$$E_{k1} = E_{k1}^{(0)} + k^2 E_{k1}^{(2)} = -\frac{1}{z}\left\{\sum_{(g)} A_g^{(2)} + 2 \sum_{(g' < g)} A_{gg'}^{(2)}\right\} a^2 k^2 = -\frac{1}{z}\left\{\sum_{(g)} J_{gg} + 2 \sum_{(g' < g)} J_{gg'}\right\} a^2 k^2. \tag{4.8}$$

It is easy to note that the structure of the coefficients of the equations of the set (4.4) are such that the secular equation of this system can have only one zero root. Actually, the value $E_k^{(0)} = 0$ satisfies the system of equations (4.4) only when all the solutions of this system $U_k^{(0)}(g)$ are equal to one another. In all the remaining cases, the $E_k^{(0)}$ are different from zero and have real positive roots. In general, there are different, although multiple roots are also possible.

It should be pointed out that if there is any possibility of determining the roots $E_k^{(0)}$ of the secular equation of the system of first approximation, then the corresponding roots $E_k^{(2)}$ are also obtained, and consequently the eigenvalues E_k of the energy of the crystal. The values $E_{k2}^{(0)}, \ldots, E_{kz}^{(0)}$, as was shown above, are different from zero; therefore terms independent of k enter into the expressions for all the E_k except E_{kl}. Thus the character of the energy spectrum in the general case for $z > 2$ will be the same as in the particular case when $z = 2$.

The formula for the temperature dependence of the spontaneous magnetization of the ferromagnet with z uncompensated spin magnetic moments per atom will have the following form:

$$M = zN\mu_0 \left\{1 - \frac{A_1}{z}\left(\frac{k_0T}{\theta_1}\right)^{3/2} - \frac{A_2}{z}\left(\frac{k_0T}{\theta_2}\right)^{3/2} \exp\left(-\frac{\theta_2'}{k_0T}\right) \ldots - \frac{A_z}{z}\left(\frac{k_0T}{\theta_z}\right)^{3/2} \exp\left(-\frac{\theta_z'}{k_0T}\right)\right\}, \tag{4.9}$$

where $A_1, A_2, \ldots, A_z$ are certain constants of order 10^{-1}; but $\theta_2, \theta_3, \ldots, \theta_z, \theta_z', \ldots, \theta_2'$ are certain functions of the exchange integrals $J_{gg}, J_{gg'}$ $\times (g, g' = 1, 2, \ldots, z)$.

5. TEMPERATURE DEPENDENCE OF THE SPONTANEOUS MAGNETIZATION OF ORDERED BINARY ALLOYS

Let us consider a series of binary, completely ordered, ferromagnetic alloys, and for simplicity, we assume that the atoms of both components A and B possess only one ferromagnetic electron apiece ($z_A = 1$, $z_B = 1$). This permits us to omit the index g in all the expressions below.

1. *Cubic lattice of an alloy of the type NaCl.* In this case, each atom A has 6 nearest neighbors B, and conversely, each atom B has 6 neighbors A. The indices h take only two values, A and B. The system (2.11) reduces to two linear equations which are homogeneous relative to $U_k(A)$ and $U_k(B)$.

After several transformations, taking only the exchange integrals between nearest neighbors into account, and expanding the coefficients of these equations in series in small values of the wave number k, we get, with accuracy up to terms of second order:

$$(6J_{AB} - E_k)\,U_k(A) + (J_{AB}a^2|k|^2 - 6J_{AB})\,U_k(B) = 0, \tag{5.1}$$
$$(J_{BA}a^2|k|^2 - 6J_{BA})\,U_k(A) + (6J_{BA} - E_k)\,U_k(B) = 0,$$

where J_{AB} and J_{BA} refer respectively to $J(f_A, f_B)$ and $J(f_B, f_A)$. Setting the determinant of this system equal to zero, and taking it into account that $J_{AB} = J^*_{BA}$, we get a quadratic equation for E_k, which has the following solution:

$$E_k^{(1)} = J_{AB}a^2k^2, \quad E_k^{(2)} = 12J_{AB} - J_{AB}a^2k^2. \tag{5.2}$$

Carrying out the usual statistical-thermodynamical calculations, we finally get the following equation for the spontaneous magnetization:

$$M = N\mu_0 - 2\mu_0 \sum_{k=0}^{N-1} \frac{1}{\exp\{J_{AB}a^2k^2/k_0T\} - 1} - 2\mu_0 \sum_{k=0}^{N-1} \frac{1}{\exp\{[12J_{AB} - J_{AB}a^2k^2]/k_0T\} - 1}. \tag{5.3}$$

The exponent in the first sum of this expression is essentially a positive quantity for arbitary k; therefore the first sum is convergent and can be replaced by an integral in k from 0 to ∞. In the second sum, the condition of the smallness of k plays the essential role: this sum will be convergent only for $12J_{AB} - J_{AB}a^2k^2 > 0$ i.e., for the condition $k < \sqrt{12}\,a$. This means that in the transition from a sum to an integration in the second integral, it is necessary to set the upper limit equal to a sufficiently high finite quantity which, however, must be less than $\sqrt{12}/a$.

Thus, for the temperature dependence of the spontaneous magnetization of an alloy with a lattice of the type NaCl, we get the formula

$$M = N\mu_0\left\{1 - \frac{1{,}306}{\pi^2}\left(\frac{k_0T}{J_{AB}}\right)^{3/2} - \frac{1}{\pi^2}\left(\frac{k_0T}{J_{AB}}\right)^{3/2} e^{-\alpha}\right\}\int_0^B \frac{x^2\,dx}{e^{-x^2} - e^{-\alpha}}, \tag{5.4}$$

$$\alpha = 12J_{AB}/k_0T, \quad B < (12J_{AB}/k_0T)^{1/2} = \alpha^{1/2}.$$

The integral in the second term is a finite quantity, but $e^{-\alpha}$ for $T \to 0$ approaches ∞; therefore, for low temperatures, the second term falls off rapidly and plays no practical role.

2. CUBIC LATTICE OF AN ALLOY OF THE TYPE CsCl ($z_A = z_B = 1$)

This case is very much like the preceding. Here the atoms A or B also have as nearest neighbors atoms of B or A, respectively. The difference lies in the fact that the number of nearest neighbors is equal to 8 here, and these neighbors are located not along the crystallographic edges of the cube but along its spatial diagonals. In this case the indices h also take on only two values and the system (2.11) reduces to two linear equations which are homogeneous relative to $U_k(A)$ and $U_{k(B)}$. From the secular equation solution, we get for E_k the values

$$E_k^{(1)} = J_{AB}a^2k^2, \; E_k^{(2)} = 16J_{AB} - J_{AB}a^2k^2. \tag{5.5}$$

For M at low temperatures, we get the same formula as (5.4), but $\alpha = 16J_{AB}/k_0T$.

3 *Cubic lattice of the compound AB_3 of the type* $FeNi_3$ ($z_A = z_{AB} = 1$). In this case atom A will have 12 nearest neighbors of B, at a distance of $a/\sqrt{2}$ from it and located in the centers of the cube faces. Each B atom will also have 12 nearest neighbors, of which 4 will be atoms of A and 8 atoms of B. Here the atoms of A will be found in a plane while the 8 of the neighbors of type B will be found in two plane parallel to the first. Thus the atoms of A are equally distributed in the sense of symmetry of their nearest neighbors, into three types (of equal number) depending on what planes they have by way of nearest neighbors of atoms of A. It then follows that we have four types of atoms in the case under consideration and the indices h will

take on the four values A, B_1, B_2 and B_3 the system (2.11) reduces to four equations.

We identify the coordinate axes with the tetragonal axes of the cube. After the corresponding transformations and expansions of the coefficients in powers of the components k_1, k_2 and k_3 of the wave number k (with accuracy up to terms of second order) we get the following system of four linear homogeneous equations:

$$\begin{aligned}&(c_0 - E_k)\, U_k(A) + c_l\, U_k(B_l)\\ &\quad + c_m\, U_k(B_m) + c_n\, U_k(B_n) = 0,\\ &c_l\, U_k(A) + (c_{ll} - E_k)\, U_k(B_l)\\ &\quad + c_{lm}\, U_k(B_m) + c_{ln}\, U_k(B_n) = 0.\end{aligned} \tag{5.6}$$

$$c_0 = 12 J_{AB}, \tag{5.7}$$

$$c_l = \frac{1}{2} J_{AB}\, a^2 (k_m^2 + k_n^2) - 4 J_{AB},$$

$$c_{ll} = 4 J_{AB} + 8 J_{BB},$$

$$c_{ml} = c_{nl} = \frac{1}{2} J_{BB}\, a^2 (k_m^2 + k_n^2) - 4 J_{BB},$$

and the indices l, m, n run through the values 1,2,3. $J_{AB} = J_{AB_1} = J_{AB_2} = J_{AB_3}$, while $J_{BB} = J_{B\,B_m}$, since the exchange integrals here depend only on the atoms between which the electron exchange takes place, and do not depend upon the type of neighbors.

Setting the determinant of (5.6) equal to zero, we obtain a fourth degree equation for the determination of the eigenvalues E_k. We limit ourselves to the approximation solution of the problem by the method given above. Expanding the coefficients and the unknowns [in Eqs. (5.6)] in series of small k_1, k_2, and k_3 and obtaining by rough calculations systems of equations of first and second approximation, we find for $E_k^{(k)}$ the value

$$E_k^{(1)} = {}^1\!/_2\, a^2 (J_{AB} + J_{BB})\, k^2. \tag{5.8}$$

The remaining roots $E_k^{(2)}$, $E_k^{(3)}$, $E_k^{(4)}$ with the exception of the term depending on k^2 will also contain terms independent of k. We get the formula for the temperature dependence of spontaneous magnetization of the alloy under consideration (for $T \to 0°$ K) in the form

$$\begin{aligned}M = N\mu_0 \Big\{ 1 &- \frac{1{,}306}{\pi^2}\left(\frac{2k_0 T}{J_{AB} + J_{BB}}\right)^{3/2}\\ &- A\left(\frac{k_0 T}{\theta_2}\right)^{3/2} \exp\left(-\frac{\theta_2'}{k_0 T}\right)\\ &- B\left(\frac{k_0 T}{\theta_3}\right)^{3/2} \exp\left(-\frac{\theta_3'}{k_0 T}\right)\\ &- C\left(\frac{k_0 T}{\theta_4}\right)^{3/2} \exp\left(-\frac{\theta_4'}{k_0 T}\right)\Big\},\end{aligned} \tag{5.9}$$

where A, B, C are constants of the order $10,^{-1}$ and θ_2, θ_2', . . . are functions of the exchange integrals J_{AB} and J_{BB}. Here, also for low temperatures (close to $T = 0$ ° K), the terms containing exponential factors virtually vanish and the "three-halves law" must hold.

Applying the methods outlined above, we can complicate the problem and consider the case of a binary ferromagnetic alloy, the atoms of whose components have different (and not equal to unity) numbers of ferromagnetic electrons. However, as rough calculations have always shown, such a complication is not of essential interest, inasmuch as the character of the temperature dependence of spontaneous magnetization in this case is not materially changed.

---

[1] F. Bloch, Z. Physik 61, 206 (1930).

[2] S. V. Vonsovskii, *Modern theories of magnetism*, Moscow Leningrad, GTTI, 1952.

[3] S. V. Vonsovskii and E. A. Turov, J. Exptl. Theoret. Phys. (U.S.S.R.) 24, 419 (1953).

[4] N. N. Bogoliubov, *Lectures on quantum statistics*, Kiev, 1949 (in Ukrainian).

[5] N. N. Bogoliubov and S. V. Tiablikov, J. Exptl. Theoret. Phys. (U.S.S.R.) 19, 251, 256 (1949).

[6] Ch. Møller, Z. Physik 82, 559 (1933).

[7] T. Holstein and H. Primakoff, Phys. Rev. 58, 1098 (1940).

[8] M. Born and M. Goeppert-Mayer, Theory of Solids, Moscow-Leningrad, ONTI, 1938 (in Russian).

Translated by R. T. Beyer
67

SOVIET PHYSICS JETP VOLUME 5, NUMBER 2 SEPTEMBER, 1957

On Radiation in Anisotropic Media

F. V. BUNKIN
P. N. Lebedev Physical Institute, Academy of Sciences, USSR

(Submitted to JETP editor December 2, 1955)
J. Exptl. Theoret. Phys. (U.S.S.R.) **32**, 338-346 (February, 1957)

A general solution is given for the problem of the field produced by a given distribution of external currents in an infinite homogeneous medium possessing arbitrary anisotropy (including gyrotropic behavior). In the particular case of a magnetoactive medium described by a tensor of the form (3.1), the multipole expansion of the radiation field has been obtained. In conclusion, the radiation field of a dipole in a magnetoactive medium is considered in greater detail.

1. INTRODUCTION

THE classical electrodynamical problem of the radiation of a given distribution of external currents in a homogeneous anisotropic medium* has not, so far as is known to us, received a general solution up to the present time. In papers by Ginsburg[1] and Kolomenskii[2] the special case is considered of the radiation of a point charge moving in a transparent anisotropic medium (Ref. 1 deals with the case of an inactive crystal, and Ref. 2 with that of a gyrotropic crystal). These writers, moreover, employ Hamilton's method, expanding the field inside a "box" in spatial Fourier series of the harmonic functions $\exp(ik_\lambda r)$. The time-dependent coefficients of the series are determined in the general case by a system of inhomogeneous linear differential equations. In the particular case of a monochromatic radiation field, which is the only one in which we shall hereafter be interested, the system of differential equations reduces to a system of linear algebraic equations, and the problem becomes considerably easier. In principle it can then be solved for a medium with arbitrary anisotropy and an arbitrary distribution of sources of the field. But with such a general statement of the problem it is more convenient to use a different approach not involving resolution of the field in terms of spatial harmonics $\exp(i\mathbf{k}_\lambda \mathbf{r})$, which are in reality not in any way singled out in the problem in question.

Namely, we at once seek an expression for the field produced by the given distribution of external currents j in the unbounded homogeneous medium with arbitrary anisotropy in a form that corresponds in the case of an isotropic medium to the well-known expression of the field in terms of retarded potentials, for example, the Hertz vector

$$\Pi = \frac{1}{i\omega\varepsilon}\int_V je^{-ik\sqrt{\varepsilon}\rho}\, dV/\rho.$$

The general expression so obtained, including also quasistationary fields, indeed turns out to be somewhat complicated, but for radiation problems one is interested only in the asymptotic representation of the indicated expression for the field, corresponding to the wave zone of the sources. The method we use for the solution of this last problem has been illustrated in this paper in the special case of an anisotropic medium — an ionized gas in a constant magnetic field (magnetoactive medium).

2. GENERAL EXPRESSION FOR THE FIELD IN AN INFINITE HOMOGENEOUS ARBITRARILY ANISOTROPIC MEDIUM WITH SOURCES

We start with the field equations for an anisotropic medium with a given distribution of external currents (the medium is assumed nonmagnetic):

$$\operatorname{curl}\mathbf{E} = -ik\mathbf{H}, \quad \operatorname{rot}\mathbf{H} = ik\hat{\varepsilon}\mathbf{E} + \frac{4\pi}{c}\mathbf{j}_{ex} \tag{2.1}$$

where $\hat{\epsilon}$ is the dielectric permeability tensor (in the general case complex)* and $\mathbf{j}_{ex}$ is the external current density, assumed to be a continuous function of position. It is required to find the solution of the equations (2.1) satisfying the condition of finiteness at all points of space and the radiation condition. This latter condition means, as for the isotropic case, that the field from a confined source must consist at infinity of diverging waves.

It is expedient to start from the equations for the field vectors (for example, for E) without at once going over to auxiliary potentials. Eliminating the vector **H** from Eq. (2.1), we find for **E** the equation

---

* Under the name of anisotropic medium we include both optically inactive and also active (gyrotropic) crystals.

* The quantity $\hat{\epsilon}\mathbf{E}$ represents a vector with the components $\epsilon_{ik}E_k$ (summation over repeated indices is assumed).

$$\text{curl curl } \mathbf{E} - k^2\hat{\varepsilon}\mathbf{E} \tag{2.2}$$

$$= \text{grad div } \mathbf{E} - \nabla^2\mathbf{E} - k^2\hat{\varepsilon}\mathbf{E} = \frac{4\pi k}{ic}\mathbf{j},$$

where the second form of the left-hand member has meaning only in a rectangular system of coordinates, which we shall use for the time being. For simplicity in writing, the subscript "ex" has been dropped.

Exploiting the linearity of the field equations, we shall seek the solution of Eq. (2.2) in the form

$$E_i = \frac{4\pi k}{ic}\int\limits_V T_{ik}(\mathbf{r}, \mathbf{r}_1)\, j_k(\mathbf{r}_1)\, dV_1, \tag{2.3}$$

where $T_{ik}(\mathbf{r}, \mathbf{r}_1)$ is a tensor of the second rank depending on the coordinates of the point of observation and the source point ($\mathbf{r}$ and $\mathbf{r}_1$) and the integration is taken over the entire volume of the sources. In the isotropic case, with $\epsilon_{ik} = \epsilon\delta_{ik}$, where δ_{ik} is the unit tensor, we have

$$T_{ik} = \frac{1}{4\pi q^2}\left(q^2\delta_{ik} + \frac{\partial^2}{\partial x_i\,\partial x_k}\right)e^{-iq\rho}/\rho, \tag{2.4}$$

where $\rho = \mathbf{r} - \mathbf{r}_1$ and $q^2 = k^2\epsilon$. From the point of view of the theory of linear differential equations $T_{ik}(\mathbf{r}, \mathbf{r}_1)$ is the Green's tensor for the equations (2.2).

Substituting Eq. (2.3) into Eq. (2.2), we obtain the following equation for T_{ik}:

$$D_{i\alpha}T_{\alpha k} = \delta_{ik}\,\delta(\rho),$$

$$\tag{2.5}$$

$$D_{ik} = \frac{\partial^2}{\partial x_i\,\partial x_k} - \nabla^2\delta_{ik} - \alpha_{ik}.$$

Here $\alpha_{ik} = k^2\epsilon_{ik}$ and ∇^2 is the Laplacian operator. It can be verified without difficulty that for $\epsilon_{ik} = \epsilon\delta_{ik}$ the tensor (2.4) indeed satisfies the equations (2.5).

In analogy with the case of the isotropic medium [Eq. (2.4)], we shall seek the solution of Eq. (2.5) in the form

$$T_{\alpha k} = D'_{\alpha k}I_0(\mathbf{r}, \mathbf{r}_1), \tag{2.6}$$

where $D'_{\alpha k}$ is also some tensor differential operator and I_0 is a scalar function of the coordinates of the points $\mathbf{r}$ and $\mathbf{r}_1$. In order for Eq. (2.6) to be a solution of Eq. (2.5), it is necessary and sufficient that the following relations hold

$$D_{i\alpha}D'_{\alpha k} = D_0\delta_{ik}, \qquad D_0I_0 = \delta(\rho). \tag{2.7}$$

Such a separation of the problem (into an algebraic and an analytical part) decidedly simplifies its solution.

The first of the equations (2.7) indicates that the operator D_0 is equal to the determinant of the tensor D_{ik} and the tensor D'_{ik} is the algebraic complement of the tensor D_{ki}. Using the invariant representation of algebraic complements and determinants (cf. for example Ref. 3) we obtain:

$$D'_{ik} = {}^1\!/_2\, e_{k\alpha\beta}\, e_{imn}\, D_{\alpha m}\, D_{\beta n}, \tag{2.8}$$

$$D_0 = {}^1\!/_6\, e_{\alpha\beta\gamma}\, e_{ijk}\, D_{\alpha i}\, D_{\beta j}\, D_{\gamma k}, \tag{2.9}$$

where e_{ijk} is the completely antisymmetric unit pseudotensor of the third rank ($e_{123} = 1$). Substituting Eq. (2.9) into Eq. (2.7), we obtain an equation for I_0, which determines this quantity apart from a nonsingular contribution I_0 which satisfies the equation $D_0I_0' = 0$. The lack of uniqueness of the function I_0 is obviously entirely analogous to that of the Green's function. As for the Green's function, the nonsingular term I_0' is determined by the supplementary conditions (in our case, the radiation condition).

According to Eqs. (2.5) and (2.9)

$$D_0\exp\{\pm i\mathbf{p}\rho\} = \Delta(\mathbf{p})\exp\{\pm i\mathbf{p}\rho\}, \tag{2.10}$$

where $\Delta(p)$ is the determinant of the matrix $p^2\delta_{ik} - p_ip_k - \alpha_{ik}$. Consequently, we shall satisfy the second of the equations (2.7) if we set:

$$I_0(\mathbf{r}, \mathbf{r}_1) = \frac{1}{(2\pi)^3}\int\limits_{-\infty}^{\infty}\frac{\exp\{\pm i\mathbf{p}\rho\}}{\Delta(\mathbf{p})}d\mathbf{p}. \tag{2.11}$$

The validity of the expression (2.11) for I_0 from the point of view of the radiation condition (i.e., the legitimacy of setting $I'_0 = 0$) is confirmed by the asymptotic behavior of the integral (2.11) at infinity. We shall not carry out the analysis of this integral for the general anisotropic case. In the following Section the investigation is carried through for several special cases, and shows that the radiation condition is satisfied.

Thus all of the quantities of interest have been found, and for T_{ik} we have finally

$$T_{ik}(\mathbf{r}, \mathbf{r}_1) = {}^1/_2\, e_{k\alpha\beta}\, e_{imn} D_{\alpha m} D_{\beta n} I_0(\mathbf{r}, \mathbf{r}_1), \quad (2.12)$$

with $I_0(r, r_1)$ given by the expression (2.11).

The solution (2.3) can be given a different and more familiar form. We introduce the vector

$$\Pi = \frac{4\pi k}{ic} \int\limits_V I_0(\mathbf{r}, \mathbf{r}_1)\, \mathbf{j}(\mathbf{r}_1)\, dV_1. \quad (2.13)$$

Then from Eqs. (2.3) and (2.12) we obtain:

$$E_i = {}^1/_2\, e_{k\alpha\beta}\, e_{imn} D_{\alpha m} D_{\beta n} \Pi_k. \quad (2.14)$$

Thus we can regard the vector Π as the Hertz vector. But in this connection it must be kept in mind that the definition of Π by Eq. (2.13) will not reduce on passage to the isotropic case to the well-known definition of the Hertz vector for an isotropic medium, since the expression (2.11) does not* go over into $e^{-iq\rho}/\rho$.

The set of formulas (2.11), (2.13) and (2.14) [or (2.3), (2.11) and (2.12)] completely solves the problem proposed. The difficulty encountered in the practical application of these formulas is that of calculating the integral (2.11). But for the determination of the field in the wave zone ($k\rho >> 1$) it is necessary to know only the asymptotic value of this integral with accuracy to terms of the order $1/k\rho$. For this purpose it is clear that in all concrete cases the method of steepest descent can be successfully applied. In the following Section we carry out such a calculation for one special case of an anisotropic medium.

3. THE WAVE FIELD OF AN ARBITRARY DISTRIBUTION OF CURRENTS IN A MAGNETOACTIVE MEDIUM

We shall apply the results obtained above to the special case of a magnetoactive medium such as an ionized gas in a constant magnetic field. If the axis of symmetry (i.e., the magnetic field) is directed along the z axis of the coordinates, then the tensor ϵ_{ik} has the form (cf., for example, Ref. 4, p. 326):

$$\varepsilon_{ik} = \begin{Vmatrix} \varepsilon & -ig & 0 \\ ig & \varepsilon & 0 \\ 0 & 0 & \eta \end{Vmatrix} \quad (3.1)$$

In the absence of absorption ϵ, η and g are real; when there is absorption, these quantities are, generally speaking, complex. The explicit expressions for the components of ϵ_{ik} in terms of the parameters of the plasma are of no interest to us here. We note that if we formally set $g = 0$ we obtain the case of a uniaxial crystal with the axis of symmetry along the z axis*. This circumstance can be used later on to obtain various results for a uniaxial crystal.

Our problem is to calculate the asymptotic expression (for $k\rho \to \infty$) for the integral (2.11) in the case of a medium described by a tensor of the form (3.1). The determinant $\Delta(\mathrm{p})$ is biquadratic in p_3 and can be written in the form (cf., for example, Ref. 5, p. 134):

$$\Delta(\mathrm{p}) = \alpha_3 (p_3^2 - s_3^2)(p_3^2 - t_3^2), \quad (3.2)$$

where $\alpha_3 = k^2\eta$, and $s_3(p_1, p_2)$ and $t_3(p_1, p_2)$ are the z components of the wave vectors $\mathbf{s}$ and $\mathbf{t}$ corresponding to the ordinary and extraordinary plane waves, expressed in terms of the other two components p_1 and p_2. The components s_3 and t_3 are determined as the roots of the equation $(z_1 = s_3^2,\ z_2 = t_3^2)$:

$$\alpha_2 z^2 - [2\alpha_1\alpha_3 - (\alpha_1 + \alpha_3)p^2]z \quad (3.3)$$

$$+ (p^2 - \alpha_3)(\alpha_1 p^2 - \alpha_1^2 - \beta^2) = 0,$$

$$\alpha_1 = k^2\varepsilon,\ \beta = k^2 g,\ p^2 = p_1^2 + p_2^2.$$

Substituting Eq. (3.2) into Eq. (2.11), we obtain:

$$I_0(\mathbf{r}, \mathbf{r}_1) \quad (3.4)$$

$$= \frac{1}{(2\pi)^3 \alpha_3} \int\limits_{-\infty}^{\infty} \frac{\exp\{\pm i\mathrm{p}\rho\}\, dp_1 dp_2 dp_3}{(p_3^2 - s_3^2)(p_3^2 - t_3^2)}$$

This can easily be reduced to a one-dimensional integral. In fact, let us first consider the region $z > 0$ and take the minus sign in the exponent of the expression (3.4). Supposing further that, in the extraction of roots, s_3 and t_3 are defined by those branches for which $\mathrm{Im}(s_3, t_3) < 0$, we perform the integration over p_3, taking the residues at the poles $p_3 = s_3, t_3$. If we go over to polar coordinates ρ, ϑ, φ for the result obtained and introduce $p_1 = p\cos\eta$, $p_2 = p\sin\eta$, then, after integration over η, we obtain

---

* Apart from a constant factor, the quantity $(\nabla^2 + q^2)I_0$ goes over into $e^{-iq\rho}/\rho$ in the case of an isotropic medium.

* For an absorbing crystal it is here necessary to postulate that the principal axes of the dielectric permeability tensor and of the conductivity tensor coincide, i.e., to require a sufficiently high degree of symmetry of the crystal.

$$I_0 = \frac{i}{8\pi\alpha_3}\int\limits_{-\infty}^{\infty}\frac{pH_0^{(2)}(p\rho\sin\vartheta)}{s_3^2 - t_3^2}\left[e^{-is_3\rho\cos\vartheta}/s_3 - e^{-it_3\rho\cos\vartheta}/t_3\right]dp. \tag{3.5}$$

Here $H_0^{(2)}(z)$ is the Hankel function of second kind and zeroth order.

This expression for I_0 is valid for arbitrary values of the parameters ϵ, η and g. But in what follows, for simplicity of exposition, we confine ourselves to the case of no absorption, i.e., the case of real ϵ, η and g.

We apply the method of steepest descents to the integral (3.5). We first transform to a new variable of integration $\xi = \xi' + i\xi''$ by means of the equation $kn_i(\xi)\sin\xi = p$, where $n_i(\xi)$ is the index of refraction of the ith plane wave ($i = 1$ for ordinary, $i = 2$ for extra-ordinary) with its normal making angle ξ with the z axis. In the first term of Eq. (3.5) one must put $i = 1$, and in the second $i = 2$. The possibility of complex values of the angle ξ means that our consideration includes so-called inhomogeneous plane waves.

From the definition of the index of refraction it follows that

$$p^2 + s_3^2 = k^2n_1^2,\ p^2 + t_3^2 = k^2n_2^2. \tag{3.6}$$

From this we obtain

$$s_3 = kn_1\cos\xi,\ \ t_3 = kn_2\sin\xi. \tag{3.7}$$

Substitution of Eq. (3.6) into Eq. (3.3) gives an equation for n_i, with roots of the form

$$n_{1,2}^2 = \frac{[\varepsilon(\varepsilon-\eta) - g^2]\sin^2\xi + 2\varepsilon\eta \pm \sqrt{[\varepsilon(\eta-\varepsilon) + g^2]^2\sin^4\xi + 4\eta^2g^2\cos^2\xi}}{2(\varepsilon\sin^2\xi + \eta\cos^2\xi)}. \tag{3.8}$$

Noting further that

$$s_3^2 - t_3^2 = \frac{k^2}{\eta}\sqrt{(\varepsilon-\eta)^2n_i^4\sin^4\xi - 4\eta g^2(n_i^2\sin^2\xi - \eta)}, \tag{3.9}$$

we obtain for I_0 the following expression

$$I_0 = \frac{i}{8\pi k^3}\sum_{i=1}^{2}\int\limits_{C_i}\frac{(n_i'\sin\xi + n_i\cos\xi)H_0^{(2)}(k\rho n_i\sin\vartheta\sin\xi)\,\mathrm{tg}\,\xi}{[(\varepsilon-\eta)^2n_i^4\sin^4\xi - 4\eta g^2(n_i^2\sin^2\xi - \eta)]^{1/2}}\exp\{-ik\rho n_i\cos\vartheta\cos\xi\}. \tag{3.10}$$

The integration contours C_i lie in the complex ξ-plane.

In all of what follows we shall carry out the investigation only for one type of wave, dropping the index i. Omitting from consideration for the time being the region of angles around $\vartheta = 0$, we employ the asymptotic representation of the function $H_0^{(2)}(z)$. With the intent of carrying out all calculations to the accuracy of terms of order $1/k\rho$, we can keep only the first term in the asymptotic representation of $H_0^{(2)}(z)$. Substitution of this into Eq. (3.10) and introduction of the polar angles θ and χ of the vectors $\mathbf{r}$ and $\mathbf{r}_1$ (Fig. 1) gives the following expression for I_0:

$$I_0(\mathbf{r}, \mathbf{r}_1) = \frac{ie^{i\pi/4}}{8\pi k^3}\sqrt{\frac{2}{\pi k\rho\sin\vartheta}}\int\limits_C F[(\xi, \mathbf{r}_1)\,e^{-ikrn\cos(\xi-\theta)}d\xi, \tag{3.11}$$

$$F(\xi, \mathbf{r}_1) = \sqrt{\frac{\sin\xi}{n(\xi)}} \times \frac{(n'\sin\xi + n\cos\xi)\exp\{ikr_1n\cos(\xi-\chi)\}}{\cos\xi\,[(\varepsilon-\eta)^2n^4\sin^4\xi - 4\eta g^2(n^2\sin^2\xi - \eta)]^{1/2}}. \tag{3.12}$$

From the condition $k\rho \gg 1$ it necessarily follows that $kr \gg 1$ and $kr_1 \gtrsim 1$. Thus the integral (3.11) satisfies the requirements for applicability of the method of steepest descents[6]. The saddle point $\xi_0(\theta)$ is determined by the equation

$$(d/d\xi)[n(\xi)\cos(\xi-\theta)] = 0,$$

from which we have

$$n'(\xi_0)/n(\xi_0) = \mathrm{tg}(\xi_0 - \theta). \tag{3.13}$$

But $n'(\xi_0)/n(\xi_0) = \operatorname{tg}\alpha(\xi_0)$, where $\alpha(\xi_0)$ is the angle between the wave normal and the energy-flux vector of the plane wave, under the condition that the angle between the normal and the z axis is equal to ξ_0 (cf., for example, Ref. 4, p. 463). Thus[4] $\alpha(\xi_0) = \xi_0(\theta) - \theta$, i.e., $\xi_0(\theta)$ is that angle between the wave normal of the plane wave and the direction of the magnetic field for which the energy-flux vector of this wave makes the angle θ with the magnetic field. From this it is clear that the angle $\xi_0(\theta)$ is always real.

The integration path of steepest descent is determined by the equation

$$n(\xi)\cos(\xi - \theta) = \psi(\theta) - i\zeta^2, \qquad (3.14)$$
$$\psi(\theta) = n(\xi_0)\cos\alpha(\xi_0),$$

where ζ is a real variable ranging from $-\infty$ to $+\infty$. Integrating over the path of steepest descent and taking the function $F(\xi, \mathbf{r}_1)\,d\xi/d\zeta$ for $\xi = \xi_0$ out from under the sign of integration, we obtain an asymptotic expression for $I_0(\mathbf{r}, \mathbf{r}_1)$ valid to terms of order $1/k\rho$:

$$I_0(\mathbf{r}, \mathbf{r}_1) = A(\theta)\, e^{ikr_1 n(\xi_0)\cos\gamma}\, e^{-ikr\psi(\theta)}/kr. \qquad (3.15)$$

Here $\gamma = [\chi - \xi_0(\theta)]$ is the angle between $\mathbf{r}_1$ and the wave normal $\mathbf{N}$ of the plane wave that has its energy-flux vector directed at the angle θ (see Fig. 1), and the function $A(\theta)$ has the form [$(n_0 = n(\xi_0),\ \alpha_0 = \alpha(\xi_0)$]:

$$A(\theta) = \frac{i}{4\pi k^3}\,\frac{\cos\theta}{\cos\xi_0\cos\alpha_0} \qquad (3.16)$$
$$\times\left[\frac{n_0\sin\xi_0}{\sin\theta\,[(n_0'' - n_0)\cos\alpha_0 - 2n_0'\sin\alpha_0]\,[(\varepsilon-\eta)^2 n_0^4\sin^4\xi_0 - 4\eta g^2(n_0^2\sin^2\xi_0 - \eta)]}\right]^{1/2}.$$

Substitution of Eq. (3.15) into Eq. (2.11) gives the expression for the wave field:

$$\mathbf{\Pi} = 4\pi k^2 A(\theta)\, e^{-ikr\psi(\theta)}\,\mathbf{Z}(\theta)/kr, \qquad (3.17)$$

$$\mathbf{Z}(\theta) = \frac{1}{i\omega}\int_V \mathbf{j}(\mathbf{r}_1)\, e^{ikr_1 n(\xi_0)\cos\gamma}\, dV_1. \qquad (3.18)$$

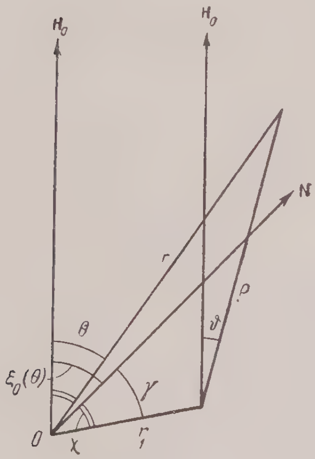

FIG. 1

4. EXPANSION OF THE WAVE FIELD IN TERMS OF MULTIPOLES

Expansion of the function $\mathbf{Z}(\theta)$ into a series in powers of a/λ (a is the order of magnitude of the linear dimensions of the system of currents and λ is the wavelength) must give the expansion of the wave field (3.17) in terms of multipoles:

$$\mathbf{\Pi} = \sum_{s=0}^{\infty}\mathbf{\Pi}_s \qquad (4.1)$$
$$= 4\pi k^2 A(\theta)\,(kr)^{-1}\, e^{-ikr\psi(\theta)}\sum_{s=0}^{\infty}\mathbf{Z}_s(\theta).$$

The expression for the multipole of sth order is found by expanding the function $\exp\{ikr_1 n(\xi_0) \times \cos\gamma\}$ in a series of powers of kr_1. Thus we obtain:

$$\mathbf{Z}_s = \frac{[in(\xi_0)]^s}{i\omega s!}\int_V (kr_1\cos\gamma)^s\,\mathbf{j}(\mathbf{r}_1)\,dV_1. \qquad (4.2)$$

In the case of an isotropic medium, the zeroth term of the expansion ($s = 0$) corresponds, as is well known[7], to dipole radiation, while the following approximation ($s = 1$) corresponds to magnetic dipole and electric quadrupole radiations. The same holds true, naturally, also in the case now considered. In fact, introducing the electric and magnetic dipole moments

$$\mathbf{p} = \frac{1}{i\omega}\int_V \mathbf{j}\,dV_1, \quad \mathbf{m} = \frac{1}{2c}\int_V [\mathbf{r}_1\mathbf{j}]\,dV_1, \qquad (4.3)$$

and the tensor $\hat{\pi}$ of the electric quadrupole moment of the given current distribution

$$\pi_{ik} = \frac{1}{2c}\int\limits_V (\xi_i j_k + \xi_k j_i)\, dV_1 \tag{4.4}$$

(ξ_i are the coordinates of the point $\mathbf{r}_1$), we find*:

$$\mathbf{Z}_0 = \mathbf{p}, \quad \mathbf{Z}_1(\theta) = n(\xi_0)([\mathbf{mN}] + \hat{\pi}\mathbf{N}). \tag{4.5}$$

$\mathbf{N} = \mathbf{N}(\theta)$ is as before the unit vector of the wave normal (Fig. 1). The difference between the result (4.5) and the corresponding result in the case of an isotropic medium consists only in the fact that the unit vector of the direction of observation, grad $\mathbf{r}$, (isotropic medium) is replaced by the vector $\mathbf{N}$ making the angle $\alpha(\xi_0)$ with grad $\mathbf{r}$.

5. THE WAVE FIELD OF AN ELECTRIC DIPOLE

We introduce the explicit expression for the field of a dipole $\mathbf{p}$. To do this, we must substitute

$$\Pi_0 = 4\pi k^2 A(\theta)\, e^{-ikr\psi(\theta)}\, \mathbf{p} / kr \tag{5.1}$$

into Eq. (2.14) and carry out the indicated operations to the accuracy of terms of the order $1/kr$.

Working out the operator (2.8) in Cartesian coordinates for the present case of a magnetoactive medium, we obtain for the components of the electric field the following expressions:

$$E_i(\mathbf{r}) = 4\pi k^6 A(\theta)\, e^{-ikr\psi(\theta)}\, a_{ik}(\theta, \varphi)\, p_k / kr, \tag{5.2}$$

where we have introduced the notations

$$\begin{aligned} a_{11} &= (\sigma_+^2 \cos^2\varphi - \varepsilon)\gamma_3 + (\varepsilon - \eta)\sigma_-^2, \\ a_{22} &= (\sigma_+^2 \sin^2\varphi - \varepsilon)\gamma_3 + (\varepsilon - \eta)\sigma_-^2, \\ a_{33} &= (\sigma_-^2 - \varepsilon)\gamma_1 - g^2, \\ a_{12,21} &= (\sigma_+^2 \sin\varphi\cos\varphi \mp ig)\gamma_3 \pm ig\sigma_-^2, \\ a_{13,31} &= \sigma_+\sigma_-(\gamma_1\cos\varphi \mp ig\sin\varphi), \\ a_{23,32} &= \sigma_+\sigma_-(\gamma_1\sin\varphi \pm ig\cos\varphi); \end{aligned} \tag{5.3}$$

$$\gamma_1 = n^2(\xi_0) - \varepsilon, \quad \gamma_3 = n^2(\xi_0) - \eta, \tag{5.4}$$

$$\sigma_+ = n(\xi_0)\sin\xi_0, \quad \sigma_- = n(\xi_0)\cos\xi_0.$$

From the relations that have been obtained it is seen that this result is correct for arbitrary angles θ, and thus the assumptions made above ($z > 0$, angle θ not too close to zero) are not essential. As regards the first assumption ($z > 0$), this follows from the fact that the right-hand side of Eq. (5.2) is a function of θ symmetric with respect to $\theta = \pi/2$. The validity of the expression (5.2) at $\theta = 0$ follows from the continuity (absence of singularity) of the right-hand member of Eq. (5.2) at this point.

Let us examine the surfaces of constant phase

$$\Psi(r, \theta) = kr\psi(\theta) = krn(\xi_0)\cos\alpha(\xi_0) = \text{const}$$

(Fig. 2). Calculation of $\nabla\Psi$ gives

$$(\nabla\Psi)^2 = k^2 n^2(\xi_0), \tag{5.5}$$

$$\cos(\widehat{\mathbf{N}, \rho}) = (\nabla\Psi)_r / kn(\xi_0) = \cos\alpha(\xi_0). \tag{5.6}$$

Equation (5.5) is, obviously, the special form of the eikonal equation corresponding to the case of a homogeneous medium with axially symmetrical anisotropy.

Equation (5.6) shows that the angle between the normal $\mathbf{N}$ to the front of the wave produced by a point source and the direction of observation $\mathbf{r}$ (the angle θ) is always equal to the angle between the

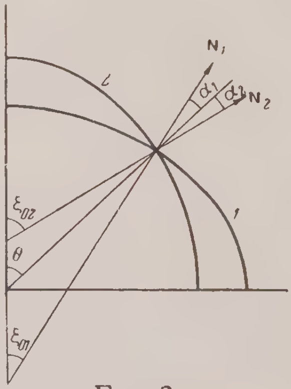

FIG. 2

$1 - \Psi_1(\rho, \theta) = \text{const}$,
$2 - \Psi_2(\rho, \theta) = \text{const}$

---

* Corresponding calculations can be found in Ref. 7, p. 382.

wave-normal and the energy-flux vector of the plane wave propagated in the direction $\xi_0(\theta)$ (Fig. 2). This result is seen to be quite natural if we take into account the fact that in the wave zone the field of an arbitrary distribution of sources can always be represented in a sufficiently small region of space as the field of a plane wave.

It is of interest to consider the radiation of a dipole for several special cases of the orientation of the dipole itself and of the choice of the direction of observation. Without presenting the corresponding calculations from Eqs. (5.2), (5.3) and (5.4), we give only the final results.

1. *Dipole orientated along the magnetic field* ($\theta = 0$). Just as in the case of an isotropic medium, the dipole does not radiate along its own axis. In a direction perpendicular to the axis of the dipole there is emitted only the ordinary linearly polarized wave, with the amplitude

$$\frac{k^2}{r} p \sqrt{\left|\frac{\varepsilon(\eta-\varepsilon)+g^2}{\eta(\eta-\varepsilon)}\right|}. \qquad (5.7)$$

2. *Dipole orientated perpendicular to the field* ($p_1 = p,\ p_2 = p_3 = 0$). Along its own axis the dipole emits the extraordinary wave elliptically polarized in the plane (x, y) perpendicular to the magnetic field. The amplitudes along the x and y axes are, respectively,

$$\frac{k^2}{r} p \sqrt{\left|\frac{\varepsilon[\varepsilon(\eta-\varepsilon)+g^2]}{\varepsilon[\varepsilon(\eta-\varepsilon)+g^2]+\eta g^2}\right|} \quad \begin{cases} g^2/\varepsilon^2 \\ g/\varepsilon \end{cases} \qquad (5.8)$$

Radiation along the axis of the dipole is characteristic of a magnetoactive medium. When we go over to the uniaxial crystal ($g = 0$), or even further to the isotropic medium ($g = 0,\ \epsilon = \eta$), the amplitudes (5.8) go to zero. Along the magnetic field both waves are emitted, and now with circular polarizations. The amplitudes of the waves are

$$(k^2/r)\, p\, |\eta/(\varepsilon + \eta \pm g)| \qquad (5.9)$$

(the upper sign refers to the ordinary wave).

In conclusion the writer takes occasion to express his deep gratitude to Prof. S. M. Rytov for directing and aiding in the work, and also to M. L. Levin for several remarks.

---

[1] V. L. Ginzburg, J. Exptl. Theoret. Phys. (U.S.S.R.) **10**, 601 (1940).

[2] A. A. Kolomenskii, J. Exptl. Theoret. Phys. (U.S.S.R.) **24**, 167 (1953)

[3] O. Veblen, *Invariants of Differential Quadratic Forms*, IIL (Foreign Lit. Press), 1948.

[4] Al'pert, Ginzburg and Feinberg, *Radio Wave Propagation*, GITTL, 1953.

[5] S. M. Rytov, *Theory of Electric Fluctuations and Thermal Radiation*, Acad. Sci. Press, 1953.

[6] R. Courant and D. Hilbert, *Methods of Mathematical Physics*, vol. 1.

[7] J. Stratton, *Electromagnetic Theory*.

Translated by W. H. Furry
69

SOVIET PHYSICS JETP VOLUME 5, NUMBER 2 SEPTEMBER, 1957

Scattering of Fast Protons on Protons

D. I. BLOKHINTSEV
Atomic Station, Academy of Sciences, USSR

(Submitted to JETP editor February 12,1956)
J. Exptl. Theoret. Phys. (U.S.S.R.) 32, 347–349 (February, 1957)

It is shown that the main term in the interaction of two protons with $J = 0$ should have a singularity of the order $1/r^3$.

As is known, the cross section for fast proton-proton scattering is characterized by isotropy and energy independence.[1] This isotropy occurs in the energy range from 100 mev to 400-500 mev; beyond that the isotropy is violated in account of meson production inelastic processes.[2,3]

Another characteristic of proton elastic scattering is the appreciable magnitude of the elastic cross section in comparison with its limiting value for S–wave scattering $-\lambda^2$. Actually, the cross section amounts to $2\lambda^2$. This indicates the essential contribution to the proton scattering of states with total angular momentum $J = 0$, i.e., of the states ${}^1S_0$ and ${}^3P_0$ [1,2] and the suppression of other waves with respect to these. The spin orbit coupling in the interaction ought to be small.

In this paper, we did not intend to go into the physical nature of such a character of proton–proton interaction. The interaction between fast protons does not reduce to any sort of potential. We will restrict ourselves to ask a somewhat phenomenological question: what should be the singularity in the main part of the interaction between two protons with $J = 0$, if this interaction is considered in the coordinate (space) representation?

For a suggestive treatment, we will start from the Born approximation. The phase δ_l of the scattered wave is determined by the known relation

$$\sin \delta_l = -\frac{1}{k}\int_0^\infty g_l(kr)\, V(r)\, u_l(kr)\, dr, \qquad (1)$$

where k is the vector wave number relative to the nucleon motion; $g_l\,(kr)$ is the outgoing wave of orbital angular momentum 1, in the absence of interaction [it has the asymptotic form $\sin(kr - \pi l/2)$] ; $u_l\,(kr)$ is the same but with the interaction present [it has the asymptotic form $\sin[kr - (\pi l/2) + \delta_l\,\}$] $V(r)$ is the interaction energy for $J = 0$ (or its main term) multiplied by $2m^*/\hbar^2$ (m^* is the nucleonic reduced mass).

Let us first consider a $V(r)$ of the form

$$V(r) = 2m^* U_0 \hbar^{-2} (a/r)^n, \qquad (2')$$

where a is a certain length and V_0 is the value of the interaction energy at $r = a$.

Let us now introduce the dimensionless variable $\rho = kr$. Then (1) can be written in the form:

$$d_l = \frac{\sin\delta_l}{k} \qquad (2)$$
$$= -aV_0\,(ak)^{n-3}\int_0^\infty g_l(\rho)\,\rho^{-n}\,u_l(\rho)\,d\rho.$$

Here d_l is the scattering length (the differential scattering cross section is proportional to $\sim d_l^2$). $V_0 = 2m^* U_0\, a^2/\hbar^2$ is a dimensionless quantity characterizing the value of the interaction energy.

In the Born approximation, this integral depends on the nucleon energy, only through the cutoff at the lower integration limit, which is necessary for $n > 2$. For $n = 3$, this dependence will be still weak–logarithmic. The principal energy dependence is contained in the factor $(ak)^{n-3} \sim E^{(n-3)/2}$ (E is the nucleon energy, which multiplies the integral. It follows that for $n = 1$ (Coulomb law), the cross section will depend on the energy as E^{-2}; for $n = 2$ (quadratic law), as E^{-1} and, finally, for $n = 3$, it is constant (not counting a weak dependence on the cutoff at the lower limit which will lead to a logarithmic rise of the cross section).

For laws with a stronger r–dependence than $1/r^3$, the cross section will increase appreciably with energy.

The qualitative behavior of the cross section for $V \approx r^{-3}$ shows that this law can be brought into agreement with the experimental data on $p-p$ scattering. Such an interaction law would, however, be in disagreement with meson theory, which requires the presence of an exponential factor $e^{-\varkappa r}$, where $\varkappa = \mu c/\hbar^2$ and where μ is the meson mass. This factor introduces deviations from the pure Coulomb law which are the smaller, the larger the proton energy. Indeed, if we write the interaction $e^{-\varkappa r}/r^3$ in a dimensionless form, we get $V(\rho) \sim e^{-\alpha\rho}/\rho^3$ where $\alpha = \varkappa/k$: hence the larger the value of k, the smaller the α and the smaller the role of the exponential.

The qualitative analysis reported above is the basis of an exact quantative calculation (not using the Born approximation) of $^1S_0$ and $^3P_0$ proton elastic scattering for the interactions

$$V = V_0 e^{-\alpha\rho}/\rho^3 \quad \text{for} \quad \rho > ak, \qquad (4)$$
$$V = V_0 e^{-\alpha ak}/(ak)^3 \quad \text{for} \quad \rho < ak,$$

i.e., for a cut–off cubic law with an exponential. It was assumed that $a = \hbar/mc = 2 \times 10^{-14}$ cm, $\varkappa = \mu c/\hbar = 7 \times 10^{12}$ cm^{-1} (for π-mesons); two values were assumed for V_0 : 15 and 30.

The graph shows the calculated proton elastic scattering versus energy (the cross–hatched area is between the curves for $V_0 = 15$ and $V_0 = 30$). The vertical lines represent a compilation[1] of the expermental data. The calculations for the energies above 400 mev are doubtful because the relativistic corrections become excessively large. For a reasonable evaluation of the obtained agreement with the experimental data, it should be noted that at small energies ($E \ll 100$ mev), the interaction will contain terms with singularities of lower degree ($V \sim 1/r^2$ and $V \sim 1/r$). In the energy range between 100 and 300 mev, however, the cross section would have changed 9 times for a $V \sim 1/r$ interaction law, and 3 times for $V \sim 1/r^2$. For $V \sim 1/r^3$ the cross section is almost constant and close to the experimental values. This result can be considered as an indication of the substantial role of terms of the type $e^{-\varkappa r}/r^3$ in the proton interaction.

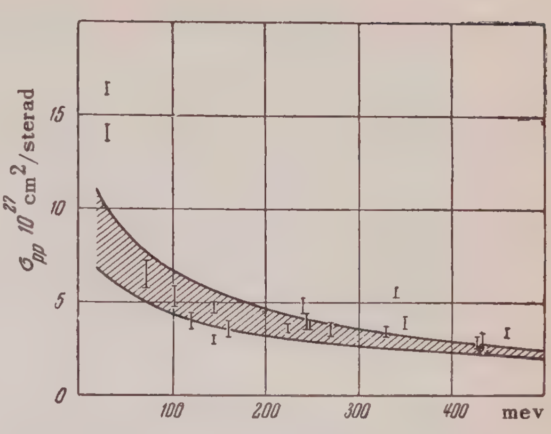

Region between the curves denotes the calculated cross section as a function of the energy. Experimental data are shown as vertical lines.

The numerical calculations were carried out under the supervision of G. I. Marchuk and V. V. Smelov to whom the author expresses his gratitude.

---

[1] Ia. A. Smorodinskii: *Prob. sovrem. fiz.* 7, 7 (1954).

[2] Meshcheriakov, Bogachev, Neganov and Piskarev, Dokl. Akad. Nauk SSSR 99, 955 (1954).

[3] Meshcheriakov, Neganov, Soroko and Vzorov, Dokl. Akad. Nauk SSSR 99, 959 (1954).

Translated by E. S. Troubetzkoy
70

SOVIET PHYSICS JETP VOLUME 5, NUMBER 2 SEPTEMBER, 1957

Some Remarks on the Validity of the Hydrodynamic Description of Quantum Systems

D. I. BLOKHINTSEV
Atomic Station, Academy of Sciences, USSR

(Submitted to JETP editor February, 1956)
J. Exptl. Theoret. Phys. (U.S.S.R.) **32**, 350-352 (February, 1957)

It is shown that the hydrodynamic description of quantum systems imposes some serious restrictions on the dimensions of the investigated system. A result of this is that the description is not valid for atomic nuclei or multiple creation of mesons at the initial stages of expansion of the meson liquid.

THE hydrodynamic description of motion assumes that it is possible to assign to each element of the considered medium an energy density ϵ, a momentum density g, a medium density ρ and a pressure p, which are functions of coordinates and time. The whole medium has to be broken up into physically infinitely small volumes Δx^3, and the time into physically infinitely small intervals Δt.

It is only formally that one can consider the space-time lattice thus formed, as having infinitely small interpoint distances. Actually, these distances are subject to lower, as well as upper bounds. The upper bounds are trivial: $\Delta x \ll L$, $\Delta t \ll T$, where L is the dimension of the system and T is a time, characteristic of the considered process. As far as the lower bounds are concerned, the classical and the quantum theories give different restrictions. We are going to consider the restrictions characteristic of a quantum system.

Let Δx^3 be the volume element, with $\Delta x = L/n$, $n \gg 1$. The momentum of the element will be $g\Delta x^3$. On the other hand, the momentum dispersion Δp related to the localization of matter in the interval Δx, will be $> \hbar/\Delta x$. In order that it be possible to describe the motion with a momentum density g, it is required that the mean value of the momentum $g\Delta x^3$ be larger than the possible dispersion, i.e., that $g\Delta x^3 \gg \hbar/\Delta x$ or

$$g \gg \hbar/\Delta x^4. \qquad (1)$$

In the nonrelativistic case, the energy density is $\epsilon = g^2/2\rho$; hence

$$\varepsilon \gg n^8\hbar^2/2L^8\rho. \qquad (2)$$

In the relativistic case $\epsilon \approx gc$, i.e.,

$$\varepsilon \gg n^4\hbar c/L^4. \qquad (3)$$

These relationships for the energy can also be obtained from the relation $\Delta E\Delta t > \hbar$ for $\Delta t \approx \Delta x/v$ or $\Delta t \approx \Delta x/c$ respectively, let us note that any more detailed model consideration can only increase the values of the right hand sides of these inequalities.

We now apply these inequalities to two definite problems.

A. HYDRODYNAMIC DESCRIPTION OF THE ATOMIC NUCLEUS

In this case, the characteristic dimension is the nuclear radius $L = R = r_0 A^{1/3}$, $r_0 = 1.3 \times 10^{-13}$ cm, A = atomic weight of the nucleus. The matter density is mA/V, where m is the nucleon mass and $V = 4\pi R^3/3$.

Let us now make use of the inequality (2) and apply it to the total nuclear excitation energy $E \approx \epsilon V$ due to the hydrodynamic motions. It then follows from (2) that:

$$E \gg \frac{n^8\hbar^2}{2R^8}\frac{V^2}{mA} = \frac{1}{2}\left(\frac{4\pi}{3}\right)^2 n^8 \frac{\hbar^2}{2mr_0^2} A^{-5/3}. \qquad (4)$$

We have $\hbar^2/2mr_0^2 \approx 10$ mev. Even if the nuclear radius is divided only into three parts ($n = 3$), we still get a tremendous excitation energy — so large that the nucleus cannot exist as a whole (for $A = 200$, $E \gg 80$ mev). Therefore it is not possible to expect, for instance, that the moment of inertia of a nucleus computed from the motion of an ideal liquid in an ellipsoidal container have any relation to the actual situation.

The quantization of the hydrodynamic rotational motion of the nucleus will not help, because the most important parameter of the problem — the moment of inertia — is calculated from the classical theory. This does not mean that one cannot at all speak of a rotation of the nucleus. In the quantum theory, the reciprocal of the moment of inertia, $a = 1/I$, is an operator. In order to be able to speak of a rotation of the nucleus it is necessary that the dispersion $\overline{\Delta a^2}$ be much smaller than $\bar{a}^2$, i.e., there must be a certain "rigidity" of the nuclear shape.

B. HYDRODYNAMIC DESCRIPTION OF MULTIPLE MESON CREATION

Recently, attempts have been made[1-3] to consider the multiple meson creation in the collision of two relativistic nucleons as the process of expansion of the excited meson liquid. When a large number of mesons is present, it can be expected that the quantization will have no sizable effect, because the mesons are subject to Bose statistics. The restrictions for such a classical description come, however, from the fact that one has to apply this concept not to the system as a whole, but to small space-time regions.

In the case considered here, we are talking about a meson liquid occupying the volume of an oblate ellipsoid: $V = (4\pi/3)(\hbar/\mu c)^3\, 2mc^2/E$ (here μ is the meson mass, m – the nucleon mass and E – the nucleons' energy in the center-of-mass system). The minor half axis of the ellipsoid is, taking into account the Lorentz contraction, equal to $L = (\hbar/\mu c)\, mc^2/E$. Because of the large magnitude of this contraction, we can restrict ourselves to a one-dimensional problem. Instead of (3), we get for the energy density per unit length:

$$\varepsilon \gg n^2\hbar c/L^2 \quad \text{for} \quad E \gg n^2\hbar c/L. \tag{5}$$

If we substitute the value of L, we find that

$$n^2 \ll m/\mu. \tag{6}$$

This inequality shows that in the initial stage of the process immediately following the nucleon collision, the hydrodynamic description is absolutely inapplicable: in this stage the meson liquid which occupies the ellipsoid undergoes quantum fluctuations of momentum and energy.

The further behavior of this liquid becomes quite indefinite from the hydrodynamic point of view, and the ellipsoid can break into "drops". One can therefore think that the process of multiple meson creation is actually a purely quantum effect.

If one still assumes that, in this quantum phase, the motion is a more or less regular one-dimensional expansion of the ellipsoid, it is easy to show that, in order that the hydrodynamic description be valid, it is necessary that the energy of the primary nucleons be greater than $10^{14} - 10^{15}$ ev (number of layers $n \approx 10$, $\Delta p/p \approx 10\%$). The same numerical conclusion is reached when one considers the final stages of the expansion, when L becomes comparable to $\hbar/\mu c$ and the motion becomes three-dimensional.

---

[1] E. Fermi, Progr. Theoret. Phys. 5, 570 (1950).

[2] E. Fermi, Phys. Rev. 81, 683 (1955).

[3] C. Z. Belen'kii and L. D. Landau, Usp. Fiz. Nauk 56, 309 (1955).

Translated by E. S. Troubetzkoy
71

SOVIET PHYSICS JETP VOLUME 5, NUMBER 2 SEPTEMBER, 1957

Polarization Effects in the Scattering of Electrons and Positrons by Electrons

A. A. KRESNIN AND L. N. ROZENTSVEIG
Physical-Technical Institute, Academy of Sciences, Ukrainian SSR

(Submitted to JETP editor December 8, 1955)
J. Exptl. Theoret. Phys. (U.S.S.R.) **32**, 353-358 (February, 1957)

Polarization effects arising in the scattering of electrons or positrons by electrons are considered. A possibility is found for using Möller scattering in magnetized foils to analyze polarized beams of electrons or positrons.

1. INTRODUCTION

THE approach to several important physical experiments involves the production and study of polarized electron and positron beams. For example, a determination of the polarization of β-particles from oriented nuclei could provide information about the interaction responsible for β-decay[1] experiments with polarized high energy electrons would be of undoubted interest; and so on. At the present time the main method for producing and analyzing polarized electron beams is scattering in the Coulomb fields of heavy nuclei[2]: a) if the incident beam is not polarized, the scattered electrons are found to be partially polarized; b) if the incident beam is polarized at a certain angle with the direction of motion, then an azimuthal asymmetry is observed in the angular distribution of the scattered electrons. We note that these effects are due to terms of the order $(Z/137)^2$ in the scattering amplitude, and accordingly are completely absent in the first Born approximation.

As an analyzer for polarized electron and positron beams, the scattering by heavy nuclei has the following disadvantages: 1) the polarization effects disappear in the limiting cases of nonrelativistic and extreme relativistic energies, i.e., in the high-energy region this method fails completely; 2) the measurement of the azimuthal asymmetry in the scattering of a polarized beam gives the projection of the polarization vector on the normal to the plane of scattering; the presence of a longitudinal polarization can be detected by first deflecting the beam with an electric field[3], but this is not always convenient to do; 3) for positrons the polarization effects are manifested considerably more weakly than for electrons; 4) double scattering in the foil with oblique incidence of the beam can strongly distort the result at small energies; just this effect held up the experimental verification of the theory for more than 10 years.[4]

In the present note, we consider the polarization effects occurring in the scattering of an electron (positron) by an electron*. It can easily be shown that in the second approximation of the perturbation theory, which leads to the well-known Möller formula (cf., for example, Ref. 5) the scattering of an unpolarized beam by an unpolarized target leaves the beam unpolarized, and in the scattering of a polarized beam by an unpolarized target (or an unpolarized beam by a polarized target) no azimuthal asymmetry appears. These effects show up first in the third approximation of the perturbation theory, which gives the radiation corrections to the Möller formula[6].

But also in the second approximation of the perturbation theory, the following effects occur: 1) in the scattering by a polarized target (a magnetized ferromagnetic substance) the electron beam becomes polarized; 2) in the scattering of a polarized beam by a polarized target the angular distribution departs from that given by the Möller formula (a different dependence on the angle ϑ and an azimuthal asymmetry). Unlike those in the case of scattering of electrons in the Coulomb field of a nucleus, these polarization effects do not disappear in the limiting cases of nonrelativistic and extreme relativistic energies; they are of comparable magnitude for positrons and electrons (at nonrelativistic energies, however, they are absent for positrons); the presence of a longitudinal polarization in the incident beam is directly manifested in the scattering; and the registration of coincidences produced by the scattered electron (positron) and the recoil electron makes it possible to eliminate altogether the effect of double scattering in the foil.

These properties of the Möller scattering in magnetized foils lead to the idea of a new method for the analysis of polarized electron and positron beams, which for certain cases turns out to be useful.

---

* This problem was suggested to us by A. I. Akhiezer, to whom we express our indebtedness.

2. SCATTERING OF A POLARIZED BEAM BY A POLARIZED TARGET

The state of polarization of a beam of nonrelativistic particles with spin ½ is described by a density matrix $\rho = ½(1 + \zeta\sigma)$, where ζ is the polarization vector ($|\zeta| \leq 1$; for $|\zeta| = 1$ the beam is completely polarized). For relativistic particles with spin ½ and momentum p,the form of the four-rowed density matrix is given in Ref. 1 (cf. also the added note in another paper[7]); but the writers of Ref. 1 did not notice that the cumbersome expression found by them for ρ can be brought into a compact form by separating out factors $\eta^{(+)}(p)$ on the right and left:

$$\rho(\zeta^0, \mathbf{p}) = \eta^{(+)}(p)\,{}^1/_2(1 + \zeta\Sigma\gamma_4)\,\eta^{(+)}(p). \quad (1)$$

Here

$$\Sigma\gamma_4 = -i\boldsymbol{\gamma}\gamma_5 = \begin{pmatrix}\sigma & 0\\ 0 & -\sigma\end{pmatrix},$$

and $\eta^{(+)}(p)$ is the projection operator onto states of positive energy $p_0 = \varepsilon = \sqrt{m^2 + \mathbf{p}^2} > 0$,

$$\eta^{(+)}(p) = (1/2\varepsilon)(m - i\hat{p})\gamma_4 \quad (\hat{p} = p_\mu\gamma_\mu). \quad (2)$$

The polarization vector ζ is given by

$$\zeta = \zeta^0_\perp + (\varepsilon/m)\zeta^0_\parallel, \quad (3)$$

where ζ^0 is the polarization vector in the system of reference in which the electrons are at rest ($|\zeta^0| \leq 1$), and $\zeta^0{}_\perp$ and $\zeta^0{}_\parallel$ are the components of ζ^0 perpendicular and parallel to the vector p. We note that in the relativistic case an unpolarized beam ($\zeta = 0$) is described by a projection operator and not by the unit matrix.

The analogous formulas for positrons with momentum p and energy $\epsilon > 0$ are:

$$\rho^{(p}(\zeta^0, \mathbf{p}) = \eta^{(\bar{p})}(p)\,{}^1/_2(1 - \zeta\Sigma\gamma_4)\,\eta^{(p)}(p), \quad (4)$$

$$\eta^{(p)}(p) = -(1/2\varepsilon)(m + i\hat{p})\gamma_4. \quad (5)$$

In the case of $e - e$ scattering the density matrix ρ_i for the initial state is a "direct product" of matrices ρ_1 and $\rho_{1'}$ which describe respectively the incident beam (momentum $\mathbf{p}_1$) and the electrons of the target (momentum $\mathbf{p}_{1'}$):

$$\rho_i = \rho(\zeta^0_1, \mathbf{p}_1) \times \rho(\zeta^0_{1'}, \mathbf{p}_{1'}). \quad (6)$$

Similarly, for the final state,

$$\rho_f = \rho(\zeta^0_2, \mathbf{p}_2) \times \rho(\zeta^0_{2'}, \mathbf{p}_{2'}). \quad (7)$$

The cross section for the scattering of a polarized electron beam by a polarized target is given by the "trace"

$$\sigma(\vartheta, \varphi) \sim \mathrm{Sp}\,[S\rho_i S^+ \eta^{(+)}(p_2)\,\eta^{(+)}(p_{2'})], \quad (8)$$

where S is the scattering matrix, whose opposite element is given, apart from a factor, by

$$S \approx \frac{(\bar{u}_2\gamma_\mu u_1)(\bar{u}_{2'}\gamma_\mu u_{1'})}{(p_2 - p_1)^2} - \frac{(\bar{u}_{2'}\gamma_\mu u_1)(\bar{u}_2\gamma_\mu u_{1'})}{(p_{2'} - p_1)^2}. \quad (9)$$

Substituting Eqs. (1) and (6) into the "trace" (8), we obtain four terms: one of them, independent of ζ_1 and $\zeta_{1'}$ agrees, to within a constant factor, with the Möller cross section; two others, depending linearly on the components of ζ_1 or $\zeta_{1'}$, are identically equal to zero; the fourth term contains the components of the vectors ζ_1 and $\zeta_{1'}$ bilinearly, and is given by

$$(p_2 - p_1)^{-4}\mathrm{Sp}\,\Gamma_{\overline{\mu\nu}}(p_1, p_2, \zeta_1)\,\mathrm{Sp}\,\Gamma_{\mu\nu}(p_{1'}, p_{2'}, \zeta_{1'})$$

$$+ (p_{2'} - p_1)^{-4}\,\mathrm{Sp}\,\Gamma_{\mu\nu}(p_{1'}, p_2, \zeta_{1'})$$

$$\times \mathrm{Sp}\,\Gamma_{\mu\nu}(p_1, p_{2'}, \zeta_1) - 2(p_2 - p_1)^{-2}$$

$$\times (p_{2'} - p_1)^{-2}\,\mathrm{Sp}\,[\Gamma_{\mu\nu}(p_1, p_{2'}, \zeta_1)\,\Gamma_{\mu\nu}(p_{1'}, p_2, \zeta_{1'})],$$

$$\Gamma_{\mu\nu}(p_1, p_2, \zeta_1) = (1/16\varepsilon_1^2\varepsilon_2)\,\gamma_\mu(m - i\hat{p}_1)$$

$$\times (\zeta_1\Sigma)\,(m - \hat{i}p_1)\,\gamma_\nu(m - i\hat{p}_2).$$

Introducing a rectangular system of coordinates with the unit vectors **k**, **l**, **n**, where **k** is a unit vector in the direction of the incident beam, **n** is a unit vector normal to the plane of scattering, and $\mathbf{l} = [\mathbf{n} \times \mathbf{k}]$, and going over from ζ_1, $\zeta_{1'}$ to ζ_1^0, $\zeta^0_{1'}$, we write the cross-section for scattering of electrons by electrons in the form

$$\sigma(\vartheta, \varphi) = \sigma_0(\vartheta)\;[1 + T_{ik}(\xi, \vartheta)\,\zeta^0_{1i}\zeta^0_{1'k}]; \quad (10)$$

Here $\sigma_0(\vartheta)$ is the Möller cross section, ϑ is the scattering angle in the center-of-mass system, and $\xi = \epsilon_{1\,\mathrm{lab}}/m$ is the energy of the incident electron in the laboratory reference system, expressed in units m. As the result of rather cumbersome developments we obtain the following formulas for the coefficients T_{ik}:

$$T_{11} = \tau(\xi, \vartheta)\,[4\xi(2\xi - 1) - (\xi - 1)(\xi + 3)\sin^2\vartheta],$$

$$T_{22} = \tau(\xi, \vartheta)\,[4\xi + (\xi - 1)(\xi + 3)\sin^2\vartheta], \qquad (11)$$

$$T_{33} = \tau(\xi, \vartheta)\,[4(2\xi - 1) - (\xi - 1)^2\sin^2\vartheta],$$
$$T_{12} = T_{21} = \tau(\xi, \vartheta)(\xi - 1)\sqrt{2(\xi + 1)}\sin 2\vartheta,$$
$$T_{31} = T_{13} = T_{23} = T_{32} = 0;$$

$$-\tau(\xi, \vartheta) = \sin^2\vartheta\,[4\xi^2(1 + 3\cos^2\vartheta) \qquad (12)$$
$$+ (\xi - 1)^2(4 + \sin^2\vartheta)\sin^2\vartheta]^{-1}.$$

The values of T_{ik} at $\vartheta = \pi/2$ are shown in Fig. 1.

In limiting cases, the cross-section (10) can be represented by relatively simple formulas.

a) The nonrelativistic case ($\xi - 1 \ll 1$)

$$\sigma(\vartheta) \approx \sigma_0(\vartheta)\left[1 - \frac{\sin^2\vartheta}{1 + 3\cos^2\vartheta}(\zeta^0_{1}\zeta^0_{1'})\right]; \qquad (13)$$

There is no azimuthal asymmetry, but the dependence on ϑ differs from Möller's result.

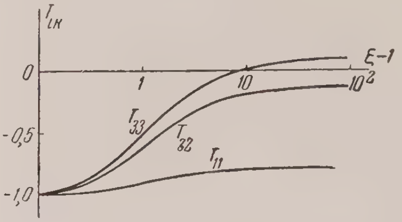

FIG. 1. The coefficients T_{ik} in Eq. (11), at $\vartheta = \pi/2$

b) The extreme relativistic case ($\xi \gg 1$)

$$\sigma(\vartheta, \varphi) \approx \sigma_0(\vartheta)\left\{1 - \frac{\sin^4\vartheta}{(3 + \cos^2\vartheta)^2}\right. \qquad (14)$$
$$\times\left[\left(\frac{8}{\sin^2\vartheta} - 1\right)(\mathbf{k}\zeta^0_{1})(\mathbf{k}\zeta^0_{1'}) + (\mathbf{l}\zeta^0_{1})(\mathbf{l}\zeta^0_{1'})\right.$$
$$\left.\left. - (\mathbf{n}\zeta^0_{1})(\mathbf{n}\zeta^0_{1'})\right]\right\}.$$

The scattering cross section for positrons by electrons is found in a similar way:

$$\sigma^{(p)}(\vartheta, \varphi) = \sigma^{(p)}_0(\vartheta)\,[1 + T^{(p)}_{ik}(\xi, \vartheta)\,\zeta^0_{1i}\zeta^0_{1'k}]; \qquad (15)$$

$$T^{(p)}_{11} = \tau^{(p)}(\xi, \vartheta)\,[(\xi + 1)^2(7\xi + 1) + (\xi + 1)(7\xi^2 - 4\xi + 5)\cos\vartheta$$
$$+ (\xi - 1)(\xi + 3)^2\cos^2\vartheta + (\xi - 1)^2(\xi + 3)\cos^3\vartheta],$$

$$T^{(p)}_{22} = \tau^{(p)}(\xi, \vartheta)\,[(\xi + 1)^2(\xi + 7) + (\xi + 1)(\xi^2 + 4\xi - 13)\cos\vartheta$$
$$- (\xi - 1)(\xi + 3)^2\cos^2\vartheta - (\xi - 1)^2(\xi + 3)\cos^3\vartheta],$$

$$T^{(p)}_{33} = \tau^{(p)}(\xi, \vartheta)\,[-(\xi + 1)(\xi^2 - 8\xi - 17) - (\xi^2 - 1)(\xi - 11)\cos\vartheta \qquad (16)$$
$$+ (\xi - 1)^2(\xi + 3)\cos^2\vartheta + (\xi - 1)^3\cos^3\vartheta],$$

$$T^{(p)}_{12} = T^{(p)}_{21} = \tau^{(p)}(\xi, \vartheta)\,2\sqrt{2(\xi + 1)}\sin\vartheta\,[2(\xi + 1) + (\xi - 1)(\xi + 3)\cos\vartheta +$$
$$+ (\xi - 1)^2\cos^2\vartheta],$$
$$T^{(p)}_{31} = T^{(p)}_{13} = T^{(p)}_{23} = T^{(p)}_{32} = 0;$$

$$\tau^{(p)}(\xi, \vartheta) = (\xi - 1)(1 - \cos\vartheta)\,[(\xi + 1)(9\xi^3 - \xi^2 - \xi + 25) +$$
$$+ 4(\xi^2 - 1)(3\xi + 11)\cos\vartheta + 2(\xi - 1)^2(3\xi^2 + 12\xi + 11)\cos^2\vartheta + \qquad (17)$$
$$+ 4(\xi - 1)^3\cos^3\vartheta + (\xi - 1)^4\cos^4\vartheta]^{-1}.$$

The dependence of $T^{(p)}_{ik}$ on ξ at $\vartheta = \pi/2$ is given in Fig. 2.

The limiting cases are: a) $\xi - 1 \ll 1$

$$\sigma^{(p)}(\vartheta) \approx \sigma^{(p)}_0(\vartheta), \qquad (18)$$

i.e., in the nonrelativistic case, the polarization has no effect on the positron electron scattering; b) $\xi >> 1$

$$\sigma^{(\pi)}(\vartheta, \varphi) \cong \sigma_0^{(\pi)}(\vartheta)\Big\{1 + \frac{\sin^4\vartheta}{(3+\cos^2\vartheta)^2}\Big[\Big(\frac{8}{\sin^2\vartheta} - 1\Big)(\mathbf{k}\zeta_1^0)(\mathbf{k}\zeta_{1'}^0) + (\mathbf{l}\zeta_1^0)(\mathbf{l}\zeta_{1'}^0) - (\mathbf{n}\zeta_1^0)(\mathbf{n}\zeta_{1'}^0)\Big]\Big\} \tag{19}$$

We shall show how the relations obtained here can be used for the experimental determination of the polarization of an electron beam. All measurements are to be carried out in such a way that the normal N to the plane of the scattering foil and the vector k form a fixed angle $\alpha \sim 45°$ (cf. Fig. 3). The electron counters 1 and 2 are set in the plane (k, N) at the angles θ_1 and θ_2 corresponding to the angles ϑ and $\pi - \vartheta$ in the center-of-mass system ($\vartheta \sim \pi/2$), and connected to a coincidence circuit. The polarization of the incident beam is determined in three steps.

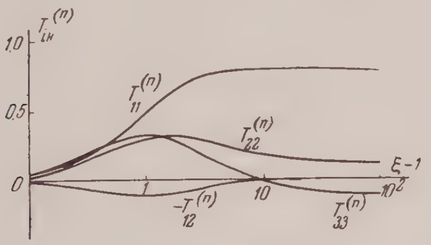

FIG. 2. The coefficients $T_{ik}^{(p)}$ in Eq. (15), at $\vartheta = \pi/2$

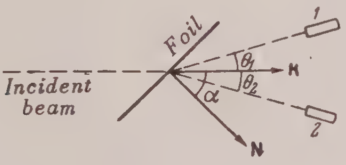

FIG. 3

1) The polarization $\zeta_{1'}^0$ of the foil is directed along the normal n to the plane of the scattering. We determine the number of coincidences D_1, referred to unit current in the incident beam. Then we turn the foil and the counters through 180° around the axis **k**, so that $\zeta_{1'}^0$ is in the direction –n, and determine the number of coincidences D_2. The ratio $D_1:D_2$ gives the projection $(\zeta_1^0\mathbf{n})$ by the formula

$$D_1/D_2 = [1 + T_{33}(\xi, \vartheta)\zeta_{1'}^0(\zeta_1^0\mathbf{n})] / [1 - T_{33}(\xi, \vartheta)\zeta_{1'}^0(\zeta_1^0\mathbf{n})].$$

2) We carry out analogous measurements after turning the foil and counters through 90° and 180° around the axis **k**, so that the new normal **n′** coincides with our former vector **l**. Obviously,

$$D_1'/D_2' = [1 + T_{33}(\xi, \vartheta)\zeta_{1'}^0(\zeta_1^0\mathbf{l})] / [1 - T_{33}(\xi, \vartheta)\zeta_{1'}^0(\zeta_1^0\mathbf{l})].$$

3) Having thus determined $\zeta_{1\perp}^0$, we turn the counters and foil around the axis k so as to bring them into the plane perpendicular to the vector $\zeta_{1\perp}^0$, then turn the foil around the axis N so that the vector $\zeta_{1'}^0$ lies in the plane of the scattering, and again carry out measurements. Then

$$D_1''/D_2'' = [1 + T_{11}(\xi, \vartheta)(\zeta_{1'}^0\mathbf{k})(\zeta_1^0\mathbf{k})] / [1 - T_{11}(\xi, \vartheta)(\zeta_{1'}^0\mathbf{k})(\zeta_1^0 k].$$

The procedure set forth here is, of course, not a universal one: at energies $\xi \sim 10$, where T_{33} changes sign (but $T_{22} \neq 0$), it must be changed. In the case of scattering of positrons, it is assumed that counter 1 registers only positrons, and counter 2, only electrons.

A weak aspect of this method is that it gives not ζ_1^0, but the product $\zeta_{1'}^0 \zeta_1^0$. If we take the number of "polarized" electrons per iron atom equal to 2.06[8] and assume that all of the atomic electrons scatter like free electrons (which is correct for sufficiently large energies ϵ_1), then for $\zeta_{1'}^0$ we get the value $\zeta_{1'}^0 = 0.08$, i.e., the asymmetry is small even for $\zeta_1^0 = 1$. The magnetized foil used as an analyzer must be calibrated in a corresponding way, i.e., the value of $\zeta_{1'}^0$ for it must be determined.

3. POLARIZATION IN THE SCATTERING OF AN UNPOLARIZED ELECTRON BEAM BY A POLARIZED TARGET

By the use of Eq. (1) it is not difficult to show that the polarization of the scattered beam (momentum p_2) is given by

$$\zeta_2 = (\varepsilon_2/m)\,\mathrm{Sp}\left(\Sigma\rho_f\right), \tag{20}$$

where ρ_f is obtained from ρ_i by means of the scattering matrix S:

$$\rho_f = \eta^{(+)}(p_2)\,\eta^{(+)}(p_{2'})\,S\rho_i S^+\eta^{(+)}(p_2)\,\eta^{(+)}(p_{2'})\,/\,\mathrm{Sp}\,[S\rho_i S^+\eta^{(+)}(p_2)\,\eta^{(+)}(p_{2'})]. \tag{21}$$

If the incident beam is not polarized (momentum $\mathbf{p}_1$, $\zeta_1 = 0$), and the electrons of the target are polarized $(\mathbf{p}_{1'} = 0,\ \zeta_{1'} = \zeta^0_{1'} \neq 0)$, then the polarization of the scattered beam

$$\zeta^0_2 = \zeta_{2\perp} + (m/\varepsilon_2)\,\zeta_{2\parallel} \tag{22}$$

can be written in the form

$$\zeta^0_{2i} = M_{ik}\zeta^0_{1'k}; \tag{23}$$

The coefficients M_{ik} are given by

$$\begin{aligned} M_{11} = \mu(\xi,\vartheta)\{8\xi^2 - \xi(1+\cos\vartheta)\,[2(\xi+1)^2 + (\xi-1)(\xi+3)\cos\vartheta \\ + (\xi^2-1)\cos^2\vartheta]\}, \end{aligned} \tag{24}$$

$$\begin{aligned} M_{22} &= \mu(\xi,\vartheta)\{8\xi^2 - \xi(1+\cos\vartheta)\,[\xi^2 + 6\xi + 1 - (\xi-1)^2\cos\vartheta \\ &\quad - 2(\xi-1)\cos^2\vartheta]\}, \\ M_{33} &= \mu(\xi,\vartheta)\{8\xi^2 + (1+\cos\vartheta)\,[(\xi+1)(\xi^2-8\xi+3) \\ &\quad - (\xi-1)(\xi^2+2\xi-1)\cos\vartheta]\}, \\ M_{12} &= \mu(\xi,\vartheta)\,\xi(\xi-1)\sqrt{2(\xi+1)}\,\sin\vartheta\,(2 - 3\cos\vartheta - \cos^2\vartheta), \\ M_{21} &= -\mu(\xi,\vartheta)\,\xi(\xi-1)\sqrt{2(\xi+1)}\,\sin\vartheta\,(4 + \cos\vartheta + \cos^2\vartheta), \\ M_{31} &= M_{13} = M_{23} = M_{32} = 0, \\ \mu(\xi,\vartheta) &= (1-\cos\vartheta)\{[\xi + 3 + (\xi-1)\cos\vartheta]\,[4\xi^2(1+3\cos^2\vartheta) \\ &\quad + (\xi-1)^2(4+\sin^2\vartheta)\sin^2\vartheta]\}^{-1}. \end{aligned} \tag{25}$$

The values of M_{ik} for $\vartheta = \pi/2$ and various energies ξ are shown in Fig. 4. (We recall that the vectors **k**, **l**, **n** are taken as coordinate axes).

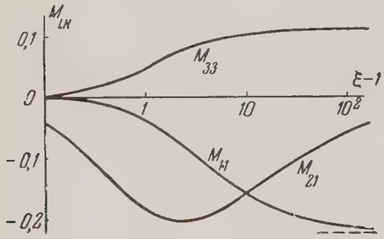

FIG. 4. The coefficients M_{ik} in Eq. (23) for $\vartheta = \pi/2$;
$M_{22} = {}^1/_2 M_{11}$; $M_{12} = -{}^1/_2 M_{21}$

Equation (23) is decidedly simplified in the limiting cases:

a) the nonrelativistic case

$$\zeta^0_2 \approx -\zeta^0_{1'}(1-\cos\vartheta)\cos\vartheta\,/\,2(1+3\cos^2\vartheta); \tag{26}$$

b) the extreme relativistic case

$$\zeta^0_2 \approx -\frac{(1-\cos\vartheta)}{(3+\cos^2\vartheta)^2}\,\{(2+\cos\vartheta+\cos^2\vartheta) \tag{27}$$

$$\times(\zeta^0_{1'}\mathbf{k})\,\mathbf{k} + (1-\cos\vartheta)\,[(\zeta^0_{1'}\mathbf{l})\,\mathbf{l} - (\zeta^0_{1'}\mathbf{n})\,\mathbf{n}]\}.$$

We note that the polarization of nonrelativistic electrons is a purely exchange effect and is due to the second term in the expression (9) for the matrix element of the scattering. It is natural that in the case of positron-electron scattering the polarization effects vanish in the nonrelativistic approximation.

---

1 H. A. Tolhoek and S. R. de Groot, Physica **17**, 81 (1951).

2 N. Mott and H. Massey, *Theory of Atomic Collisions*.

3 H. A. Tolhoek and S. R. de Groot, Physica **17**, 17 (1951).

4 Shull, Chase and Myers, Phys. Rev. **63**, 29 (1943); G. Goertzel and R. T. Cox, Phys. Rev. **63**, 37 (1943).

5 A. I. Akhiezer and V. B. Berestetskii, *Quantum Electrodynamics*, Moscow, 1953.

6 A. Akhiezer and R. Polovin, Dokl. Akad. Nauk SSSR **90**, 55 (1953).

7 F. W. Lipps and H. A. Tolhoek, Physica **20**, 85 (1954).

8 P. Argyres and C. Kittel, Acta Metallurgica **1**, 241 (1953).

Translated by W. H. Furry
72

SOVIET PHYSICS JETP VOLUME 5, NUMBER 2 SEPTEMBER, 1957

On the Nature of the Cone-like Shape of Tracks of Multi-charged Ions in Nuclear Emulsions

O. V. LOZHKIN
Radiation Institute, Academy of Sciences, USSR

(Submitted to JETP editor June 27, 1956)
J. Exptl. Theoret. Phys. (U.S.S.R.) 32, 208-213 (February, 1957)

Photometric investigations of the tracks of multi-charged particles in fine grained nuclear emulsions of various sensitivity indicate that the thinning down of the track near the end of the range is not due to variation of the total specific energy losses but to variation of the energy spent by δ-electrons with $E \geq 2$ kev near the track axis. A new method for measuring the total charge of multi-charged particles in fine grained nuclear emulsions is described.

---

1. INTRODUCTION

THE tracks of multiply-charged ions in nuclear emulsion of medium and high sensitivity have the peculiarity of a thinning down at the end of the ion path. Beginning with the work of Freier[1], this thinning down was connected by many investigators[2-5] with a decrease of the specific ionization energy loss dE/dx at the end of the ion path because of electron pickup. The thinning-down length was understood to mean the average path length after which a fragment of initial charge Z_0 captured its first orbital electron. This led to the method of determining Z_0 from the thinning down length of the track. However, the decrease of dE/dx in the capture of an electron by the ion is not as it would seem from first examination since at the same time as the charge is decreased the velocity of the ion is decreased, and $dE'/dx \sim Z^2_{\text{eff}}/v^2$. Therefore there is doubt that a particular thinning-down length exists, especially since the actual thinning down (because of change of dE/dx), if it does exist, can easily be masked by changes of the track half width which are caused by the δ-electrons.

In the past few years Güer and Lonchamp[6-8] developed new ideas about the mechanism responsible for changes of track thickness in nuclear emulsion. The thinning down is explained primarily by changes in the space density of δ-electrons and not only by changes in the specific ionization loss. Confirmation of this point of view comes from the results of Ref. 9 on measurements of specific ionization loss of nitrogen isotopes in emulsion.

2. EXPERIMENTAL PART

In order to describe the relative shares of changes in specific ionization along the path length and the spatial distribution of δ-electrons causing the thinning down of the track at its end, it is essential to have a method of separating both these effects. This was attained by using emulsions strongly different in sensitivity.

For the investigation, fine grained nuclear emulsions type P-9 prepared in the laboratory of N. A. Perfilov were used. If the sensitivity of an emulsion is characterized by specific ionization dE/dx for particles causing a visible track, then the emulsion P-9_0 had a minimum value of dE/dx near 50 kev/μ, while for the emulsion P-9_s– approximately 4.5 kev/μ. The plates were exposed to completely ionized nitrogen atoms with an energy of 90 mev at an angle of 10° at the surface of the emulsion. After development the nuclear tracks were studied with the aid of a photometric installation. The dependence of the track darkening $(I_\varphi - I_c)/I_\varphi$ in an interval of 5μ on the remaining ion path length in the emulsion was measured. The slit size in the objective plane was $(0.8 \times 5)\ \mu^2$.

3. RESULTS OF THE MEASUREMENTS AND DISCUSSION

The observed dependence of darkening on path length for the N^{14} ion is given in Fig. 1. The appearance of N^{14} ion tracks in emulsions of different sensitivities is seen in the microphotographs of Fig. 2.

As can be easily seen from the curves of Fig. 1, the thinning down of the N^{14} ion tracks is clearly shown for the sensitive emulsions, but does not appear for the insensitive emulsions. Since in the low sensitivity emulsion (P-9_0) the N^{14} ion forms a track consisting of separate grains, the entire darkening characterizes the specific ionization loss dE/dx of the nitrogen ion along its path. In agreement with the results of Ref. 9 we can conclude from curve *A* that the energy loss of a nitrogen ion along its path changes insignificantly and can not be the cause of the observed changes of darkening of tracks in more sensitive emulsions (P-9_s).

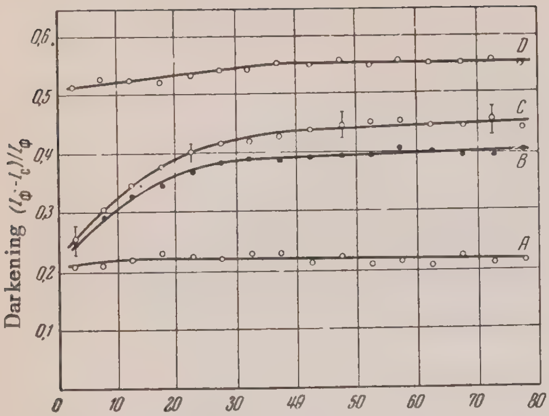

FIG. 1. Dependence of total darkening in a N^{14} ion track, on range. *A* – Low sensitivity emulsion (P-9_0); *B* and *C* – sensitive emulsions of two different batches (P-9_s); *D* – Ilford E-1 emulsion.

The indicated peculiarities of multiply charged ions in sensitive and insensitive emulsions can be understood if we assume that the thinning down of the tracks is caused not by the full dE/dx energy loss of the particle, but only by a small part of the total collision losses which cause the appearance of δ-electrons with energy more than a certain $E_{\min}$. In the sensitive emulsion these δ-electrons cause an additional broadening of the track which decreases as the ion speed decreases because of the lesser δ-electron energy. In the insensitive emulsion these δ-electrons do not give any observable photographic effect.

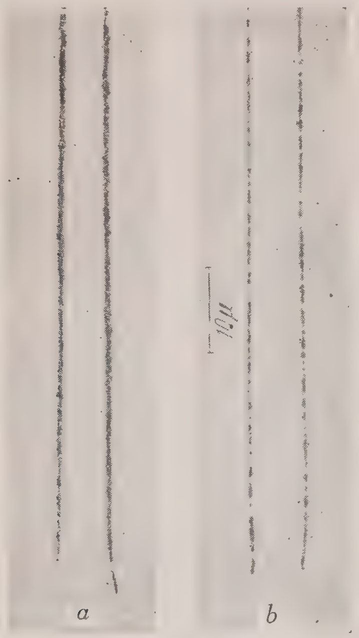

FIG. 2. Microphotographs of N^{14} tracks. *a* – in sensitive emulsion *b* – in low sensitivity emulsion.

To further examine this viewpoint we have calculated the dependence of the energy of the emitted δ-electrons near the track axis on the remaining range of the particle for the ions N^{14}, B^8, Li^8. The energy emitted by δ-electrons in 1μ of path for a multiply charged particle in emulsion of normal composition is determined by the equation:

$$K_\delta = 2.33\cdot 10^{19}\cdot \frac{Z^2_{\mathrm{eff}}}{v^2} \ln \frac{E_{\max}}{E_{\min}} \ \mathrm{kev}/\mu,$$

where v is the particle speed, Z_{eff} is the particle charge at the given speed, $E_{\max} = 2mv^2$ is the maximum energy of the δ-electrons, $E_{\min}$ is the minimum energy of the δ-electrons which can cause track broadening. The dependence of the charge of the particle on speed has been taken from Refs. 10 and 11. The dependence of speed on range was determined from Ref. 12 for Li^8 and B^8, and from Ref. 9 for N^{14}.

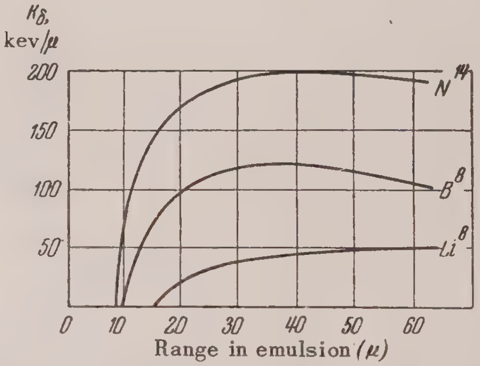

FIG. 3. Dependence on the range of energy lost as δ-electrons of energy ≥ 2 kev in the vicinity of the axis of a multiply charged particle track for ions N^{14}, B^8 and Li^8.

Taking into account the results of Demers[13], with fine grained emulsions where it was shown that δ-electrons with $E = 2$ kev are capable of sometimes causing development of a single grain near the track, it is reasonable to take 2 kev as the minimum δ-electron energy capable of broadening the track. Calculations of the dependence of K_δ on the range under this assumption is given in Fig. 3. In Fig. 4, we present the results of photometric analysis of Li^8, B^8 and N^{14} tracks in emulsion P-9_s. From a comparison of Figs. 3 and 4 the qualitative dependence of $(I_\varphi - I_c)/I_\varphi$

and K_δ on range for ions of various charge is seen. One difference is that within the limits of the examined ranges K_δ goes through a maximum, whereas the full darkening (or the track half width) continues to increase. This circumstance is undoubtedly connected with the increased percentage of high range δ-electrons with increase of particle velocity. An exact calculation of the influence of the δ-electrons on the characteristics of the track involves knowledge of the range energy relation for electrons in emulsion. The above mentioned experimental results and calculations allow definite conclusions to be drawn about the cone formations of multiply charged particles in emulsion. The thinning down of the tracks of multiply charged ions at the end of their range is determined by the change in energy lost to δ-electrons with energy $> E_{\min}$ in the vicinity of the track axis, and also on their energy distribution. The $E_{\min}$ used here, the minimum δ-electron energy capable of broadening the track, is determined not only by the emulsion sensitivity, but by the size of the developed silver grains in the emulsion. The larger the developed grains, the larger must the δ-electron energy be in order to cause a photo reaction in a micro crystal of AgBr near the trajectory of the multiply charged particle, but beyond normally developed silver grain. From this point of view, it is clear why emulsions of similar sensitivity (P-9_s and Ilford E-1), but of different grain size, show different degrees of track thinning for N^{14} near the end of path (Fig. 1). The discrimination of fine grain emulsions for multiply charged particles is clearly seen.

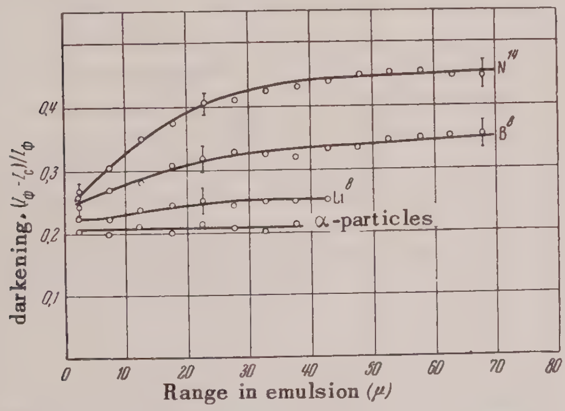

FIG. 4. Total darkening as a function of range for N^{14}, B^8 and Li^8 in P-9_s emulsion ,

The influence of the δ-electrons (with energy greater than $E_{\min}$) can also be used to explain the observation that in fine grain emulsion there is a noticeable difference in darkening in tracks and heavy fission fragments of uranium at the beginning of their path[14,15]. The darkening caused by a light fragment is on the average 15-20% greater than that caused by a heavy fragment[16]. In Ref. 15, Mathieu and Demers conclude from the observed difference in darkening that the light fragment has a higher specific ionization loss at the beginning of its track than the heavy fragment (11.6 and 9.4 mev/μ, respectively). This conclusion is in contradiction with other experimental data and with theory, as the authors themselves note. These difficulties disappear if the assumption is made that the difference in darkening is not due to difference in dE/dx, but rather to a different energy distribution of δ-electrons for the light and heavy fragment. If we calculate the maximum δ-electron energy at the beginning of the track for the light and heavy fragment, we get respectively 2.2 and 1.0 kev. Thus the energy loss to electrons of energy greater than 1 kev in the vicinity of the track axis will be an important quantity for the light fragment, and negligible for the heavy fragment. The result will be a broadening of the light particle track at its beginning. The specific ionization losses for the light fragment will be smaller than for the heavy fragment.

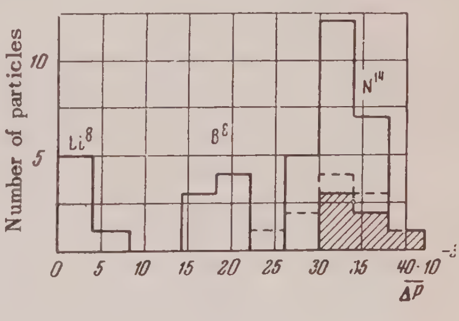

FIG. 5. Distribution of $\overline{\Delta P}$ for particles of various charge, N^{14}, B^8, Li^8. ($\overline{\Delta P}$ – the average change in darkening $(I_\Phi - I_c)/I_\Phi = P(R)$ in the last 25 μ of track).

Thus the characteristics of multiply charged particle tracks in sensitive emulsion make it difficult, if not impossible, to measure the specific ionization loss without taking into account the secondary ionization caused by fast δ-electrons.

4. METHOD OF CHARGE DETERMINATION

In the course of this investigation, a new method of determining the charge of a multiply charged particle from the characteristics of its last 25μ of track was evolved. Since the thinning down of a track at its end is determined by the number and energy distribution of the δ-electrons, which in turn are determined by the type of ion, it is clear that the relationship between track characteristics and particle charge can be found. Calculation of this dependence with sufficient accuracy is impossible at the present time, although an empirical relationship using particles of known charge can be found. It is essential to note that the proposed method is most effective with fine grained emulsions (grain size of AgBr 0.06 μ) since we then have a close approximation of the dependence of the full darkening $(I_\varphi - I_c)/I_\varphi$ on range to the function $K_\delta = f(R_{\mathrm{rem}})$, for small remaining range.

Charge determination can be made as follows. Using photometric analysis of a multiply-charged particle track, the dependence of darkening $(I_\varphi - I_c)/I_\varphi = P(R_{\mathrm{rem}})$ on range is determined for the last 25μ of track. This dependence is characterized by some average change in darkening ΔP between adjacent scanning fields. The average change in darkening was calculated from the average change in slope of the $P(R_{\mathrm{rem}})$ curve, $\overline{\Delta P} = A \tan \overline{\varphi}$, where $\overline{\varphi} = \frac{1}{n}\sum_{i=1}^{n} \operatorname{arc\,tan}(\Delta P_i / A)$ the average angle, ΔP_i is the change in darkening for adjacent regions, A is the ratio of the scales used for $P(R_{\mathrm{rem}})$ and R, $(n+1)$ is the number of regions measured in the 25μ. In our measurements the scanning slit was 5μ long in the objective plane, so that $n = 4$. The absolute charge is then determined from a smooth curve relating average darkening change ΔP to particle charge. This curve is constructed for particles of known charge.

This method has the following properties, which are also seen from the experimental results presented below: 1) the possibility of limiting observations to a small region near the end of the particle track which is made possible by the strong dependence of the particle charge on the slope of the curve $(I_\varphi - I_c)/I_\varphi = P(R_{\mathrm{rem}})$ just near the end of the particle range; 2) the weak dependence of ΔP on the angle of the particle track in the emulsion allows charge measurement on tracks entering at angles up to 30° without corrections; 3) the weak dependence of ΔP on small variations of emulsion sensitivity and development allow the use of a single calibration curve for emulsions of different batches and different experiments.

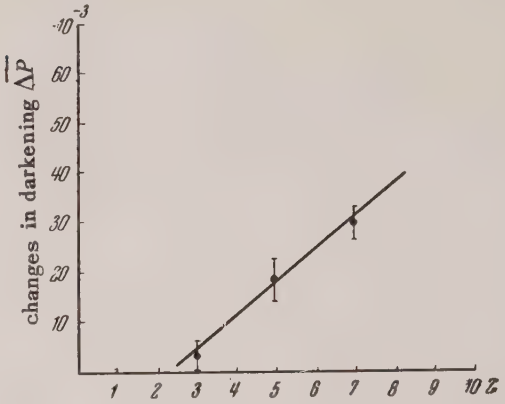

FIG. 6. Dependence of $\overline{\Delta P}$ on ion charge Z.

Figures 5 and 6 show some results typical of the described method. Figure 5 shows the distribution of ΔP for particles of various charge (N^{14}, B^8, Li^8); for the N^{14} ion results are also shown for tracks entering at 15° to the emulsion (lined section) and for less sensitive emulsion (dotted line). Figure 6 shows the dependence of ΔP on particle charge for P-9$_s$ emulsion, Good discrimination of charge is seen from the curve, at least up to a $Z = 10$.

The accuracy of charge measurement by this method evaluated by measurements of N^{14} tracks is about 0.8 units of charge. It must however be pointed out that the charge measurement by the above method is influenced by the particle mass. If we take into account the various possible isotopes of the measured ions with mass differences up to 20 or 30%, this will lead to variations of like magnitude in residual range at a given velocity, and will lead to an error of about 0.5 units of charge. Thus the probable error in determining the charge of an unknown multiply charged particle is not higher than ± 1.3 units of charge.

In conclusion the author would like to thank Prof. G. N. Flerov and D. M. Parfanovich for their help in the work, and Prof. N. A. Perfilov for discussions of the results.

The author is indebted to I. R. Novikov and to E. I. Prokof'ev for preparation of the nuclear emulsions used.

---

[1] P. Freier and E. J. Lofgren, Phys. Rev. **74**, 1818 (1948).

[2] Hoong Tchang Fong, J. Phys. Radium **12**, 739 (1951).

[3] A. Beiser, Am. J. Phys. **20**, 124 (1952).

[4] N. A. Dobrotin, *Cosmic Rays*, Moscow, 1954, p. 204.

[5] D. H. Perkins, Proc. Roy. Soc. (London) **203A**, 399 (1950).

[6] P. Güer and P. Lonchamp, Compt. Rend. **236**, 70 (1953).

[7] P. Lonchamp, J. Phys. Radium **14**, 433 (1953).

[8] Güer , Lonchamp, and Gegauff, Compt. rend. **240**, 856 (1955).

[9] H. L. Reynolds, and A. Zucker, Phys. Rev. **96**, 393 (1954).

[10] Brunnings, Knipp and Teller, Phys. Rev. **60**, 567 (1941).

[11] Reynolds, Scott and Zucker, Phys. Rev. **95**, 671 (1954).

[12] W. H. Barkas, Phys. Rev. **89**, 1019 (1953).

[13] P. Demers and Z. Lechno-Wesintynska, Canad. J. Phys. **31**, 480 (1953).

[14] Z. I. Solov'ev, Thesis, Radiation Inst. Acad. Sci., 1955.

[15] R. Mathieu and P. Demers, Canad. J. Phys. **31**, 78 (1953).

[16] M. I. Kuznetsov, Thesis, Radiation Inst. Acad. Sci. 1954.

Translated by G. L. Gerstein
50

Letters to the Editor

Particle with Spin 3/2 in an Electromagnetic Field

E. E. FRADKIN
Leningrad State Pedagogical Institute

(Submitted to JETP editor July 9, 1956)
J. Exptl. Theoret. Phys. (U.S.S.R.) **32**, 363-365
(February, 1957)

LET us consider the relativistically invariant equations for particles of spin 3/2 in an electromagnetic field:*

$$(\alpha^k \pi_k + i\varkappa)\Psi = 0, \tag{1}$$

$$\pi_k = \partial / \partial x_k - ie\mathrm{A}_k, \ (k = 0,\ 1,\ 2,\ 3).$$

We write the matrices α_k in the parametric form of Petras[1]:

$$\alpha^k = \gamma^k + \gamma_i (B^{ik} - B^{ki}) / \sqrt{3}, \ \gamma^k\gamma^i + \gamma^i\gamma^k = 2g^{ik},$$
$$B^{ik} B^{ls} = g^{kl} B^{is}, \ \ \gamma^l B^{ik} = B^{ik}\gamma^l.$$

From Eqs. (1) we find the supplementary conditions in relativistically covariant form:

$$D\gamma_i B^{ml}\Psi / \sqrt{3} = - iaF_{nl}\gamma^n B^{ml}\Psi, \tag{2}$$

$$D = I - {}^1/_2\, iaF_{ps}\gamma^p\gamma^s, \quad a = {}^2/_3 (2 + \sqrt{3})\, e / \varkappa^2;$$

$$(Q^{kls}\pi_k + i\varkappa R^{ls})\,\Psi = 0,$$

$$Q^{kls} = - Q^{lks} = \gamma^k B^{sl} - \gamma^l B^{sk} \tag{3}$$

$$+ (\gamma^l\gamma^k - \gamma^k\gamma^l)\, \gamma_i B^{si} / 2\sqrt{3},$$

$$R^{ls} = B^{sl} - \gamma^l\gamma_i B^{si} / (1 + \sqrt{3})$$

(F_{nl} is the tensor of the electromagnetic field). Since $Q^{lls} = 0$, then the term with π_l is missing in condition (3). For $l = 0$, the term with a time derivative is absent from (3).

Multiplying Eq. (1) by the matrix

$$\omega = I -- {}^1/_2 (2 - \sqrt{3})\, \gamma_s\gamma_i B^{si}$$

and applying condition (2), we get the relativistically invariant equation

$$(\mathscr{L}^k\pi_k + i\varkappa M)\,\Psi = 0, \tag{4}$$

$$\mathscr{L}^k = \gamma^k - i\,\frac{1 - \sqrt{3}}{2}\, aF_{nm}\gamma^k\gamma_i D^{-1}\gamma^n B^{im}$$

$$+ i\,(2 - \sqrt{3})\, aF_{nm} D^{-1}\gamma^n B^{km},$$

$$M = I + i\,\frac{2\sqrt{3} - 3}{2}\, aF_{nm}\gamma_i D^{-1}\gamma^n B^{im}$$

$$- i\,\frac{1 - \sqrt{3}}{2}\,\frac{a}{\varkappa}\left(\frac{\partial}{\partial x_p} F_{nm}\gamma^p\gamma_i D^{-1}\right)\gamma^n B^{im}$$

$$- (1 - \sqrt{3})\left(\frac{\partial}{\partial x_p} F_{nm} D^{-1}\right)\gamma^n B^{pm}.$$

Condition (3) is now the condition for the compatibility of Eq. (4) and condition (2). The fundamental equation (1) is equivalent to Eq. (4) with conditions (2) and (3). We note that Eq. (4) is non-linear relative to the electromagnetic field.

Taking into account the smallness of the dimensionless parameter ($aF_{nm} = 10^{-19} F_{nm}$, where F_{nm} is measured in the Gaussian system of units), we solve the equation relative to $\partial/\partial x_0$, neglecting terms of second and higher order relative to aF_{nm}. We then get an equation in the Schrödinger form

$$i\partial\Psi / \partial x_0 = H\Psi,$$

where H is the Hamiltonian of the particle with spin 3/2 in the electromagnetic field in the linear approximation relative to the small parameter aF_{nm}. We remark that the extreme smallness of aF_{nm} guarantees as negligibly small the magnitude of the contribution in the Hamiltonian from the higher approximations in aF_{nm}, even for strong fields.

The Hamiltonian H has the form*

$$H = H_0 + F_{nm}R^{nm\nu}(p_\nu - eA_\nu) + F_{nm}P^{nm} + \frac{\partial F_{nm}}{\partial x_p} Q^{nmp},$$

$$H_0 = \gamma_0\gamma^\nu (p_\nu - eA_\nu) + e\varphi + \varkappa\gamma_0,$$

$$p_\nu = - i\partial / \partial x_\nu, \ \varphi = - A_0, \tag{5}$$

$$R^{nm\nu} = i\,\frac{1 + \sqrt{3}}{\sqrt{3}}\,\frac{e}{\varkappa^2}\,\{(\gamma_0\gamma^\nu\gamma_i\gamma^n - \gamma_i\gamma^n\gamma_0\gamma^\nu)\, B^{im}$$

$$- (1 - \sqrt{3})\,\gamma_0\gamma^n (B^{\nu m} - \gamma_0\gamma^\nu B^{0m})\},$$

$$P^{nm} = \frac{ie}{\sqrt{3}\varkappa}\left\{\gamma_0\gamma_i\gamma^n B^{im}\right.$$

$$\left. - \frac{1 + \sqrt{3}}{\sqrt{3}}\,\gamma_i\gamma^n\gamma_0 B^{im} - \frac{2}{\sqrt{3}}\,\gamma_0\gamma^n\gamma_0 B^{0m}\right\},$$

$$Q^{nmp} = i\,\frac{1 + \sqrt{3}}{\sqrt{3}}\,\frac{e}{\varkappa^2}\,\gamma_0\,\{\gamma^p\gamma_i\gamma^n B^{im} - (1 - \sqrt{3})\,\gamma^n B^{pm}\}.$$

As can be seen, a particle with spin 3/2 possesses dipole and quadrupole kinematic moments and, moreover, the Hamiltonian H possesses an unusual term of a dipole type which depends on the momentum.[**]

Averaging is carried out over the charge density. Therefore the normalization condition has the form

$$\int \Psi^* \rho \Psi \, (dr) = 1,$$

$\rho = \eta\alpha^0$ is the Hermitian charge density matrix. The matrix η which determines the invariant bilinear Hermite form $(\Phi^*\eta\Psi)$ is found in the form

$$\eta = -\gamma_0 B^{ii} + (2 - \sqrt{3})\, \gamma_i \gamma_0 \gamma_k B^{ik}.$$

Correspondingly,

$$\rho = -B^{ii} + (1 - \sqrt{3})\, \gamma_i \gamma_k B^{ik} / \sqrt{3} + \gamma_i \gamma_0 B^{i0} / \sqrt{3} + \gamma_0 \gamma_i B^{0i} / \sqrt{3}.$$

The mean value of the energy of a particle with spin 3/2 in an electromagnetic field will be determined by the formula:

$$E = \int \Psi^* \rho i \frac{\partial}{\partial x_0} \Psi \, (dr) = \int \Psi^* \rho H \Psi \, (dr).$$

Hence for a guarantee of the reality of E we have the condition of the quasi-hermiticity of the operator H:

$$\int \{(H\Phi)^* \rho \Psi - \Phi^* \rho H \Psi\} \, (dr) = 0. \tag{6}$$

For the Hermitian (5), the condition (6) is satisfied by taking into account the additional conditions (2) and (3).

The value of the energy in the linear approximation relative to the small parameter aF_{nm} is represented in the following form (at the same time we transform to the Gaussian units):

$$E = \int \Psi^* (-B^{ii}) \Big\{ H_0 + \frac{2}{3}(2 + \sqrt{3}) \frac{\hbar e}{M^2 c^2} \times [R_E^{\mu\nu} E_\mu + R_H^{\mu\nu} H_\mu] \Big(p_\nu - \frac{e}{c} A_\nu\Big) - \frac{2}{3}(2 + \sqrt{3}) \frac{\hbar e^2}{M^2 c^3} [R_E^{\mu 0} E_\mu + R_H^{\mu 0} H_\mu] \varphi + \frac{2}{3}(2 + \sqrt{3}) \frac{\hbar^2 e}{M^2 c^2} \Big[Q_E^{\mu\nu} \frac{\partial E_\mu}{\partial x_\nu} + Q_H^{\mu\nu} \frac{\partial H_\mu}{\partial x_\nu} \Big] \Big\} \Psi \, (dr). \tag{7}$$

Thus a contribution to the energy, in addition to terms of the Hamiltonian of the Dirac type H_0, is made by supplementary terms of the dipole type, which depend on the momentum, and on the quadrupole electric and magnetic moments. Averaging in Eq. (7) is carried out over $\Psi^* (-B^{ii}) \Psi$ – the charge density of free particles.

For comparison we note that particles with spins 0 and ½ do not possess kinematic moments while a particle with spin 1 possesses kinematic dipole moments, which do not make a direct contribution to the energy but, in spite of this, are said to be electromagnetic interactions[3-5].

I consider it my pleasant duty to express my thanks to Dozent S. V. Izmailov for pointing out the theme and for his constant interest in the work.

---

[*] The analysis is carried out in a system of units in which $\hbar = c = 1$. The metric tensor g^{ik} is chosen in the form

$$g^{00} = -g^{11} = -g^{22} = -g^{33} = 1, \quad g^{ik} = 0 \ (i \neq k).$$

[*] In the summation the Latin indices run, as above, over the values 0, 1, 2, 3, and the Greek over the values 1, 2, 3.

[**] Terms of such a type were first obtained by Darwin[2] in the non-relativistic approximation for particles with spin ½ in an electromagnetic field.

1 M. Petras, Czech. J. Phys. **5**, 160 (1955).
2 C. G. Darwin, Proc. Roy. Soc. (London) **118A**, 654 (1928).
3 H. Kemmer, Proc. Roy. Soc. (London) **173A**, 91 (1939).
4 V. L. Ginzburg, J. Exptl. Theoret. Phys. (U.S.S.R.) **12**, 425 (1942).
5 S. V. Izmailov, Uch. zap. Leningrad State Pedagogical Inst. **103**, 219 (1955).

Translated by R. T. Beyer
74

Experimental Comparison of the Energy Spectra of γ–Quanta from the Decay of π°–Mesons Formed on Carbon and Lead Nuclei by 600 Mev Protons

Iv. D. Baĭukov, A. N. Sinaiev,
A. A. Tiapkin
United Institute for Nuclear Research

(Submitted to JETP editor November 2, 1956)
J. Exptl. Theoret. Phys. (U.S.S.R.) 32,
385–386 (February, 1957)

In experiments conducted up to the present time there has not been discovered any noticeable difference in the γ–spectra formed by light and heavy elements [1,2]. Since the energy and angular distributions are interelated, the conclusion was made,[3] from the similarity of the energy spectra, that the angular distributions of the γ–quanta formed by light and heavy elements are coincident. However, direct measurements of angular distribution of γ–quanta[4] have disclosed a considerable dependence on the mass number of the nuclei irradiated by 660 mev protons. The dependence of the angular distribution of γ–quanta on the mass number of the nuclei obtained in the work of Ref. 4 can be satisfactorily explained by the relative capacity of nuclei to protons and by accounting for absorption of mesons in the nucleus. Computations made for this case showed that the γ–spectra formed by light and heavy elements should differ significantly only in the region of low energies (ϵ_γ < 70 mev). The coincidence of γ–spectra in this energy region cannot be considered as a definitely established fact, inasmuch as at these energies the background of chance coincidences is high and the spectrometer efficiency is relatively low.

To obtain a more accurate comparison of γ–spectra formed in light and heavy nuclei, relative measurements were made in this study of the flow of γ–quanta in different regions of the γ–spectra resulting from the decay of mesons formed in carbon and lead by 600 mev protons at 0° observation angle with reference to the motion of the protons. Measurements were made with a 12 channel double coil magnetic spectrometer.

Targets of lead and graphite, placed inside the vacuum chamber of the accelerator were changed successively every minute. Simultaneously with the change of targets, the registration system of the spectrometer was automatically switched so that one group of electromechanical counters registered the spectrum of the paris formed on the graphite target and the other those formed on the lead target. The energy of the γ–quanta to be registered was selected by changing the field intensity in the gap of the spectrometer magnet. For control purposes, simultaneously with the measurements of the relative γ–flow in different regions of the γ–spectrum, measurements were also made of the full flow of quanta by means of a γ–telescope described in Ref. 4.

According to Ref. 4, the full output of γ–quanta at 0° is 3.6 ±0.1 greater in lead nuclei than in carbon. Taking this ratio for the full γ–quanta outputs, the ratios of the differential outputs (on $d\omega d\omega\epsilon_\gamma$) for different γ–quanta energies, as obtained in this work, can be presented in table form (see below). Thus for γ–quanta in the region of low energy (ϵ_γ < 70 mev), there is observed a difference in the γ–spectra formed on the nuclei of carbon and lead. The difference between the γ–spectra is, apparently, connected with the previously discovered change in the angular distribution of π°–mesons related to the interaction effect between the bombarding protons and the nucleons in the presence of strong meson absorption. Hard γ–quanta at 0° observation angle are formed basically by the decay of π^+ mesons, produced on the surface of the nucleus; which is highly screened from the bombarding protons by the rest of the nucleons in the nucleus. Soft γ–quanta are formed basically on the opposite nuclear surface which is freely irradiated by protons. For this reason, in the case of π°–meson formation on heavy nuclei, when the effects of proton and meson interactions with the nuclei are considerable, there is observed a relative increase in soft γ–quanta in the spectrum.

ε_γ (mev)	$(d\sigma_{Pb}/d\sigma_C)\ 0^\circ$
30	6.4±0.4
52	4.9±0.15
90	4.15±0,15
144	3.5±0.1
222	3.3±0,1
303	3.2±0.1
348	3,1±0;1
379	3.6±0.2
472	4,1±0.3

To the extent that the effects connected with absorption of π°–mesons and the slowing down of the bombarding protons in the nuclear substance substantially change the angular distribution of the mesons and decrease the full cross section of meson formation on heavy nuclei, it is natural to expect also a considerable difference in the energy distributions of mesons formed on light and heavy nuclei. This difference between the spectra must be due to the change of the meson absorption and scattering cross section with energy and also to the greater loss of energy by the bombarding protons in heavy nuclei.

On the other hand, it can be concluded, from the comparison of spectra in the energy region above 120 mev, that the energy distributions of π°–mesons formed at 0°–angle on nuclei of carbon and lead do not exhibit any noticeable difference. More accurate data concerning spectra of π–mesons, formed on light and heavy nuclei, could be obtained by making relative measurements of differential cross sections of the formation of charged mesons. For a quantitative evaluation of the expected difference in the spectra of π–mesons, it is necessary to make computations by the method of probability trials to account for the deceleration of the protons and the absorption and scattering of π–mesons in the nuclei.

---

[1] Kozodaiev, Tiapkin, Baiukov, Markov, and Prokoshkin, Izv. Akad. Nauk SSSR, Fiz. Ser. 19, 589 (1955).

[2] Crowe, Panofsky, Phillips and Walker, Phys. Rev. 83, 893 (1951).

[3] R. Hales and B.Moyer, Phys. Rev. 89, 1047 (1953).

[4] Tiapkin, Kozodaiev and Prokoshkin, Dokl. Akad. Nauk SSSR, 100, 689 (1955).

Translated by J.L.Herson
87

Production of Very Strong Magnetic Fields by Rapid Compression of Conducting Shells*

IA. P. TERLETSKII
Moscow State University

(Submitted to JETP editor November 5,1956)
J. Exptl. Theoret. Phys. (U.S.S.R.) 32, 387–388 (February,1957)

FOR the practical realization of cyclic accelerators of charged particles to energies in excess of 10^{10} ev, it is necessary to learn to create very strong magnetic fields, in excess of 10^5 oe. At the indicated energies, both for electrons and for protons, the formula

$$V = 3\cdot 10^4\, RH, \qquad (1)$$

holds, where V is the energy of the accelerated particles, expressed in electron volts, R is the radius of curvature of the trajectory in meters, and H is the magnetic field intensity in oersteds. Consequently, in a cyclic accelerator for 10^{11} ev or 100 bev, with a directing magnetic field $H = 10^5$ oe, the radius of the largest orbit must be 30 m, whereas with $H = 10^6$ oe, it needs to be only 3 m. Thus only at fields exceeding 10^5 Oe is there hope of building 100 bev apparatus of not too huge dimensions. If we learn to create magnetic fields of intensities 10^7 to 10^8 oe, we may hope for the practical production of compact cyclic accelerators for energies exceeding even 100 bev.

The strongest magnetic fields have been obtained by passage of powerful current impulses of short duration through ironless electromagnets (P. L. Kapitza). By this impulsive method, fields of order 3×10^5 Oe have been obtained. Further increase of the field was limited by the mechanical strength of the electromagnet coils, which were ruptured by the interaction forces of the currents.

There occurs to us an alternative method of creating very strong magnetic fields: by the rapid compression of conducting shells or loops. By this method it is in principle possible to obtain magnetic fields considerably stronger than the largest attainable by the impulsive method.

Let us consider a conducting hollow sphere, placed in an external magnetic field H_0 created by any practicable method. If the source of external field H_0 is suddenly shut off, the field inside the sphere, because of induced currents, will decay exponentially with relaxation time

$$\tau = \alpha\,(4\pi\sigma / c^2)\, R^2, \qquad (2)$$

where R is the radius of the sphere, σ is the conductivity in absolute units, c is the speed of light, and α is a numerical coefficient of order unity, determined by the form of the conductor. For a 10 cm copper sphere, the relaxation time according to (2) exceeds 1 sec.

Let us now suppose that the sphere, located in an external field H_0, is subjected to an intense hydrostatic pressure, so that the linear dimensions of the internal cavity decrease by a factor n in a time interval T much shorter than the relaxation time τ. In this case, during the time interval T the conducting material of the sphere may be considered as having practically infinite conductivity, and consequently the magnetic lines of force may be considered rigidly connected to the material ("frozen" magnetic field). Since in the process of compression the magnetic lines of force cannot cross the conducting wall of the sphere, the magnetic flux through the cross section of the sphere will remain constant, i.e.,

$$\Phi = \int_0^R H(r)\, 2\pi r\, dr = \text{const.} \qquad (3)$$

Consequently, for an initially uniform magnetic field we get $\pi R^2 H = \text{const}$, whence

$$H / H_0 = (R_0 / R)^2 = n^2, \qquad (4)$$

where R_0 and H_0 are the initial values of the inside radius of the sphere and of the magnetic field.

In the process of compression of the sphere, work will be performed against the ponderomotive force of the magnetic field, and therefore the energy of the field undergoing compression will increase. Since in a uniform field the full energy is $\epsilon = H^2 v/8\pi$, where v is the volume of the cavity; therefore, according to (3),

$$\mathcal{E}/\mathcal{E}_0 = R_0/R = n. \qquad (5)$$

Thus as a result of an n–fold compression of a hollow sphere, the magnetic field inside the cavity increases by a factor n^2.

The same reasoning holds not only for a spherical shell but for any solid loop; for example, for a torus. In all cases the magnetic field will increase in proportion to the square of the diminution of linear dimensions.

A uniform and intense hydrostatic compression of a sphere, or an inward compression of a solid loop, is quite realizable by means of cumulative explosion of an explosive material. Thus if, by means of implosion, over a period of a second, one compresses a hollow copper sphere so that its internal diameter contracts, say, by a factor 10, the magnetic field inside the sphere will increase by a factor 100. Consequently, an initial magnetic field of 10^5 oe will increase in the example considered to 10^7 oe.

Obviously an accelerator based on the application of very strong magnetic fields obtained by the method under consideration will not be a device with periodic action. Such an accelerator can be designed only for obtaining single pulses of accelerated particles. This circumstance, however, does not constitute a serious disadvantage; for with the known cyclic methods of acceleration, the frequency of the pulses of accelerated particles decreases rapidly with increase of energy, and this is equivalent to operation of the apparatus under single–pulse conditions.

---

*The present article reproduces, with unimportant abridgments, a report of the Institute of Nuclear Problems of the U. S. S. R. Academy of Sciences, November 14, 1952.

Translated by W. F. Brown, Jr.
89

The Influence of the Entrainment of Electrons by Phonons on Thermomagnetic Effects in Semiconductors

V. L. GUREVICH AND IU. N OBRAZTSOV
Semiconductor Institute,
Academy of Sciences, USSR

(Submitted to JETP editor November 10,1956)
J. Exptl. Theoret. Pyys. (U.S.S.R.) 32, 390–392 (February, 1957)

THE effect of a nonequilibrium distribution of phonons (entrainment of electrons by phonons) on thermoelectric and thermomagnetic effects was first calculated for metals by L. E. Gurevich.[1,2] In semiconductors at temperatures of the order of room temperature, this entrainment has practically no effect on the thermoelectric power. But it is important at low temperatures [3–5]. The purpose of the present note is the calculation of the effect of electron entrainment by phonons on the transverse and longitudinal Nernst–Ettinghausen (N–E) effects in semiconductors.

We shall assume that the electron distribution function in the conduction band is $n = n^0 + n'$, where n' is the small deviation from the equilibrium value n^0. Similarly for phonons $N = N^0 + N'$. At low temperatures, electrons are entrained principally by the acoustic phonons with the highest velocity ω_1; these have considerably longer mean free time τ_{ph} than the phonons which belong to the other two acoustic branches,[6] and the optical vibrations are not excited. A solution of the transport equation on the assumption that the electrons have relaxation time $\tau_e(\epsilon)$, and that their effective mass m is isotropic, gives

$$n' = \frac{\tau_e}{m}\frac{1}{1+(e\tau_e H/mc)^2}\left\{\left(\frac{\varepsilon-\mu_0+g}{T}\nabla T+\nabla\mu,\mathbf{p}\right) + \frac{e\tau_e}{mc}\left(\frac{\varepsilon-\mu_0+g}{T}[\mathbf{H}\nabla T]+[\mathbf{H}\nabla\mu],\ \mathbf{p}\right)\right\}\frac{\partial n^0}{\partial\varepsilon}. \qquad (1)$$

Here $\mu = \mu_0 - e\varphi$ is the electrochemical potential, ϵ is the electron energy and p is their quasi-momentum; the magnetic field H is perpendicular to ∇T and $\nabla\mu$. The term which results from the entrainment is of the order

$$g \approx m w_1^2 \tau_{ph}/\tau_e', \qquad (2),$$

where τ_e' is the relaxation time of electrons which are only scattered by phonons.

The function in (1) leads to the following expression for the current:

$$\mathbf{i} = \sigma_1 \nabla\mu + \sigma_2 \nabla T + \sigma_3 [\mathbf{H} \nabla T] + \sigma_4 [\mathbf{H} \nabla\mu]. \quad (3)$$

Here the coefficients σ_1 and σ_2 are of the same form as in the absence of entrainment and $\sigma_2 = \sigma_2^{(1)} + \sigma_2^{(2)}$, where $\sigma_2^{(1)}$ results from the entrainment, while $\sigma_2^{(2)}$ corresponds to the usual mechanism. The coefficient σ_3 can be divided into two similar components, and thus also the constant of the transverse N–E effect.

$$Q = (\sigma_1\sigma_3 - \sigma_2\sigma_4)\, c/[\sigma_1^2 + (\sigma_4 H)^2] \quad (4)$$

can be represented as $Q = Q^{(1)} + Q^{(2)}$, where the term $Q^{(1)}$ is associated with entrainment.

We equate the coefficient ratio $Q^{(1)} / Q^{(2)}$ to the differential thermoelectromotive force ratio $\alpha^{(1)} / \alpha^{(2)}$ at the same temperature. The chemical potential μ_0 appears in the expression for $\alpha^{(2)}$ but not in the formula for $Q^{(2)}$. It therefore follows from (1) that in nondegenerate semiconductors, where essentially $\epsilon \approx kT$, the first ratio is greater than the second by a factor of, roughly, μ_0 / kT. Thus the entrainment has a considerably greater effect on the transverse N–E effect than on the thermoelectromotive force. The same considerations can be applied to the longitudinal N–E effect.

In a weak field we have, in order of magnitude,

$$Q^{(1)} \approx (k/c)\,(w_1^2\, kT)\,(\tau_e/\tau_e)\,\tau_{\text{ph}}. \quad (5)$$

The variation of the thermoelectromotive force in a weak magnetic field is

$$\Delta\alpha^{(1)} = \alpha^{(1)}(H) - \alpha^{(1)}(0) \approx \frac{k}{e}\frac{mw_1^2}{kT}\frac{\tau_{\text{ph}}}{\tau_e'}\left(\frac{uH}{c}\right)^2, \quad (6)$$

in order of magnitude, where u is the mobility.

According to Herring,[6] in an unbounded cubic crystal $1/\tau_{\text{ph}} = \Lambda q^2$, where q is the wave vector. Far below the Debye temperature

$$\Lambda \approx (kT)^3/\rho\hbar^2 w^3, \quad (7)$$

where ρ is the density of the crystal and ω is the average speed of sound. When $\tau_e = \tau_e'$ we have from (5) and (7) $Q \sim T^{-5}$.

If the dependence of τ_e on energy ϵ and temperature T is

$$\tau_e = f_1(T)\, f_2(\varepsilon/kT) \quad (8)$$

and τ_e' and g have the same functional form, then in an arbitrary magnetic field,

$$Q^{(1)}(H) = Q^{(1)}(0)\,\psi_1(uH/c), \quad (9)$$

$$\Delta\alpha^{(1)}(H) = (c/u)\, Q^{(1)}(0)\,\psi_2(uH/c)\,(uH/c)^2, \quad (10)$$

where ψ_1 and ψ_2 depend on temperature only through the indicated argument, and $\psi_2(0) \approx \psi_1(0) = 1$

In particular, from the usual assumptions regarding the character of the interaction between electrons and phonons, which lead to energy-independence of the mean free path l ($\tau_e = \tau_e' \sim \epsilon^{-1/2}$):

$$Q^{(1)}(H) = \frac{4\hbar^2 w_1^2}{9\pi mc\Lambda kT^2 (uH/c)^2}\,\frac{\rho(H) - \rho(0)}{\rho(0)}, \quad (11)$$

$$\Delta\alpha^{(1)}(H) = -\frac{\hbar^2 w_1^2}{6m\Lambda ukT^2}\,\frac{R(H) - R(0)}{R(0)}. \quad (12)$$

Here $\rho(H)$ and $R(H)$ are the resistivity and Hall constant in a transverse magnetic field. The ratios $R(H) / R(0)$ and $\rho(H)/\rho(0)$ depend only on the parameter uH/c and were calculated in Refs. [8–10].

We note that in any field $Q^{(1)} > 0$, and thus $Q^{(1)}$ and $Q^{(2)}$ have opposite signs.

All of the above conclusions are also valid for holes but with a reversed sign in (12).

The effect of entrainment on thermomagnetic effects has been observed experimentally in p-type germanium [11]. The character of the field and temperature dependences of the transverse N–E effect constant agreed with Eq. (9). However, in comparing the theory and experiment, one must keep in mind the degeneracy of the germanium valence band (the presence of two kinds of holes). The above results can easily be extended if it is assumed that the currents of light and heavy holes can be combined additively. It is then easily shown that if the ratios of the concentrations and mobilities of light and heavy holes are temperature-independent the relations (9) and (10 continue to be valid.

---

[1] L. E. Gurevich, J. Exptl. Theoret. Phys. (U.S.S.R.) 16, 193 (1946).

[2] L. E. Gurevich, J. Exptl. Theoret. Phys. (U.S.S.R.) 16, 416 (1946).

[3] G. E. Pikus, J. Exptl. Theoret. Phys. (U.S.S.R.) 21, 852 (1951).

[4] H. P. R. Frederikse, Phys. Rev. 91, 491 (1953).

[5] C. Herring, Phys. Rev. 96, 1163 (1954).

[6] C. Herring, Phys. Rev. 95, 954 (1954).

[7] B. I. Davydov and I. M. Shmushkevich, Usp. Fiz. Nauk 24, 21 (1940).

[8] Harding, Proc. Phys. Soc. (London) A140, 205 (1933).

[9] Johnson and Whitesell, Phys. Rev. 89, 941 (1953).
[10] O. Madelung, Z. Naturforsch 8a, 791 (1953).
[11] Mochan, Obraztsov and Krylova, J. Tech. Phys. (U.S.S.R.) 27, 2 (1957).

Translated by I. Emin
91

The Role of Three–Particle Forces in the Three–Body Problem

E. B. TEODOROVICH AND N. N. KOLESNIKOV
Moscow State University

(Submitted to JETP editor November 10, 1956)
J. Exptl. Theoret. Phys. (U.S.S.R.) 32, 392–393 (February, 1957)

THE possible role of the so–called many-particle forces has been discussed recently.[1–6] There are indications that by taking account of three–particle forces, the calculated energies of light nuclei show improved agreement with experiment[7,8] In studying the contribution of three–particle forces, we have confined ourselves to three-body problems: a) the calculation of the binding energies of H^3 and He^3; b) the calculation of the neutron–deuteron scattering cross section. For simplicity, we have neglected the noncentral character and the spin dependence of two-particle nuclear forces. As the total energy operator of tritium we took the sum

$$H = -\sum_{i<j} V_0 \frac{\exp\{-\mu r_{ij}\}}{\mu r_{ij}} + f\frac{K_1(\mu(r_{12}+r_{23}+r_{31}))}{\mu^3 r_{12} r_{23} r_{31}} + \frac{\hbar^2}{2M}(\nabla_1^2+\nabla_2^2+\nabla_3^2),$$

with $i, j = 1,2,3$, where the first term represents the ordinary (two–particle) interaction, the constants $V_0 = 52$ mev and $1/\mu = 1.4 \times 10^{-13}$ cm being chosen to yield the correct deuteron binding energy.[9] The term representing the three–particle interaction was taken in the same form as in Refs.[1–3]. The constant f was not given a fixed value but was chosen to give the correct binding energy of H^3. The choice of the trial function in the variational problem took into account the smallness of the probability, because of strong three–particle repulsion, that the three particles would simultaneously be in very close proximity.

	0.42	2.63	6.71	14.7	26,9	35,0	42,0	60.4	82,2
a	3.76	2.68	1,47	0.485	0,141	0,082	0,049	0.020	0,010
b	3.51	2.48	1,41	0.543	0.211	0,152	0.120	0.074	0,054
c		2.74	1,39	0.784	0.470	0.371	0,315	0,224	0.162

In this way we obtained $f = 153$ mev, which agrees in order of magnitude with the value of 375 mev obobtained by Drell and Huang.[1] For He^3 the calculated value of the Coulomb energy (0.745 mev) was very close to the experimental value, whereas worse results were obtained[7,8] when three–particle forces were neglected. For the potential scattering of neutrons by deuterons, we took into account only the s and p states of the incident particle, with the system able to be in either a doublet or quartet state.[10] The phases of the scattered waves were determined by means of Schwinger's variational method[11,12] with the trial function

$$(a+br)\sin kr + (c+dr)\cos kr,$$

where a, b, c are the variational parameters.

The total cross sections in barns are given in the Table (E is the energy in mev in the laboratory system of coordinates. The letters a and b denote variants of the calculation).

In the Table, a denotes that only two–particle interactions were taken into account; b denotes that both two–particle and three–particle interactions were taken into account with $f = 153$ mev; c denotes the experimental values of the cross sections.[13] The inclusion of three–particle forces somewhat improves the agreement with experiment. But one cannot simultaneously obtain the correct binding energy of H^3, the correct neutron–deuteron scattering cross section and saturation of nuclear forces in heavy nuclei[1] by selecting a single value of the constant f, even when noncentral forces are taken into account. It can therefore be assumed that three–particle interactions play a relatively small part in nuclei, and that these cannot be the principal cause of the saturation of nuclear forces.

The authors are deeply grateful to Professor D. D. Ivanenko, who directed this work.

---

[1] S. D. Drell and K. Huang, Phys. Rev. 91, 1527 (1953).

2 K. Brueckner and K. M. Watson, Phys. Rev. 92, 1023 (1953).
3 A. Klein, Phys. Rev. 89, 1158 (1953).
4 M. Levy, Phys. Rev. 88, 725 (1952).
5 G. Wentzel, Helv. Phys. Acta, 15, 111 (1942); 25, 569 (1952).
6 A. Sokolov and D. Ivanenko, *The Quantum Theory of Fields*, Moscow, 1951.
7 R.L. Pease and H.Feshbach, Phys. Rev. 88, 945 (1952).
8 T. Hu and K. Hsu, Proc. Roy. Soc. (London) A204, 476 (1951).
9 L. Hulthen and K. Laurikainen, Rev. Mod. Phys. 23, 3 (1951).
10 G. Massey and M. Buckingham, Proc. Roy. Soc. A173, 123 (1941); A211, 183 (1952).
11 J. Schwinger and B. A. Lippmann, Phys. Rev. 79, 469 (1950).
12 S. Altschuler, Phys. Rev. 89, 1278 (1953).
13 J. Seagrave and R. Henkel, Phys. Rev. 98, 666 (1955).

Translated by I. Emin
92

New Short–Lived Isomers in the Millisecond Range

O. I. LEIPUNSKII, A. M. MOROZOV,
IU. V. MAKAROV AND P. A. IAMPOL'SKII
Physical Chemistry Institute,
Academy of Sciences, USSR

(Submitted to JETP editor November 13, 1956)
J. Exptl. Theoret. Phys. (U.S.S.R.) 32, 393–394
(February, 1957)

WE have investigated isomeric states with half–lives in the millisecond range which resulted from interactions with 20 mev protons. In addition to previously observed isomers,[1] data have recently been obtained concerning new isomeric radioactivity in a number of elements.

The method of investigating short–lived activities was described in our previous article.[1] in the present measurements, the γ–energy was determined by the use of a FEU–19 photomultiplier with a (2.9 × 1.6 cm) NaI (Tl) crystal and single–channel differential analyzer. For each γ–energy measurement the spectrometer was calibrated by the Cr^{51} line ($E_\gamma = 0.33$ mev, $T_{1/2} = 26.5$ days). In addition, the accuracy of the apparatus was controlled by the γ–emission which results from proton irradiation of Ta ($T_{1/2} = 5.5 \pm 1.0$ m sec)[1,2] .

The Table contains our average values for the half–lives and energies of the observed γ–radiation. The errors are the mean deviation of results in different experiments.

In some cases we used control targets consisting of different chemical compounds which contain a given element. The half–lives measured in compounds of a given element are in good mutual agreement.

After we had obtained the data in the Table, information concerning a few short–lived isomeric radioactivities was published in the literature. These findings can be compared with our own values.

Softky[2] showed that the γ–emission with $E_\gamma = 0.305$ mev which accompanies K capture in Se^{75} has the half–life $T_{1/2} = 18.0 \pm 1.5$ m sec. and must be assigned to an isomeric state of As^{75m} The short–lived radioactivity which we obtained from proton irradiation of Ge has a half–life and an energy which agree with the corresponding values for the γ–emission of As^{75m} ($T_{1/2} = 17.5 \pm 2.0$ m sec, $E_\gamma = 0.310$ mev) and must result from the reaction Ge^{76} $(p, 2n)$ As^{75m} with

Target	$T_{1/2}$ *m* sec	E_γ, mev	Data from other authors		Suggested reaction
			$T_{1/2}$, *m* sec	E_γ, mev	
Ge	17.5±2.0	0,31	18±1.5[3] 14[4]	0.305 [3] 0.315 [4]	Ge^{76} $(p, 2n)$$As^{75m}$
$SrCO_3$	16.5±2.0	0.41±0.02	—	—	—
Y_2O_3	13	0.20±0.02	—	—	—
Zr	10±1	0.24±0.02	10÷20[5]	0.250 [5]	$Zr^{90}(p, n)Nb^{90m}$
SmO	A few *m* sec	—	—	—	—
HgO	42±5 5±1	0.37±0.02 —	— —	— —	— —
Ga	несколько *мсек*	—	—	—	—
Cd	47±10	0.28	45±10[6]	0,312±0,01 [6]	Cd (p, n) или Cd$(p, 2n)$

~ 13 mev threshold. Our data on Ge radioactivity is also in good agreement with the values obtained for As γ–emission after irradiation in the 22–mev betatron.[4]

The short–lived radiation from Zr ($T_{1/2} = 100 \pm 1.0$ m sec, $E_\gamma = 0.24 \pm 0.02$ mev) can be assigned to an isomeric transition of Nb^{90m} [reaction (p, n) with threshold ~ 12 mev], because our values for the half–life and energy of the transition are in good agreement with the corresponding values for Nb^{90m} ($T_{1/2}$ = 10–20 m sec, E_γ=0.250 mev) which result from the β^+ –decay of Mo^{90} [5].

When Zr was irradiated, in addition to the radioactivity with $T_{1/2} = 10.0 \pm 1.0$ m sec we detected a shorter–lived activity with $T_{1/2} \sim 0.6$ m sec as well as a longer–lived activity with $T_{1/2} > 10^{-1}$ sec.

Our earlier article[1] reports the isomeric radioactivity which results from the irradiation of cadmium with fast protons ($T_{1/2} = 40 \pm 10$ m sec). In connection with the abstract,[6] which reports isomeric radioactivity in indium ($T_{1/2} = 45 \pm 10$ m sec, $E_\gamma = 0.312 \pm 0.010$ mev) after irradiation with 22–mev γ–rays, it can be assumed that the radioactivity which we had observed in cadmium was the isomeric radioactivity of indium resulting from a (p, n) or $(p, 2n)$ reaction on a cadmium isotope.

The authors consider it their pleasant duty to thank K. D. Sinel'nikov, P. M. Zeidlits, A. P. Kliucharev and A. M. Smirnov for important assistance in this work, and O. B. Likin and V. I. Smirnov for assistance in the construction and adjustment of the electronic apparatus.

---

[1] Leipunskii, Miller, Morozov and Iampol'skii, Dokl. Akad. Nauk SSSR **109**, 935 (1956).

[2] S. D. Softky, Phys. Rev. **98**, 736 (1955).

[3] A. Schardt, Bull. Am. Phys. Soc. **1**, 85 (1956).

[4] S. H. Vegors and P. Axel, Bull. Am. Phys. Soc. **30**, No. 7, 11 (1955).

[5] H. B. Mathur and E. K. Hyde, Phys. Rev. **98**, 79 (1955).

[6] S. H. Vegors and E. B. Duffield, Bull. Am. Phys. Soc. **1**, 206 (1956).

Translated by I. Emin
93

Negative Ions of Silicon, Germanium, Tin and Lead

V. M. Dukel'skii and V. M. Sokolov
Leningrad Physico–Technical Institute,
Academy of Sciences, USSR

(Submitted to JETP editor November 21, 1956)
J. Exptl. Theoret. Phys. (U.S.S.R.) 32, 394–395
(February, 1957)

In continuing the study of negative atomic ion production we looked for such ions of elements in the right–hand column of the fourth group of the periodic table. For one of these elements, carbon, negative ions had been found[1,2]. In the present work we established the existence of negative atomic ions of the remaining elements in the subgroup IV *B*: Si, Ge, Sn and Pb.

The negative ions were produced in an ion source through the interaction of an electron beam with molecules of a halide of the element under investigation. We also obtained negative ions by "charge exchange", that is, by the transfer of an extra electron from donor ions to atoms of the investigated substance[3]. For the purpose of analyzing and recording the negative ions, we used a magnetic mass spectrometer with resolving power sufficient to separate the isotopes of lead. In order to obtain the line intensities needed for measurements of the negative ion spectrum, it was necessary to maintain a higher vapor density of the working substance in the ion source than had been sufficient for the recording of positive pions, and also to use stronger electron currents in the ionization chamber. Both of these factors somewhat reduced the resolving power of the mass spectrometer for negative ions.

We now outline the experimental details and results for the individual elements.

Silicon. The ion source contained $SiCl_4$ vapor. The electron energy in the ionization chamber was 60 ev and the electron beam current was 6 mA. In the negative ion spectrum we observed the following groups of lines: Si^- (28,29,30), Cl^-, $SiCl^-$, Cl_2^-, $SiCl_2^-$, $SiCl_3^-$ and $SiCl_4^-$. The Si^- lines were easily identified by comparison with the Cl^-(35,37) lines and from the peak ratios for the isotopes with masses 28, 29 and 30. The dissociation and ionization of $SiCl_4$ molecules by electron impact was studied by Vought[4]; for low $SiCl_4$ vapor density in the ion source the negative ion spectrum revealed only Cl^- and $SiCl_2^-$ ions. Bates [5], who by extrapolating the electronic binding energy in isoelectronic sequences of atoms and ions calculated the electron affinity of a number of light elements, gives 1.7 ev for this quantity in Si.

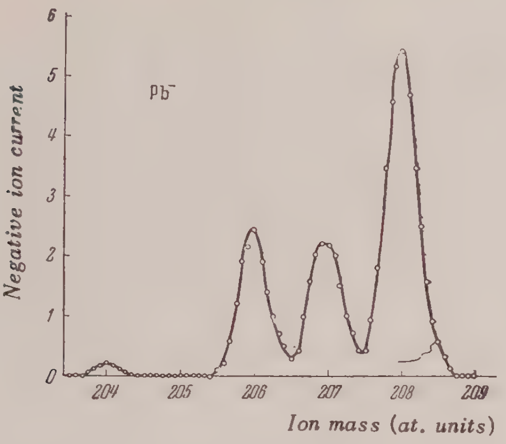

Germanium. For this element we tested the possibility of producing negative ions by "charge exchange" between negative antimony ions and germanium atoms. The source was equipped with two vaporizers: one for the volatilization of germanium and the other for the vaporization of antimony. The germanium vapor at $< 5 \times 10^{-4}$ mmHg pressure consists principally of atoms;^{6} therefore it could be expected that the process of "charge exchange" would produce negative atomic ions of germanium. When the ion source chamber contained only germanium vapor negative ions were not observed. When the source also contained antimony vapor we detected negative ions of this element (Sb^-, Sb_2^-, Sb_3^-) and Ge^- ions (70,72, 73, 74, 76). The Ge^- lines were identified by comparison with the Sb^- (121, 123) lines and by the relative intensities of the individual isotopes.

Tin. The ion source contained $SnCl_4$ vapor. Negative ions were produced by 80 ev electrons in a 4 mA electron current. The negative ion spectrum contained, in addition to Cl^- and Cl_2^- ions, the ions Sn^-(112, 114, 116, 117, 118, 119, 120, 121, 124), $SnCl^-$, $SnCl_2^-$, $SnCl_3^-$ and $SnCl_4^-$

Negative Sn^- ions were also obtained by "charge exchange" of negative bismuth ions and tin atoms. But it was not possible to resolve all of the tin isotopes in the mass spectrometer.

Lead. The working substance in the ion source was PbI_2 vapor. The electron energy was 40 ev and the electron current 2 mA. The negative ion spectrum contained the lines of I^-, Pb^- (204, 206, 207, 208), I_2^-, PbI^- and PbI_2^-. The Pb^- ions were identified by comparison with the I ions and by the relative isotopic intensities. The Figure shows the mass spectrogram of Pb^- ions obtained by plotting different ion energies with constant magnetic field strength of the analyzer. The Figure shows that the lead isotopes are well resolved and the height of the individual peaks corresponds to the relative isotopic abundances in ordinary lead.

We also performed an experiment to obtain Pb^- ions by "charge exchange" between antimony ions and lead atoms. When lead and antimony vapor were simultaneously introduced into the ion source the negative ion spectrum revealed a broad line for Pb^- ions which were not resolved into isotopes.

The atoms of C, Si, Ge, Sn and Pb which form the Iv *B* subgroup of the periodic table possess two *p*—electrons in their outer electron shells. The electron affinity of these elements must be attributed, as for the elements of groups V, VI, and VII, to the existence of an incomplete group of equivalent *p*—electrons into which the extra electron is introduced.

---

1 L. G. Smith, Phys. Rev. 51, 263 (1937).
2 R. E. Honig, J. Chem.Phys. 22, 126 (1954).
3 V.M.Dukel'skii, Dokl. Akad. Nauk SSSR 105, 595 (1955).
4 R. H. Vought, Phys. Rev. 71, 93 (1947).
5 D. R. Bates, Proc. Roy.Irish, Acad. A51, 151 (1447).
6 R. E. Honig, J.Chem. Phys. 21, 573 (1953).

Translated by I. Emin
94

Peculiarities of Cerenkov Radiation in Anisotropic Media

V. E. Pafomov
P. N. Lebedev Physical Institute,
Academy of Sciences, USSR

(Submitted to JETP editor July 27, 1956)
J. Exptl. Theoret. Phys. (U.S.S.R.) 32, 366-367
(February, 1957)

THE problem of Cerenkov radiation in anisotropic media has been discussed in a series of articles$^{1-6}$. Here we turn our attention to those interesting peculiarities that were not pointed out in the enumerated articles. For the sake of simplicity we consider these peculiarities in the case of a charge moving along the optic axis of a uniaxial dielectric crystal.

Taking the *z* axis along the velocity we obtain, according to Ref. 2, the Fourier component of the vector potential at large distances from the trajectory of the particle ($|\sigma r| \gg 1$) in the following form

$$A_{z\omega} = \frac{e}{c\sqrt{2\pi\sigma r}} \exp\{i(k_z z + k_r r - \omega t)\} \qquad (1)$$

$$= \frac{e}{c\sqrt{2\pi\sigma r}} \exp\{i(z - vt)\,\omega / v \pm isr\},$$

$$\sigma^2 = (\omega/v)^2 [1 - \beta^2 \varepsilon_r(\omega)]\, \varepsilon_z(\omega) / \varepsilon_r(\omega) = -s^2. \qquad (2)$$

The original Bessel equation (see Ref. 2) contains σ^2; therefore (1) is a solution independent of the sign of σ. The choice of the sign is determined by the requirement that the field must vanish at infinity. But in the absence of attenuation in the medium this criterion is insufficient. Again it is necessary to require that the Poynting vector be directed away from the radiating system. This implies a positive component W_r of the group velocity. In anisotropic media there is a range of frequencies where an outflow of energy from a moving charge ($W_r > 0$) corresponds to advanced potentials, which must also be taken as the type of the solution.

An analogous situation occurs in the refraction of plane waves incident upon a dielectric from vacuum. As is known, two refracted waves satisfy the boundary conditions. Usually one takes that wave whose wave vector forms an acute angle α with the normal to the interface pointing into the dielectric. In the region of negative group velocity, however, energy is carried out of the boundary by a wave with a wave vector that forms an obtuse angle ($\pi - \alpha$) with the normal. As Mandelshtam[7] has remarked, the direction of energy flow must also be a criterion in choosing the refracted wave.

We calculate the radial component of the group velocity by means of a formula, which has been derived in Ref. 8, and obtain

$$W_r = \partial\omega / \partial k_r = n^2 c \sin\vartheta / \varepsilon_z (n + \omega \partial n / \partial\omega), \qquad (3)$$

where ϑ is the angle between the wave vector and the z axis, and n is the refractive index for the extraordinary wave (see Ref. 1). Unattenuated waves will exist only for a real refractive index n. If $\epsilon_r(\omega)$ and $\epsilon_z(\omega)$ depend on the frequency in the same way as, e.g., in Ref. 2, then the derivative $\partial n/\partial\omega$ is positive over the entire frequency range. Thus the region of negative group velocity is determined only by the sign of $\epsilon_z(\omega)$ ($\epsilon_z < 0$), in which case it is necessary to take advanced potentials ($k_r < 0$) as the type of the solution.

If retarded potentials are taken as the type of the solution over the entire frequency range, then the force acting on the particle will have the form

$$F_z = -(e/c)^2 \int [1 - (1/\varepsilon_r(\omega)\,\beta^2)]\, \omega d\omega, \qquad (4)$$

where the integration is carried out over the region σ^2. Just that frequency range, where the parentheses in the integrand remains negative, corresponds to the range with negative group velocity. Here it is necessary to take advanced potentials as the type of the solution, which leads to formula (4) with the modulus of the integrand.

Another peculiarity of Cerenkov radiation in crystals is that the angle γ between the light ray W and the direction of electron motion may be larger than 90°. To show this we write

$$\operatorname{tg}\gamma = \frac{W_r}{W_z} = \frac{\partial\omega/\partial k_r}{\partial\omega/\partial k_z} = \frac{\varepsilon_z}{\varepsilon_r} \operatorname{tg}\vartheta.$$

In the region of negative group velocity we have $k_r < 0$; therefore $\tan\vartheta = k_r/k_z < 0$ and $\tan\gamma > 0$. Hence the charge radiates at velocities smaller than a certain value in accordance with the radiation condition $\epsilon_r\beta^2 < 0$.

In the region where $\epsilon_r > 0$ and $\epsilon_z < 0$ the charge radiates at any velocity. Here we have $\tan\vartheta > 0$ and ϵ_z and ϵ_r have different signs; therefore $\tan\gamma < 0$, i.e., the light ray (the direction of energy propagation) forms an obtuse angle with the direction of electron motion. It is obvious that these peculiarities occur also in the most general case.

In conclusion the author expresses deep gratitude to V. L. Ginzburg for valuable instructions and a discussion of the results and to B. M. Bolotovskii for a discussion of the results of this work.

---

[1] V. L. Ginzburg, J. Exptl. Theoret. Phys. (U.S.S.R.) 10, 608 (1940).

[2] A. Kolomonskii, Dokl. Akad. Nauk SSSR **86**, 1097 (1952).

[3] M. I. Kaganov, J. Tech. Phys. (U.S.S.R.) **23**, 507 (1953).

[4] Katsumi Tanaka, Phys. Rev. **93**, 459 (1954).

[5] A. G. Sitenko and M. I. Kaganov, Dokl. Akad. Nauk SSSR **100**, 681 (1955).

[6] V. E. Pafomov, J. Exptl. Theoret. Phys. (U.S.S.R.) **30**, 761 (1956); Soviet Physics JETP **3**, 597 (1956).

[7] L. I. Mandelshtam, J. Exptl. Theoret. Phys. (U.S.S.R.) **15**, 475 (1945).

8 V. L. Ginzburg, *Theory of Propagation of Radiowaves in the Ionosphere*, Moscow-Leningrad, State Technical Publishers, 1949.

Translated by J. Heberle
76

Concerning Even-Even Nuclei having the Characteristic 2+ for the Second Excited State

N. N. DELIAGIN AND V. S. SHIPNEL'
Moscow State University

(Submitted to JETP editor Sept. 24, 1956)
J. Exptl. Theoret. Phys. (U.S.S.R.) **32**, 373-374
(February, 1957)

T is well known[1,2] that even-even nuclei, as a rule, have in the ground state zero spin and positive parity, (characteristic 0^+), and in the first excited state spin equal 2 and also positive parity (characteristic 2+). Such a general rule does not exist for the second excited states, where characteristics 4+ and 2+ are encountered with equal frequency and also others. If the sequence of characteristics 0+, 2+, 4+ (corresponding to the ground and the first two excited states) is successfully explained, at least in the region of strongly deformed nuclei, by the generalized nuclear model proposed by Bohr and Mottelson[3] the sequence 0+, 2^+, 2^+, does not have at the present time a satisfactory explanation. It is of interest to examine experimental data pertaining to nuclei now known to have such a sequence of characteristics (nuclei: Fe^{56}, Zn^{66}, Se^{76}, Kr^{84}, Cd^{110}, Sn^{116}, Te^{122} Te^{126}, Xe^{126}, Xe^{128}, Os^{186}, Os^{188}, P^{192}, Pt^{194}, Pt^{196}, Hg^{198}, Hg^{200}).

It can be noticed that nuclei with $Z > 36$ are grouped in the immediate vicinity of values $Z = 50$ and $Z = 82$ at which the successive proton shells become filled. This location of these nuclei can be connected with their deformation. Inasmuch as the deformation parameters of these nuclei are unknown, the quantity $\delta = (\Delta Z + \Delta N)/2$ is taken conditionally as a measure of deformation, where ΔZ is the absolute value of the difference between Z of the nucleus and the value of Z nearest to it corresponding to a filled shell; ΔN is the analogous quantity for the number of neutrons. For all the examined nuclei, $4 \leq \delta \leq 12$. The sequence of characteristics 0+, 2+, 2+ is not encountered in nuclei situated close to the "two magic ones" ($\delta = 4$) nor in strongly deformed nuclei ($\delta = 12$). It can be assumed that this interval corresponds to nuclei of intermediate deformations, where the binding of the nucleons to the surface is not yet sufficient for the appearance of rotational levels, but the overall properties of the nuclei already manifest themselves. The excitation in this case can be either of a mixed nature, when, together with the overall excitation, there is also a change in the configuration of the nucleons, or it can be purely collective excitation, not of a rotational but of a vibrational nature. The ratio of energies of the second and first excited states, which is in most of the studied nuclei close to 2, points in favor of the vibrational nature of the excitation.

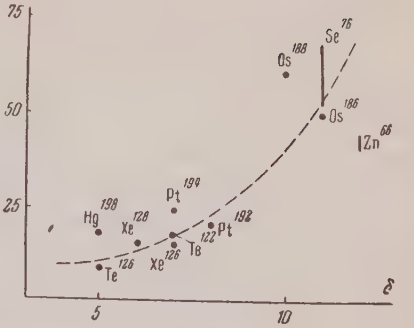

For the investigated nuclei the intensity of the direct transition from the second excited state to the ground state (2+ – 0+) is frequently comparable with the intensity of the cascade (2+ – 2+) transition and sometimes even exceeds it. This is in contradiction with the concept of single particle transition (Weisskopf's formula[4]). Besides, it is known that the first transition in the cascade 2+ – 2+ represents generally a mixed transition $E^2 + M$. There is thereby exhibited a characteristic increase in the relative intensity of the direct transition with increase of δ. The indicated dependence is shown in the Figure, which represents data on 11 nuclei for which the relative intensities have been reliably measured (intensity of direct transition in % relative to cascade along the axis of ordinates). The dotted curve indicates the possible average form of this dependence.

Such a redistribution of intensities of two competing transitions in favor of the direct transition with the increase of δ can be explained by the increased contribution of component $E2$ to the mixed transition 2+ – 2+ with increased deformation. Theoretical basis for such an increase was given by Shapiro[5]. Unfortunately, there are no sufficiently reliable experimental data at the present time concerning the magnitude of $E2$ in mixed transitions, making it impossible to relate the value of $E2$ to the deformation of the nucleus. However, an explanation of the increase in intensity of the direct transition with increased deformation can be given independently of the composition of the mixed transition 2+ — 2+. As was shown recently by Ford and Levinson[6], considerable increase in the probability of $E2$ transition may take place even in the case of relatively slight deformed nuclei. The intensity of the direct transition $E2$ can thereby exceed considerably the cascade transition, even if the latter has the nature of a pure transition $M1$. Apparently, also in this case, the relative intensity of the direct transition must increase with the increase in the deformation of the nucleus.

For some of the studied nuclei there are also known to exist higher excitations in addition to the two lower excited states having characteristics 2+. Inasmuch as the characteristics of the two lower excitations are equal, transitions from any higher level take place with the same change in spin and parity. If the multipole order of both transitions of such a pair were equal, the higher energy quantum, i.e., the transition to the first excited state, would always have the greater intensity. Actually, however, there are cases in which the inverse ratio of intensities is observed. Such a case was noted earlier by the authors[7] in the example of the Pt^{192} nucleus. Similar relation of intensities is observed for certain transitions of excited states of Pt^{194} and Os^{188}. The anomalous ratio of intensities can be connected with either additional selection rules (for example, type K forbiddenness[8]) or with the different nature of competition between the transitions.

---

[1] M. Goldhaber and A. Sunyar, Phys. Rev. **83**, 906 (1951).

[2]. G. Scharff — Goldhaber, Phys. Rev. **90**, 587 (1953).

[3] A. Bohr and B. Mottelson, Kgl. Don. Math — Fys. Medd. **27**, 16 (1953).

[4] J. Blatt and V. Weisskopf, *Theoretical Nuclear Physics*.

[5] I. S. Shapiro, J. Exptl. Theoret. Phys. (U.S.S.R.) **30**, 975 (1956); Soviet Phys. JETP **3**, 779 (1956).

[6] K. Ford and C. Levinson, Phys. Rev. **100**, 1 (1955).

[7] Deliagin, Kuznetsova and Shpinel', Izv. Akad. Nauk SSSR Fiz. Ser. **20**, 909 (1956).

[8] Alagie, Alder, Bohr and Mottelson, Kgl. Dan Mat. Fys. Medd, **29**, 9 (1955).

Translated by J. L. Herson
80

Dependence of the Polarization of (D + D) Neutrons on the Energy of the Deuterons.

I. I. Levintov, A. V. Miller, E. Z. Tarumov,
Vn. Shamshev
Institute of Chemical Physics,
Academy of Sciences, USSR

(Submitted to JETP editor October 1, 1956)
J. Exptl. Theoret. Phys. (U.S.S.R.) **32**, 375-376
(February, 1957)

THE method described in detail in Ref. 1 made possible polarization measurements of (D + D) neutrons and their dependence on energy D. We had at our disposal a tabular accelerator of the Institute of Chemical Physics, Academy of Sciences, USSR, which yields deuterons of 1800 kev maximum energy.

Polarization measurements were made with thick and thin zirconium targets. In all measurements the turning center of the counters was located at an angle of 49° to the neutron beam and the turning angle $\varphi_\alpha = 22°$. The cut-offs of the five discriminator channels were equal to 0.4; 0.5; 0.6; 0.7; 0.8. Computations of the maximum polarization of (D + D) neutrons was made from the asymmetry data measured in channels with cut-offs 0.4 and 0.7. The channel with cut-off 0.4 corresponded to poorer geometry at which the widening of the solid angle $\Delta\Omega$ [see Eq. (1), Ref. 1] was equal to 19°. For the channel of cut-off 0.7 this angle was 11°. In all experiments the values of P_{max}, obtained for both these channels, were in satisfactory agreement. In the following presentation of results, the mean value of P_{max} for these two channels is used, while the experimental errors in P_{max} correspond only to the statistical inaccuracies of the measurements.

Results of asymmetry measurements with the thick target are shown in Table 1.

The maximum polarization of (D + D) neutrons computed from these data is shown in Fig. 1. Computations were made for energy $E_d = 2/3\, E_d^*$. Such averaging corresponds to the linear dependence of the effective cross section of the reaction on the deuteron energy and somewhat decreases the uncertainty existing in those experiments introduced by the thick target. The results shown in Fig. 1 should thus be regarded as the "exit" polarization for a thick target at the corresponding deuteron energies.

In the second series of experiments, a thin

TABLE 1

E_d(mev)		0.4	0.6	0,9	1,2	1,5	1,8
Pressure in counters (atm.)		1,034	1,143	1.263	1.380	1.449	1,566
Asymmetry R	0.4	1.119 ±0,029	1,170 ±0.028	1,141 ±0.016	1.119 ±0,011	1,125 ±0.013	1,106 ±0.011
	0,7	1.228 ±0.045	1,221 ±0,042	1.249 ±0,039	1.284 ±0,021	1,288 ±0,027	1,248 ±0,022

zirconium target (150 kev) was used. With prolonged bombardment of the target by D ions a redistribution takes place in the deuteron layer and a change in the thickness of the target. For this reason thin targets were replaced after 20-30 hours of operation.

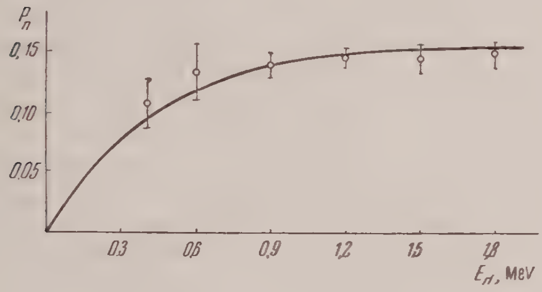

FIG. 1. "Exit" polarization of (D + D) neutrons for angle θ_n (lab) = 49° obtained from measurements using a thick target for various deuteron energies E_d.

Results are shown in Table 2 of asymmetry measurements in the conducted experiments, and values are given in Fig. 2 of P_{max} for (D + D) – neutrons computed from these data. In the same Figure are shown results of measurements by Meir, Scherrer and Trumpy[2] for $E_d = 600$ kev (target thickness 70 kev).

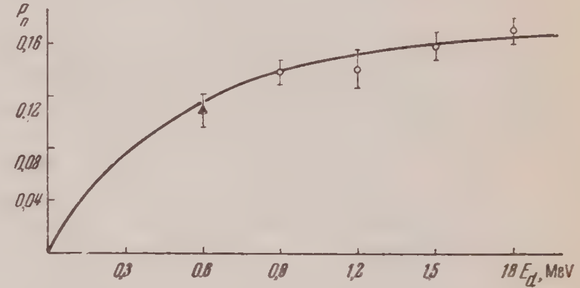

FIG. 2. Polarization of (D + D) neutrons at angle θ_n(lab) = 49° obtained from measurements with a thick target for various deuteron energies E. Δ: results of measurements by Meier, Scherrer and Trumpy[2].

TABLE 2

Ed (mev)		0.9	1.2	1,5	1,8
Pressure in counters (atm.)		1,263	1.380	1.449	1.566
Asymmetry R	0.4	1,114 ±0.013	1,114 ±0.024	1.142 ±0,018	1.148 ±0,012
	0,7	1,261 ±0.024	1.253 ±0.049	1.273 ±0.037	1,348 ±0,027

In spite of the difference in methods our results agree well with their data which up to the present time were the only accurate experimental data on polarization of (D + D) neutrons. Thus, the results shown in Fig. 2 increase considerably our knowledge concerning polarization of neutrons in this reaction. It follows from these results that the dependence of the polarization of (D + D) neutrons on the neutron energy is monotonic up to $E_d = 1.8$ mev. This monotonic property and the good accuracy of the values of $P_{\max}$, as determined by us, make the (D + D) reaction a convenient source of neutrons with a colibrated polarization.

We thank the group which operates the accelerator of the Chemical Physics Institute, Academy of Sciences, USSR for their help in carrying out the experiments.

---

* Editor's note: That's what it says!

1 Levintov, Miller and Shamshev, J. Exptl. Theoret. Phys. (U.S.S.R.) 32, 274 (1957); Soviet Phys. JETP 5, 258 (1957).

2 Meier, Scherrer and Trumpy, Helv. Phys. Acta 27, 577 (1954).

Translated by J. L. Herson
81

Altitude Dependence of Broad Atmospheric Showers According to the Various Models of the Elementary Act of Nuclear Collisions

V. V. GUZHAVIN AND G. T. ZATSEPIN
P. N. Lebedev Physical Institute,
Academy of Sciences, USSR

(Submitted to JETP editor July 20, 1956)
J. Exptl. Theoret. Phys. (U.S.S.R.) 32, 365-366
(February, 1957)

CALCULATIONS of the development in the atmosphere of nuclear-active and electron-photon components of broad atmospheric showers from primary protons of three different energies (10^{14}, 10^{16}, 10^{18} ev) were carried out for two variants of nuclear collision models. In both variants, the free path in air of the nucleons and pions was taken to be independent of the energy, and equal to 65 gm/cm^3, which corresponds to the geometric cross section of the nuclei of the atoms of the air.

In the first variant, it was assumed that for energies of the nucleons and pions higher than 5×10^{12} ev, creation of particles in nuclear collisions is described by the theory of Landau[1]. The energy spectrum and the composition of the secondary particles were assumed to be independent of whether a nucleon or a pion collided with the nucleus, and were taken from Ref. 2. The energy taken off by the secondary π-mesons was taken to be equal to 10% of the energy of the generating particle. The decay of the nuclear-active particles in the energy range $E > 5 \times 10^{12}$ ev could be neglected. In the energy region $E' < 5 \times 10^{12}$ ev, it was assumed that, independently of the nature of the generating particle of the energy E', in a collision of it with a nucleus, there is a nucleon among the secondary particles with energy $E = 0.7\,E'$, while the remaining energy $0.3\,E'$ is distributed among the created π^{+-0} mesons, the number of which is

$$n\,(E') = 2\,(AE'/2Mc^2)^{1/4},$$

where A is the average atomic weight of the nuclei of the air atoms, Mc^2 is the rest energy of the nucleon.

In the second variant of the calculations, in agreement with the assumption of Vernov,[3] it was taken into account that a nucleon of any energy (even for $E > 5 \times 10^{12}$ ev) loses only 30% of its energy in the formation of mesons in nuclear collisions, retaining 70%. It was further assumed that in the the collision acts only π^{+-0} mesons are produced, the multiplicity of which $n(E')$ was computed by Eq. (1), where the meson spectrum produced in the act is mono-energetic.

The development of the showers of nuclear-active particles in both variants was considered by the method of successive generation[4], with account taken of the decay of π^{+-0} mesons. The summation of the electron-photon showers arising from π^0-mesons was carried out graphically.

The results of the computations are shown in the Table where, in each column there is given the numbers obtained from the two variants (the upper is the first, the lower, the second). In the first column, we give the ratio of the energy flux $(EN_n)_p/(EN_n)_M$ carried by the nuclear-active particles for a high mountain (Pamir) to that for sea level (Moscow). The results of the calculations of the number of electrons at the altitude of Pamir N_{eP} and Moscow N_{eM} are given in the second and third columns, while the ratios of these numbers are given in the fourth. In the fifth and sixth columns, we have the computed and experimental values of the altitude dependence C_P/C_M between levels of Pamir and Moscow of the number of showers registered by usual method with the counters of corresponding area. As is evident from the Table, the experimental data on the altitude dependence of the number of showers from particles of energy $E \approx 10^{14}$-10^{16} ev agree better with the assumption on the loss of the nucleon in the nuclear collisions of only 30% of its energy. We have no experimental data on the altitude dependence of the number of showers from

TABLE

E_0	Computed values					Experimental values
	$(EN_n)_p/(EN_n)_M$	N_{ep}	N_{eM}	$N_{ep}\ N_{eM}$	$\frac{C_p}{C_M}=\left(\frac{N_{ep}}{N_{eM}}\right)^{\varkappa}$	
10^{14}eV	6.0	$3.8\cdot10^4$	$4.5\cdot10^3$	8.5	20 ($\varkappa = 1.4$)	≈13
	5.33	$2.5\cdot10^4$	$4.2\cdot10^3$	6.0	12.4 ($\varkappa = 1.4$)	
10^{16}eV	5.2	$6.7\cdot10^6$	$9.6\cdot10^5$	7.0	22 ($\varkappa = 1.6$)	≈15
	5.30	$4.5\cdot10^6$	$9.0\cdot10^5$	5.0	13.0 ($\varkappa = 1.6$)	
10^{18}eV	4.7	$9.2\cdot10^8$	$2.1\cdot10^8$	4.4	15 ($\varkappa = 1.8$) 20 ($\varkappa = 2.0$)	
	5.14	$6.2\cdot10^8$	$1.8\cdot10^8$	3.5	9.6 ($\varkappa = 1.8$) 12.2 ($\varkappa = 2.0$)	

particles with energies $E \approx 10^{18}$ ev, but the data on the magnitude of the barometric effect at sea level for showers from primary particles of the same energy[5] agree better with the calculations based on Landau's theory.

The results of the calculations of the altitude dependence depend slightly on the energy spectra of the created mesons, but are very sensitive to the amount of energy remaining with the nucleon; therefore the results present a weighty argument that in the region $E > 5 \times 10^{12}$ ev (at least, up to $E \approx 10^{14}$-10^{16} ev) the nucleon in collisions with nuclei of the atoms of the air loses, on the average, only about 1/3 of its energy. Conversely, for the region of very high energies ($E \approx 10^{18}$ ev), we conclude that a significant breaking down in the energy of the nucleon takes place in nuclear collisions.

The authors express their gratitude to N. S. Strunin and E. G. Natrusov who carried out a large part of the computations.

---

[1] L. D. Landau, Izv. Akad. Nauk SSSR, Ser. Fiz. **18**, No. 1 (1953).

[2] O. A. Guzhavina, V. V. Guzhavin and G. T. Zatsepin, J. Exptl. Theoret. Phys. (U.S.S.R.) **31**, 819 (1956);

[3] Vernov, Grigorov, Zatsepin and Chudakov, Izv. Akad. Nauk SSSR, Ser. Fiz. **19**, 493 (1955).

[4] G. T. Zatsepin and I. L. Rozental', Dokl. Akad. Nauk SSSR **99**, 369 (1954).

[5] Galbraith and T. E. Cranshaw, Conference on broad atmospheric showers, Harwell, April, 1956.

Translated by R. T. Beyer
75

The Construction of a Phenomenological Scattering Matrix with Non-local Interaction

V. S. BARASHENKOV
Chief Administration for the Use of Atomic Energy

(Submitted to JETP editor August 6, 1956)
J. Exptl. Theoret. Phys. (U.S.S.R.) 32, 368–369
(February, 1957)

IN recent years, detailed studies have been made on the possibility of introducing relativistically invariant cut-off form factors in the Schrödinger equation or in the equation of motion described in the Heisenberg representation.[1–3] It was shown that in all cases, multi-time equations become non-integrable, while the conditions of macroscopic causality are violated[2–4]. However, we can attempt to introduce the form factors directly into the relativistically invariant equation for the S-matrix which was obtained earlier in the theory with local interaction. Wataghin and Rayski [5] suggested the construction of the S-matrix, juxtaposing to each angle of the Feynman diagram (which corresponds to the theory with local interaction) a form factor while each internal line of this diagram is a causal function D^c or Δ^c [5].

Analytically, this suggestion can be formulated by writing the S matrix in the form*:

$$S = \sum_{n=0}^{\infty} \frac{(ie)^n}{n!} \tag{1}$$

$$\times \int_{-\infty}^{+\infty} P\{\varphi^*(x_1)\, A(x_1')\, \varphi(x_1'') \ldots \varphi^*(x_n)\, A(x_n')\, \varphi(x_n'')\}$$

$$\times F(x_1 x_1' x_1'') \ldots F(x_n x_n' x_n'')\, d^4(x_1 \ldots x_n'').$$

Actually, we can apply to the S matrix (1) the theorems of Wick on the reduction of the P derivative to the N derivative . The operator packets are expressed by D^c and Δ^c functions just as in the theory with local interaction. We cannot take the operator packets $\varphi^*(x_i)$ and (x_i) into account, since the corresponding matrix elements are equal to zero; this can easily be shown by a calculation in momentum space. However, it is not difficult to show that the S matrix (1) is not unitary, and, consequently, cannot be interpreted as the scattering matrix.**

It was shown in Ref. 6 that it is possible to satisfy the unitarity condition and macroscopic causality simultaneously if we add to the original Hermite "Lagrange function" $L(x_1 x_2 x_3)$ an anti–Hermitian part which is expressed in the form of an infinite series in powers of the interaction constant. It will be shown below that we can construct a unitary and macroscopically causal expression for the S matrix without the introduction of additional series, the physical meaning and convergence of which are not explicit. For this purpose, we write down the expression for the S matrix in the form:

$$S = \sum_{n=0}^{\infty} \frac{(-i)^n}{n!} \int_{-\infty}^{+\infty} P^* \{H_1 H_2 \ldots H_n\}\, d^4(x_1 x_2 \ldots x_n),$$

$$H_i \equiv H(x_i) = -ie \int \varphi^*(x_1)\, A(x_2)\, \varphi(x_3) \times \sum_{i=1}^{3} F_i(x_1 x_2 x_3)\, \delta(x_i - x)\, d^4(x_1 x_2 x_3) \qquad (2)$$

(for the definition of the operator p^*, see below). If we write the expression for the operator H_i in the form

$$H_i = -ie \int \varphi^*_p(x_i)\, A_k(x_i)\, \varphi_q(x_i)\, \{\Phi_1(k+q; q) + \Phi_2(p; q) + \Phi_3(p; p-k)\}\, d^4(pqk),$$

$$\varphi^*_p(x_i) = \varphi^*(p)\, e^{-ipx_i}; \quad \varphi_q(x_i) = \varphi(q)\, e^{iqx_i};$$

$$A_k(x_i) = A(k)\, e^{ikx_i};$$

[$\varphi^*(p)$; $\varphi(q)$; $A(k)$; Φ_i are the Fourier components of the operators $\varphi^*(x)$; $\varphi(x)$; $A(x)$ and the form factors F_i] , then we can apply the same rule for the calculation of the matrix elements (2) as in the theory with local interaction. We thus obtain for the matrix element of the energy eigenvalue of the field A:

$$\int \langle k \,|\, A_k(x_1)\, A_k(x_2) \,|\, k_1 \rangle \langle 0 \,|\, P^* \{\varphi^*_{p_2}(x_2)\, \varphi_{q_1}(x_1)\} \,|\, 0 \rangle \langle 0 \,|\, p^* \{\varphi^*_{p_1}(x_1)\, \varphi_{q_2}(x_2)\} \,|\, 0 \rangle \qquad (3)$$
$$\times \{\Phi_1(k+q_1; q_1) + \Phi_2(p_1; q_1) + \Phi_3(p_1; P-k)\} \{\Phi_1(k+q_2; q_2) + \Phi_2(p_2; q_2) + \Phi_3(p_2; p_2-k_2)\}\, d^4(x_1 x_2 p_1 p_2 q_1 q_2).$$

In space–time regions

$$e^2_{ij} \equiv (\bar{x}_i - \bar{x}_j)^2 - c^2 (t_i^2 - i_j)^2 < 0; \quad e^2_{ij} \gg \lambda^2$$

(λ is a constant which defines the characteristic dimension in the theory), the operator P^* does not differ from the known chronological operator P, since in these regions the operator P in (2) can be defined in a relativistically invariant fashion.[1] In microscopic regions $e^2_{ij} \lesssim \lambda$ one can generalize the definition of the operator P in relativistically invariant fashion. This generalization is, to a marked degree, arbitrary. Thus, if we set

$$P^* \{H_i H_j\} = {}^1\!/_2 [H_i H_j]_+ + {}^1\!/_2\, \varepsilon^*_{ij} [H_i H_j]_-; \qquad (4)$$
$$[H_i H_j]_\pm = H_i H_j \pm H_j H_i;$$
$$\varepsilon^*_{ij} \equiv \varepsilon^*(x_i - x_j) = \begin{cases} +1 & \text{for } e^2_{ij} \leqslant 0; \quad (t_i - t_j) > 0; \\ 0 & \text{for } e^2_{ij} > 0; \\ -1 & \text{for } e^2_{ij} \leqslant 0; \quad (t_i - t_j) < 0; \end{cases}$$

then

$$\langle 0 \,|\, P^* \{\varphi_p(x_1)\, \varphi_q(x_2)\} \,|\, 0 \rangle =$$
$$= {}^1\!/_2 \langle 0 \,|\, [\varphi^*_p(x_1)\, \varphi_q(x_2)]_+ \,|\, 0 \rangle$$
$$+ {}^1\!/_2\, \varepsilon^*(x_1 - x_2) \langle 0 \,|\, [\varphi^*_p(x_1)\, \varphi_q(x_2)]_- \,|\, 0 \rangle$$
$$= -{}^1\!/_2 i\, (1 + \varepsilon^*(x_2 - x_1))\, \Delta^+_q(x_2 - x_1)\, \delta(p - q)$$
$$- {}^1\!/_2 i\, (1 - \varepsilon^*(x_2 - x_1))\, \Delta^-_q(x_2 - x_1)\, \delta(p - q)$$

and Eq. (3) is rewritten in the form:

$$\int \langle k \,|\, A_k(x_1)\, A_k(x_2) \,|\, k \rangle\, \widetilde{\Delta}^c(x_2 - x_1; k)\, \widetilde{\Delta}^c(x_1 - x_2; k)\, d^4(x_1 x_2);$$

$$\widetilde{\Delta}^c(x; k) = {}^1\!/_2 (1 + \varepsilon^*(x))\, \widetilde{\Delta}^+(x; k) + {}^1\!/_2 (1 - \varepsilon^*(x))\, \widetilde{\Delta}^-(x; k);$$

$$\widetilde{\Delta}^\pm(x; k) = \int \Delta^\pm(q)\, \{\Phi_1(k+q; q) + \Phi_2(q; q) + \Phi_3(q; q-k)\}\, e^{iqx} d^4 q.$$

It follows from the properties of the form–factors

F_i that the commutator $[H_i H_j]_- \approx 0$ in the macroscopic regions $e^2_{ij} >> \lambda^2$, i.e., we can replace ϵ^*_{ij} by ϵ_{ij} in all regions $|e^2_{ij}| >> \lambda^2$ and, consequently, the function $\widetilde{\Delta}^c_{ij}$ will contain only positive frequencies for $t_i > t_j$. In other words, the S matrix (2), in macroscopic regions of space–time, satisfies the conditions of causality. The unitarity of (2) can be shown in the same way as for the S matrix without the form factor, where the operator P^* can always be replaced by P[3].

We can also determine P^* by the normal product in correspondence with wick's theorem:

$$P^* \{\varphi^*_p(x_1)\,\varphi_q(x_2)\}$$

$$= N\{\varphi^*_p(x_1)\,\varphi_q(x_2)\} + {}^1\!/_2\,\widetilde{\Delta}^c(x_1 - x_2; p)\,\delta(p - q).$$

From the viewpoint of computation, such a definition of the operator P^* is much more satisfactory than (4).**

In conclusion, I wish to thank Prof. D.I. Blokhintsev for his interest and discussions.

---

*As an example, we consider the simple case of the interaction of the scalar charged and neutral fields φ and A.

**The unitary condition $SS^+ = 1$ in the second approximation of perturbation theory reduces to the requirement that all the matrix elements of the expression $S_2^+ + S_2 + S_1 S_1^+$ vanish. In a theory with a form function, this is impossible. We can establish this fact by considering, for example, the matrix element of the eigenvalue of the energy of the field A or φ.[3]

*One can express $\epsilon^*(x)$ in the form of an exponent with dependence only on x, as a consequence of which, calculation of the integrals in the matrix elements presents well known difficulties.[7]

1 M. A. Markov, J. Exptl. Theoret. Phys. (U.S.S.R.) 25, 527 (1953); V. S. Barashenkov, J. Exptl. Theoret. Phys. (U.S.S.R.) 32, 566 (1957).

2 P. Kristensen and C.Moller, Det. Kon. Dan. Vid. Selsk, Med. 27, 7 (1952) ; C. Hayashi, Progr. Theor. Phys. 10, 533 (1953); 11, 226 (1954).

3 V. S. Barashenkov, Dissertation, 1955.

4 E. C. G. Stueckelberg and D. Wanders, Helv. Phys. Acta 27, 667 (1954).

5 G. Wataghin, Nuovo Cimento 10, 1602 (1953); J. Rayski, Proc. Roy. Soc. (London) 206A, 578 (1951).

6 B. M. Medvedev, Dokl. Akad. Nauk SSSR 103, 37 (1955).

7 D. Yennie, Phys. Rev. 80, 1953 (1950); H. Shimazu and O. Hara, Progr. Theor. Phys. 9, 187 (1953).

Translated by R.T. Beyer
77

An Experiment on the Measurement of the Viscosity of an Expanded Liquid

A. P. TOROPOV AND A. I. KITOVA
Central Asia State University

(Submitted to JETP editor September 10, 1956)
J. Exptl. Theoret. Phys. (U.S.S.R.) 32, 372-373
(February, 1957)

STUDY of the viscosity of expanded liquids would be of considerable interest for the development of the theory of viscosity. In the literature there is not indication of work in this field. We therefore set ourselves the task of investigating whether such measurements could be carried out. Reported below are some results of experiments we performed.

The substance chosen for investigation was benzene. The sample used had physical constants that agreed fully with handbook values. The benzene was put through an additional distillation just before the experiments for removal of absorbed water and for partial degasification, and the first and last fractions were rejected. Since we did not undertake to attain maximum expansion of the liquid complete degasification of the benzene was not carried out.

The method of Stokes was chosen for making the measurements as being easiest to apply. For manufacture of glass beads of the necessary diameter, we adopted the method of fusion of glass powder granules in the flame of a gas burner. This method was used by Bloomquist and Clark[1]; we modified and simplified their method to some extent. For our task we selected a few beads of 3C-5K molybdenum glass of diameter 0.05 to 0.06 mm, of accurately spherical shape and containing no gas inclusions. Since glass beads in benzene are hard to see, the ones chosen were coated with aluminum by evaporation in a vacuum. The density of the spheres was determined by the method of free flotation and was 2.268 g/cm^3 at 25° C.

The experiments on measurement of the viscosity of the expanded benzene were carried out in cylindrical ampoules, made of 3C-5K molybdenum glass, of inside diameter 6 mm. At the ends of the ampoules were intakes, 150 mm apart. The inside diameter of the intakes was about 1 mm. The ampoule was filled with benzene in such a way that after sealing, a bubble of gas remained in it. The glass bead was inserted into the ampoule

Results of measurements of viscosity (in millipoises) of expanded and unexpanded benzene

Temperature, °C	Unexpanded liquid			Expanded liquid		
	Time of fall, sec	Density	Viscosity	Time of fall	Density	Viscosity
Ampoule No. 1. Solution temperature 32.2 °C Lowest rupture temperature 28.5 °C						
30.00	17.30	0.8680	5.613	17.06	0.8657	5.54
31.00	17.06	0.8670	5.536	16.90	0.8657	5.49
Ampoule No. 2. Solution temperature 34.6°C Lowest rupture temperature 30.8 °V						
32.00	15.65	0.8659	5.462	15.49	0.8631	5.42
33.00	15.44	0.8648	5.389	15.30	0.8631	5.35
34.00	15.23	0.8637	5.318	15.20	0,8631	5,31
Ampoule No. 3. Solution temperature 61.2°C Lowest rupture temperature 56.3 °C						
58.00	12.74	0.8378	3.979	12.46	0.8343	3.90
60.00	12.44	0.8356	3.892	12.35	0.8343	3.87
60.50	12.37	0.8351	3.871	12.30	0.8343	3.85

filled with benzene; the benzene in the ampoule was frozen, and the ampoule was sealed. Three such ampoules were prepared; they differed from one another in the size of the gas bubbles contained in them. In conducting the experiments, the ampoules were clamped in a stand that permitted rapid inversion of the ampoule, with immediate establishment of accurate verticality of its axis; in addition, it was also possible to set the ampoule in a horizontal position. On the stand were two sights, fastened 100 mm apart. This stand, with the ampoule clamped in it, was set in a water thermostat with transparent walls; the temperature could be varied continuously and could be held constant to within ± 0.02°C.

The experiment was conducted as follows. First the ampoule was set horizontal, and the temperature of the thermostat was very slowly raised until the whole volume of the ampoule appeared full of liquid. Then the temperature ("solution temperature") was recorded, and immediately there began a slow cooling of the thermostat to the point of rupture of the liquid. This procedure was repeated many times, until the solution and rupture temperatures remained constant to within ±0.2 °C. After such a training of the ampoule had been completed, the bead was transferred to one end of the ampoule, the thermostat was heated to the solution temperature, and then – after disappearance of the gas bubble in the ampoule – the temperature of the thermostat was fixed a little below the solution temperature. The ampoule was held at this temperature 20 to 25 minutes; then it was quickly set vertical, with the end containing the bead upward, and the time of fall of the bead from the upper to the lower sight was measured. Such measurements were taken at least 10 to 15 times for each ampoule at each temperature chosen for measurement.

The mean absolute error in the determination of the time of fall of the beads was ±0.04 sec. The density of the expanded liquid was calculated from the density of benzene at the solution temperature and from the coefficient of linear expansion of the molybdenum glass. The calculations gave a value of the density of the expanded liquid that did not differ appreciably from the density of benzene at the solution temperature. The values of the viscosity and density of benzene that were needed for the calculation were calculated with an interpolation formula taken from Ref. 2. The absolute error in the measurement of the viscosity of the expanded benzene was in all cases within ±0.03 millipoise.

Worthington[3] indicates that the presence of a glass bead in an ampoule with an expanded liquid makes the expanded liquid very unstable, and that upon the slightest motion of the bead, the liquid ruptures. However, the data presented in the Table show quite convincingly in our opinion, that measurement of the viscosity of an expanded liquid by the Stokes method is possible. The problem in further investigations is to improve the accuracy of the necessary measurements and to explore methods of extending the temperature interval in which the expanded liquid exists.

---

[1] C. R. Bloomquist and A. Clark, Ind. Eng. Chem., Anal. Ed., 12, 61 (1940).

[2] Tekhn. ents., Spr. fizich., khimich. i tekhnologich. velichin [Technical Encyclopedia, Handbook of Physical, Chemical and Technological Data], 5, 10.

[3] A. M. Worthington, Phil. Trans. Roy. Soc. (London) **A183**, 355 (1893).

Translated by W. F. Brown Jr.
79

Concerning the Possibility of an Experimental Investigation of the Structure of the Electron

V. A. Petukhov
P. N. Lebedev Physical Institute,
Academy of Sciences, USSR

(Submitted to JETP editor Oct. 31, 1956)
J. Exptl. Theoret. Phys. (U.S.S.R.) **32**, 379-380
(February, 1957)

IN connection with successes in the construction of different electron accelerators, the latter find greater applications as the activating agent in investigations of electric charge distributions in atomic nuclei. In particular, the study of elastic scattering of 100, 188 and 236 mev electrons by protons at rest permitted the determination of the mean square radius of the proton[1].

All these computations and interpretations of experimental results, however, were based on the assumption of a dimensionless electron. The question of charge distribution inside the electron is important not only from the point of view of using this particle for investigations of structures of heavy nuclei, but is also independently of interest in physics. An experimental solution of this question makes it necessary to have a source of ~ 40 bev electrons for the case of the immovable electron target. Besides, in view of the small value of the effective cross section, currents of the order of several amperes are required for a responsible frequency of observation.

The choice of electron energy is determined by experimental capabilities to determine the angular distribution of the differential cross section in elastic scattering of electrons by electrons computed for two extreme cases: 1) the electron is treated as a mathematical point; 2) the electron has the classical radius $r_0 = e^2/mc^2$. The effective cross section for the first case is determined by the known Meller formula[2]. Quantum electrodynamic computations of scattering of extended electrons by electrons was carried out by M. A. Markov and I. V. Polubarinov. Accounting for the extension of the electron consisted of replacing the Hamiltonian of local interaction by the Hamiltonian of interaction with non local current, which formally lead to a change in the propagation function of the virtual photon. The dependence of the differential cross section on the scattering angle in the center-of-mass system is shown graphically in the Figure for the two types of selected form factors. It is seen from the Figure that the ratio of scattering cross sections at these energies $\gamma\ (= E/mc^2)$ is quite distinguishable experimentally.

At the present time there are no known methods of developing accelerators for obtaining electrons of such high energy (> 40 bev) especially for currents in amperes.

The possibility of conducting an experiment as indicated above is based on utilizing the principle of the ring phasotron, proposed by Kolomenski, Petukhav and Rabinovich[3] back in 1953. In this accelerator the magnetic field remains constant in time, but a small width of the magnetic path is preserved due to high gradients (large n) and the introduction of sectors with reverse direction of the magnetic field. The constancy of the magnetic field permits to apply the principle of charge accumulation in the limiting energy orbit and, in view of the repeated passage of the particles through the same meeting place, permits to circumvent the second difficulty connected with the need for high currents.

As far as the energy phase of the problem is concerned, the operation of two opposing electron beams, i.e., bringing into coincidence the system of center of mass with the laboratory system gives a considerable energy gain for relativistic particles (electrons). Thus, for example, a 100 bev accelerator in its physical effect is equivalent to two opposing electron beams of only ~ 150 mev. An electron accelerator of these energies from the standpoint of dimensions and power, is a relatively modest installation.

The problem of the meeting of two beams can be solved in different ways. For example, Kerst and others[4] considered the possibility of meeting of protons in the case of two adjacent but independently operating ring accelerators. There is however, still another possibility which, it seems to us, opens wide possibilities for the future.

The theory of the ring phasotron, shows that in the characteristic phasotron operation the particles are drawn as it were into the region of higher magnetic fields and we have thereby computed the direct as well as the inverted variant of this accelerator. In the first case, the orbit of the particles represent an unwinding spiral of a very small pitch while for the inverted variant the radius of the orbit decreases slightly as the particle is speeded up.

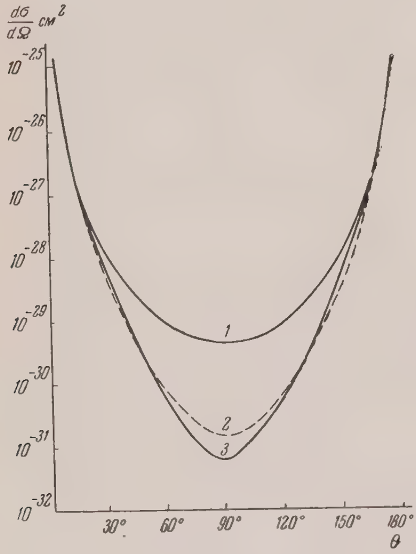

FIG. 1. $1 - r_0 = 0$; $2 - r_0 = e^2 mc^2 = 2.8 \cdot 10^{-23}$ см, $F(q^2) = (1 + q^2 r_0^2)^{-2}$; 3 — same for $F(q) = \exp(-{}^1/_2\, q^2 r_0^2)$; $\gamma = 200$

If the azimuthal dimensions of the sectors with direct and reversed directions of the magnetic field are made equal. and the sectors themselves are made so that the field intensities in the outer and inner halves are different, then there appears the possibility of combining in one magnetic system the direct and inverted ring of the phasotron. In this case with the sectors arranged with alternating strong and weak fields the electrons may revolve in the straight variant (i.e., inside the ring), for example in the clockwise direction and in the inverted variant (i.e., outside the ring) in the counterclockwise direction, moving in the same operating cycle against each other. The distance between the moving in opposite directions electron beams which began the acceleration process on the inner and outer radii of the electromagnet respectively, will decrease as the energy of the particles increases.

By the introduction of a suitably selected azimuthal asymmetry it is possible, in principle, to bring about the intersection of the trajectories of the electron beams which acquired maximum energy within the limits of a small azimuth. In this manner there is also avoided the first difficulty arising from the need to have available electron beams accelerated up to several tens of bev.

A very important characteristic which determines the feasibility of such an experiment is the effectiveness of computing electron scattering at a given angle considering the fact that the effective cross section of the physical phenomenon under consideration is very small (10^{-29} to 10^{-30} cm^2). Computation shows that with 10^{12} particles in the beam, effective length of the intersection ~ 10 cm, and cross section dimensions of the beams ~ 10 cm^2, the number of counts per unit solid angle for $\sigma = 10^{-29}$ is one count per 10 seconds. A quantity of 10^{12} particles in a beam rotating with the velocity of light is equivalent to ~ 2.5 amps, which is quite permissable from the standpoint of distortion of the accelerator magnetic field by the magnetic field of the beam itself.

The physical equipment for the investigation is envisaged in the form of special coincidence circuits of high resolving power ($\tau = 10^{-8}$ sec), which together with special absorbers which transmit only electrons of maximum energy will enable to make observations in the background of a large number of electrons scattered in the usual manner by the electrons and nuclei of the residual gas atoms in the vacuum chamber. The most dangerous in this respect is the effect of the elastic scattering by nitrogen nuclei, which may result in a high number of chance coincidences thereby considerably distorting the result.

The ratios of false counts, due to the finite resolving time τ of the coincidence circuits, to the number of true counts at 10^{-6} mm pressure in the vacuum chamber, are 3 and 0.1, corresponding to values of angle of 45° and 90 °. Inasmuch as the value of τ varies as the square of the pressure, the experiment can be conducted only in a very high vacuum ~ 10^{-7} mm.

The selected electron energy (150 mev) will make it possible not only to investigate experimentally the variation of the cross section with angle and thereby obtain the answer concerning the size of electrons, but also to traverse a very interesting energy region near the formation thresholds of μ and π mesons.

[1] R. Hofstadter and R. W. McAllister, Phys. Rev. **98**, 217 (1955).

[2] A. I. Akhiezer and V. B. Berestetskii, *Quantum Electrodynamics*, Moscow, 1953 p. 297

[3] Kolomenskii, Petukhov and Rabinovich, Reports (Otchet) Physical Institute, Acad. Sci. USSR, 1953; *Some questions in the theory of cyclic accelerators*, Acad. Sci. Press.

[4] D. W. Kerst and others, Phys. Rev. **102**, 590 (1956).

Translated by J. L. Herson
83

Force Fluctuations in an Electron Gas

M. Ia. Mints

(Submitted to JETP editor November 15,1956)
J. Exptl. Theoret. Phys. (U.S.S.R.) 32, 386–387
(February, 1957)

FOR the calculation of the microscopic parameters of an electron gas, it is important to known the fluctuation of the random force distribution $w(\mathbf{F})$ which acts on the individual electron. A calculation of $w(\mathbf{F})$ under the assumption that the a priori probability $\tau(\mathbf{r})$ of the particle distribution about an individual particle is a constant, i.e., that there is no correlation in the positions of the particles, was carried out by Holtsmark.[1] In this case a distribution function was obtained such that all its moments diverge, beginning with the second. On the other hand, it is clear that there will be an appreciable correlation only at distances $r_0 \sim e^2/kT$, at which the mean kinetic energy of the particles is of the order of the value of the potential barrier. For $T \sim 10^5$, the value of r_0 is $\sim 10^{-8}$.

At large distances, there is virtually no correlation, since the gas is assumed to be in a state of statistical equilibrium with constant density. Since the relaxation length and the mean distance between particles are appreciably greater than r_0 under ordinary circumstances, we can neglect the interaction of the surrounding particles located in a sphere of radius r_0. In other words, the motion of the particles in the vicinity of the isolated one is the ordinary Rutherford scattering. The distribution of the particles near the particle under examination can be found by solving the kinetic equation

$$v_i \frac{\partial f}{\partial x_i} - \frac{1}{m}\frac{\partial u}{\partial x_i}\frac{\partial f}{\partial v_i} = 0 \qquad (1)$$

with boundary condition $f(\mathbf{r},\mathbf{v}) = \exp(-mv^2/kT)$ for $u = 0$, where $u(\mathbf{r})$ is the potential established by the isolated electron. This equation has the integral $f = \Omega(mv^2/2 + u)$ where Ω is an arbitrary function. Consequently, solving this equation, we get

$$\tau(\mathbf{r}) = \exp(-e^2/rkT). \qquad (2)$$

It is of interest to note that in the limiting case of very strong interaction, for which the particles out to the distance $\ll r_0$ are in equilibrium with the field of the isolated electron, $\tau(\mathbf{r})$ is obtained in the same fashion.

Making use of the Markov procedure:

$$w(\mathbf{F}) = \frac{1}{8\pi^3}\int \exp(-i\rho\mathbf{F})\, A(\rho)\, d\rho,$$

$$A(\rho) = \lim_{N\to\infty}\left[\int \exp(-e^2\rho\mathbf{r}/r^3)\,\tau(\mathbf{r})\,d\mathbf{r}\right]^N,$$

we can show that for large F the function $w(\mathbf{F})$ falls off more rapidly than any power of F. Consequently, the moments of all orders of $w(\mathbf{F})$ must exist. These can be computed by expanding the eigenfunction $A(\rho)$ in a series in powers of ρ. For example,

$$\langle \mathbf{F}^2\rangle = \int \mathbf{F}^2 w(\mathbf{F})\, d\mathbf{F} = -(\Delta_\rho A(\rho))_{\rho=0} = 4\pi e^2 nkT.$$

In a similar fashion, all the moments of even order can be calculated. [Moments of odd order are equal to zero because of spherical symmetry of $w(\mathbf{F})$.] The value obtained can serve for a rough estimate of the coefficient of viscosity:

$$\mu \sim \sqrt{\langle \mathbf{F}^2\rangle / m\overline{v^2}} = \sqrt{4\pi e^2 n/kT}.$$

An exact calculation ought to take into account the correlation of force fluctuations at different points of space, for which it is necessary to compute $\langle F_i(x)\, F_k(x')\rangle$. However, the consideration just given shows that the principal contribution to the viscosity, the diameter, the relaxation length for particles with long range interaction will not be given by an account of well regulated, averaged forces (pair collisions, interaction with vibrations) since this contribution is proportional to the first moment of $w(\mathbf{F})$ and the interaction with the fluctuations of the electric field. For these quantities, a consideration of the fluctuation scattering is more important than consideration of the well regulated deceleration.

---

[1] J. Holtsmark, Ann. Physik 58, 577 (1919); Phys. Z. 20, 162 (1919); 25, 73 (1924).

Translated by R. T. Beyer
88

Effect of a Longitudinal Magnetic Field on the Multiple Scattering of Particles

N. A. CERENKOV
United Institute of Nuclear Studies

(Submitted to JETP editor November 6,1956)
J. Exptl. Theoret. Phys. (U.S.S.R.) 32, 389–390
(February,1957)

LET there be a homogeneous magnetic field in a scattering medium. Let us consider how an infinitely narrow pencil, generally speaking, of relativistic particles, directed parallel to the magnetic induction vector, will be scattered. As is well known, the magnetic field does not change the energy of the particles. Thus, if we neglect the energy losses of the particles in thescattering, we can limit ourselves to the case in which all the particles have the same energy. We take the axis of the pencil to be the z axis. We assume that the properties of the medium do not depend on x and y, and that, in the mean, the angle between the velocities of the particles and the z axis is small. This problem has been solved by Fermi[1] in thecase in which the medium is homogeneous and the magnetic field is absent.

Let a current of particles arise at the origin. For $z > 0$, the equation of the process under consideration has the form:

$$\frac{\partial n}{\partial z} + \alpha\frac{\partial n}{\partial x} + \beta\frac{\partial n}{\partial y} + L\left(\beta\frac{\partial n}{\partial \alpha} - \alpha\frac{\partial n}{\partial \beta}\right) + \frac{n}{l(z)} = \frac{a^2(z)}{4}\left[\frac{\partial^2 n}{\partial \alpha^2} + \frac{\partial^2 n}{\partial \rho^2}\right] \qquad (1)$$

with the boundary condition

$$n = A\delta(x)\,\delta(y)\,\delta(\alpha)\,\delta(\beta)$$

for $z = 0$, where α and β are the projections of the angular deviations of the particle velocity from the z axis on the planes zx and zy; n is the particle distribution function in x, y, z, α, β; A is the ratio of the particle flux through the plane $z = 0$ to its velocity; $1/l(z) = (mT/p) + \Sigma N_i(z)\sigma_i$ $N_i(z)$ is the number of atoms of type i per unit volume of the medium; σ_i is the absorption cross section of the particles by atoms of type i; m is the rest mass, p is the momentum, T is the characteristic lifetime of the particles relative to random decay. Let the cross section of single scattering of particles on the atoms of type i have the form $d\sigma_i = R_i(\theta)\, d(\theta$. Then

$$a^2(z) = \sum_i N_i(z)\int R_i(\theta)\,\theta^2 d\theta.$$

Finally, $L = eB/cp$, B = magnetic induction, e = electric charge of the particle, c = velocity of light.

Equation (1) is solved by a decomposition of the function

$$F = A^{-1} n \exp\left\{-\int_0^z l^{-1}(\zeta)\,d\zeta\right\}$$

into a Fourier integral in x, y, α, β; as a result,

$$F = \frac{\exp\left\{\dfrac{-\gamma_0 r^2 + 2\gamma_1 r\theta\cos(\varphi_0-\varphi) + \gamma_2 Lr\theta\sin(\varphi_0-\varphi) - \gamma_2\theta^2}{\gamma_0\gamma_2 - \gamma_1^2 - \gamma_2^2 L^2/4}\right\}}{\pi^2\left[\gamma_0\gamma_1 - \gamma_1^2 - \gamma_2^2 L^2/4\right]}, \qquad (2)$$

$$r\cos\varphi_0 = x, \quad r\sin\varphi_0 = y, \quad \theta\cos\varphi = \alpha, \quad \theta\sin\varphi = \beta,$$

$$\gamma_0 = \int_0^z a^2(\zeta)\,d\zeta, \quad \gamma_1 = \frac{1}{L}\int_0^z a^2(\zeta)\sin L(z-\zeta)\,d\zeta,$$

$$\gamma_2 = \frac{4}{L^2}\int_0^z a^2(\zeta)\sin^2\frac{L(z-\zeta)}{2}\,d\zeta.$$

The angular distribution without reference tothe transverse displacement, as is easy to understand, does not depend on L:

$$\int\!\!\int_{-\infty}^{+\infty} n\,dx\,dy = \frac{A}{\pi\gamma_0}\exp\left\{-\frac{\theta^2}{\gamma_0} - \int_0^z \frac{d\zeta}{l(\zeta)}\right\}. \qquad (3)$$

The spatial distribution without reference tothe angles has the form:

$$\int\!\!\int_{-\infty}^{+\infty} n\,d\alpha\,d\beta = \frac{A}{\pi\gamma_2}\exp\left\{-\frac{r^2}{\gamma_2} - \int_0^z \frac{d\zeta}{l(\zeta)}\right\}. \qquad (4)$$

We note two effects, produced by the magnetic field in the narrow beam. The principal effect consists of the fact that under otherwise equal conditions the pencil is narrower in the magnetic field than without it. This follows from the fact that

$$\frac{4}{L^2}\sin^2\frac{L(z-\zeta)}{2} < (z-\zeta)^2,$$

and means $\gamma_2(L) < \gamma_2(0)$ if $L \neq 0$. This is also understandable because in the intervals between collisions in the magnetic field, the scattered particle moves in a helical path and departs from the axis of the pencil less than in the absence of the field, when it moves along a straight line.

The other effect is the following. In the absence of the magnetic field, the mean value of the angle $\varphi - \varphi_0$ is equal to zero. In this case we have a radial "polarization" of the pencil. In the magnetic field,

$$\overline{\varphi - \varphi_0} = -\operatorname{arctg}(\gamma_2 L / 2\gamma_1).$$

This means that in the magnetic field, the axis of polarization is turned by this angle.

---

[1] B. Rossi and K. Gresisen, *The interaction of cosmic rays with matter*, p. 45 (Russian translation).

Translated by R. T. Beyer
90

s-d Exchange in Ferromagnetic Metals

F. M. GAL'PERIN

(Submitted to JETP editor October 22, 1956)
J. Exptl. Theoret. Phys. (U.S.S.R.) 32, 381-382
(February, 1957)

LANDAU first pointed out the possibility of the fundamental phenomenon of "submagnetization" of the external *s*-electrons of a ferromagnetic crystal in the exchange "field" of the internal *d*-electrons of the atoms, as a result of exchange between the electrons under consideration (*s-d* exchange).

Vonsovskii developed in detail the theory of *s-d* exchange. His results contain exchange integrals between *s*- and *d*-electrons of a single atom (I_0) and of neighbor atoms (I), and also the transport integral of an *s*-electron. In the present state of the theory, these integrals cannot be calculated. Consequently, as the same author pointed out, a quantitative comparison with experiment is not possible; the theory gives only a qualitative explanation of many phenomena[1].

The aim of the present work is to show that the integrals mentioned can be found by an empirical method, and that substitution of their values in Vonsovskii's relations for pure ferromagnetic metals[1,2] gives satisfactory agreement with experiment.

We make the simple and natural assumption that the *s-d* exchange interaction depends on the interelectronic distances and on the number of electrons participating in the interaction. As an example, we consider the approximation of tight binding of the *s*-electron[1-3]. In this case, an *s*-electron spends most of the time in an *s*-state at distance R_s from the nucleus of some atom, and the *d*-electrons spend most of the time at a distance R_d from nuclei of atoms, where R_s and R_d are the radii of the *s*- and *d*-shells, respectively, of an isolated atom. Under these conditions the minimum distances between nearest *s*- and *d*-electrons in a single atom and in neighbor atoms (along a straight line connecting the nuclei of the atoms) are, respectively, R_s-R_d and r_1-R, where $R = R_s + R_d$, r_1 is the distance between an atom and the atoms nearest to it (first c.s., c.s. = coordination sphere), $(r_2 - R)$ is the distance between an *s*-electron and the next nearest *d*-electrons, r_2 is the distance between an atom and the next nearest atoms (second c.s.). In order to preserve the accuracy with which r_1 and r_2 are usually measured, the magnitude of R is computed with the same accuracy (to the fourth decimal place) by our relation[4]; the values of R thus obtained differ by no more than 1% from those calculated by Slater's method[5].

According to the sign of $r_i - R$, the metals divide into two groups: Co falls in group 1 $[(r_i/R) < 1]$, Ni (Dy and Er) in group 2 $[(r_i/R) > 1]$, Fe(Gd) with respect to its first c.s. in group 1, where $i = 1$ for Ni (second c.s. not taken into account because of the large distance of the next-nearest atom: $r_2/r_1 = 1.414$), $i = 1, 2$ for Co and Fe (second approximation); $i = 1, 2$ for Co $(r_2 \approx r_1)$, $i = 1$ for the other metals (first approximation); i = number of the c.s.

We postulate that the exchange integral I is

$$I = 1 \pm \sum_i \Delta E_i; \quad \Delta E_i = 0.641\, n_i (r_i - R); \tag{1}$$

here and hereafter, the upper sign refers to group 1, the lower to group 2. We denote by I_1 the integral I in first approximation.

The exchange integral I_0 is similarly expressed:

$$I_0 = -[1 - 0.641\,(R_s - R_d) \pm 0.065\,(N_d - 2/e)]; \tag{2}$$

$$R_s - R_d = 1.56\{1 - 0.13\,[eN_d/(N_d - 1) \mp (N_d/2 - 1)/e]\}, \tag{2$'$}$$

where N_d is the number of unpaired d-electrons in the atom, $e = 1$ for Co and Ni, $e = 2$ for Fe, $e = 7$ for Gd. In the tight binding approximation being considered, we neglect the transport integral of the s-electron. Upon evaluating (2) and (2′), we find $I_0 = \pm 0.13\, eN_{d(f)}/N_{d(f)} - 1$; the minus sign applies to Fe, Ni and Co, the plus to Gd.

By substituting (1) and (2) in Vonsovskii's relation (1.13)[1], we find the atomic magnetic moments

$$m/M_B = N_d + N_f + 0.15\,(I_0/I - 4)n_s \quad (n_s = 2). \tag{3)*}$$

By reversing the sign before ΔE in (1) and substituting (1) in our relation

$$m_p/M_B = N_{d(f)} - n_s + \sum_i (1 \mp \Delta E_i); \tag{3$'$}$$

$i = 1$ for Ni and Fe, $i = 1, 2$ for Co,

we find the paramagnetic atomic magnetic moments m_p. By differentiating m with respect to pressure P, and by assuming that under hydrostatic compression only the interatomic distances and the moments m change, we find

$$\frac{1}{m}\frac{dm}{dP} = \pm 0.0641\,\frac{xI_0}{mI^2}\,(n_1r_1 - n_2r_2), \tag{4}$$

where x is the compressibility. It follows from (4) that $dm/dP < 0$ for Gd and Fe and > 0 for Ni. We furthermore get fot exchange energy of the "3/2-power law" of Bloch and Möller

$$A = kn^2N_d^2(N_f)I_1/e^2. \tag{5}$$

Here $e = m_0/M_B$ for group 1, $e = (m_0/M_B) + 1$ for group 2, where m_0 is the integral part of the atomic moment m (0, 1, 2 and 7 M_B for Ni, Co, Fe and Gd respectively).

Properties of pure ferromagnetic metals.

Metal		Gd	Ni	Co	Fe
$n_1(r_1$, Å)		6(3.561)	12(2,4868)	6(2.499)	8(2.4777)
$n_2(r_2$, Å)		6(3.629)		6(2.507)	6(2,8610
R, Å		3.566	2,4082	2.5382	2.7332
$N_{d(f)}; n_{d(f)}$		1(7);1(7)	2; 8	3; 7	4; 6
$\Delta E_1(\Delta E_2)$		—0,02(0,24)	0.60	—0.15(—0,12)	—1.31(0.49)
$\sum_i \Delta E_i$		0.22	0.60	—0,27	—0.82
$I(I_1)$; I'/K		1,22(0,98)	0.40(0.40) ;1	0,73(0.73); 1	0.18 (0,69); 1
I_0; I'_0/K		1,06; —1	—0.260; —1	—0.195; —1	—0.347; — 1
m/M_B	calc.	7,06	0.605	1.720	2,220
	expt.	7,10	0.605	1.715	2,217
m_p/M_B	calc.		1.6	3,27	3,31
	expt.		1,6	3,27	3.37
$\frac{1}{m}\frac{dm}{dP}\cdot 10^7\,\frac{\text{cm}^2}{\text{kg}}$	calc.		30	—1	—5
	expt.		60	—	—6
A/k	calc.	5	230	946	177
	expt.	4.5[6]	226[8], 220[7]	—	207[7], 183[8]
Θ°K	calc.	266	642	1385	1043
	expt.	289	631	1393	1043

The Curie point is calculated by a relation similar to (1.8) of Ref. 1:

$$\Theta = 2nA_{dd}[A_{sf}] / 1 - \delta / nI'[nI_1])$$

(the quantities in square brackets are those for Gd, determined, according to our hypothesis, by *s-f* exchange), where $A_{sf} = -\frac{1}{2}(1 - N_f)(I_0 + nI_1)$, $A_{dd} = \frac{1}{2}(1 + N_d^2)(I'_0 + nI')$, $\delta = 0.15 \times (I_0 - 4I_1)^2 n_s \div I_1 n_{d(f)}$, cf. the Table and (22.1) of Ref. 2.

---

* The same value of m is given by our relation m/M_B

$$m / M_B = N_{d(f)} - n_s + \frac{1}{2}(N_d \mp 1)I.$$

[1] S. V. Vonsovskii and K. B. Vlasov, J. Exptl. Theoret. Phys. (U.S.S.R.) 25, 327 (1953).

[2] S. V. Vonsovskii and Ia. S. Shur, *Ferromagnetism*, GTTI, 1949.

[3] H. Bethe and A. Sommerfeld, *Electron Theory of Metals*, ONTI, 1938. [Handbuch der Physik, Bd. 24/2, pp. 333-622 (1933)].

[4] F. M. Gal'perin, J. Exptl. Theoret. Phys. (U.S.S.R.) 31, 150 (1956); Soviet Phys. JETP 4, 147 (1957).

[5] J. C. Slater, Phys. Rev. 36, 57 (1930).

[6] Elliott, Legvold and Spedding, Phys. Rev. 91, 28 (1953).

[7] M. Fallot, Ann. de Physique 6, 305 (1936).

[8] E. I. Kondorskii and A. N. Fedotov, Izv. Akad. Nauk SSSR Ser. Fiz 16, 432 (1954).

Translated by W. F. Brown, Jr.
84

Quasi-Magnetic Interaction of the Spin of a Nucleon with the Rotation of the Nucleus

D. F. ZARETSKII AND A. V. SHUT'KO

(Submitted to JETP editor August 31, 1956)
J. Exptl. Theoret. Phys. (U.S.S.R.) 32, 370–371
(February, 1957)

BOHR and Mottelson[1,2] have interpreted the rotational levels of nuclei with spin 1/2 by starting out from the assumption that the Ω-projection of the total angular momentum of nucleons on the axis of symmetry of the nucleus is an integral of the motion. We can conceive of a different interpretation of the rotational levels of the nuclei, however, if we start from the following two assumptions: 1) there are absent from these nuclei the $^2\Sigma$ states which are considered according to a coupling scheme which corresponds to the case of *b* coupling according to Gund.[3] Then in the first approximation, the levels with total momenta $I = K \pm 1/2$ are degenerate (K is the rotational quantum number); 2) this degeneracy is taken into account by the introduction into the Hamiltonian of Bohr and Mottelson of an interaction of the type

$$H_{Rs} = -(\lambda / mc^2)\, \mathbf{s}[(\nabla U \mathbf{v}_{\mathrm{coll}}],$$

where λ is the dimensionless phenomenological constant which has the same meaning and value as in the usual nuclear spin–orbit coupling (see, for example, Ref. 4); s is the spin vector of the nucleon, $U(\mathbf{r})$ = self-consistent potential of the nucleus, mc^2 = rest energy of the nucleon, $\mathbf{v}_{\mathrm{coll}}$ = velocity with which the nucleon takes part in the collective motion. Introduction of the interaction (1) into the Hamiltonian of the system can be justified if we start out from the model of independent particles which move in a rotating self-consistent field.[5,6]

First, we shall make clear the meaning of $\mathbf{v}_{\mathrm{coll}}$. Consideration of the rotation of the field, as is well known, leads to the appearance in the Hamiltonian of the system (which is written relative to the rotating system of coordinates) of a perturbation of the form $H' = -\hbar\,\omega_x L_x$, where ω_x is the frequency of rotation of the field $U(\mathbf{r})$ relative to the x–axis, perpendicular to the axis of symmetry of the nucleus, L_x is the projection of the orbital momentum of the nucleons on the corresponding axis. The unperturbed Hamiltonian H_0 describes the motion of particles in the non–rotating field. We can write the perturbed wave functions, with accuracy up to first order in ω_x, in the form

$$\psi = \psi_0 + i\omega_x\psi_1, \qquad (2)$$

where ψ_0 is the unperturbed wave function, which is real for the Σ state; ψ_1 is also a real function. Then, with the same accuracy as (2), we get an expression for the current density:

$$\mathbf{j} = \psi_0^2 \mathbf{v}_{\mathrm{coll}}, \quad \mathbf{v}_{\mathrm{coll}} = (h\omega_x / m)\,\mathrm{grad}\,(\psi_1 / \psi_0). \qquad (3)$$

We can interpret this expression that for a rotation of the nucleus, each nucleon acquires an additional irrotational velocity $\mathbf{v}_{\mathrm{coll}}$.

We now make clear the meaning and origin of the interaction (1). We represent the wave function (2), with corresponding accuracy, in the form

$$\psi = \psi_0 \exp\{i\omega_x \psi_1 / \psi_0\}. \qquad (4)$$

Then the Schrödinger equation in the new representation has the form

$$H_{tr}\psi_0 = E\psi_0, \qquad (5)$$

$$H_{tr} = \exp(-i\omega_x\psi_1/\psi_0)\,H\exp(i\omega_x\psi_1/\psi_0),$$

$$H = H_0 + H'.$$

The nuclear spin–orbital interaction, which enters into H_0, has the form

$$H_{ls} = -(\lambda/m^2c^2)\,[\nabla U\mathbf{s}]\,\mathbf{p} \qquad (6)$$

(p is the momentum of the nucleon). Carrying out the transformation, it is easy to see that there is an additional interaction of first order in ω_x in H_{tr}, in addition to the interaction of type (6):

$$H_{Rs} = -(i\lambda/m^2c^2)\,[\mathbf{s}\nabla U]\,\mathbf{p}\,(\psi_1/\psi_0). \qquad (7)$$

Taking into consideration the definition for the collective velocity (3), we bring the interaction (7) to the form (1):

The velocity $\mathbf{v}_{\text{coll}}$ as a function of the coordinates is for us, strictly speaking, unknown, since it is necessary for its determination to know the wave function of the nucleons in the nucleus. Therefore, as an estimate of the magnitude of the interaction (1), we shall consider that it coincides with the velocity of the irrotational flow of an ideal incompressible fluid which is found in a rotating vessel of spheroidal form.[2] Moreover, as an estimate, we shall consider the interaction (1) in the first non–vanishing approximation in the deformation. In the $^2\Sigma$ states, the integrals of the motion are K and s, where $\mathbf{K} = \mathbf{L} + \mathbf{R}$, where $\mathbf{L}$ is the total orbital momentum of the nucleons, R is the moment of rotation of the nucleus. The rotational frequencies of the nucleus about an axis perpendicular to the axis of symmetry are given in the following form: $\omega_{x,y} = R_{x,y}/I$, where I is the moment of inertia. Averaging (1) over the wave functions of the $^2\Sigma$ states, we obtain

$$\langle H_{Rs}\rangle = \gamma\mathbf{K}\mathbf{s}, \qquad (8)$$

$$\gamma = \frac{3\lambda}{2mc^2}\langle H_{\text{int}}\rangle\frac{\hbar^2}{I}, \qquad \langle H_{\text{int}}\rangle = -\beta\langle r\frac{\partial U}{\partial r}\cdot Y_{20}\rangle,$$

$<H_{\text{int}}>$ is the energy of interaction of the nucleon with the deformations, β is a parameter of the deformation.

Different estimates[7,8] give for the quantity $<H_{\text{int}}>$ a value of the order of several mev. Assuming that $\lambda \approx 20$,[4] we get

$$\gamma \approx 0.1\,\hbar^2/I. \qquad (9)$$

Nucleus	energy of rotational level (kev)				nuclear term	$3\hbar^2/I$ (keV)	$\gamma/\left(\frac{\hbar^2}{I}\right)$
	1	2	3	4			
Tm^{169} [9]	8.40	118.30	138,10	—	Σ_g^- a Σ_u^+	74.4	0,23
W^{183} [10]	46.80	99.07	207.00	308.94	Σ_u^- a Σ_g^+	78.0	0.81
Pu^{239} [11]	7.85	57.25	75.67	—	Σ_g^- a Σ_u^+	37.5	0.42

We shall make a series of remarks on the character of the $^2\Sigma$ states in the nucleus. If the nucleus has a center and axis of symmetry, then there can exist one of the following states: $\Sigma_g^+, \Sigma_u^+, \Sigma_g^-, \Sigma_u^-$. The sign + or – characterizes the behavior of the wave function for reflection in a plane passing through the axis of symmetry, while the indices g and u characterize the behavior for inversion of the coordinates of the nucleon relative to the origin. In the case of the nucleus, the indices g and u also determine the total parity of the level. Moreover, the states $\Sigma_{g,u}^+$, just as in the shell model, correspond to single nucleon configurations, while the $\Sigma_{g,u}^-$ arise as multi–nucleon configurations. In states Σ_g^+ and Σ_u^-, the quantum number K has the values 0,2,4,. . . , while in the states Σ_u^+ and Σ_u^- it has the values 1,3,5, . . .

Results are shown in the Table of the analysis of the rotational spectra of several nuclei with spin 1/2 from the viewpoint just given. The values found for γ do not contradict, in general, the estimate (9). Therefore, it has not been excluded that for these nuclei there exist $^2\Sigma$ states. The magnetic moment of the nucleus Tm^{149}, computed under the assumption of Σ_u^+ states, agrees with the experimental value if we assume that the gyromagnetic ratio for the collective motion $g_R \approx 1$. Σ states can arise in those cases in which the energy of interaction of the nucleon with deformations is greater than the energy of spin–orbital coupling. Evidently the multiplicity of the radiative transition between components of the doublet ${}^2\Sigma$ in the rotation spectrum of nuclei with spin 1/2 ought to correspond to a magnetic dipole The available data relative to the multiplicity of the transitions in rotational spectra of the nuclei Tm^{169}, W^{183} and Pu^{239} do not contradict this rule.

In conclusion, we note that the interaction (1) will also play a role in the coupling scheme of Bohr and Mottelson, since in this case the state with given $\Omega = 1/2$ is a combination of Σ and Π states.

---

1 A. Bohr and B. Mottelson, Probl. sovrem. Fiz. 9, 34 (1955) (Russian translation).

2 A. Bohr, Probl. sovrem. fiz. 1, 5 (1956) (Russian translation).

3 G. Hersberg, *Spectra and the structure of diatomic molecules.*

4 W . Heisenberg, *Theory of the atomic nucleus.*

5 D. Inglis, Probl. sovrem. fiz. 1, 139 (1956) (Russian translation).

6 G. C. Wick, Phys. Rev. 73, 51 (1948).

7 E. Feenberg and K. C. Hammack, Phys. Rev. 81, 285 (1951).

8 D. Hill and J.Hiller, Usp. Fiz. nauk 52, 83 (1954) (Russian translation).

9 Cork, Brice , Martin, Schmid and Helmer, Phys. Rev. 101, 1042 (1956).

10 Murray, Boehm, Marmier and DuMond, Phys. Rev. 97, 1007 (1955).

11 Hollander, Smith and Mihelich, Phys. Rev. 102, 740 (1956).

Translated by R. T. Beyer
78

The Threshold of "Creation" and the Threshold of "Generation" of Negative *K*-Particles*

M. DANYSH AND B. PONTECORVO
United Institute of Nuclear Studies

(Submitted to JETP editor November 22, 1956)
J. Exptl. Theoret. Phys. (U.S.S.R.) **32**, 398-399
(February, 1957)

GELL-MANN and Pais[1] were the first to analyze the peculiar behavior of the θ^0-particles. Starting from the notion of simultaneous creation of *K*-particles and hyperons, which has been confirmed experimentally[2], the small probability for producing two hyperons in a nucleon-nucleon collision[3] leads to the idea that the *K*-particle has isotopic spin ½. This is in agreement with the Gell-Mann classification[4], and implies that the θ^0-particle is not transformed into itself by charge-conjugation, i .e., the θ^0 and $\tilde{\theta}^0$ are distinct particles. Then, when one considers the weak interactions responsible for the θ^0 decay, the transitions $\theta^0 \rightleftarrows \tilde{\theta}^0$ are no longer forbidden. This led Gell-Mann and Pais[1] to the conclusion that the θ^0-particle is a mixture of two particles $\theta_1{}^0$ and $\theta_2{}^0$ having different charge-parity and different modes of decay. Pais and Piccioni[5] proposed various versions of an experiment to test the particle-mixture character of the θ^0-particle. We suppose the experimental arrangement of Pais and Piccioni to be known to the reader.

The present paper contains some remarks on the properties of charged *K*-particles, following immediately from the considerations of Pais and Piccioni but nevertheless not yet stated explicitly in the literature. We also propose a version of the Pais-Piccioni experiment which appears to us simpler than the other schemes which have been published.

Consider the process of creation of negative *K*-particles. According to Gell-Mann[4], the threshold for creating these particles (or $\tilde{\theta}^0$-particles) in pion-nucleon or in nucleon-nucleon collisions is much higher than the threshold for creating K^+ (or θ^0) particles. This is because a K^+ or θ^0 can be created together with a hyperon, whereas a K^- or $\tilde{\theta}^0$ cannot be created with a hyperon because of the conservation of strangeness. Thus for example, in nucleon-nucleon collisions the threshold for creation of K^+ or θ^0 is around 1580 mev, while the threshold for creating K^- is around 2500 mev. However, if one looks in detail at the properties of the θ^0-particle predicted by Pais and Piccioni, then it is clear that K^--particles can be obtained from a nucleon or pion beam at an energy below the threshold for the "creation" of K^-, i.e., below the threshold for the production of a pair of *K*-particles. For at an energy below the *K*-particle pair threshold one can produce a θ^0-particle which then undergoes the transition $\theta^0 \to \tilde{\theta}^0 \to K^-$, the first step occurring in the absence of matter and the second step resulting from nuclear scattering with charge exchange. Thus the threshold for the "generation" of K^--particles in thick targets is lower than the threshold for their "creation".

The special feature of our proposed experiment is that the observation of K^--particles below the threshold for K-particle pair-production is by itself sufficient to show the correctness of the particle-mixture theory.

The experimental arrangement[5], in which it was proposed to study the variation with time of the composition of a beam of θ^0-particles by observing the decay of the short-lived $\theta_1{}^0$ and Λ^0 components, requires the use of either a cloud-chamber or a bubble-chamber. Since K^--particles have a long life-time, they could be observed in our version of the experiment at a large distance from a suitably designed synchrophasotron target. The method of observing the K -particles could then be the usual one (magnetic deflection and focussing) which was used for example in the experiments on the nuclear interactions of stopped K^--particles. This makes the experiment technically simpler.

In one possible arrangement of the experiment, the ratio (K^-/K^+) or (K^-/π^+) could be measured as a function of target size, using for example cylindrical targets with height and diameter equal. The (K^-/K^+) ratio, obtained from a proton beam of constant energy below the K^--particle "creation" threshold, should increase with the size of the target. In principle one could obtain from the experiment not only information about the $\theta_1{}^0$ and $\theta_2{}^0$ decay modes but also about the charge-exchange scattering process. One might expect that the upper limit of the (K^-/K^+) ratio at energies below the pair-creation threshold will be given by

$$(K^- / K^+) \leqslant 1/4\, (\theta^0 / K^+) \cdot \delta_{\text{opt}} / \lambda\, (\widetilde{\theta}^0 \rightarrow K^-),$$

Here (θ^0/K^+) is the ratio of the numbers of neutral and positive K-particles initially created, ¼ is the maximum number of $\widetilde{\theta}^0$-particles which can arise from a single θ^0 by the Gell-Mann-Pais-Piccioni effect, δ_{opt} is the thickness of the target* in grams per cm^3, and $\lambda(\widetilde{\theta}^0 \rightarrow K^-)$ is the mean free path for the charge-exchange process. The order of magnitude of the (K^-/K^+) ratio works out at about 0.01.

When a thick target is bombarded with protons above the K-particle pair threshold, the Gell-Mann-Pais-Piccioni effect may still markedly increase the flux of K^--particles. M. Podgoretskii has remarked that this may be important in designing experiments in which a high (K^-/π^-) ratio is required.

One may also find a relatively large probability for "charge exchange" of K^+-particles through two successive nuclear interactions $(K^+ \rightarrow \theta^0 \rightarrow \widetilde{\theta}^0 \rightarrow k^-)$. When a beam of K^+-particles bombards a thick target, the ratio of the numbers of charged K-particles which are scattered with and without charge-exchange will be, as in the previous case, of the order of magnitude 0.01.

---

* Presented at the Tiflis Conference on High-Energy Physics, October, 1956.

* The thickness δ_{opt} ought to be less (by about a factor 3) than the absorption mean free path of the K^--particles.

1 M. Gell-Mann and A. Pais, Phys. Rev. **97**, 1387 (1955); Ia. Zel'dovich, Usp. Fiz. Nauk **59**, 377 (1956).
2 Fowler, Shutt, Thorndike and Whittemore, Phys. Rev. **93**, 861 (1954); J. Steinberger, Proc. Rochester Conference, (Interscience, 1956).
3 Balandin, Balashov, Zhukov, Pontecorvo and Selivanov, J. Exptl. Theoret. Phys. **29**, 265 (1955); Soviet Phys. JETP **2**, 98 (1956).
4 M. Gell-Mann, Proc. Pisa Conference, 1955.
5 A. Pais and O. Piccioni, Phys. Rev. **100**, 1487 (1955).

Translated by F. J. Dyson
96

Nuclear Saturation and the Lévy–Klein Potential of Pseudoscalar Meson Theory

B. K. Kerimov
Moscow State University

(Submitted to JETP editor October 4, 1956)
J. Exptl. Theoret. Phys. (U.S.S.R.) 32, 377–378 (February, 1957)

THE question of nuclear saturation has been investigated[3,4] on the basis of two models of the nuclear forces[1,2] derived from pseudoscalar meson theory. The authors of Ref. 3 came to the conclusion that the Lévy potential,[1], which has a strong Wigner–type attraction produced by two–meson exchange, satisfies the requirements of nuclear saturation if one includes the repulsive three-particle force arising from pair terms. In Ref. 4 it was shown that the two–particle potential[2] derived from pseudoscalar meson theory with gradient coupling (and without pair terms), including single and double meson exchange, gives a satisfactory degree of saturation for heavy nuclei without considering three–particle repulsion, provided that one takes in account not only the repulsive core of radius r_c but also the weak repulsion in the odd P–states.

It was found earlier [5–8] that the second–order potentials of neutral pseudoscalar and scalar meson theory, supplemented by an ordinary repulsive force (independent of σ and τ), give the correct saturation at the binding energy and density of heavy nuclei. The present paper deals with the problem of nuclear stability, using the non-relativistic two-particle potential $V_{12} = V_2 + V_4{}^{(a)} + V_4{}^{(b)}$ of pseudoscalar meson theory, including terms of second and fourth order. Our result is that when the one-pair term $V_4{}^{(b)}$, which is a repulsive potential, is included in V_{12}, nuclear stability cannot be obtained even by bringing in three-particle repulsions. This contradicts the conclusions of Ref. 3.

In the non-relativistic approximation, the interaction potential between two nucleons, calculated in pseudoscalar charge-symmetric meson theory with pseudoscalar coupling, including effects of single and double meson exchange, has the form[3,9-13]

$$V_{12} = V_2 + V_4^{(a)} + V_4^{(b)}, \tag{1}$$

where

$$V_2 = \frac{1}{3}\frac{G^2}{4\pi}\left(\frac{\mu}{2M}\right)^2 (\tau_1\tau_2)\left\{\sigma_1\sigma_2 + S_{12}\left[1 + \frac{3}{\mu r} + \frac{3}{(\mu r)^2}\right]\right\}\frac{e^{-\mu r}}{r}, \tag{2}$$

$$V_4^{(a)} = -3\left(\frac{G^2}{4\pi}\right)^2\left(\frac{\mu}{2M}\right)^2 \frac{1}{\mu r^2}\,\frac{2}{\pi} K_1(2\mu r), \tag{3}$$

$$V_4^{(b)} = 6\left(\frac{G^2}{4\pi}\right)^2\left(\frac{\mu}{2M}\right)^3 \frac{1}{\mu r^2}\left(1 + \frac{1}{\mu r}\right)^2 e^{-2\mu r}. \tag{4}$$

Here S_{12} is the tensor force operator, K_1 is the first-order Hankel function, $r = |\mathbf{r}_1 - \mathbf{r}_2|$ is the distance between the nucleons, μ and M are the meson and nucleon masses, and $\hbar = c = 1$.

The strongly attractive potential $V_4{}^{(a)}$ is largely compensated by the repulsive potential $V_4{}^{(b)}$, and so the fourth-order interaction $V_4 = V_4{}^{(a)} + V_4{}^{(b)}$ produced by double meson exchange gives a weak attraction for intermediate values of r around $\mu r = 1$. This differs from the strong attraction $V_4{}^{(a)}$ which appears in the Lévy potential calculated by the Tamm-Dancoff method. Lévy made an error[9,13] in the calculation of V_{12}. The repulsive potential $V_4{}^{(b)}$, which was not included in our earlier analysis[1,3] of the properties of nuclei, will significantly change the results we obtained.

In this note we use the two-nucleon potential (1) supplemented by a repulsive core of radius r_c:

$$V_{12} = \begin{cases} V_2 + V_4^{(a)} + V_4^{(b)} & \text{for } r > r_c, \\ \infty & \text{for } r < r_c. \end{cases} \tag{5}$$

following the usual method[3,5-8] and assuming a uniform density of nuclear matter, we obtain expressions for the mean nuclear potential produced by the interaction (5):

$$\langle V_{12}\rangle = \langle V_2\rangle + \langle V_4^{(a)}\rangle + \langle V_4^{(b)}\rangle, \tag{6}$$

$$\langle V_2\rangle = -A\,\frac{9}{8}\,\mu\lambda\,\frac{\mu}{2M}\,\frac{1}{\eta^3}\int_b^\infty x e^{-x} D(\alpha x)\,dx, \tag{7}$$

$$\langle V_4^{(a)}\rangle = -A\,\frac{9}{\pi}\,\mu\lambda^2\,\frac{1}{\eta^3}\left[\frac{1}{2}K_0(2b) - \frac{1}{4}\int_b^\infty K_1(2x)\,D(\alpha x)\,dx\right], \tag{8}$$

$$\langle V_4^{(b)}\rangle = A\,9\mu\lambda^2\,\frac{\mu}{2M}\,\frac{1}{\eta^3}\left[\frac{b+2}{2b}\,e^{-2b} - \frac{1}{4}\int_b^\infty \left(1 + \frac{1}{x}\right)^2 e^{-2x}\,D(\alpha x)\,dx\right] \tag{9}$$

The notations are those of Ref. 3;

$$D(\alpha x) = [3j_1(\alpha x)/\alpha x]^2,$$

j_1 is the first-order spherical Bessel function, $R = \eta A^{1/3}\mu^{-1}$ is the nuclear radius, $(1/\mu) = 1.4 \times 10^{-13}$ cm is the meson Compton wave-length, $\alpha = 1.52/\eta$, $b = \mu r_c$, $\lambda = (G^2/4\pi)(\mu/2M)$, A is the nuclear mass number, and η is a parameter measuring the departure of the nuclear radius from its equilibrium value $R_s = A^{1/3}\mu$.

The kinetic energy of the nucleon gas, considered as a gas of hard spheres of radius r_c, is given[3] by

$$T = 14.7\,A\,(\eta^{-2} + 2.16\,b\eta^{-3})\ \text{MeV}. \tag{10}$$

The total energy of the nucleus is

$$E = \langle V_{12}\rangle + T. \tag{11}$$

a function of the parameters η, μ, λ.

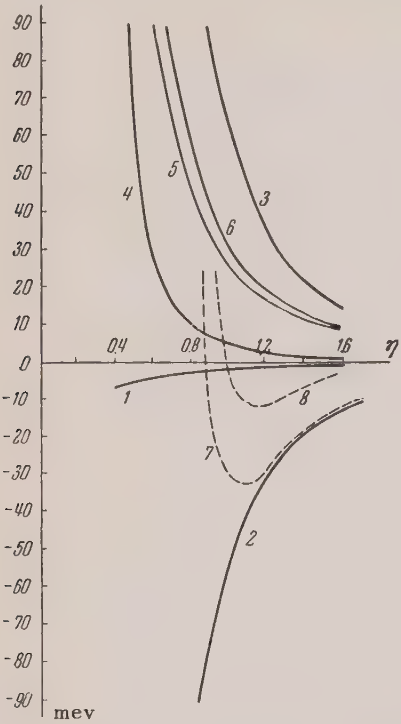

1– $<V_2>/A$; 2– $<V_4^{(a)}>/A$; 3– $<V_4^{(b)}>/A$; 4 – $<V_{12}>/A$; 5 – T/A; 6 – E/A; 7 – $<V>/A = (<V_2> + <V_4^{(a)}> + <V_{123}>)/A$; 8 – $E/A = (<V> + T)/A$. Curves 1–6 were computed by us, curves 7–8 taken from Ref. 3. All refer to $G^2/4\pi = 10$, $r_c = 0.38\ \hbar/\mu c$.

In the figure we show the potential, kinetic and total energy per nucleon as a function of η, assuming $G^2/4\pi = 10$, $r_c = 0.38\ (\hbar/\mu c)$. The curves show that the energies $(<V_{12}>/A)$ and (E/A) are positive in the range $0.3 \leq \eta \leq 1.6$. The energy $<V_4^{(b)}>$ due to two–particle repulsions completely cancels the attractive energy $<V_2> + <V_4^{(a)}>$, and so the binding energy does not saturate at normal nuclear density ($\eta \sim 1$). The same behavior of (E/A) occurs also for $(G^2/4\pi) = 7.5$, 5.2, 1 and $r_c = 0.38\ (\hbar/\mu c)$. Thus it is not necessary, in considering the nuclear saturation problem with the potential (5) derived from pseudoscalar meson theory, to introduce the three–particle repulsion which adds a positive term $<V_{123}>$ to the nuclear energy. This result contradicts our earlier statement[3] that the Lévy potential (without the $V_4^{(b)}$ term)

$$V_{12} = \begin{cases} V_2 + V_4^{(a)}, & r > r_c, \\ \infty & r < r_c, \end{cases}$$

supplemented by the three–particle repulsion, will produce saturation in heavy nuclei. Actually, the term $(<V_{123}>/A)$ due to three–particle repulsions, in the absence of the $V_4^{(b)}$ term, just sufficiently weakens the strong attraction $(<V_{12}>/A)$ so that the total energy per nucleon (E/A) has a minimum of –12 mev at normal nuclear density (η = 1– 1.5). Our calculation shows that the Lévy–Klein potential defined by Eq. (5) gives no nuclear saturation, either with or without the addition of a three–particle repulsion.

In conclusion I thank Professor A. A. Sokolov for criticism and valuable comments.

---

1 M. M. Levy, Phys. Rev. 88, 725 (1952).
2 K. A. Brueckner and K. M. Watson, Phys. Rev. 92, 1027 (1953).
3 S. D. Drell and K. Huang, Phys. Rev. 91, 1527 (1953).
4 Brueckner, Levinson and Mahmond, Phys. Rev. 95, 217 (1954).
5 B. Kerimov, J. Exptl. Theoret. Phys. (U.S.S.R.) 24, 299 (1953).
6 A. Sokolov and B. Kerimov, J. Exptl. Theoret. Phys. (U.S.S.R.) 26, 430 (1954).
7 B. Kerimov and A. Dzhavadov, J. Exptl. Theoret. Phys. (U.S.S.R.) 30, 900 (1956); Soviet Phys. JETP 3, 713 (1956).
8 D. Ivanenko and B. Kerimov, J. Exptl. Theoret. Phys. (U.S.S.R.) 31, 105 (1956); Soviet Phys. JETP 4, 417 (1957).
9 A. Klein, Phys. Rev. 90, 1101 (1953).
10 T. Hamada and M. Sugawara, Progr. Theor, Phys. 9, 555 (1953).
11 I. A. Kvasnikov, Diploma research, Moscow State Univ., 1954.
12 D. Feldman, Phys. Rev. 98, 1456 (1955).
13 H. A. Bethe and F. DeHoffman, *Mesons and Fields*, Vol. 2, New York, 1955.

Translated by F. J. Dyson
82

The Problem of Parity Non-conservation in Weak Interactions

B. L. IOFFE, L. B. OKUN' AND A. P. RUDIK

(Submitted to JETP editor November 21, 1956)
J. Exptl. Theoret. Phys. (U.S.S.R.) 32, 396–397
(February, 1957)

ONE of the possible theoretical explanations of the paradox of the θ and τ–decay of K-mesons[1] is the hypothesis of parity non-conservation in weak interactions. Lee and Yang[2] showed that parity non-conservation in weak interactions could not have been detected by any experiments which have yet been performed (except, of course, the K-meson decay experiments), and they proposed several experiments by which the conservation of parity could be tested. However, Yang and Lee did not require that the weak interactions be invariant under time-reversal or charge-conjugation.* If one assumes that space-parity is not conserved, and that the θ and τ particles are identical, then the existence of a long-lived K°-particle [4] can be explained by supposing either that charge-parity or time-parity is conserved. The analysis of correlation experiments by Lee and Yang assumes that time-parity is conserved and charge-parity is not conserved.

We have found that, in the absence of conservation of space-parity, there exists an experimental test to decide whether charge-parity or time-parity is conserved in weak interactions. Namely, if time-parity is conserved, the long-lived (odd with respect to time-reversal) K°-particle can decay into 3 pions or into 3 π°-mesons forming an S-state, while this process is forbidden if charge-parity is conserved. We shall show that if one assumes conservation of charge-parity one is led to results quite different from those of Lee and Yang.

The invariance of the Hamiltonian under charge conjugation implies certain well-known phase-relations[3,5] between the coefficients multiplying the various interactions. Consider first of all the decay $\Lambda^\circ \rightarrow p + \pi$. If parity-conservation is dropped, the interaction Hamiltonian for this process must have the form

$$H = g\,(\bar{\psi}_p\,\psi_\Lambda)\,\varphi_\pi + iG\,(\bar{\psi}_p\gamma_5\psi_\Lambda)\,\varphi_\pi \qquad (1)$$

$$+ g^*\,(\bar{\psi}_\Lambda\psi_p)\,\overset{+}{\varphi}_\pi + iG^*\,(\bar{\psi}_\Lambda\gamma_5\psi_p)\,\overset{+}{\varphi}_\pi .$$

assuming that interactions containing derivatives are excluded. The operation of charge-conjugation is as usual described by

$$\varphi'(x) = \varphi^+(x);$$

$$\psi'(x) = -\bar{\psi}(x)\,C^{-1}; \quad \bar{\psi}'(x) = C\psi(x),$$

where the matrix C satisifies the conditions

$$C^T = -C; \quad CC^+ = 1; \quad \gamma_\mu^T = -C\gamma_\mu C^{-1}.$$

We use the Feynman notations

$$\gamma_\mu = \{\beta\alpha,\ \beta\}; \quad \gamma_5 = -i\gamma_1\gamma_2\gamma_3\gamma_4,$$

$$\hat{a} = \gamma_\mu a_\mu = -\beta\alpha\mathbf{a} + \beta a_4.$$

We apply the operation of charge-conjugation to Eq. (1),rememberingthat $\gamma_5{}^T = C\gamma_5 C^{-1}$, and conclude that for invariance it is necessary that g and G be real*.

When parity is not conserved, the square of a transition matrix element may contain pseudoscalar as well as scalar terms. To determine whether pseudoscalar terms appear in the Λ°-decay, we consider the decay of a polarized Λ° at rest. Assuming the Hamiltonian (1), the square of the matrix element, summed over the proton spin and with neglect of the proton-meson interaction, becomes

$$\sum |M|^2 = \{g^2\bar{u}_\Lambda\,(\hat{p}+m)\,u_\Lambda - G^2\bar{u}_\Lambda\,\gamma_5\,(\hat{p}+m)\,\gamma_5 u_\Lambda$$

$$+ igG\bar{u}_\Lambda\,[\gamma_5\,(\hat{p}+m) + (\hat{p}+m)\,\gamma_5]\,u_\Lambda\}\,/\,2E_p, \qquad (2)$$

Here $\hat{p}$ is the proton momentum and m its mass. A pseudoscalar term (proportional to σp, where σ is the spin of the Λ°) can only appear in the interference term, but it anyway vanishes since

$$\bar{u}_\Lambda\gamma_5 u_\Lambda = 0.$$

In a similar way, it is easy to show that pseudoscalar terms proportional to pσ must vanish even when both scalar and vector interactions are present. It follows that in the two-step process, $\pi^- + p \rightarrow \Lambda^\circ + K^\circ$, $\Lambda^\circ \rightarrow p + \pi^-$, considered by Lee and Yang, the differential probability will not contain any pseudoscalar term proportional to $(\mathrm{p}_\pi\,\mathrm{p}_\Lambda\,\mathrm{p}_p)$; in this case the only effect of the first strong interaction is to produce polarized Λ°-particles. Hence it is impossible to detect any non-conservation of parity by observing the angular distribution of protons in Λ°-decay. A test of parity conservation is possible only by observing radiative Λ°-decay. In the radiative decay the pseduoscalar interference terms again vanish, but the photon spectrum will be different according as parity is or is not conserved. Only if parity is not conserved can terms proportional to g^2 and to G^2 exist together in the expression for the spectrum*. All these remarks apply equally to the decay of $\Sigma^\pm$-particles.

The beta-decay is another weak process in which effects of non-conservation of parity might be observed. If parity is not conserved, the interaction

Hamiltonian becomes

$$H=(\overline{\psi}_p\psi_n)\,(c_S\overline{\psi}_e\psi_\nu+ic'_S\overline{\psi}_e\gamma_5\psi_\nu) \tag{3}$$

$$+(\overline{\psi}_p[\gamma_\mu,\,\gamma_\nu]\,\psi_n)\;\{c_T\,(\overline{\psi}_e\,[\gamma_\mu,\,\gamma_\nu]\,\psi_\nu)$$

$$+ic'_T\,(\overline{\psi}_e\gamma_5\;[\gamma_\mu,\gamma_\nu]\,\psi_\nu)\}+\text{Herm. conj.}$$

$$[\gamma_\mu,\;\gamma_\nu]={}^1/_2\,(\gamma_\mu\gamma_\nu-\gamma_\nu\gamma_\mu),$$

We confine the discussion to the scalar and tensor interactions which have been experimentally observed. Invariance under charge conjugation implies that C_S, $C_S{}'$, C_T, $C_T{}'$ be real.

We consider the β-decay of a polarized nucleus. We calculate from Eq. (3) the square of the transition matrix element and sum over the neutrino spin. The only surviving pseudoscalar terms are those arising from interference of the scalar and tensor interactions, since the terms proportional to C_S, $C_S{}'$ and to $C_T\,C_T{}'$ vanish identically. After summing over the electron spin, we find

$$(4/E_\nu E_e)\,(c'_S\,c_T-c_S\,c'_T) \tag{4}$$

$$\times\Big\{\mathrm{Im}\Big(\int\overline{\psi}_p\psi_n\exp\,[-i\,(\mathbf{p}_e-\mathbf{q})\,\mathbf{r}]\;d\mathbf{r}$$

$$\times\int\overline{\psi}_n\sigma\psi_p\exp\,[i\,(\mathbf{p}_e-\mathbf{q})\,\mathbf{r}]\,d\mathbf{r}\Big)\Big(\mathbf{q}E_e-\mathbf{p}E_\nu\Big)$$

$$+\mathrm{Re}\Big(\int\overline{\psi}_p\psi_n\,\exp\,[-i\,(\mathbf{p}_e-\mathbf{q})\,\mathbf{r}]\,d\mathbf{r}$$

$$\times\int\overline{\psi}_n\alpha\psi_p\exp\,[i\,(\mathbf{p}_e-\mathbf{q})\,\mathbf{r}]\,d\mathbf{r}\;\Big)\;[\mathbf{pq}]\Big\}$$

where $\mathbf{q}$ is the neutrino momentum. Equation (4) is easy to evaluate in the case of the beta-decay of a polarized free neutron. If we suppose that the polarization of the proton is not observed and sum over the proton spin, the result is again zero.

In the case of any allowed transition, Eq. (4) still vanishes. For an allowed transition we may keep only the first term in the curly bracket and replace the exponential exp $[i\,(\mathbf{p}_e-\mathbf{q})\,\mathbf{r}\,]$ by unity. Then the presence of the scalar interaction requires that initial and final state have the same values of total angular momentum and of z-component of angular momentum. But the diagonal elements of the Hermitian matrices σ are real, so that Eq. (4) is zero. For allowed transitions, Eq. (4) still vanishes, at least to order $(Ze/\hbar v)$, when the Coulomb interaction is taken into account.

Thus we have shown that for the simplest beta-decay processes, if charge-conjugation invariance holds, there is no difference between the consequences of conservation and non-conservation of space-parity.

The authors express their sincere appreciation to Professors V. B. Berestetskii and V. V. Sudakov for criticism and to I. Ia. Pomeranchuk for his interest in this work.

---

*Pauli[3] has discussed these problems in a general way. It is important to observe that, when parity is not conserved, charge conjugation ceases to be equivalent to time reversal. Pauli proved that, assuming the ordinary relation between spin and statistics, the Lagrangian must be invariant under the combined operation of charge-conjugation and inversion of all four coordinates.

*We assume that spinors belonging to different fields anticommute. If we assumed that they commute, we should obtain only a common unobservable phase-factor.

*This situation could however be simulated if there exist two Λ^0-particles with opposite parity and almost equal lifetime.

Note added in proof. (February 14, 1957)

We recently heard of the results of the experiments of Professor Wu on the β-decay of oriented cobalt nuclei. In these experiments a correlation was found between the nuclear spin and the direction of the electron momentum (a term $\sigma\mathbf{p}$). The arguments given above show that this implies a non-conservation in beta-decay of both space-parity and charge-parity.

1 Orear, Harris and Taylor, Phys. Rev. 102, 1676 (1956).

2 T. D. Lee and C. N. Yang, Phys. Rev. 104, 254 (1956).

3 W. Pauli, *Niels Bohr and the Development of Physics*, (Pergamon Press, London, 1955).

4 Lande, Booth, Impeduglia, Lederman and Chinowsky, Phys. Rev. 103, 1901 (1956); Fry, Schneps and Swami, Phys. Rev. 103, 1904 (1956).

5 H. A. Tolhoek and S. R. DeGroot, Phys. Rev. 84, 150 (1951).

Translated by F.J. Dyson
95

Diffractive Production of Proton-Antiproton Pairs by High Energy Photons

A. G. Sitenko and L. N. Rosentsveig
Physico-Technical Institute,
Ukrainian Academy of Sciences

(Submitted to JETP editor October 15, 1956)
J. Exptl. Theoret. Phys. (U.S.S.R.) 32, 383
(February, 1957)

THE production of a proton-antiproton pair by a photon may be considered as a first-order process for which the matrix element is given by

$$S_{i\to f}=-\frac{e}{\sqrt{2\omega}}\int\bar{\psi}_p^{(-)}(\gamma\mathrm{e})\,e^{ikx}\,\psi^{(+)}_{-\tilde{p}}\,d^4x; \qquad (1)$$

Here $\psi_p^{(-)}$ is the wave function of a proton in the field of the nucleus, behaving asymptotically like a plane wave of momentum p together with an ingoing spherical wave. $\psi^{(+)}_{-\tilde{p}}$ is the wave-function of a proton with negative energy $-\tilde{E}$, behaving asymptotically like a plane wave of momentum $-\tilde{\mathrm{p}}$ with an outgoing spherical wave. e is the polarization vector of the photon. The proton-antiproton interaction is neglected; this is allowable when the photon energy ω is not too close to the threshold. The wave-functions $\psi_p^{(-)}$ and $\psi_{-\tilde{p}}^{(+)}$ are constructed by means of the optical model, in which the interactions of the proton and antiproton with the nucleus are described phenomenologically.

The problem becomes very simple in the limit $\omega \gg 2M$, when the important part of the matrix element comes from a region far from the nucleus, where the wave functions behave like a superposition of a plane wave and a wave diffracted by the nucleus. Akhiezer[1] has worked out the theory of diffraction for spinor waves, and he finds for the wave function of a spin $-1/2$ particle scattered by a completely black absorbing nucleus of radius R

$$\psi^{(+)}_{-\tilde{p}}=-\frac{1}{4\pi}\int\left(\gamma\frac{\partial}{\partial\mathrm{x}}+\gamma_4\tilde{E}-M\right) \qquad (2)$$

$$\times\frac{e^{i\tilde{p}\,|\mathrm{x}-\rho|}}{|\mathrm{x}-\rho|}(\gamma\tilde{\mathrm{n}})\,v_{-\tilde{p}}\,d\rho\cdot e^{i\tilde{E}t},$$

$$(\rho\geqslant R,\ \rho\perp\mathrm{n}).$$

Here the integration extends over a plane through the center of the nucleus and perpendicular to the unit vector $\tilde{\mathrm{n}}=(\tilde{\mathrm{p}}/|\tilde{\mathrm{p}}|)$. $v_{-\tilde{p}}$ is the spinor amplitude of the plane wave with momentum $-\tilde{\mathrm{p}}$ and negative energy $-\tilde{E}$. Similarly,

$$\bar{\psi}_p^{(-)}=\frac{1}{4\pi} \qquad (3)$$

$$\times\int\bar{u}_p(\gamma\mathrm{n})\left(\gamma\frac{\partial}{\partial\mathrm{x}}+\gamma_4E+M\right)\frac{e^{ip\,|\mathrm{x}-\rho|}}{|\mathrm{x}-\rho|}\,d\rho\cdot e^{iEt},$$

$$(\rho\geqslant R,\ \rho\perp\mathrm{n}),$$

with $\mathrm{n}=(\mathrm{p}/|\mathrm{p}|)$. The Coulomb interaction between the nucleons and the nucleus is neglected.

The idea of diffractive scattering only makes sense at small angles. Supposing the angles between the pair momenta p, $\tilde{\mathrm{p}}$ and the phonon momentum k to be small, and the energies E, $\tilde{E}$ large compared with M, the cross-section for proton-antiproton pair production by a black uncharged nucleus becomes

$$d\sigma=\frac{e^2}{32\pi^3}\frac{E\tilde{E}}{\omega^3} \qquad (4)$$

$$\times\frac{R^2J_1^2(MR\,|\xi+\eta|)}{|\xi+\eta|^2}\left[\frac{2(\xi+\eta)^2}{(1+\xi^2)(1+\eta^2)}\right.$$

$$+\frac{\omega^2}{E\tilde{E}}\left(\frac{\xi}{1+\xi^2}-\frac{\eta}{1+\eta^2}\right)^2$$

$$\left.+\left(2+\frac{\omega^2}{E\tilde{E}}\right)\left(\frac{1}{1+\xi^2}+\frac{1}{1+\eta^2}\right)^2\right]d\tilde{E}\,d\xi\,d\eta;$$

with the vectors ξ and η defined by

$$\begin{gathered}\mathrm{p}=(\mathrm{p}\varkappa)\varkappa+M\xi,\qquad\tilde{\mathrm{p}}=(\tilde{\mathrm{p}}\varkappa)\varkappa+M\eta.\\ \varkappa=\mathrm{k}/\omega,\qquad\xi\varkappa=\eta\varkappa=0;\\ d\xi=(E/M)^2\,d\Omega,\qquad d\eta=(\tilde{E}/M)^2\,d\tilde{\Omega}.\end{gathered} \qquad (5)$$

Unlike the Born approximation formulas, the expression (4) cannot be obtained from the corresponding expression[1] for the bremsstrahlung of a proton diffractively scattered by a black uncharged nucleus by substituting $-\tilde{p}$, p, $-k$ for p, p', k. The reason is that in the extreme relativistic limit the diffracted waves hardly overlap at all in bremsstrahlung but overlap strongly in pair-production.

If we assume a finite size for the nucleon,[2] a form-factor will appear in Eq.(4). We have not included any effect of the anomalous magnetic moment of the nucleon.

---

[1] A. I. Akhiezer, Dokl. Akad.Nauk SSSR 94, 651(1954).

[2] I. Ia. Pomeranchuk, Dokl. Akad. Nauk SSSR 96, 265 and 481 (1954).

Translated by F. J. Dyson
85

Internal Compton Effect in Pair Conversion

E. G. MELIKIAN
Moscow State University

(Submitted to JETP editor October 30,1956)
J. Exptl. Theoret. Phys. (U.S.S.R.) 32, 384–385
(February, 1957)

IF the energy difference between excited and ground state is greater than $2\,mc^2$ (m is the electron mass), then a nucleus in the excited state may decay by emission of an electron-positron pair togetherwith a photon. We call this process the internal Compton effect in pair conversion. We exhibit below the formulas for the relative differential probability of this process (i. e., the ratio of the absolute probability of internal Compton effect in pair conversion to the probability of a simple radiative transition), calculated in Born approximation.

The Feynman diagrams for this process are analogous to those appearing in the calculation[1] of internal Compton effect involving the atomic electrons. We maintain the notations of the earlier calculation[1], except that ϵ_+, ϵ_-, p_+, p_- now denote the energy and momentum of the positron and electron.

The relative differential cross-section for a magnetic 2^j-pole transition is

$$\begin{aligned} d\gamma_j^{(\mathrm{M})} = {} & \frac{4(2j+1)\alpha^2 k p_+ p_-}{(2\pi)^3 P}\left(\frac{P}{\Delta E}\right)^{2j+1}\frac{1}{(P^2-\Delta E^2)^2}\Big\{kp_+\left[\cos(\mathbf{p}_+\mathbf{k})-\cos(\mathbf{p}_+\mathbf{P})\cos(\mathbf{kP})\right] \\ & \times\Big[\frac{m^2+(p_-k)}{(p_-k)^2}+\frac{(p_+p_-)}{(p_-k)(p_+k)}\Big]+kp_-\left[\cos(\mathbf{p}_-\mathbf{k})-\cos(\mathbf{p}_-\mathbf{P})\cos(\mathbf{kP})\right]\Big[\frac{m^2+(p_+k)}{(p_+k)^2} \\ & +\frac{(p_+p_-)}{(p_+k)(p_-k)}\Big]+p_+p_-\left[\cos(\mathbf{p}_+\mathbf{p}_-)-\cos(\mathbf{p}_+\mathbf{P})\cos(\mathbf{p}_-\mathbf{P})\right]\Big[\frac{m^2}{(p_-k)^2}+\frac{m^2}{(p_+k)^2} \\ & +\frac{(p_+p_-)+(p_++p_-,k)}{(p_-k)(p_+k)}\Big]+\frac{m^2k^2}{(p_-k)(p_+k)}\sin^2(\mathbf{kP})-\frac{p_-^2}{(p_-k)}\sin^2(\mathbf{p}_-\mathbf{P})-\frac{p_+^2}{(p_+k)}\sin^2(\mathbf{p}_+\mathbf{P}) \\ & -\frac{m^2(p_+P)}{(p_-k)^2}-\frac{m^2(p_-P)}{(p_+k)^2}-\frac{m^2+(p_+k)}{(p_-k)}-\frac{m^2+(p_-k)}{(p_+k)} \\ & -2\frac{(p_+p_-)\left[(p_+p_-)+(p_++p_-,k)-m^2\right]}{(p_+k)(p_-k)}\Big\}\sin\vartheta_-d\vartheta_-do_+dk\,d\varepsilon_+, \end{aligned}$$

Here $(p_+p_-) = \mathbf{p}_+\mathbf{p}_- - \epsilon_+\epsilon_-$ is the scalar product of the 4-vectors p_+ and p_-. The z-axis is taken along the direction of $\mathbf{k}$, $\vartheta_\pm$ are the polar angles of the vectors $\mathbf{p}_\pm$, and

$$do_+ = \sin\vartheta_+ d\vartheta_+\,d\varphi_+;\ \mathbf{P} = \mathbf{p}_+ + \mathbf{p}_- + \mathbf{k}.$$

The relative differential cross-section for an electric $2j$-pole transition is

$$\begin{aligned} d\gamma_j^{(\mathrm{э})} = {} & \frac{4(2j+1)\alpha^2 p_+p_-k}{(2\pi)^3(j+1)P}\left(\frac{P}{\Delta E}\right)^{2j+1}\frac{1}{(P^2-\Delta E^2)^2}\Big\{2\Big[\frac{m^2+(p_-k)}{(p_-k)^2}+\frac{(p_+p_-)}{(p_-k)(p_+k)}\Big] \\ & \times\Big[jk\varepsilon_+-jk\varepsilon_+\frac{\Delta E}{P}\cos(\mathbf{kP})-jkp_+\frac{\Delta E}{P}\cos(\mathbf{p}_+\mathbf{P})+\frac{k\Delta E^2}{2P^2}p_+((j+1)\cos(\mathbf{kp}_+) \\ & +(j-1)\cos(\mathbf{kP})\cos(\mathbf{p}_+\mathbf{P}))\Big]+2\Big[\frac{m^2+(p_+k)}{(p_+k)^2}+\frac{(p_+p_-)}{(p_+k)(p_-k)}\Big] \\ & \times\Big[jk\varepsilon_--jk\varepsilon_-\frac{\Delta E}{P}\cos(\mathbf{kP})-jkp_-\frac{\Delta E}{P}\cos(\mathbf{p}_-\mathbf{P})+p_-\frac{k\Delta E^2}{2P^2}((j+1)\cos(\mathbf{p}_-\mathbf{k}) \\ & +(j-1)\cos(\mathbf{kP})\cos(\mathbf{p}_-\mathbf{P}))\Big]+2\Big[\frac{m^2}{(p_-k)^2}+\frac{m^2}{(p_+k)^2}+\frac{(p_+p_-)+(p_++p_-,k)}{(p_-k)(p_+k)}\Big] \\ & \times\Big[j\varepsilon_+\varepsilon_--j\varepsilon_+p_-\frac{\Delta E}{P}\cos(\mathbf{p}_-\mathbf{P})-j\varepsilon_-p_+\frac{\Delta E}{P}\cos(\mathbf{p}_+\mathbf{P})+p_+p_-\frac{\Delta E^2}{P^2}((j+1)\cos(\mathbf{p}_+\mathbf{p}_-) \\ & +(j-1)\cos(\mathbf{p}_+\mathbf{P})\cos(\mathbf{p}_-\mathbf{P}))\Big]-\frac{2}{(p_-k)}\Big[j\varepsilon_-^2-2j\varepsilon_-p_-\frac{\Delta E}{P}\cos(\mathbf{p}_-\mathbf{P}) \\ & +\frac{p_-^2\Delta E^2}{2P^2}((j-1)\cos^2(\mathbf{p}_-\mathbf{P})+2)\Big]-\frac{2}{(p_+k)}\Big[j\varepsilon_+^2-2j\varepsilon_+p_+\frac{\Delta E}{P}\cos(\mathbf{p}_+\mathbf{P}) \\ & +\frac{p_+^2\Delta E^2}{2P^2}((j-1)\cos^2(\mathbf{p}_+\mathbf{P})+2)\Big]+\frac{2m^2k^2}{(p_+k)(p_-k)}\Big[j-2j\frac{\Delta E}{P}\cos(\mathbf{kP}) \\ & +\frac{\Delta E^2}{2P^2}((j-1)\cos^2(\mathbf{kP})+2)\Big]+\Big[j-(2j+1)\frac{\Delta E^2}{P^2}\Big]\Big[\frac{m^2}{(p_-k)^2}(p_+P) \\ & +\frac{m^2}{(p_+k)^2}(p_-P)+\frac{m^2+(p_+k)}{(p_-k)}+\frac{m^2+(p_-k)}{(p_+k)}+2\frac{(p_+p_-)\left[(p_+p_-)+(p_++p_-,k)-m^2\right]}{(p_+k)(p_-k)}\Big]\Big\} \\ & \times\sin\vartheta_-d\vartheta_-do_+dk\,d\varepsilon_+. \end{aligned}$$

These formulas become much simpler in the extreme relativistic limit. After integrating over angles, the relative differential probability becomes identical for magnetic and electric transitions, namely

$$d\gamma_j = \frac{(2j+1)\,\alpha^2}{2\,(2\pi)^3}$$

$$\times\left(1 - \frac{m^2\,(\Delta E - k)}{\Delta E\,\varepsilon_+\varepsilon_-}\right)^j \frac{(\varepsilon_+^2 + \varepsilon_-^2)\,k)}{(\Delta E - k)^2\,\Delta E^3}\,dk\,d\varepsilon_+.$$

The ratio of the differential probability for internal Compton effect to the probability for ordinary internal pair-conversion is roughly given by

$$d\gamma_j/d\beta_j = (\alpha/2\pi)\,k\,dk/(\Delta E - k)^2,$$

provided that $\Delta E\text{-}K >> m$.

In conclusion the author thanks I. S. Shapiro for valuable advice and assistance.

---

1. E. G. Melikian, J. Exptl, Theoret, Phys. (U.S.S.R.) 31, 1088 (1956); Soviet Phys. JETP

Translated by F. J. Dyson
86

The Momentum Distribution of Interacting Fermi Particles

A. B. MIGDAL

(Submitted to JETP editor November 22,1956)
J. Exptl. Theoret. Phys. (U.S.S.R) 32, 399–400
(February, 1957)

WE consider a system composed of a large number of interacting Fermi-particles. It is to be expected that among the excited states of the system there will exist states whose energy can be expressed as a sum of energies of quasi-particles. The energy of a quasi-particle of momentum p is

$$\varepsilon_p = v_0\,(p - p_0),$$

where p_0 is the momentum at the top of the Fermi sea of the quasi-particles, $v_0 = v\,(p_0)$ is the velocity of a quasi-particle at the Fermi surface, $p > p_0$ for quasi-particles and $p < p_0$ for holes. The momentum p_0 need not coincide with the limiting momentum p_0^0 determined by the density,

$$p_0^0 = (3\pi^2 n)^{1/3}, \qquad (\hbar = 1).$$

It is easy to see that the quasi-particles have an attenuation proportional to $(p - p_0)$.[2] This means that for p_0 not close to p_0 an excited state of a system with strong interactions cannot be described in terms of quasi-particles. As $p \to p_0$ the state becomes describable in terms of quasi-particles even when the interaction is strong. We shall prove that the momentum distribution of the particles in the ground state has a discontinuity at $p = p_0$, for any kind of interaction. This result refers to the distribution of particles and not of quasi-particles.

The one-particle Green's function is defined by

$$G\,(\mathbf{r}_1, t_1, \mathbf{r}_2, t_2) \tag{1}$$

$$= i\,\langle T e^{iHt_1}\,\Psi\,(\mathbf{r}_1)\,e^{-iH\,(t_1 - t_2)}\,\Psi^+\,(\mathbf{r}_2)\,e^{iHt_2}\rangle,$$

where the expectation value is taken in the ground state of the system $\Psi\,(\mathbf{r}) = \Sigma\, a_{\mathbf{p}}\, e^{i\,\mathbf{pr}}$, and $a_{\mathbf{p}}$ is the annihilation operator for a particle of momentum p. If there is no external field, G is a function only of $r = |\mathbf{r}_1 - \mathbf{r}_2|$ and $\tau = t_1 - t_2$. Expressing G as a Fourier series in coordinate space, we find

$$G\,(r, \tau) = \sum G\,(p, \tau)\, e^{i\,\mathbf{pr}}; \tag{2}$$

$$G\,(p, \tau) = \begin{cases} i e^{iE_0\tau} < a_p e^{-iH\tau} a_p^+ >, & \tau > 0, \\ -i e^{-iE_0\tau} < a_p^+ e^{iH\tau} a_{\mathbf{p}} >, & \tau < 0. \end{cases}$$

This equation connects the function $G\,(p, \tau)$ with the momentum distribution of particles in the ground state, which is

$$n\,(p) = < a_p^+ a_{\mathbf{p}} > = iG\,(p, \tau)\,|_{\tau \to -0}.$$

Writing

$$G\,(p, \tau) = \int G\,(p, \varepsilon)\, e^{-i\varepsilon\tau}\, d\varepsilon\,/\,2\pi,$$

we obtain

$$n(p) = i\int G(p, \varepsilon)\, e^{-i\varepsilon\tau}\, d\varepsilon / 2\pi,$$
$$\tau \to -0.$$

In the last integral we must not take the limit $\tau = 0$ before integration, since the integral $\int G(p, \epsilon)\, d\epsilon$ diverges along the real axis. For finite negative τ, we can replace the integral along the real axis by an integral round a closed contour C consisting of the real axis together with a semi-circle at infinity in the upper half-plane. After this we can set $\tau = 0$. Thus we have

$$n(p) = i\int_C G(p, \varepsilon)\, d\varepsilon / 2\pi. \qquad (3)$$

The Green's function must have poles corresponding to quasi-particles. This follows from the representation of the Green's function in terms of the eigenstates of the whole system, according to the procedure of Lehmann.[1] Therefore, for p close to p_0,

$$G(p, \varepsilon) = Z / (\varepsilon_p - \varepsilon - i\gamma(p)) + f(p, \varepsilon)$$

where $f(p, \epsilon)$ is a function regular at $\epsilon = \epsilon_p - i\gamma$, and γ defines the attenuation of a quasi-particle and changes sign at $p = p_0$ as is required in order to give the correct sign for the attenuation of holes. The constant Z may be called the renormalization constant of the Green's function. When $p < p_0$, $\gamma < 0$ and G has a pole in the upper half-plane near to the real axis. When $p > p_0$, $\gamma > 0$ and this pole crosses to the lower half-plane where it is outside the contour C. Therefore,

$$n(p_0 - 0) - n(p_0 + 0) = Z, \qquad (4)$$

and since $0 \leq n(p) \leq 1$, the renormalization constant satisfies the inequality $|Z| \leq 1$.

---

[1] H. Lehman, Nuovo Cimento 11, 342 (1954); reproduced in "Problems of Modern Physics," 3, 1955.

Translated by F. J. Dyson
97

The μ-decay of K-particles and Hyperons

L. B. OKUN'

(Submitted to JETP editor November 22, 1956)
J. Exptl. Theoret. Phys. (U.S.S.R.) 32, 400–402
(February, 1957)

RECENTLY Schwinger[1] suggested that the weak interactions of μ-mesons and neutrinos with pions and K-particles are primary, and that the interactions of μ-mesons with hyperons and nucleons are secondary effects of the weak primary boson-fermion interaction. We here consider some elementary consequences of this hypothesis and discuss possible experimental tests of it.*

We suppose that the decays

$$\pi^\pm \to \mu^\pm + \nu \text{ and } K^\pm \to \mu^\pm + \nu, \qquad (1)$$

are primary, and that all other interactions of μ-meson and neutrino with baryons and heavy mesons are results of a chain of interactions of which the process (1) constitutes one link. Such a chain of interactions can describe in particular the μ-decay of hyperons (e. g., $\Lambda^\circ \to p + K^- \to p + \mu^- + \nu$) and the so-called $K_{\mu 3}$-decay of K-particles (e. g., $K^+ \to \pi^\circ + K^+ \to \pi^\circ + \mu^+ + \nu$). The other links in the chain must be strong interactions. Thus the other links cannot be processes in which strangeness is not conserved, such as $K^+ \to \pi^+ + \pi^\circ$, $\Lambda^\circ \to p + \pi^-$, etc.

The last remark implies that every μ-decay of particles with strangeness $+1$ (the K^+ and K°-particle and the anti-hyperons $\bar{\Lambda}$ and $\bar{\Sigma}$) must go via the μ-decay of the K^+ ($K^+ \to \mu^+ + \nu$) while the μ-decay of particles with strangness -1 (K^- and $\bar{K}^\circ$ and the hyperons Λ and Σ must go via the K^- decay ($K^- \to \mu^- + \nu$). So for the K°-particle, the decay

$$K^0 \to \mu^+ + \nu + \pi^- \qquad (2)$$

is allowed, while

$$K^0 \to \mu^- + \nu + \pi^+; \qquad (2')$$

is forbidden, and for the $\bar{K}^\circ$, the decay

$$\bar{K}^0 \to \mu^- + \nu + \pi^+ \qquad (3)$$

is allowed while

$$\bar{K}_0 \to \mu^+ + \nu + \pi^-. \qquad (3')$$

is forbidden. Also, in order to construct the two-step chain for the $K_{\mu 3}$ decay, we must have two types of K-particle, a scalar θ and a pseudoscalar τ, if the K-particle spin is zero. Otherwise, since the pion is pseudoscalar, parity would not be conserved in the process $K \to K + \pi$, and this is a strong interaction which must conserve parity. If we assume that the processes $\theta \rightleftarrows \tau + \pi$ and $\tau \rightleftarrows \theta + \pi$ conserve isotopic spin, it is easy to derive a relation between the probabilities of the processes

$$a)\ K^0 \rightarrow \mu^+ + \nu + \pi^-, \quad b)\ K^+ \rightarrow \mu^+ + \nu + \pi^0.$$

We find* that $w_a = 2w_b$.

It is well known[2–4] that the ratio of μ^+ to μ^- decays in a beam of K°-particles will vary with time or with distance from the point of origin of the beam. This depends on the fact that the ratio of $\overline{K}^\circ$ to K° in the beam is variable. Consider for definiteness a beam of θ°-particles. At $t = 0$ there are no $\overline{\theta}^\circ$-particles present:

$$N(\theta^0,\ t = 0) = N_0; \quad N(\overline{\theta}^0,\ t = 0) = 0.$$

Then[3] after a time t,

$$N(\theta^0,\ t) = \frac{1}{4} N_0 [e^{-t/\tau_1} + e^{-t/\tau_2} + 2e^{-t/2\tau_1 - t/2\tau_2} \cos \Delta mt],$$

$$N(\overline{\theta}^0,\ t) = \frac{1}{4} N_0 [e^{-t/\tau_1} + e^{-t/\tau_2} - 2e^{-t/2\tau_1 - t/2\tau_2} \cos \Delta mt].$$

Here τ_1 and τ_2 are the θ_1° and θ_2° lifetimes, and Δm is the difference between their masses; we recall that the particles which have definite charge-parity[5] are θ_1° and θ_2°, and not θ° and $\overline{\theta}^\circ$. Since processes (2′) and (3′) are forbidden, while the probabilities of (2) and (3) are equal by virtue of charge-symmetry, the ratio of μ^+ to μ^- decays will vary in the beam according to the formula

$$\frac{n_{\mu^+}}{n_{\mu^-}} = \frac{e^{-t/\tau_1} + e^{-t/\tau_2} + 2e^{-t/2\tau_1 - t/2\tau_2} \cos \Delta mt}{e^{-t/\tau_1} + e^{-t/\tau_2} - 2e^{-t/2\tau_1 - t/2\tau_2} \cos \Delta mt}. \qquad (4)$$

This is a special case of a more general formula found by Zel'dovich[4] . A similar law holds for the μ-decay of the τ°-particle.

If the hypothesis of the primary character of the $K\mu\nu$-interaction is correct, then in the $K_{\mu 4}$-decay

$$(K \rightarrow \mu + \nu + 2\pi)$$

the K^+ and K° must emit μ^+-mesons while the K^- and $\overline{K}^\circ$ must emit μ^--mesons. However, the probability of $K_{\mu 4}$ decay must be very small compared with that of $K_{\mu 3}$-decay. The decay of Λ and Σ hyperons, which have strangeness -1, must go via the μ-decay of a K^--particle. This means that hyperon decays can only produce μ^- and never μ^+-mesons. Thus the processes

$$\Lambda^0 \rightarrow p + \mu^- + \nu, \quad \Sigma^- \rightarrow n + \mu^- + \nu$$

are allowed, while the μ-decay of the Σ^+-hyperon is forbidden.

Finally we consider the μ-decay of the cascade Ξ-hyperon. Our hypothesis requires that in μ-decay the strangeness is either conserved (if the μ-decay goes via a pion) or is changed by one unit (if the μ-decay goes via a K-particle). Since the Ξ-hyperon has strangeness -2, it can decay by

$$\Xi^- \rightarrow \Lambda^0 (\Sigma^0) + \mu^- + \nu, \quad \Xi^0 \rightarrow \Sigma^+ + \mu^- + \nu$$

but not by

$$\Xi^- \rightarrow n + \mu^- + \nu, \quad \Xi^0 \rightarrow p + \mu^- + \nu$$

Decays with μ^+ emission are of course forbidden for Ξ-hyperons.

If these various consequences of Schwinger's hypothesis are not confirmed by experiment, it means that the hypthesis is incorrect. However, an experimental confirmation of the effects will not imply that the hypothesis is correct. In fact the same consequences can be derived from quite different assumptions. For example, they follow from a hypothesis of Sachs,[6] according to which μ-decays conserve "attribute" and the "attribute" of μ^- and neutrino together is equal to that of K^- or Λ or Σ. All the selection rules which we have found hold in the Sachs theory, independently of whether the primary interaction of μ, ν is with pions and K-particles or with nucleons and hyperons. In particular, the forbiddenness of (2′) and (3′) was deduced by Sachs,[6] and Eq. (3) by Sachs and Trieman,[7] starting from the "attribute" hypothesis.

The author expresses his thanks to Professor I. Ia. Pomeranchuk for much valuable criticism.

---

*After this letter was in print we received a typescript of the second part of Schwinger's work, including some of the results reported here.

*This result was found independently by S. G. Matinian (private communication).

1 J. Schwinger, Phys. Rev. 104, 1164 (1956).

2 M. Gell-Mann and A. Pais, Phys. Rev. 97, 1387 (1955).

3 A. Pais and O. Piccioni, Phys. Rev. 100, 1487 (1955).

4 Ia. B. Zel'dovich, J. Exptl. Theoret . Phys. (U.S.S.R.) 30, 1168 (1956); Soviet Phys. JETP 3, 989 (1957).

5 Ia. B. Zel'dovich, Uspekhi Fiz. Nauk 59, 377 (1956).

6 R. G. Sachs, Phys. Rev. 99, 1573 (1955).

7 S. B. Trieman and R. G. Sachs, Phys. Rev. 103, 1545 (1956).

Translated by F. J. Dyson
98

Conservation Laws in Weak Interactions

L. D. Landau
Institute for Physical Problems,
Academy of Sciences, USSR

(Submitted to JETP editor December 11, 1956)
J. Exptl. Theoret. Phys. (U.S.S.R.) 32, 405–406
(February, 1957)

THE properties of *K*-particles have led to a difficult situation in present–day theoretical physics. The angular distribution of the τ–decay $(K^+ \to 2\pi^+ + \pi^-)$ requires that the K^+-particle be in a 0^- state. But this state cannot then decay into two π-mesons $(K^+ \to \pi^+ + \pi^0)$. We are faced with the dilemma, either to believe that there are two distinct *K*-particles, or to believe that conservation laws are violated in the *K*-particle decay. In the first case, we have to explain the equality of the masses (accurate to within 2 electron masses), and the approximate equality of the lifetimes, associated with the θ and τ decays. One may try to explain the equality of masses, as Lee and Yang[1] propose, by postulating an unknown symmetry property of the nuclear forces, under which the θ and τ states can be interchanged. However, if one supposes that the neutrino decay modes

$$(K^+ \to \mu^+ + \nu, \quad K^+ \to \mu^+ + \nu + \pi^0, \quad K^+ \to e^+ + \nu + \pi^0)$$

are equally probable for the two parity-states, one should expect a difference in the lifetimes arising from the different frequencies of the τ and θ decays (around 8% and 25% respectively). The difference in lifetimes should be 30–40% and is in conflict with recent experimental data.[2]

We are apparently forced to the conclusion that the two *K*-particle hypothesis disagrees with experiment, and the only alternative is to suppose that presently accepted conservation laws are violated in the *K*-particle decay. Since there is not the slightest reason to doubt the validity of the law of conservation of momentum, we have to envisage a direct violation of the law of conservation of parity.

At first glance it appears that non-conservation of parity would imply an asymmetry of space with respect to inversion. Such an asymmetry, in view of the complete isotropy of space (conservation of momentum), would be more than strange. In my opinion a simple denial of parity-conservation would place theoretical physics in an unhappy situation. I wish to point out that there exists a way out of this situation. We know that the strong interactions are invariant not only with respect to space-inversion but also with respect to charge-conjugation. We assume that in weak interactions these two invariance properties do not hold separately. But we can suppose that we still have invariance with respect to the product of the two operations, which we call combined inversion. Combined inversion consists of space reflection with interchange of particles and antiparticles. If all interactions are invariant with respect to combined inversion, space remains completely asymmetrical, and only electric charges are asymmetrical. This asymmetry destroys the symmetry of space just as little as the existence of chemical stereoisomers.

For charged particles there will not be any law of conservation of parity, since the combined inversion does not transform a charged particle into itself. It is also clear that all the constants (masses, lifetimes) characteristic of a particle are identical for particle and anti-particle. For the processes which are possible for particle and anti-particle differ only by a space-inversion, if the whole system is invariant under combined inversion. Speaking pictorially, a K^--particle is a K^+-particle reflected in a mirror.

Truly neutral particles, i.e., particles which are identical with their antiparticles, transform into themselves under combined inversion. For such particles the combined inversion becomes an ordinary space inversion, and so parity is conserved in all their interactions. It is to be emphasized that the conserved parity is the product of the ordinary parity and the charge-parity of these particles. In this sense the π^0-meson is an odd particle, the K_1^0 (θ^0) which decays into two pions is an even particle, and the K^0 which was predicted by Gell-Mann and Pais[3] and recently discovered experimentally[4] is an odd particle. For photons, combined inversion reverses the sign of the magnetic field and leaves the electric field invariant. The ordinary parities of electric and magnetic multipoles are just reversed under combined inversion. It is easy to show that in this scheme, in spite of the non-existence of ordinary parity, particles cannot possess dipole moments. In fact, the only vector which can be constructed from the wave-function of a particle at rest is the spin-vector, which is even under reflection and odd under charge conjugation. Thus the spin-vector is odd under combined inversion, and in view of what was said earlier about the electromagnetic field the spin-vector can carry only a magnetic and not an electric moment.

As Lee and Yang[5*] have shown, the non-conservation of parity would imply correlations in various hyperon creation and decay processes. One can prove that invariance under combined inversion requires that the coefficients multiplying the weak interaction terms in the Lagrangian are real. This does not however change the qualitative picture which appears in the general case of parity nonconservation. The asymmetry of hyperon decay with respect to the plane of production, which was predicted by Lee and Yang,[5] still occurs in our proposed scheme.

In conclusion I wish to express deep gratitude to L. Okun', B. Ioffe and A. Rudik, for the discussions in which the ideas of this letter originated.

---

*I wish to thank these authors for kindly sending me the manuscript of their paper before publication.

1 T. Lee and C. Yang, Phys. Rev. 102, 290 (1956).

2 Proceedings of the Sixth Annual Rochester Conference, April, 1956, (Interscience 1956).

3 M. Gell-Mann and A. Pais, Phys. Rev. 97, 1387 (1955).

4 Lande, Booth, Impeduglia, Lederman and Chinowsky, Phys. Rev. 103, 1901 (1956).

5 T. Lee and C. Yang, Phys. Rev. 104, 254 (1956).

Translated by F. J. Dyson
102

Possible Properties of the Neutrino Spin

L. D. Landau
Institute for Physical Problems,
Academy of Sciences, USSR

(Submitted to JETP editor December 11, 1956)
J. Exptl. Theoret. Phys. (U.S.S.R.) 32, 407–408
(February, 1957)

If the law of conservation of parity is abandoned, then new properties of the neutrino become possible. In the case of zero mass, the Dirac equation separates into two uncoupled pairs of equations. In the usual theory it is impossible to restrict attention to one pair of equations, since the two pairs are interchanged by a space-inversion. But if we require only invariance under combined inversion[1], then we can suppose that the neutrino is described by a single pair of equations. In ordinary language, this implies that the neutrino is always polarized along (or always opposite to) the direction of its motion. The antineutrino is then polarized always in the opposite sense. In this scheme the neutrino is not a truly neutral particle, in agreement with the observed absence of double β-decay and especially with the experiments on induced β-decay. We call this kind of neutrino a longitudinally polarized neutrino, or a longitudinal neutrino for short.

In the usual theory the neutrino mass is zero "accidentally." And if one takes into account the neutrino interactions, a non-zero rest-mass appears automatically, although it is of negligible magnitude. The mass of a longitudinal neutrino is automatically zero, and this fact is not disturbed by any interactions.

If we assume the neutrino to be longitudinal, the number of possible types of weak interaction operator is greatly reduced. Consider the decay of a μ-meson into an electron and two neutrinos. We write the interaction operator in the usual way as a product of two factors, one composed of the μ-meson and electron field-operators, and the other composed of two neutrino field-operators. With longitudinal neutrinos, we can construct from two ψ-operators only a single combination, a scalar. It is a scalar under rotations only, the operation of ordinary inversion not being applicable to it. The tensor combination vanishes for two identical particles obeying Fermi statistics. From the μ-meson and electron fields we can construct two combinations, a scalar and a pseudoscalar (in the ordinary sense).

If the μ-decay produces a neutrino and an antineutrino, the situation is different. In this case, from the longitudinal neutrino and antineutrino fields, we can construct only a 4-vector. From the μ-meson and electron fields we can construct two combinations, a vector and a pseudovector. Thus in both cases, in spite of the lack of invariance under space-inversion, we have only two possible interaction operators.

It is easy to calculate the energy spectrum of the electron in μ-decay. The result agrees with the calculation of Michel.[2] In the case of two neutrinos we find the Michel parameter $\rho = 0$, and in the case of neutrino and antineutrino we find $\rho = 0.75$. The first alternative is contradicted by experiment, while the second agrees with the existing data,[3,4] which give $\rho = 0.64 \pm 0.10$. Thus the experiments on μ-decay do not contradict the longitudinal neutrino hypothesis, and they further lead to the unambiguous conclusion that the μ-decay involves one neutrino and one antineutrino.

Next we consider the decay $\pi \rightarrow \mu + \nu$. Since the pion has spin zero, the operator responsible for the $\pi \rightarrow \mu + \nu$ decay must contain a scalar combination of the μ and ν fields. This automatically implies that, in a $\pi \rightarrow \mu + \nu$ decay with a longitudinal neutrino, the μ-meson will be completely polarized along its direction of motion (or in the opposite direction). As Lee and Yang[5] observed, the nonconservation of parity can lead to a correlation between the directions of the μ-meson and electron in a $\pi \rightarrow \mu \rightarrow e$ cascade. In our scheme, a simple calculation leads to the following distribution of the outgoing electrons in energy and angle,

$$dN / N = 2\varepsilon^2 \left[(3 - 2\varepsilon) + \lambda \cos\theta\, (2\varepsilon - 1)\right] d\varepsilon. \quad (1)$$

Here ϵ is the ratio of the electron energy to the maximum possible energy, θ is the angle between the directions of motion of the μ-meson and the electron, and λ is a constant depending on the ratio between the vector and pseudovector terms in the combination of μ-meson and electron field-operators. Explicitly we have

$$\lambda = 2ab / (a^2 + b^2), \quad (2)$$

where a and b are the coefficients of the two terms. In our earlier paper[1] we argued that a and b should be real. The quantity λ must lie between -1 and 1, and the value zero is not excluded. The integrated angular distribution of the electrons is proportional to $(1 + 1/3\ \lambda \cos\theta)$, so that the maximum possible forward-backward asymmetry is a factor of two. Even if λ should be markedly different from zero, the observation of the $\mu - e$ correlation may be very difficult because of the depolarization of the mesons in the course of their slowing down, and especially for μ^+-mesons because of the formation of muonium (the system $\mu^+ + e^-$).

Next we consider the effect of the longitudinal neutrino in β-decay. It is known from experiment that the β-decay interaction operator is a sum of scalar and tensor covariants. Either interaction term gives rise to a polarization of the electrons along the direction of their motion, of magnitude (v/c) (or $-v/c$), the ratio of the electron velocity to light velocity. The high-energy electrons are thus completely polarized in the direction of their motion.

Note added in proof.(February 21, 1957).

Very recently Wu, Ambler, Hayward, Hoppes and Hudson showed that in the β-decay of oriented Co^{60} nuclei there is actually a lack of mirror-symmetry. This definitely establishes the non-conservation of parity in β-decay. The experiments of Wu et al. agree with the theory of the longitudinal neutrino; however, the precision of the experiments does not seem high enough for a quantitative verification. The experiments of Wu et al. imply that the neutrino has its spin parallel to its direction of motion, while the antineutrino has its spin antiparallel.

Garwin, Lederman and Weinrich have observed a correlation in the $\pi \to \mu \to e$ decay. The magnitude of the correlation is large, which seems to imply a value of the parameter λ equal to unity. The energy-dependence of the correlation seen in this experiment does not agree with Eq. (1). It is difficult to say at present whether the discrepancy is within the limits of error of the measurements.

I am very much obliged to Professor Lederman for kindly sending me the manuscripts of both papers before publication.

[1] L. D. Landau, J. Exptl. Theoret. Phys. (U.S.S.R.) 32, 405 (1957).
[2] L. Michel, Proc. Phys. Soc. (London) A63, 514 and 1371 (1950).
[3] Sargent, Rinehart, Lederman and Rogers, Phys. Rev. 99, 885 (1955).
[4] Boneth, Levi-Setti, Panetti, Rossi and Tomasini, Nuovo Cim. 3, 33 (1956).
[5] T. Lee and C. Yang, Phys. Rev. 104, 254 (1956).

Translated by F. J. Dyson
103

Concerning a Possible Method for the Polarization of a Proton Beam

E. K. ZAVOISKII

(Submitted to JETP editor December 14,1956)
J. Exptl. Theoret. Phys. (U.S.S.R.) 32, 408
(February,1957)

A BEAM of protons (likewise deuterons, tritons, He^3, etc.) passing through a thin ferromagnetic slab, magnetized to saturation, should become "magnetized" due to pick-up by the protons of the polarized ferromagnetic electrons. As a result of such electron pick-up, the atoms of hydrogen obtained will be polarized as regards their electron spin and if, outside the magnetic field, they are again ionized by passage through a thin foil (or a gas beam), then the protons will come out partly polarized.

The fraction of polarized protons coming out of the second foil (only atoms of hydrogen being considered entering the foil), will be equal to half the fraction of the neutral atoms polarized according to their electron spin. The degree of polarization of the hydrogen atoms is determined by the probability of the protons picking up the "ferromagnetic" electrons in comparison with the probability of picking up the unpolarized electrons. The magnitude of the polarization obviously will depend on the velocity of the protons and the type of the ferromagnet. If it is assumed that $3d$ and s electrons will be picked up with equal probability, then the degree of polarization of a proton beam passing through an iron foil should approach ~ 15%.

The beam intensity of the polarized protons depends on the proton beam passing through the ferromagnetic slab. Experiments show that thin foils bombarded by 10–40 kilovolt protons can withstand a beam of several micro amperes/cm^2 , and the degree of electron pick–up by the protons reaches tems of percent.

The possibility of using a pulsed technique for such a polarizer should be mentioned. This should be very practical for many accelerators. This method also makes possible the direct formation of negative ions of hydrogen with polarized muclei. For this, of course, one must use the negative ions emerging from the second foil.

A study of the polarization of the protons and its dependence on velocity may also be of interest in elucidating questions on the nature of ferromagnetism.

In conclusion it should be mentioned that, in principle, polarization of the protons should be achievable likewise using the polarized electrons of paramagnetic substances and metals.

Translated by A. Turkevich
104

Inelastic Interaction of Protons with Energies Greater than 7 bev with Carbon and Hydrogen Nuclei

K. I. ALEKSEEVA AND N. L. GRIGOROV
Moscow State University

(Submitted to JETP editor December 7,1956)
J. Exptl. Theoret. Phys.(U.S.S.R.) 32, 404–405
(February,1957)

WE have measured the cross section for inelastic interaction of high energy protons with carbon and hydrogen nuclei. The measurements were carried out in the stratosphere at an altitude of 20–25 km at a geomagnetic latitude of 31° N, where the minimum kinetic energy of the primary protons is 7 bev and 60% of all the protons have energies between 7 and 20 bev.

The apparatus for determining these inelastic interaction cross–sections was constructed as follows. The telescope defining the vertical beam of cosmic rays consisted of three rows of self quenching Geiger–Müller tubes connected in three-fold coincidence (referred to as the counter telescope); some distance below these was a row of hodoscopic counters covering almost the complete solid angle of the apparatus. In between the middle and lower rows of telescopic counters there was placed an absorber made of 8 cm of lead and 0.9 cm aluminum. The absorbers being investigated, for example, of graphite (density $d = 1.0 - 1.1$ gm/cm^3 ; thickness per unit area of absorber $d = 16.0$ gm/cm^2), were placed on a trolley and every three minutes were interposed into the space between the top and middle rows of the telescopic counters in such a manner that the measurements with the graphite and without the graphite (and likewise the measurements with the paraffin and graphite) alternated. In order to register the products of the interaction of the protons with the material of the absorber, the telescope and absorbers were surrounded by a large number of counters. All the counters (including those in the telescope) were connected to a vacuum tube hodoscope. The apparatus was lifted into the stratosphere in September 1955 by sounding balloons. The results were sent to the ground by radio.

The cross section for inelastic interaction of protons with carbon nuclei was determined by two methods: (1) From the attenuation of the flux of single shower producing particles falling on the lead absorber by the graphite absorber in the telescope; this attenuation was governed by the inelastic interactions of the protons with the carbon nuclei (the measurements gave the decrease in the number of electron-nucleon showers from the Pb due to the insertion of the graphite into the telescope): (2) Through the direct measurement of the number of electron–nucleon showers arising in the graphite.

Using the attenuation method, we obtained the following values of the mean free path and the cross section for inelastic interaction of protons with carbon nuclei (corrections have been made for accidental coincidences, for the formation of δ-showers in the graphite and for interactions due to α particles in the primary cosmic rays):

$$L_p^{\mathrm{C}} = 67^{+13}_{-9}\ g/\mathrm{cm}^2\ ;\ \sigma_p^{\mathrm{C}} = 300 \pm 50\ \mathrm{mb}.$$

Direct measurements of the number of interactions in the graphite gave the following values for the mean free path and for the inelastic interaction cross section:

$$L_p^{\mathrm{C}} = 73 \pm 7\ g/\mathrm{cm}^2\ ;\sigma_p^{\mathrm{C}} = 270 \pm 30\ \mathrm{mb}.$$

All the values have indicated statistical errors.

The cross section for inelastic interaction of protons with protons was established from the difference of numbers of electron–nucleon showers registered with paraffin and with graphite using an apparatus of the same type (the paraffin absorber had a density $d = 0.90 - 0.95$ gms/cm^3

and a thickness of $d_1 = 18.8$ gms/cm^2 ; the pulverized graphite absorber had a density $d = 1.0 - 1.0$ gms/cm^3 ; $d_1 = 16.0$ gms/cm^2). The mean free path and inelastic scattering cross section for proton–proton interaction came out to be

$$L_p^{\mathrm{H}} = 47^{+37}_{-15} g/\mathrm{cm}^2 ; \sigma_p^{\mathrm{H}} = 35 \pm 16 \text{ mb}.$$

In getting this value of the cross–section we did not know sufficiently accurately the contribution of δ-showers produced in the hydrogen. However, on the basis of experimental data available, it can be said that the values of the cross–section will not change more than ± 10% after correcting for these δ-showers. At the present time we are carrying out measurements at sea level to determine the formation of delta showers in graphite and paraffin.

Translated by A. Turkevich
101

On the Theory of Scattering of Particles by Nuclei

I. G. IVANTER AND L. B. OKUN

(Submitted to JETP editor November 29,1956)
J. Exptl. Theoret. Phys. (U.S.S.R.) 32, 402–403
(February, 1957)

IN the study of the scattering of nucleons by nuclei, a model[1,2] has often been used which considers the nucleus as a Fermi gas of nucleons at a temperature $T = 0$. It seems reasonable to use this same model to study the nuclear scattering of particles having masses different from that of a nucleon. Such a study would allow one to start evaluating the effect of the Pauli principle in the scattering of π and K-mesons.

Let a particle 1 with mass m_1 and momentum p_1 impinge on a Fermi gas of particles 2 of mass m_2 and momenta p_2 $(0 \leq p_2 \leq p_F)$, at a temperature $T = 0$. Let the differential scattering cross section for the free particles 1 and 2 be isotropic, independent of energy, and equal to $\sigma_0 / 4\pi$. We will calculate the total cross section $\sigma = \sigma_0 F$ for the collision of particle 1 with one of the particles of the gas. It is obvious that the factor F must be less than 1 since, because of the Pauli principle, not all of the final states for particle 2 are allowed, but only those with $p_2' > p_F$. In order to calculate F let us consider the collision of two particles (Fig. 1). We will let p_1' and p_2' be the momenta of particles 1 and 2 in the laboratory system of coordinates after the collision; p and p′ will be the momenta of particle 1 in the center of mass before and after the collision, respectively. Then

$$p_2' = | -\mathrm{p}' + m_2 (\mathrm{p}_1 + \mathrm{p}_2) / (m_1 + m_2) | > p_F.$$

Keeping in mind that

$$p' = p = | m_2 \mathrm{p}_1 - m_1 \mathrm{p}_2 | / (m_1 + m_2)$$

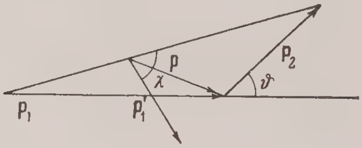

FIG. 1

and introducing the variables

$$\alpha = m_1 / m_2, \; u = p_2 / p_1,$$
$$w = p_F / p_1, \; x = \cos \vartheta, \; y = \cos \chi,$$

we obtain the equation for the surface S in the space u, y, x that determines the allowed region of the variables u, y, x:

$$\begin{aligned} S(\alpha, w; u, y, x) &= (1 + \alpha^2 u^2 - 2\alpha u x) + (1 + u^2 + 2ux) \\ &- 2 [(1 + \alpha^2 u^2 - 2\alpha u x)(1 + u^2 + 2ux)]^{1/2} y \\ &- w^2 (1 + \alpha)^2 = 0. \end{aligned}$$

This surface depends on α and w parametrically. Schematically, the allowed region is presented in Fig. 2. It is bounded by the surface S and the planes $y = -1$, $x = +1$, $x = -1$, $u = 0$, $u = w$.

Calculating the number of collisions suffered by particle 1 in unit time, we obtain for the factor F the following expression:

$$F = (3/4w^3) \int\int\int u^2 \sqrt{1 + \alpha^2 u^2 - 2\alpha u x} \, du \, dx \, dy.$$

Here the integration has to be carried out over the allowed region described above. Different

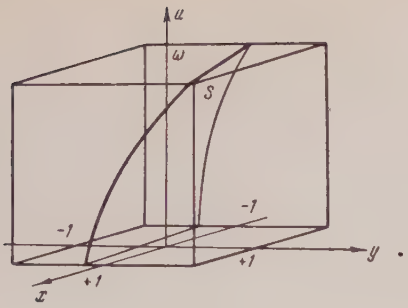

FIG. 2

values of F result from different values of the parameters α and w. In the general case ($0 \leq \alpha \leq 1$) we get:

$$0 < w < 1 \quad : \quad F = 1 - w^2(1 + 2\alpha)/5,$$

$$1 < w < 1/\alpha : \quad F = [\alpha^2 - 2 + 10w^2 - 20\alpha w^3 + 15\alpha^2 w^4 - 4\alpha^3 w^5]/10w^3(1-\alpha)^2,$$

$$1/\alpha < w < \infty : \quad F = (1+\alpha)^2/10\alpha^2 w^3.$$

As is easily seen these formulae simplify considerably in the limiting situations $\alpha = 0$ and $\alpha = 1$.

We express our sincere gratitude to Prof. I. Ia. Pomeranchuk and L. A. Ter-Martirosian for interesting and productive discussions.

---

[1] Hayakawa, Kawai and Kikuchi, Progr. Theor. Phys. 13, 415 (1955).

[2] M. L. Goldberger, Phys. Rev. 74, 1269 (1948).

Translated by A. Turkevich
99

The Spatial Distribution of the Penetrating Component of Wide Atmospheric Showers

E. L. ANDRONIKASHVILI AND
M. F. BIBILASHVILI
Physical Institute, Academy of Sciences, Georgia SSR

J. Exptl. Theoret. Phys.(U.S.S.R.) 32, 403–404
(February, 1957)

STUDIES have been carried out on the spatial distribution of the penetrating component of wide atmospheric showers at an altitude of 400 meters above sea level in a tunnel underneath 26.6 meters of earth (65.5 meters of water equivalent, m. w. e).

The measurements of the density of penetrating particles were carried out at distances of 0, 10, 20, 30, 45, and 60 meters from a vertical axis passing through the center of the detecting system. The shower detection was carried out using two core selectors similar to those used in previous work.[1] In addition, the apparatus contained correlating hodoscopic systems which served to determine the total number of particles and the point of passage of the core of the wide atmospheric shower. There was also an underground apparatus registering the particles in the penetrating component. The showers were recorded with the help of a movie camera. This set-up was most efficient for showers containing between 10^5 and 5×10^5 particles. During 2156 hours of running data were obtained on the spatial distribution of the penetrating component of showers with this number of particles and these are presented in the Table.

Distance from the axis of detecting system	Time of observation, hours	No. of showers registered	Rate of counting, Days^{-1}	Calculated density of penetrating particles, *Particles/m^2*
0	276.0	72	6.25	0.55±0.065
10	250.0	61	5.9	0.51±0.078
20	244.0	58	5.7	0.49±0.064
30	246.0	48	4.7	0.39±0.056
45	395.0	38	2.3	0.17±0.027
60	745.0	31	1.0	0.07±0.013

The experimental data obtained are represented satisfactorily, within statistical error, by a Gaussian of the form:

$$\rho(r) = 0{,}61 \exp[-0{,}00059 r^2]. \qquad (1)$$

We note, however, that in carrying out the measurements we did not take into consideration the angular distribution of the cores of the wide atmospheric showers and the inaccuracy in determining the position of passage of this core. Consideration of the two distributions shows that the axes

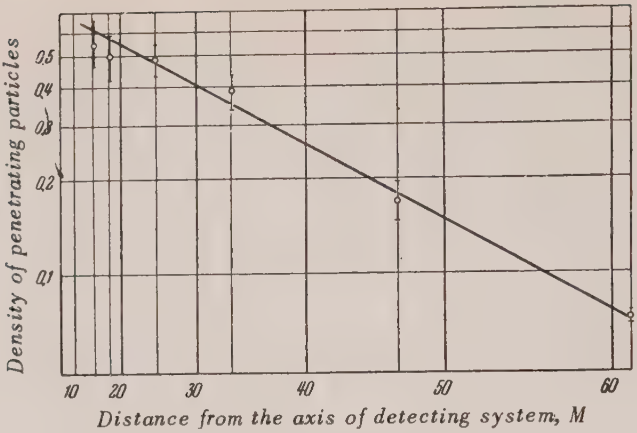

Spatial distribution of the penetrating component of wide atmospheric showers having a total number of particles in the interval between 10^5 and 5×10^5.

of the wide atmospheric showers are inclined relative to the underground system and this is especially important for measurements in the central parts of the shower. The spatial distribution of the density of the penetrating particles (per m^2) is constructed from the corrected data presented in the Figure. It obeys a Gaussian law on the form:

$$\rho(r) = (0.66 \pm 0.09) \exp[-(0.00058 \pm 0.00009) r^2]. \tag{2}$$

The total number of penetrating particles calculated on the basis of distribution (2) turns out to be $(3.5 \pm 1.1) \times 10^3$ particles.

Consideration of the minimum energy needed to get a depth of 65.5 m. w. e. leads to a value of 5×10^{13} ev carried by the penetrating component. The soft component of these same showers at sea level carries an energy of 3×10^{13} ev. Thus 60 to 70% of the energy reaching sea level as electronic-photonic component penetrates to a depth of 65.5 m. w. e. Considering the energy carried by penetrating particles that are absorbed in the ground up to 65.5 m. w. e. we conclude that at least 75% of the energy of wide atmospheric showers at sea level is concentrated in their penetrating component.

---

[1] Cocconi, Cocconi-Tongiorgi and Greisen, Phys. Rev. 76, 1020 (1949).

Translated by A. Turkevich
100

CONTENTS—(*continued*)

Russian Reference

s-d Exchange in Ferromagnetic Metals . . . . . F. M. Gal'perin 321 32, 381
Quasi-Magnetic Interaction of the Spin of a Nucleon with the Rotation of the Nucleus . . . . . D. F. Zaretskii and A. V. Shut'ko 323 32, 370
The Threshold of "Creation" and the Threshold of "Generation" of Negative *K*-Particles . . . . . M. Danysh and B. Pontecorvo 325 32, 398
Nuclear Saturation and the Levy-Klein Potential of Pseudoscalar Meson Theory . . . . . B. K. Kerimov 326 32, 377
The Problem of Parity Non-conservation in Weak Interactions . . . . . B. L. Ioffe, L. B. Okun' and A. P. Rudik 328 32, 396
Diffractive Production of Proton-Antiproton Pairs by High Energy Photons . . . . . A. G. Sitenko and L. N. Rozentsveig 330 32, 383
Internal Compton Effect in Pair Conversion . . . . . E. G. Melikian 331 32, 384
The Momentum Distribution of Interacting Fermi Particles . . . . . A. B. Migdal 333 32, 399
The μ-Decay of *K*-Particles and Hyperons . . . . . L. B. Okun' 334 32, 400
Conservation Laws in Weak Interactions . . . . . L. D. Landau 336 32, 405
Possible Properties of the Neutrino Spin . . . . . L. D. Landau 337 32, 407
Concerning a Possible Method for the Polarization of a Proton Beam . . . . . E. K. Zavoiskii 338 32, 408
Inelastic Interaction of Protons with Energies Greater than 7 bev with Carbon and Hydrogen Nuclei . . . . . K. I. Alekseeva and N. L. Grigorov 339 32, 404
On the Theory of Scattering of Particles by Nuclei . . . . . I. G. Ivanter and L. B. Okun' 340 32, 402
The Spatial Distribution of the Penetrating Component of Wide Atmospheric Showers . . . . . E. L. Andronikashvili and M. F. Bibilashvili 341 32, 403

CONTENTS – (*continued*)

Russian Reference

Scattering of Fast Protons on Protons . . . . D. I. Blokhintsev 284 32, 347
Some Remarks on the Validity of the Hydrodynamic Description of Quantum Systems . . . . D. I. Blokhintsev 286 32, 350
Polarization Effects in the Scattering of Electrons and Positrons by Electrons . . . . A. A. Kresnin and L. N. Rosentsveig 288 32, 353
On the Nature of the Cone-like Shape of Tracks of Multi-charged Ions in Nuclear Emulsions . . . . O. V. Lozhkin 293 32, 208

Letters to the Editor:

Particle with Spin 3/2 in an Electromagnetic Field. . . . . E. E. Fradkin 298 32, 363
Experimental Comparison of the Energy Spectra of γ Quanta from the Decay of π^0-Mesons formed on Carbon and Lead Nuclei by 600 Mev Protons . . . . Iu. D. Baiukov, A. N. Sinaiev and A. A. Tiapkin 299 32, 385
Production of Very Strong Magnetic Fields by Rapid Compression of Conducting Shells . . . . Ia. P. Terletskii 301 32, 387
The Influence of the Entrainment of Electrons by Phonons on Thermomagnetic Effects in Semiconductors . . . . V. L. Gurevich and Iu. N. Obraztsov 302 32, 390
The Role of Three-Particle Forces in the Three-Body Problem . . . . N. N. Kolesnikov 304 32, 392
New Short Lived Isomers in the Millisecond Range . . . . O. I. Leipunskii, A. M. Morozov, Iu. V. Makharov and P. A. Iampol'skii 305 32, 393
Negative Ions of Silicon, Germanium, Tin and Lead . . . . V. M. Dukel'skii and V. M. Sokolov 306 32, 394
Peculiarities of Cerenkov Radiation in Anisotropic Media 307 32, 366
. . . . V. E. Pafomov 307 32, 366
Concerning Even-Even Nuclei Having the Characteristic 2+ for the Second Excited State . . . . N. N. Deliagin and V. S. Shipnel' 309 32, 373
Dependence of the Polarization of (D + D) Neutrons on the Energy of the Deuterons . . . . I. I. Levintov, A. V. Miller, E. Z. Tarumov and Vn. Shamshev 310 32, 375
Altitude Dependence of Broad Atmospheric Showers According to the Various Models of the Elementary Act of Nuclear Collisions . . . . V. V. Guzhavin and G. T. Zatsepin 312 32, 365
The Construction of a Phenomenological Scattering Matrix with Non-Local Interaction . . . . V. S. Barashenkov 313 32, 368
An Experiment on the Measurement of the Viscosity of an Expanded Liquid . . . . A. P. Toropov and A. I. Kitova 315 32, 372
Concerning the Possibility of an Experimental Investigation of the Structure of the Electron . . . . V. A. Petukhov 317 32, 379
Force Fluctuations in an Electron Gas . . . . M. Ia. Mints 319 32, 386
Effect of a Longitudinal Magnetic Field on the Multiple Scattering of Particles . . . . N. A. Cerenkov 320 32, 389

(*Contents continued on adjacent page*)

Soviet Physics JETP   Volume 5, Number 2   September, 1957

CONTENTS

Russian Reference

Emission of Negative Ions from Metallic Surfaces Bombarded with Positive Hydrogen Ions . . . . . I. M. Mitropan and V. S. Gumeniuk 157 32, 214
Some Cases of Very Small Life Times of Low Nuclear Levels . . . . . E. E. Berlovich and G. V. Dubinkin 164 32, 223
Two Limiting Momenta in Scalar Electrodynamics . . . . . L. P. Gor'kov 167 32, 359
Measurement of the Relative Intensities of γ-Lines by a Two Meter Crystal Diffraction γ-Spectrometer . . . . . O. I. Sumbaev 170 32, 247
Structure of the Periphery of Extensive Atmospheric Cosmic Ray Showers . . . . . Iu. N. Antonov, Iu. N. Vavilov, G. T. Zatsepin, A. A. Kutuzov, Iu. V. Skvortsov, G. B. Khristiansen 172 32, 227
Soft 15–800 kev Radiation Accompanying the Thermal Neutron Fission of Uranium . . . . . V. K. Voitovetskii, B. A. Levin, and E. V. Marchenko 184 32, 263
Investigation of Slow Electron Emission Induced by High Energy Protons . . . . . E. S. Mironov and L. M. Nemanov 188 32, 269
Level Shifts In Helium . . . . . G. F. Filimonov 192 32, 311
Non Linear Theory of Betatron Oscillations in a Strong Focusing Synchrotron . . . . . Iu. F. Orlov 195 32, 316
Measurement of the C^{12} (p,γ) and C^{12} (d,n) Effective Cross Sections for Low Energy Bombarding Particles . . . . . A. S. Deineko A. Ia. Taranov and A. K. Val'ter 201 32, 251
Equilibrium Spectrum of Electrons and Photons with Account of Scattering . . . . . I. P. Ivanenko 204 32, 333
Behavior of an Electron in a Periodic Electric and a Uniform Magnetic Field . . . . . G. E. Zil'berman 208 32, 296
The Acceleration of a Plasma by a Magnetic Field . . . . . A. I. Morozov 215 32, 305
Investigation of U^{235} Fission γ Rays in the Energy Region up to 250 kev . . . . . V. V. Skliarevskii, D. E. Fomenko and E. P. Stepanov 220 32, 256
Quantum States and Optical Transitions of the F_2^+ Center Electron . . . . . M. F. Deigen, V. L. Vinetskii 226 32, 289
Investigation of the Energy Levels of the F^{20} Nucleus by Magnetic Analysis . . . . . L. M. Khromchenko 231 32, 194
Optical Contact of Polished Glass Surfaces . . . . . I. V. Obreimov and E. S. Trekhov 235 32, 185
Explosion of a Metal by an Electric Current . . . . . S. V. Lebedev 243 32, 199
Fission of U, Th, Bi and Tl Induced by High Energy γ-Quanta . . . . . E. V. Minarik and V. A. Novikov 253 32, 241
A New Method for Measuring the Polarization of Medium Energy Neutrons and the Phase Shift Analysis of $n-He^4$ Scattering . . . . . I. I. Levintov, A. V. Miller and V. N. Shamsev 258 32, 274
Decay of the τ Meson . . . . . I. N. Mikhailov 265 32, 284
The Theory of Ferromagnetism af Metals and Alloys at Low Temperatures . . . . . E. S. Kondorskii and A. S. Pakhomov 269 32, 323
On Radiation in Anisotropic Media . . . . . F. V. Bunkin 277 32, 338

(*Contents continued on inside back cover*)